Abimaelle Silva Chibério

Graduate in Chemical Engineering

Single-Column Chromatography with Recycle Lag Analog to Simulated Moving Bed Processes

Thesis submitted in partial fulfillment
of the requirements for the degree of

Doctor of Philosophy in
Chemical and Biochemical Engineering

Adviser: Doutor José Paulo Barbosa Mota, Full Professor,
NOVA University of Lisbon

Examination Committee

Chair:	Doutor Paulo Manuel Assis Loureiro Limão-Vieira
Rapporteurs:	Doutor Alírio Egídio Rodrigues
	Doutor Ricardo Jorge Sousa da Silva
Members:	Doutor José Paulo Barbosa Mota
	Doutor Francisco Avelino da Silva Freitas
	Doutor Mário Fernando José Eusébio
	Doutora Cristina Maria da Costa Peixoto Lisboa

FACULDADE DE
CIÊNCIAS E TECNOLOGIA
UNIVERSIDADE NOVA DE LISBOA

October, 2019

Abimaelle Silva Chibério

Graduate in Chemical Engineering

Single-Column Chromatography with Recycle Lag Analog to Simulated Moving Bed Processes

Thesis submitted in partial fulfillment
of the requirements for the degree of

Doctor of Philosophy in
Chemical and Biochemical Engineering

Adviser: Doutor José Paulo Barbosa Mota, Full Professor,
NOVA University of Lisbon

Examination Committee

Chair:	Doutor Paulo Manuel Assis Loureiro Limão-Vieira
Rapporteurs:	Doutor Alírio Egídio Rodrigues
	Doutor Ricardo Jorge Sousa da Silva
Members:	Doutor José Paulo Barbosa Mota
	Doutor Francisco Avelino da Silva Freitas
	Doutor Mário Fernando José Eusébio
	Doutora Cristina Maria da Costa Peixoto Lisboa

FACULDADE DE
CIÊNCIAS E TECNOLOGIA
UNIVERSIDADE NOVA DE LISBOA

October, 2019

Single-Column Chromatography with Recycle Lag Analog to Simulated Moving Bed Processes

This document was created using the (pdf)LaTeX processor, based on the "novathesis" template[1], developed at the Dep. Informática of FCT-NOVA [2].
[1] https://github.com/joaomlourenco/novathesis [2] http://www.di.fct.unl.pt

To my incredible family, Negídio, Núbia and Abimael, my sources of inspiration. And to my beloved Diego, for the endless care and support.

Acknowledgements

The walk to get here was not the easiest, but the effort was certainly worth it. None of this would have been possible without the support received.

First of all, I would like to thank the mentor Professor Paulo Mota, not only for his guidance, but also for the trust he placed in my work, for the patience and availability he provided, and for the immense knowledge shared.

I also acknowledge the Conselho Nacional de Desenvolvimento Científico e Tecnológico (CNPq-Brasil), for funding and monitoring the project during these four years through grant [234180/2014-5]. To Laboratório Associado para Química Verde (LAQV/REQUIMTE) and M-ERA.NET through NESSIE project (New Structured Substrates for Downstream Processing of Complex Biopharmaceuticals, project nº4319) for the financial support to the work.

To colleagues of the office, thank you very much. Especially Tiago Santos, Raquel Serra, Laura Esteves, Rui Ribeiro and Snežana Reljić. You were very important, discussing work issues and also sharing pleasant conversations. You gave the emotional support I needed in the final stretch of the thesis and warmed my heart, thank you. To the researchers Gonçalo Policarpo and João Antunes, thank you for the assistance in the laboratory work and discussion of the project.

A thank you very dearly to the friends Rúbia Risso and Elena Surra, you became very special for me, sharing great chats accompanied by a coffee or a good lunch. Of you, I will never forget and I will be waiting for a visit wherever I am.

A special thanks to my family, you are everything to me. To my parents, Negídio Chibério and Núbia Da Silva, for their emotional support and for always having done everything so that I would grow at every step taken. You have taught me to always keep my head up and smiling without fearing what is to come. To my brother, Abimael Chibério, for the good humor and clowning, as well as for the incentive dialogues, always passing me good energies and leaving my life lighter. I love you so much!

To my husband, Diego da Câmara, I lack words to thank. You were the key piece during this whole journey. Your daily cares, constant words and attitudes of encouragement, and the sharing of incredible moments here in Portugal allowed me to continue throughout this journey and get here. You were the main propellant in the last few months of my doctorate and you didn't let me doubt my abilities. To you I will be eternally grateful.

To the other members of the family, uncles, cousins, brothers-in-law and in-laws,

thank you for the visits received, bringing a small piece of Brazil into my home and the coziness of the family, making this walk easier.

Finally, my sincere thanks to all those who contributed, directly or indirectly, to the conclusion and success of this thesis.

Abstract

The chromatography steps dominate the Downstream Processing (DSP) costs of a new biopharmaceutical, which has propelled the biopharmaceutical industry to invest a lot of effort on their improvement in order to reduce the costs of the biopharmaceutical production. Liquid chromatography (LC) is currently the core technique within the DSP strategy for the purification of biopharmaceuticals. Although single-column batch chromatography is simpler to operate than continuous (multicolumn) chromatography, the latter has many advantages over the former, including improved purity, yield, and productivity.

The main objective of this thesis is the development of a new chromatographic platform based on a novel single-column device that mimics the operation of multicolumn chromatography through ingenious management and recycling of the mixed fractions exiting the chromatographic column. The platform shares the benefits of the Simulated-Moving-Bed (SMB) technology. However, the newly developed process uses only a single chromatographic column.

The conceptual design of the set-up and its mathematical model were successfully established. The laboratory prototype was built focusing on a simple, compact, and versatile design with small footprint. The binary separation of nucleosides by reversed-phase chromatography was experimentally realized as proof of concept of the new system. An effort was made in 3D manufacturing of flow distributors and internals to ensure the proper operation of the recycle device and the improvement of its efficiency. A second case study—the capture step of monoclonal antibodies by affinity chromatography on protein A—was successfully used as a demonstration of the applicability of the newly developed process.

The new system offers a more compact, less expensive, and simpler-to-operate alternative to multicolumn SMB chromatography. Depending on the efficiency of the recycle device, the single-column process can achieve the same purities as the analogous SMB unit while keeping the specific productivity constant. Moreover, the single-column chromatograph can be easily integrated into the existing downstream processing platforms of complex biopharmaceuticals.

Keywords: Biomolecules Separation/Purification, Continuous Chromatography, Simulated Moving Bed, Single-column with Recycle Lag.

Resumo

As etapas cromatográficas inseridas no trem de purificação a jusante da bioreação dominam largamente os custos dessa componente do processo de produção de um biofármaco, o que tem levado a indústria biofarmacêutica a investir esforços na sua melhoria a fim de reduzir os custos globais de produção. A cromatografia líquida é atualmente a técnica principal para a purificação de produtos biofarmacêuticos. Embora a cromatografia descontínua monocoluna seja mais simples de operar do que a cromatografia contínua multicoluna, a última apresenta muitas vantagens sobre a primeira, incluindo pureza mais elevada e melhorias de rendimento e produtividade.

O objetivo principal desta tese é o desenvolvimento de uma plataforma cromatográfica baseada num novo processo monocoluna capaz de mimetizar a operação da cromatografia multicoluna em contracorrente simulada por meio de um dispositivo engenhoso de gestão e reciclo das frações do efluente da coluna cromatográfica. Apesar da plataforma desenvolvida utilizar apenas uma única coluna cromatográfica, ela partilha os benefícios dos chamados processos de Leito Móvel Simulado (LMS). Este último é a realização física do conceito de cromatografia sólido-líquido em contracorrente.

O desenho conceptual da instalação e o seu modelo matemático foram estabelecidos com sucesso. O respetivo protótipo laboratorial foi construído visando a minimização de equipamento, simplicidade, versatilidade e volume, sem, no entanto, limitar a ampla variedade mimetizável de processos multicoluna LMS e suas variantes. Procedeu-se ao desenho e dimensionamento do ciclo de operação de uma separação binária de nucleosídeos por cromatografia em fase reversa como prova de conceito do novo sistema e validou-se o processo experimentalmente. Desenharam-se e fabricaram-se diversos distribuidores de fluxo e dispersores internos através de impressão 3D para garantir a operação adequada do dispositivo de reciclo e melhoria de sua eficiência. O passo de captura de anticorpos monoclonais por cromatografia de afinidade com proteína A foi o segundo caso de estudo ao qual foi aplicado o novo processo, demonstrando a sua aplicabilidade.

O novo cromatógrafo de coluna única com atraso no reciclo oferece uma alternativa mais compacta, barata e simples de operar do que a cromatografia LMS multicoluna. Dependendo da eficiência do dispositivo de reciclo, o novo processo pode alcançar as mesmas purezas da unidade LMS análoga, mantendo a produtividade específica constante. Para além disso, ele pode ser facilmente integrado nas plataformas existentes de purificação de biofármacos complexos.

Palavras-chave: Separação/Purificação de Biomoléculas, Cromatografia Contínua, Leito Móvel Simulado, Monocoluna com Atraso no Reciclo.

Contents

List of Figures

List of Tables

Listings

Glossary

gPROMS — gPROMS, for general PROcess Modelling System, is among the most advanced general purpose process modelling and simulation software available today. For more information: `https://www.psenterprise.com/products/gproms`.

Julia — Julia is a high performance Programmimg Language, open source, that uses a flexible dynamic language, suitable for scientific and numerical computing. The Julia community has over 2400 Julia packages, and it also supports libraries from Python, R, C/Fortran, C++, and Java [34].

Acronyms

ABS	acrylonitrile butadiene styrene
AC	Affinity Chromatography
AEX	Anion exchange
AM	Additive Manufacturing
ATF	Alternating tangential flow
BC	Batch Chromatography
BJ	Binder Jetting
CC	Continuous Chromatography
CEX	Cation exchange
CHO	Chinese hamster ovary
CIP	cleaning-in-place
CIPP	Capture, intermediate purification and polishing
CLI	command line interface
CMCCC	Chemistry Manufacturing Controls Coordinating Committee
CNPq	National Council for Scientific and Technological Development
COG	Cost of goods
CSS	Cyclic steady-state
CST	Continuous Stirred Tank
CU	Capacity utilization
DLP	Direct Light Processing
DMD	digital mirror device
DMLS	Direct Metal Laser Sintering
DOD	Drop on Demand
DSE	Distortion Standard Equipments
DSP	Downstream processing

EAM	Equal Area Method
EBM	Electron Beam Melting
ELISA	Enzyme-linked immunosorbent assay
EPDM	ethylene propylene diene monomer
FDA	Food and Drug Administration
FDM	Fused Deposition Modeling
GC	Gas Chromatography
GF	Gel Filtration
gPROMS	general PROcess Modelling System
GSSR	Gradient with Steady State Recycle
HCP	Host cell protein
HIC	Hydrophobic Interaction Chromatography
HPLC	High Performance Liquid Chromatography
IEX	Ion Exchange Chromatography
IT	integration time
LC	Liquid Chromatography
LDF	Linear-driving-force
LOM	Laminated object manufacturing
mAbs	Monoclonal antibodies
MCSGP	Multicolumn Countercurrent Solvent Gradient Purification
MJ	Material Jetting
MMC	Multimodal Chromatography
PEEK	polyether ether ketone
PLA	polylactic acid
PrA	Protein A
R&D	Research and Development
RPC	Reversed Phase Chromatography
SEC	Size Exclusion Chromatography

SFF	Solid-FreeForm Technology
SLA	Stereolithography
SLM	Selective Laser Melting
SLS	Selective Laser Sintering
SMB	Simulated Moving Bed
SSR	steady-state recycling
TFF	Tangential flow filtration
TGA	Thermal Gravimetric Analysis
TMB	True Moving Bed
UPS	Upstream processing
WB	Western blot

Symbols

a_i^{P}	amount of component i (mAb or impurity) collected in the product fraction during some step (g)
A_P	cross-sectional area of the piston (cm^2)
K	cycle steps (-)
c_i	concentration of solid i in the fluid (g/cm^3)
c_i^{in}	inlet solute concentration (g/cm^3)
COL	column apparatus
COM	communication port
c_i^{out}	outlet solute concentration (g/cm^3)
D	desorbent flowrate or stream
D_L	axial dispersion coefficient (cm^2/s)
D_m	molecular diffusivity (cm^2/s)
E	eluent flowrate or stream; can be extract in some cases
ϵ	interparticle void fraction (-)
ϵ_p	intraparticle porosity (-)
ϵ_t	total porosity of the packed bed (-)
F	feed flowrate or stream
$FLOW_i$	pump flowrate (mL/min)
G	gradient flowrate or stream; can be extract in some cases
γ	empirical constant (-)
h	dimensionless plate height (-)
H	Henry's constant (-)
H^{app}	apparent Henry's constant (-)

H^r	real Henry's constant (-)
ID	internal diameter
Y	dimensionless solid phase concentration of the mAb (-)
k	LDF mass transfer coefficient (-)
k_{m}	mass transfer coefficient (-)
k_{m}^{∞}	maximum value of the mass transfer coefficient (-)
L	column or piston length (cm)
λ	wavelength (nm)
m_{ads}	adsorbed mass on the chromatographic column (g)
μ	arithmetic mean (-)
OD	external diameter
Pe	Péclet number (-)
$\mathrm{Pe_d}$	Péclet number based on the diameter, D_P, of the piston (-)
$\mathrm{Pe_h}$	hydraulic Péclet number (-)
$\mathrm{Pe_m}$	molecular Péclet number (-)
PI	Purity Index
$PUMP$	pump F, pump E or pump G
Pur_i	purity of component i (-)
q	amount of solute adsorbed at any given time (g/cm^3)
Q_0	volumetric flow rate at the piston's inlet (cm^3/s)
q^*	solute concentration at solid phase in equilibrium with the solute concentration at liquid phase (g/cm^3)
$\overline{Q_F}$	productivity (mL/min)
q^{∞}	adsorption capacity of the resin for the mAb (g/L)
Q_L	volumetric flow rate at the piston's outlet (cm^3/s)
R	raffinate flowrate or stream; can be recycle stream in some cases
RP	recycle piston apparatus
s	dimensionless pH (-)

S_1	coefficient that describes the maximum hindrance to the mass transfer (-)
S_2	coefficient that describes the non-linearity of the increase in hindrance (-)
σ	standard deviation (-)
t	time coordinate (s)
τ	time interval, or reference time
θ	reduced time coordinate scaled by a reference time τ (-)
T_i	flowrate exiting the corresponding tank in the Analog with mixed tanks
t_R	retention time (s)
UV_i	UV cell
v	fluid linear velocity (cm/s)
v_0	inlet fluid linear velocity (cm/s)
θ_{ads}	adsorbed volume on the chromatographic column (cm^3)
$VALUE$	max. pressure (bar)
$VALUE_i$	wavelengths (nm)
V_c	column volume (cm^3)
v	coefficient that relates Henry's constant to the pH value (-)
v_ϵ	interstitial velocity (cm/s)
V_F^{cycle}	feed volume injected per cycle (cm^3)
V_i	on-off pneumatic valve
V_i	apparent volume (cm^3)
v_L	outlet fluid linear velocity (cm/s)
V_L	dead volume of piston outlet (cm^3)
V_{matrix}	stationary phase volume (cm^3)
V_0	dead volume piston inlet (cm^3)
V_P	piston volume (cm^3)
θ_R	retention volume (cm^3)
w	dimensionless impurities concentration (-)
W	volumes of fluid (cm^3)
x	dimensioless domain for axial position z (-)
X	extract flowrate or stream

y	dimensionless mAb concentration (-)
Y	E (eluent), F (feed), G (gradient), R (recycle piston) or E+F
Y'	P (product), W (waste) or R (recycle piston)
Y^*	dimensionless equilibrium solid phase concentration of the mAb (-)
z	axial coordinate along the piston or column (cm)

Chapter 1

Research Purpose

1.1 Motivation

The biopharmaceutical industry emerged from the merger of the pharmaceutical industry with the biotechnology industry in the 1990s [55]. Traditionally, while the pharmaceutical industry produced and marketed drugs through chemical synthesis, biotech companies developed therapies manufactured in or extracted from living organisms such as yeast, bacteria, plant or mammalian cells. These therapies, or biologics, have offered potent therapeutic options for many diseases that had no available treatment, or had treatment with limited efficacy. In 2016, seven of the top ten best-selling drugs in the world were biologics [55].

Monoclonal antibodies (mAbs) are one of the most important medical products of biopharmaceutical industrial manufacturing [96]. mAbs are specific agents applied with a high degree of efficacy for the treatment of a wide variety of cancers [240, 263], for treatment of organ rejection response [167], as well as for reduction of the symptoms of various autoimmune diseases, such as multiple sclerosis [79], among several other crucial functions in the area of medical treatments.

The synthesis and applications of peptides are gaining increasing popularity as a result of the developments in biotechnology and bioengineering areas and for a number of research purposes including cancer diagnosis and treatment, antibiotic drug development, epitope mapping, production of antibodies, and vaccine design [49]. The use of synthetic peptides approved by the health authorities for vaccine, for cancer, and in drug delivery systems is increasing with these developments.

In the struggle for health costs control, the huge cost of biological products, including mAbs and peptides, is an issue that has been explored and discussed extensively [38].

The production of biopharmaceuticals can be divided into two main steps: the Upstream processing (UPS) part—the initial stage of a bioprocess—mainly comprising the bioreaction in the case of mAbs and solid-phase synthesis in the case of synthetic peptides, up to the stage where the biomolecules of interest are produced, and the Downstream processing (DSP) part, where the (bio)reaction bulk is processed to meet the purity and quality requirements. For years, the former received much more investments to development of production technologies.

The DSP has a majority share in the total cost of manufacturing biopharmaceuticals, mainly due to the presence of chromatographic processes in some of its stages [229]. The predominant obstacles faced by the production of new bioproducts include cost reduction, through improving process economics and efficiency, and meeting the quality criteria for Food and Drug Administration (FDA) approval, which have been increasingly demanding [229]. Because of that, the biopharmaceutical economy started to demand an evolution in DSP, in order to reduce the costs of the production process while aiming, at the same time, to develop more efficient equipment with respect to productivity, recovery, yield, ease of handling and automation, and qualified products in terms of purity.

Liquid Chromatography (LC) is currently the core technique for purification of biopharmaceuticals, and its use is often integrated vertically within the DSP strategy, as it easily fits into the early capture stage as well as into the final purification phase.

Single-column batch chromatography, which because of its simplicity is routinely used by industry, isolates the pure fraction of the product peak. In this process purity is achieved at the expense of yield because the impure side fractions, containing valuable product, must be discarded.

Multicolumn continuous chromatography, whose most efficient implementation is based on the Simulated Moving Bed (SMB) concept, captures the side fractions by internal recycling until the entire product has been extracted while new feed and fresh eluent (or desorbent) are continuously or cyclically injected. This not only gives significantly higher yields of purer product, but also enables to process more feed and thereby increase overall throughput.

A SMB unit typically consists of a circular train of chromatographic columns divided into a number of sections (the standard configuration uses four sections). A section or zone is defined as one or more columns connected in series without any side streams in between; sections are separated by inlet and/or outlet streams. For example, the standard four-zone SMB has two inlet streams—fresh feed and fresh eluent (or desorbent)—and two outlets—raffinate and extract. Section I is contained between the eluent inlet and the extract outlet; section II is located between the extract outlet and the feed inlet; section III is placed between the feed inlet and the raffinate outlet; and section IV is located between the raffinate outlet and the eluent inlet.

There are already several published works on SMB processes with less than four sections, such as three [230, 281, 284] and two [21, 128, 129, 160, 227, 228] sections. Around 2003–2004 Abunasser and Wankat [6, 7] proposed a one-column SMB analog,

but their system did not fully exploited the analogy with the multicolumn system.

In 2005, a new idea of mimicking the operation of continuous multicolumn chromatography with a single column was put forward [17, 176]. The concept was called "one-column analog of continuous chromatography." This single-column chromatograph crave to imitate the operation of the multicolumn process with the same specific productivity (feed processed per unit time per resin volume) or, equivalently, absolute productivity (feed processed per unit time) divided by the number of columns. However, very little has been raised about this idea, particularly from the viewpoint of experimental realization.

Working with the limiting case of one-column chromatography is advantageous because only one column has to be (re)packed, switching from one mixture to another would be easier and take less time than with a multicolumn system, less equipment is involved and the pressure drop and solvent consumption are reduced.

Thus, in an effort to produce high-quality biopharmaceuticals at a lower cost and using a simpler set-up, the main objective of this PhD thesis is to develop a new chromatographic platform based on the "one-column analog of continuous chromatography" concept: a novel single-column device that mimics the operation of continuous multicolumn chromatography through ingenious management and recycling of mixed fractions, reaching values of purity and recovery equal to or greater than multicolumn systems.

1.2 Objective and Justification

The main aim of this work is to develop and describe the most efficient way of mimicking the behavior and performance of continuous multicolumn chromatography with just a single-column apparatus. In order to achieve this, four specific objectives were traced:

- To establish the conceptual design of set-up, its mathematical model and assemble the laboratory prototype;
- To perform experimental validation, mimicking an already validated multicolumn system;
- To optimize the set-up using 3D printing technology;
- To apply the newly-developed system to another case study aiming at comparing the results with a different multicolumn chromatographic system.

The work plan was divided into four steps according to the specific objectives outlined.

The first task consisted of the conceptual design of the new chromatographic process, the mathematical description of its time-dependent behavior and performance, and construction of a laboratory prototype.

Reducing the number of chromatographic columns in a LC process is of intense interest in biopharmaceutical DSP, due to the reduction of costs and simplification of the production platform. Based on the approach proposed in 2005 [176] by the research group in which this project was developed, the idea of a single-column chromatographic system was explored by experimentally realizing a recycle device with a moving piston, to be implemented in line with the chromatographic column, so that the mixed fractions leaving the column can be directed to the recycle device. The latter has the function of collecting, storing, and re-injecting the mixed fractions with a delay in time, in which the fluid outlet maintains the same order of the piston input. The piston is expected to achieve a dispersive plug-flow behavior therein.

For reasons of efficiency, simplicity, and cost, the laboratory prototype should be as compact as possible, with a small number of equipment involved, with the challenge of minimizing the extra volumes in the system and operating with optimal pressure values. The possibility of automation brings agility to the operation, and online monitoring is crucial for the development of modern techniques in the competitive biopharmaceutical production market.

The second specific objective, which served to guide the second stage of the thesis, was the validation of the laboratory prototype. For this purpose, the laboratory prototype was tested on the binary separation of nucleosides by reversed-phase chromatography under linear adsorption conditions in an open-loop configuration. These experimental considerations were taken from literature [228] as a convenient model separation problem. The experimental results were compared with simulations, performed in the dynamic process simulation software gPROMS, considering two different limiting behaviors of the moving-piston device with recycle lag: perfectly stirred tank and dispersed plug-flow. It was envisaged that each nucleoside would be recovered in a distinct fraction with a high degree of purity and recovery besides low solvent consumption, and the experimental concentration profile curve would be similar to the plug-flow simulation curve.

To bring the piston model closer to the desired one, 3D printing technology was widely approached for production of different distributor configurations for the inner workings of the piston. The most appropriate 3D form was used together with the complete system for the chromatographic separation of guanosine and uridine nucleosides.

The application of the newly developed chromatographic process to another case study is fundamental to prove its intended purpose. With this aim in mind the proposed physical realization of Single-Column Chromatography with Recycle Lag, representing the fourth stage of the thesis plan, was applied to the capture step of mAbs by affinity chromatography on Protein A (PrA) resin, as an analog of the commercial Twin-Column CaptureSMB process [29, 30], which in turn is a simplified instance of the more general Multicolumn Countercurrent Solvent Gradient Purification (MCSGP) process [155, 179, 180, 182].

This separation is considerably more complicated than that of nucleosides. mAbs and their derivatives are of increasing interest in the drug industry due to their important

application in the treatment of complex diseases. On the other hand, the capture step of mAbs from a clarified bioreaction bulk is challenging due to the presence of very similar impurities, with similar adsorption properties to the target product [253]. Besides this, PrA is an extremely expensive resin, thirty times more expensive than most ion-exchange resins [123]; this increases the manufacturing costs of mAb-derived bioproducts and thus provides a gigantic advantage to a system operated with the limiting case of only one chromatographic column.

The simulated concentration profiles were simulated in gPROMS for the new system. Also for evaluation purposes, it was aimed at attaining values of specific productivity, purity and recovery as good as those obtained with the continuous multicolumn processes discussed above.

1.3 Thesis Content

In addition to this Chapter, the contents of this thesis is as follows:

Chapter 2 Introduction

In this chapter the literature review is presented covering the main important subjects for understanding the work developed in this thesis. The main topics covered are: *Biopharmaceutical Industry, Products and Processes*; *Chromatography*; *Continuous Multicolumn Countercurrent Chromatographic Processes*; and *Monocolumn Processes Similar to SMB*.

Chapter 3 Single-column Analog with Recycle Lag

Chapter 3 is based on the concept of a single-column analog that mimics Continuous Multicolumn Chromatography, developed in 2005 by the research group of Prof. Paulo Mota (same group in which this thesis is inserted), and proposes the conceptual design for its prototype, the corresponding mathematical model, as well as the conditions for assembly of the laboratory prototype.

Chapter 4 Separation of Nucleosides by Reversed-phase

This chapter, as well as the ones that follow, are structured as *Introduction and Objectives*, wherein it is expressed a brief approach on the main subject and the objective of the work in question; *Materials and Methods*; *Results and Discussions*; and, finally, *Conclusions*.

After construction of the laboratory prototype, this chapter aims to validate the apparatus created and assembled. For this purpose, the binary separation of uridine and guanosine nucleosides by reversed-phase, originally processed by semi-continuous two-column chromatography in open-loop configuration, is used as reference. This process is then mimicked by the single-column system. Before the experiments, the characterization of the stationary phase, adsorption isotherms,

column dynamic behaviour and recycle device is made. The experimental results of this case study for each mode of operation are compared with the simulated results generated through gPROMS software.

Chapter 5 Improvements of Plug-flow Operation in the Recycle Device

Chapter 5 is responsible for presenting new fluid distributor configurations—pieces that compose part of the recycle device in the new set-up, printed using two different 3D technologies: Stereolithography (SLA) and Fused Deposition Modeling (FDM). The fluid concentration profile is analyzed for each printed configuration and the one with the best result is used to reproduce the nucleosides separation experiments.

Chapter 6 mAb Capture on Protein A

Still in order to prove the efficacy of the single-column system created within this thesis, in chapter 6 the single-column system is applied to another case study that uses a more complicated separation than the case of nucleosides: the purification of a monoclonal antibody, mimicking the commercial Twin-Column CaptureSMB process. The simulated results are compared with the simulations in gPROMS for the Twin-Column system.

Chapter 7 Final Considerations and Perspectives

This final chapter presents an overview of the main conclusions of the work developed in the thesis and suggestions for future research that can still be approached for the developed chromatographic system.

Chapter 2

Introduction

2.1 Biopharmaceutical Industry, Products and Processes

2.1.1 Biopharma Market Overview

The Biopharma sector is the leading growth sector within the pharmaceutical industry, accounting for about 40% of overall pharmaceutical market. This sector has been experiencing rapid growth of 15% per year, with global revenues now reaching 200 billion dollars annually [157].

Rapid growth is happening all over the world and is accompanied by fierce competition. Developing countries are the fastest growing in the manufacture and marketing of biopharmaceuticals. China and India are some of the countries that have been following this wave of growth in the biopharmaceutical area, betting on mammalian cell culture platforms, recombinant proteins and even monoclonal antibodies. Although these potential countries are developing countries, each has approximately 10–11% of the total liters capacity of bioreactors across the globe, indicating that they are gaining maturity in their technical expertise [157]. Vietnam and Cuba are some of the other developing countries that are starting to gain space in the manufacturing process of this sector.

Despite this, the United States and Europe are still the largest facility holders, with the United States dominating 35.3% and Europe 30.2% of total concentration of global biopharmaceutical manufacturing, while China and India add up a little more than 19% of biopharmaceutical production worldwide [214].

2.1.2 Challenges and Opportunities

Biopharmaceutical has long been considered one of the most sophisticated and elegant gains of modern science. Its impressive potential for market growth brings opportunities

and challenges, driving this industry for the exploration of Research and Development (R&D) work objectifying new strategies, technologies and operational approaches. R&D refers to creative investigative activities driven by an enterprise for innovation, introduction and improvement of its products and procedures, with the purpose of developing new knowledges or improving existing ones.

From the opportunity of development of ever more complex and efficient materials for healthcare application, arises the capability of biopharmaceuticals to treat previously intractable diseases. As a consequence, the greater number of diseases with treatment or complete cure leads to an increase in the acceptance and reliability of biopharmaceuticals by the population, in addition to increased marked demand, impelling the growth of this market.

The limitations of this glamorous industry are presented in different forms. The facilities are costly to manage, with processes having long duration, low yields, expensive raw materials and a highly qualified team to operate them due to complexity of manage these set-ups. All of this results in very costly installations. Large-scale biotechnology manufacturing facilities, for example, require $200 million to $500 million to build, and can take 4–5 years to build, compared to the cost of small molecule scale, ranging $30 million–$100 million [198].

In addition, and not least, the bioprocessing industry has rigid regulators involved in most decisions to ensure high-end bioproducts. As a consequence, changes occur slowly. Maybe these are some reasons companies prefer to focus on one or a few platforms to apply to as many products as possible.

The FDA[1] is the agency responsible for protecting the public health by ensuring that human and veterinary drugs and biological products intended for human use are safe and effective. New drugs and biologics must receive FDA approval before companies can market them. Some examples of biological products are therapeutic proteins, vaccines and cellular therapies. Manufacturers must prove that they are able to produce the drug in accordance with federal quality standards. The FDA does not test or develop the products, its experts analyse the results of laboratory clinical trials performed by the manufacturers. If the agency grants approval it means that the known risks of the product to the intended use are outweighed by their benefits [75].

The biopharmaceutical field has changed a lot over the last fifteen years. In the early 2000s, biopharmaceutical facilities operated at elevated levels of capacity utilization rates due to high demand and tight production capacity. The so-called “capacity crunch” was a major concern of this branch of industry in face of significant capacity shortages. In 2003, the capacity utilization rate was 79% overall compared with up to 63% overall in 2018 [217]. It is much healthier to operate at a lower capacity utilization rate, but still higher than 50%, than to operate at very big rates. When this rate approaches or exceeds

[1] FDA is an agency within the U.S. Department of Health and Human Services. The core functions of the agency are to oversee Medical Products and Tobacco, Foods and Veterinary Medicine, Global Regulatory Operations and Policy, and Operations. For more information please visit: `https://www.fda.gov`.

80%, process facilities tend to become a bottleneck and bioprocessing is limited.

The rigid rules of quality that companies must comply result in a meticulous production process, in which the purity of the material of interest is one of the factors of extreme importance. Since 2018, the main bottleneck factor has been "facility constraints" [217], highlighting the fact that a new phase of industry capacity expansion is emerging. Downstream operations are where most bottlenecks now occur, which requires increasing research for the development of better continuous and better overall downstream purification technologies.

Innovative technologies come and go over the years. An example of this is transgenic animals, for *in-vivo* manufacture of recombinant proteins, which is, at present, an relatively rejected bioprocess area. This same area was considered the apex of interest in the early 2000s. Recently, on the other hand, cellular and gene therapies, involving even both technologies (genetically-modified cells), have been presented as the next big topic for biopharmaceutical manufacturing [217]. Cell therapy Provenge, for example, is used for the treatment of cancer, while gene therapies offers even more magnificent promises of regenerative medicine and disease remission [198].

2.1.3 Bioproducts

Biopharmaceuticals are only part of the pharmaceutical industry products. In the 1980s, the term "biopharmaceuticals" appeared to refer to human health products generated through modern biological methods using engineered organisms, distinguishing these products from traditional biological products extracted directly from natural biological sources. [102].

Biopharmaceuticals are complex molecular structures with high molecular weight, 200- to 1000- fold higher than traditional medicines; moreover, because of their size and sensitivity, they are primarily absorbed by the lymphatic system. While the chemical and natural medicines have low molecular weight and simple structure, because they are made up of simple molecules with well-defined physical chemical properties. These molecules from chemical synthesis are easily absorbed by the blood through the capillaries [12, 220].

A wide range of biopharmaceutical products with different application functions are already part of healthcare, and with each passing year the number of new products only increases. Currently, biopharmaceuticals account for 60% of the new drugs approved by the FDA [28].

The composition of biopharmaceuticals can be grouped into different classes according to their nature (Figure 2.1), being nucleic acids, peptides, or proteins [270]. Cell-based systems can also be contemplated as biopharmaceuticals for applications in cell therapy [235]. Biopharmaceutical products include, but are not limited to, purified proteins, recombinant proteins, natural and synthetic peptides, recombinant hormones, recombinant enzymes, growth factors, cell and gene therapies, vaccines and monoclonal

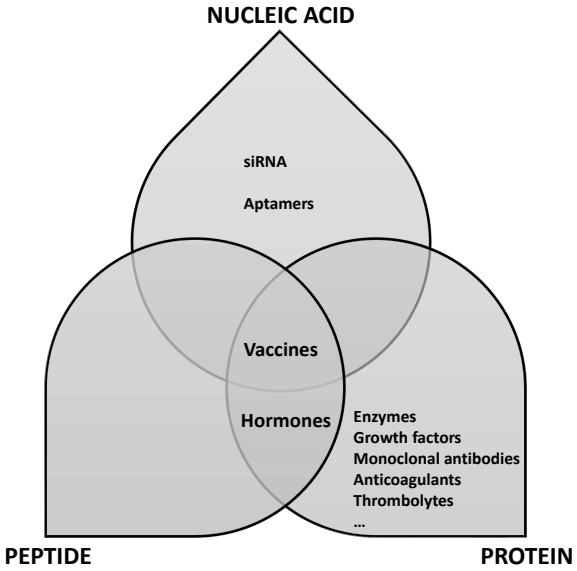

Figure 2.1: Diagram of biopharmaceuticals classes divided into groups according to their nature. Within nucleic acids there are siRNAs and aptamers [28]. In the protein group there are the enzymes, growth factors, monoclonal antibodies, anticoagulants, among others. Hormones can be divided between peptides or proteins. Vaccines can be divided into all groups.

antibodies.

Complex biomolecules undergo a purification process before usage in patients, with specific physicochemical properties and biological activity. Growth factors, for example, are used to treat cardiovascular diseases, or for bone tissue regeneration at clinical level [28].

Many of the molecules used to prevent diseases are inserted in the vaccines group. Prophylactic vaccines are made from peptides, DNA, or recombinant proteins [213]. Hepatitis B surface antigen, for example, is a protein-based vaccine used against hepatitis B [277].

Another important class of biopharmaceuticals are the therapeutic proteins, that have been targeting a great diversity of diseases for 30 years, representing one of the most promising drug families [191]. This variety of therapeutic proteins is dominated by mAbs [267]. Therefore, recombinant therapeutic proteins, including mAbs, constitute the most mature class of biopharmaceuticals, with the highest number of approved products. From 2003 to 2017, the number of recombinant therapeutics approved by FDA increased by approximately 400% [215, 216]. FDA set a record in 2017 for the number and percentage of approved biopharmaceuticals being recombinant-based, there were 31 approvals, representing 93% of the total biopharmaceutical products approved. In 2003, there were 18 approvals and 69% for recombinant products. For the production of therapeutic proteins, the most common expression system have been and continues to be Chinese hamster ovary (CHO) cells [271].

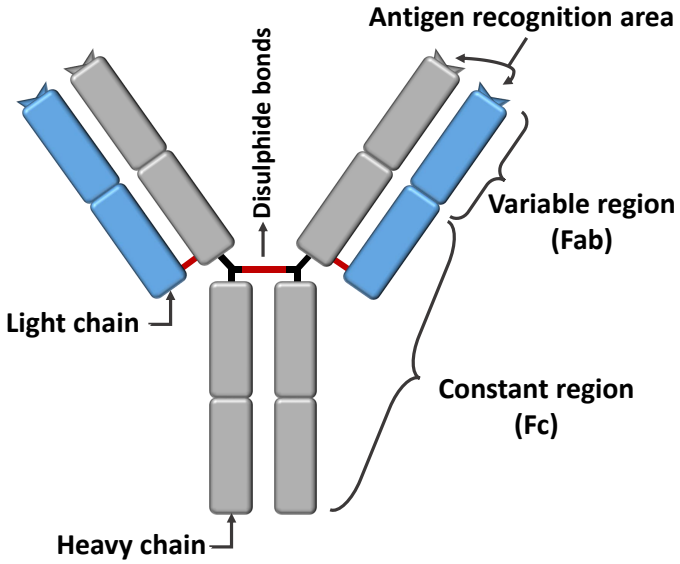

Figure 2.2: Monoclonal antibody structure. An immunoglobulin protein consists of two proteins, the light and heavy chains, linked through disulphide bonds. Each chain has a constant region(Fc) and a variable region(Fab). The antigen-recognizing part is located in the variable region.

2.1.3.1 Monoclonal Antibodies

Immune processes are divided into two types: adaptive and innate [164, 203]. While innate immunity recognizes targets common in any micro-organism structure, such as double-stranded DNA, adaptive immunity recognizes an antigen by its specific epitope. An epitope is a segment recognized by the T-cells and B-cells, the principal cells of the adaptive immune system. Both of these receptors are able to recognize a specific target of a micro-organism, usually a segment of an extracellular protein.

mAbs are complex molecules, produced by B-cells, that are specific to epitopes on antigens. Once the cells are labelled by the antibodies, the latter conduct other cells of the immune system to destroy those tagged substances [189]. Because of the ability to recognize specific molecules present on the surface of the cell or in organism fluids, mAbs affect the functions of this target cell without damage the rest of body's cells.

mAbs are made of polypeptide chains and have high molecular weight. They are Y-shaped proteins and are composed of a fixed and a variable part (Figure 2.2). It is the variable region that characterizes antibody specificity and, therefore, where antigen-antibody interactions occur. The constant region is the one that will determine which of the 5 existing classes the antibody belongs to: immunoglobulin (Ig)M, IgD, IgG, IgA, or IgE.

mAbs have revolutionized the field of research and medicine, due to its ability to be produced in large quantity and its high specificity. These molecules are one of the most structurally and functionally complex classes among protein-based biopharmaceuticals.

Mostly used to prevent and treat cancer (e.g., breast, colorectal and gastric cancers),

infectious, inflammatory, and autoimmune diseases (e.g., rheumatoid arthritis, multiple sclerosis), and transplant rejection, mAbs can be applied in multiple areas of medicine. In this way, they can identify or destroy tumor cells, activate or reduce physiological functions, stimulate or turn off receptors, stop pathological processes, and inactivate enzymes [189].

In addition, antibodies do not have valuable functions only for clinical utilization, but are also widely used for scientific research tools, such as Enzyme-linked immunosorbent assay (ELISA) [256], Western blot (WB) [39] and flow cytometry techniques; and acting as markers for diagnostic tests, being used, for example, to quantify a desired specific protein found in an immersion medium.

The commercialization of the first therapeutic mAb product occurred in 1986, the Orthoclone OKT3, approved for use in the prevention of kidney transplant rejection [71]. Since then, the commercialization of this class of biopharmaceuticals has only been growing. Therapeutic drugs based on monoclonal antibodies are the class of biotherapeutics most produced today. The annual production demanded by the marked for an approved mAb is 10–100 kilograms, using bioreactor batch sizes up to 20,000 liters [187].

By 2016, the FDA had already approved more than 50 mAbs for the treatment of a variety diseases, and another 50 were in phase three clinical trials [219]. Of these products already approved and manufactured, only three are produced in *E.coli* while all others are produced in mammalian cells [71].

The first approved biosimilar mAbs in Europe, Inflectra and Remsima [71], are included in the list of approved mAbs. They are biosimilar versions of the blockbuster mAb Remicade. A single supplier, Celltrion, is responsible for the manufacture of the bulk mAb used for the production of these biosimilars, although they are considered two different products, since the final drug for each is manufactured by a separate entity and two different manufactures are responsible by the final batch release of the products. In addition, each product has undergone separate European Marketing Authorization Applications.

The brilliant success of this class of drugs comes at a price. In 2013, global sales revenue for all mAb products accounted for approximately half of total sales of biopharmaceuticals, reaching close to $75 billion [71].

In addition to the continued growth in sales of mAb products already approved, there are still more than 300 products from this class in development [208], with the potential to come to approval, leading to the belief that not only sales of mAs will continue to grow in the coming years, but will also boost sales of biopharmaceutical products in general.

About three to six new mAb products are approved each year in Europe and/or the United States. Along these lines, approximately 70 mAb products are expected to be on the market by 2020, with worldwide sales approaching $125 billion [71, 233].

Approximately 26% of mAb products entering Phase II human clinical trials in recent years will reach market approval with an average time of seven years between the commencement of Phase II clinical trials until approval [63, 205], based on the review of the

historical success and turnover rates (i.e., time taken for a product to change from one stage of development to another).

Global sales of mAbs have been growing faster than other biopharmaceuticals in recent years, since their approval rate is also much higher than these other products. To get an idea, from 2008 to 2013 the growth in sales of mAbs jumped from $39 billion to $75 billion, an increase of 90% [71]. On the other hand, sales of the other recombinant protein therapies increased only 26% over the same period.

There are some factors that contribute to the growth of the mAb market. The emergence of new targets, from the rapid advancement of our understanding of disease at the molecular level, is one of the drivers of continued interest in developing new antibody products. The fastest route to a clinical proof-of-concept to activate, inhibit or block these new targets is usually provided by the mAb product. The risk of unexpected safety problems in human clinical trials is lower than in other types of therapeutic products, since their production uses efficient platforms and the antibodies are generally well tolerated and highly specific. Thus, mAbs are almost always the first product candidates to reach the stage of clinical trials for these new targets. And then, if proof-of-concept of these products succeed, they are already advanced to commercialization, presenting the "first-to-market" advantage [71].

The amplification of the world pharmaceutical market, due to the increase and aging of the world population and the rising standard of living in emerging markets, is also an important factor driving sales of mAbs [168].

Furthermore, the need for large-scale and cost-effective supply requires the market to develop new technologies for the production of mAbs, allowing for a noticeable improvement in process efficiency and reducing actual manufacturing costs [44, 92, 267]. As a consequence, this represents a great benefit to society as these products have the increasing opportunity to be inserted in more cost-sensitive markets.

2.1.4 Bioprocess Flow

Biopharmaceutical processes must be integrated processes designed to provide the quantity and quality of the required product utilizing as few steps as possible and in the most cost effective manner. Modern bioprocesses are diverse, with specialized designs, to suit different types of consumers and their products. The production process of biotech products, with application in the pharmaceutical field, is divided into two main steps: upstream (USP) and downstream (DSP) processing as demonstrated in Figure 2.3.

2.1.4.1 Upstream Processing

UPS is the initial phase of the bioprocess, where cells grow within bioreactors until they reach the desired density [188]. As shown in Figure 2.3, this step contains all the tasks related to the development of the inoculum (thawed cells introduced to the media), such as preparation of the media, cell culture, and bioreactor bulk collection. Thus, the

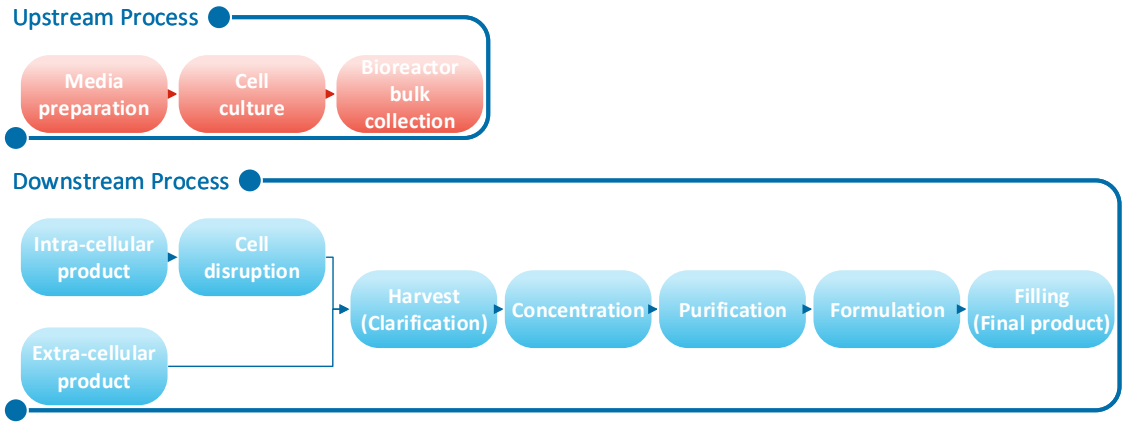

Figure 2.3: Simplified Bioprocess Flow diagram. UPS covers the development stages of the inoculum, represented by preparation of the medium, cell culture, and collection of the bioreaction bulk. The DSP covers all the steps for recovery and purification of the target product and subsequent shipment to the market, containing the stages of solid-liquid separation, concentration, purification, formulation and filling. The stages of a bioprocess may vary according to the host organism used and the desired product.

main purpose of UPS is to promote the environment necessary for cells to produce the biomolecule of interest.

The media is prepared by ensuring proper nutrition for the cells to grow and express the target product. Before introducing the cells, it is necessary to make sure the media is homogenous. In addition, the media is subjected to measurement of some parameters, such as pH, ions concentration (conductivity), glucose level and particle concentration measurement (osmolality) to assure the perfect cellular development.

The fermentation process/cell culture is monitored and its end is based on the quantity and quality of the product accumulated in the bioreactor. When the number of cells begins to decrease faster, i.e. when they begin to die, it is the indicator that the highest quantity of high quality product has been achieved in the bioreactor [267]. During the cell culture, gases and temperature are controlled to guarantee maximum cell growth.

After cell culture, the bulk is withdrawn from the bioreactor containing the product of interest and a diversity of other components. This target product can be excreted by the cell, being an extracellular production (usually it is the case of mammalian cells), or it can be an intracellular production (usually it happens with cells of bacteria), needing cell lysis to be able to release and then harvest the desired biomolecule [199].

2.1.4.2 Downstream Processing

DSP is an essential step in the manufacture of biopharmaceuticals, and refers to the recovery and purification of these products. The cell mass coming from the upstream is processed to meet the requirements of purity and quality (e.g. stability and activity of

the bioproduct). The main steps taken by DSP are harvest, concentration, purification, formulation and filling [187]. Because biotech products vary in size and nature, different principles of separation are required to isolate (recover) and purify the products.

Harvest is considered the transition stage between UPS and DSP. It is the primary recovery, where the cells and large debris are separated from the medium containing the target product. Centrifugation is one of the commonly used procedures for harvest, in which cells and some larger debris are separated from the mixture and are discarded, since they are the biggest components of the medium and suffer the effect of gravity more intensely than the rest of mix. Another procedure, that is applied generally in sequence, is the filtration, using size exclusion principle, to remove more debris. Harvest methods may change depending on the host organism used.

After solid-liquid separation, the clarified is concentrated by methods such as evaporation, ultrafiltration, adsorption, precipitation, among others, to reduce the volume of sample to be purified.

In sequence, the purification stage occurs and it is extremely important for bioprocesses. It has the function of removing compounds that may cause a safety risk for patients, supply risk, performance alteration of purification resins/membranes or damage/alteration of product. Therewith, the final drug must be free of incompletely expressed product, aggregates of the target product, or remnants of cell lysis. Endotoxins, host cell proteins, proteolytic enzymes, cellular DNA and other nucleic acids, virus, cell debris, lipids and proteases are some of the impurities and contaminants that affect the quality of the bioproduct [126].

To maintain the activity and stability of the product, the formulation step is applied, by concentrating the sample with removing most of the water (e.g., freeze-drying, spray drying), or crystallization by addition of salts.

Proteins are highly susceptible to loss of biological activity, so they deserve special attention in the formulation step. To prolong the life of the protein, some stabilizers are added for protein formulation, such as salts (ammonium sulfate, sodium chloride), sugars (sucrose, lactose), polyhydric alcohols (glycerol) and polymers (polyethylene glycol). The protein formulation may be in the form of dry powder, suspensions or solutions.

Lastly, in the filling phase the formulated product is packaged and sent to the market for consumers.

2.1.4.3 Processing of Monoclonal Antibody

mAbs became the dominant product class within the biopharmaceutical market and, as the biopharmaceutical industry matures, the number and types of diseases that will be treated with monoclonal antibody products will only increase. This demand for mAbs has as consequence the requirement of a significant improvement in design and optimization methods and processes for the manufacture of this type of product, not only to make the production process faster and more cost-effective for industry, but also to facilitate

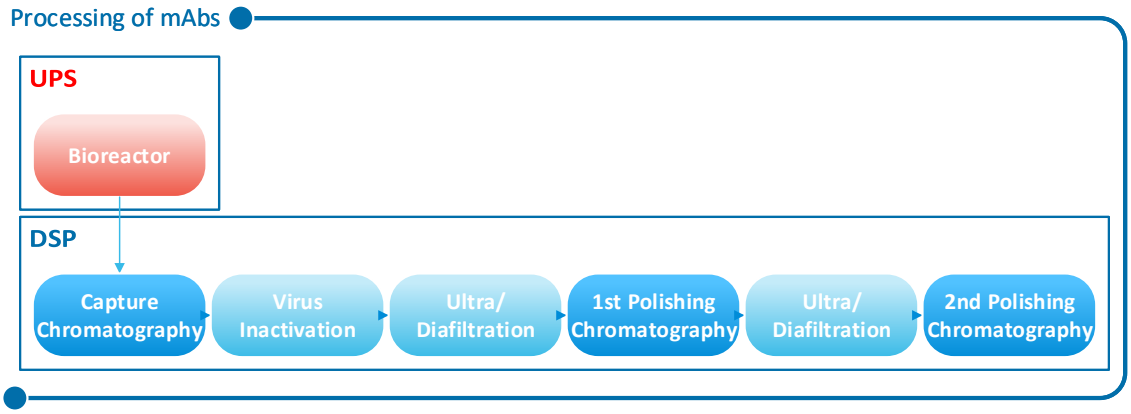

Figure 2.4: Typical integrated process for a mAb. USP usually occurs in perfusion bioreactors, whereas in DSP, purification is divided into capture and two polishing steps. Recovery is commonly performed together with a first purification by the capture chromatographic process. Purification, also called polishing steps, are generally covered by CEX chromatography (binding and elute mode) and AEX chromatography (flowthrough mode), respectively. To concentrate the solution, ultra/diafiltration procedures are repeated between different stages of the DSP. An additional step, the viral inactivation, is necessary to improve the purification. Variations may occur to the process described above.

world-wide access to the product in terms of cost-benefit in both developed and more cost-sensitive countries.

For mAb-based drug category, the most common class of biotherapeutics produced today, the conventional industrial production takes place via well-defined batch platform operations, separated into USP and DSP [87]. In the USP phase the process runs in large-scale fed-batch bioreactors, while in the DSP part the harvest and purification are performed in sub-stages through sequences of complementary chomatographic methods. Concentration steps, performed by ultrafiltration and diafiltration, may also occur more than once in DSP, interspersed with the usual chromatographic operations [44, 187]. In addition, there is a virus inactivation step [92, 267] to ensure the high level of purity and no risks for human health. The complete process schematic [123, 249] can be seen in Figure 2.4.

For the continuous production of therapeutic proteins, the USP presents two alternatives: chemostat and perfusion bioreactor [94, 151, 276], both with continuous mode of operation in terms of constant medium exchange. Their schematic setups are showed in Figure 2.5. The striking difference between the two is that the output flow in the chemostat is the same as the contents of the bioreactor, including cells, target proteins and metabolites [113], while at the perfusion set-up, a cell retention device is added, which removes only by-products from the bioreactor, which are the target proteins and metabolites, and holds the cells in, allowing process intensification and increased viable

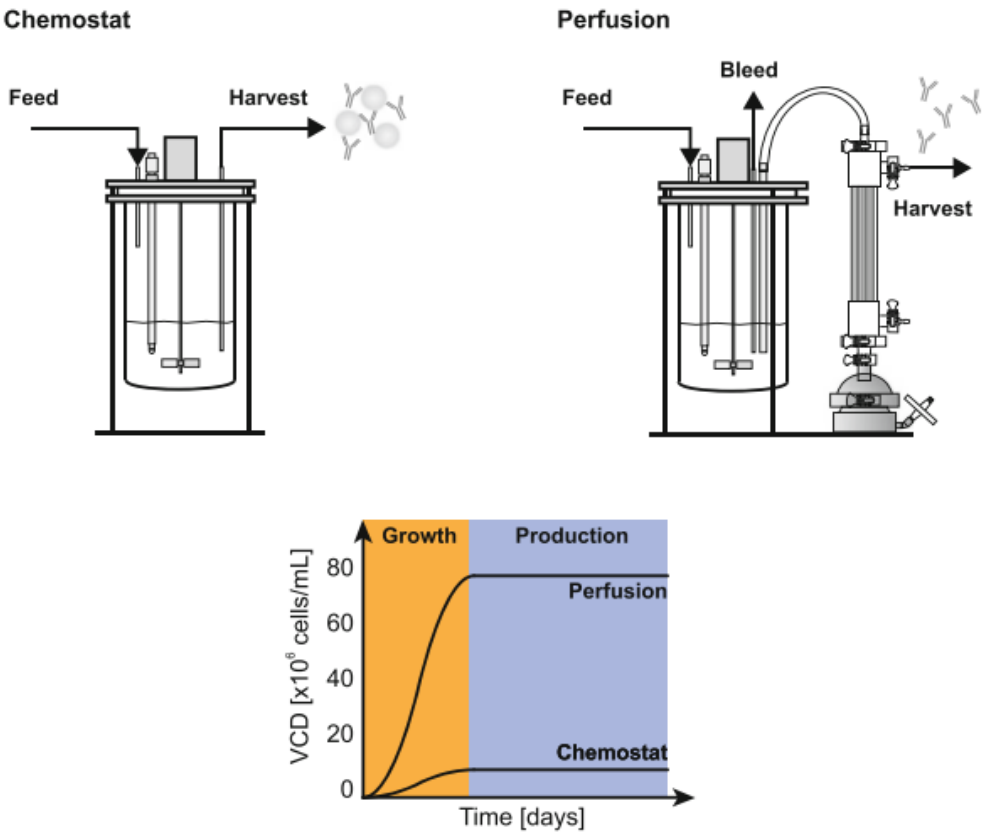

Figure 2.5: Apparatus of chemostat (left-top) and perfusion bioreactors (right-top). In the bottom, the graph compares their performance to cultures of Chinese hamster ovary (CHO) cells via viable cell density profiles. For CHO cultures, much lower viable cells densities are achieved with the chemostat than with perfusion operation, explained by the low division rate of mammalian cells. Source: [267].

cell densities. Cultures with a high rate of cell division, as typically occurs with microbial production systems, chemostat is used, while mammalian cells, which have a lower rate of cell division than the former, are applied at the perfusion setup [267].

Cell retention devices, used in the perfusion bioreactor, use the separation method based on cell size or cell density, and may be filter devices, centrifuges, gravity settlers to acoustic wave separators [51, 152, 268]. However, the devices in focus nowadays employ tangential flow, which are the Alternating tangential flow (ATF) filtration and Tangential flow filtration (TFF) systems, both using hollow fiber filter modules for cell retention. When comparing the two systems, a comparative study [57] showed that TFF device could achieve higher viable cell density than ATF. In contrast, the ATF operation reduces the probability of filter-fouling, as it induces a self-cleaning of the hollow fibers [40]. In another research [135] it was reported that the ATF device has significantly lower maximum shear stress, but on the other hand, almost no protein retention compared to the TFF.

An analysis of suitable cell specific perfusion rates is required for the appropriate

design and development of the mammalian cell perfusion process. A robust and stable operating process is the key to better integration with downstream processing for the development of an end-to-end integrated production stream, and these conditions are guaranteed by defining suitable operating set points (flow rates, viable cell density, and medium composition) [267].

The mAbs are in mixtures of different molecules themselves, exhibiting a wide heterogeneity, due to degradation processes and post-translational modifications. So there are different glycoforms, lysine variants, deamidated variants, etc. mAb purification is a challenging task, due to the presence of impurities very similar to the target product and consequently with very similar adsorption properties [253]. Besides that, their purification is generically characterized by a center-cut separation, in which the pure fraction of mAbs is eluted between two others composed by weakly adsorbing impurities (W) and strongly adsorbing impurities (S). Thus, improved separation methods are required to achieve good purity and yield in the purification process [178].

In DSP the primary separation of bioproduct and cellular debris from the bulk of the bioreactor occurs at the capture, or recovery stage, usually performed on protein A resin [267]. This stage is also a purification phase. The aim is to isolate the product by removing all microparticles and colloidal materials, in addition to removing most of the water, medium growth supplements, solutes from small molecules, proteolytic enzymes and other degradative elements by concentrating the product. In short, the goal is to isolate, concentrate and stabilize the target bioproducts [88]. Depending on the method used for capture, the recovery phase can reach 95% purity [187].

Then, mAbs undergo a first polishing step, or intermediate purification, to remove most of the bulk contaminants (impurities) [88], such as host cell proteins and accidental viruses, even as other contaminants from other materials of the process, for example, leached ligand from the capture resin (generally free protein A) which may be bound or co-eluted with the desired therapeutic.

Finally, a second polishing step, or final purification, is employed to remove trace contaminants and impurities (such as inactive or unwanted isoforms) or closely related substances (fragments or other chemical modifications of the bioproduct, like improperly combined or unfolded polypeptide chains) to achieve final purity [88]. Although this stage is a more meticulous phase, both the intermediate and final polishing phases assist in the removal of viruses, accidental or endogenous, and remaining traces of endotoxins, DNA and host cell proteins.

In brief, while capture is used to concentrate the antibody from the sample taken from the bioreactor outlet employing Protein A affinity chromatography using pH step elution with the positive effect of significantly decreasing the levels of process-related impurities (e.g., DNA), the two polishing phases aim at the removal of process- and product-related impurities (e.g., aggregates) using two chromatographic methods such as Cation exchange (CEX) and Anion exchange (AEX) [267]. There are two types of purification mode: bind/elute mode, where the target product as it passes through the

stationary phase is then retained by the medium, and the flow-through mode, in which the target product flows through the medium and the impurities are retained by the stationary phase. In the mAb case CEX acts in bind/elute mode, whereas AEX acts in flow-through mode [123].

An alternative method for the mAb capture step has been extensively studied and successfully applied in recent years—the Multicolumn Countercurrent Solvent Gradient Purification (MCSGP) [155, 179, 180, 182]. This process allows the separation of charge variants of the mAb with high yield and purity using a cost-effective cation exchange adsorbent. Using MCSGP, the specific activity of the drug may be increased by removing less active charge variants [178].

Yields and purities higher than 90% can be obtained with this procedure applied for mAb purification [180, 250], and comparing to batch operation for the same purity values, MCSGP achieves considerably higher yields [179]. Steinebach et al. [250] has recently shown, for example, that for a purity of 92% in a procedure for isolation of the main charge isoform of a mAb, a two-column MCSGP process (with 5 cm length each) achieved 94% yield after 5 cycles, while batch operation under the same parameters and using a 5 cm column obtained 50% of yield, while with a 10 cm column 85% yield was reached.

At the conventional mAb producing process (protein A affinity chromatography and two polishing steps, cation- and anion-exchange chromatography), charge variants of the mAb remain in the final product. Due to the increasingly stringent requirements related to product heterogeneity imposed by regulatory authorities, the MCSGP has gained notoriety due to its ability to remove these variants in a preparative production with small and economically viable units [253].

In addition, although protein A affinity chromatography, applied in the mAbs capture phase, produces mAbs with high yield and purity, and with short process development times, the high cost of the affinity resin dominates the overall costs of downstream processing. Thus, although the CEX stationary phase is less selective than protein A, this disadvantage is outweighed by a higher process efficiency. This increased efficiency of the MCSGP is attributable to the countercurrent movement of the stationary phase with the mobile phase and the internal recycle [180].

On the other hand, the use of cost-effective non-affinity resins in batch chromatography provides a higher Host cell protein (HCP) content in the final product. Therefore, the use of the continuous MCSGP process is favored, since it bypasses this drawback of conventional non-affinity batch chromatography, while using a much cheaper resin than Protein A. Ströhlein et al. [253] showed that MCSGP is very competitive with the capture step using protein A, achieving yield of 95%, and HCP content in the eluted product stream between 146-625 ppm, whereas at protein A capture phase is in the order of about 2000 ppm. To achieve the final specifications, a polishing step is generally added to the process using a multimodal resin.

Accordingly, for mAb purification a two-step system consisting of cation-exchange MCSGP capture step and multimodal batch chromatography polishing step may replace

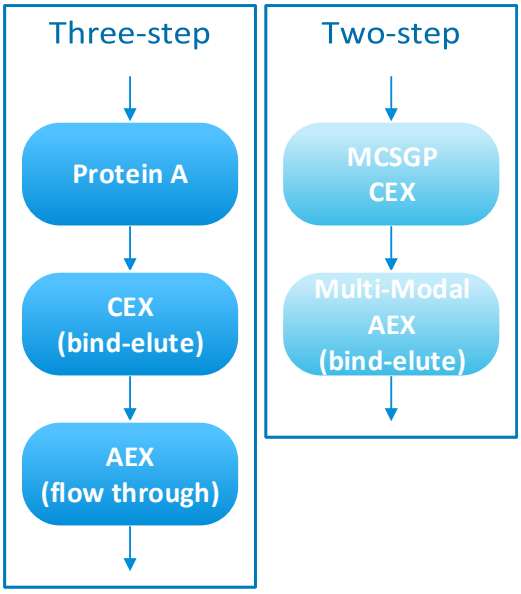

Figure 2.6: Schematic of three-step and two-step processes for monoclonal antibodies purification. The conventional sequence of chromatography steps is composed by Protein A affinity chromatography as capture phase and, as polishing phases, the cation-exchange chromatography in bind-elute mode and anion-exchange chromatography in flow through mode. The developed two-step downstream processing has the cation-exchange MCSGP process as capture step, and a multi-modal chromatography using AEX in bind-elute mode as polishing step.

the state-of-the-art three-step scheme which includes Protein A, cation-exchange, and anion-exchange, as drawn in Figure 2.6

In another study, Müller-Späth et al. [180] in collaboration with Merk-Serono[2] made an economic comparison between the two-step process and the batch protein A-based three-step process for mAb purification. The calculations took into consideration material costs, overhead costs and capital costs. As result, the case study manifested that downstream costs of the MCSGP-based process were 25 % lower than the protein A-based process, which was predominantly caused by material costs that were 50% lower. The study also showed that the cost gap between the two processes increases as the mAb titers increase, which the latter appears as a current trend in upstream process development.

2.1.4.4 Upstream *versus* Downstream Processing

The challenge of the biopharmaceutical industry focuses on ensuring optimized, robust and high-yield processes with bioproducts of a high level of purity and efficacy, but with

[2]Merck Serono (EMD Serono in the United States and Canada) is a pharmaceutical company focused on biopharmaceuticals, located in Darmstadt-Germany, and a brand and division of Merck. More information at: http://www.merckserono.com .

full attention to the costs derived from the production process.

Bioprocessing lines undergo switch-overs, maintenance, installation and validation of new equipments, training of personnel and cleaning and sterilization of stainless steel facilities, requiring a necessary downtime. Recent studies show that DSP still fights to keep up with USP improvements, so downtime with upstream versus downstream equipment is normal [217].

DSP, especially purification, continues to be the productivity limiter. The manufacturing cost of therapeutic antibodies, for example, have a considerable percentage assumed by the DSP chromatographic steps [229]. This is the main reason for the growing fascination and recent technology advances in continuous purification, which can solve many downstream bottlenecks [157]. This interest has not only promoted technological advances that point to the transition from batch to continuous processing in many industrial cases, as the conversion of batch manufacturing to continuous manufacturing has already resulted in a significant intensification of the process for a variety of industries [267].

The benefits of continuous process are not few. It offers reduced equipment size, steady state operation, low cycle times, high volumetric productivity, more homogeneous product quality, and improved controllability, and, as importantly, reduced economic costs [152, 210, 272, 280].

2.2 Chromatography

2.2.1 Principle of Operation

The history of chromatography began in 1903 and since then has had an important task in several different fields [43]. Chromatography is a separation and purification technique used to isolate, enrich and separate a target compound of interest from other compounds of a sample. Therefore, chromatography is a reliable way to identify and quantify compounds and an extraordinary way to produce pure, high quality compounds [60]. In summary, the purpose of applying chromatography is to achieve satisfactory separations in an appropriate time interval.

In the chromatographic method, the complex mixture is dissolved in a fluid (mobile phase), which traverses through another material held by a porous support (stationary phase). The various components of the mixture cross the stationary phase with different migration speeds, causing the separation of these constituents. Therefore, the factor responsible for separation of the components of the mixture is the differential interactions that these components possess with two phases: the mobile phase and the stationary phase [103]. Occasional differences in the velocity of passage through the stationary phase imply in differential retention on the stationary phase, thus changing the separation [246]. To wash out a compound through a column the elution process is carried out, where a suitable solvent is injected into the column. This solvent has a stronger interaction with the component to be eluted than the interaction between the component and the

Table 2.1: Terms commonly used in liquid chromatography. Adapted from [141].

Term	Definition
Mobile phase or carrier	Solution or solvent moving through the column.
Stationary phase or adsorbent	Substance attached to a support that stays fixed inside the column.
Analyte	Complex mixture whose individual components have to be separated and analysed.
Eluent	Fluid entering the column to assist in the dragging components of interest.
Eluate	Fluid exiting the column and being collected for quantitative and qualitative analysis.
Elution	The process of washing out a compound through a column using a suitable solvent.

stationary phase. Table 2.1 shows a brief definition of the main terms used in liquid chromatography.

Figure 2.7 illustrates the functional principle of chromatography, showing an example of feed injection, in a previously packed chromatographic column, of a mixture containing two major components, A and B. The purpose of this process is to promote a binary separation. The curves inside the column show the concentration of each component as a function of the length (L) of the column at x-axis. Thus, it is noted that by placing the mixture to run through the column, constituent A has a higher velocity, and therefore crosses the column more rapidly, due to its lesser interaction with the stationary phase material (called raffinate). Accordingly, component B, which adheres more strongly to the stationary phase (called extract), travels more slowly compared to A, that has a weaker adhesion. With this, A is the first component to be collected at the output of the column. Next, component B is collected at a further fraction of the output of the column. At the end of the process, the eluate has two practically pure compounds separated and collected at different time intervals, due to their different retention times. Retention time is the amount of time a compound spends on the column after it has been injected.

The principle of separation of different constituents of the feed mixture is determined by the differential affinities, or strength of adhesion, of the various components towards the stationary and mobile phase, in which the affinity is decreed by two conditions: adsorption and solubility [141], the adsorption being the phenomenon that measures the degree and the manner in which the component attaches to the stationary phase, while solubility is the property of how well a component dissolves in the mobile phase. Thus, the higher the adsorption to the stationary phase, the slower the molecule moves through the column. On the other hand, the higher the solubility in the mobile phase, the faster the molecule moves through the column. These two factors, adsorption and solubility,

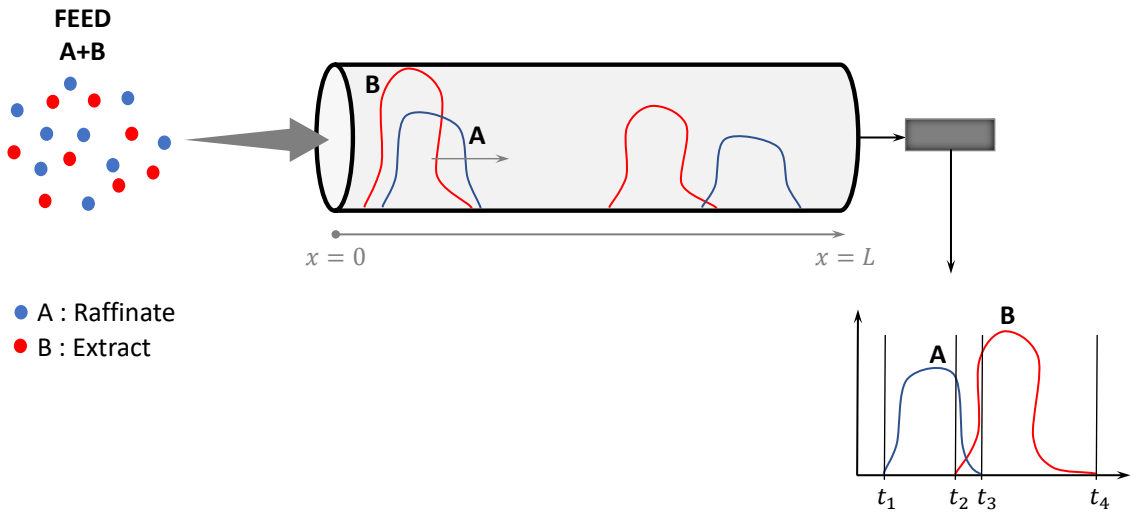

Figure 2.7: Operating principle of chromatography. A feed solution, in this case binary mixture, consisting of A and B, is injected into the chromatographic column. Concentration profiles are plotted as the compounds pass through the column length. It is possible to observe that the affinity of the B component for the stationary phase present in the column is more pronounced than the affinity of A, therefore its retention time is longer than that for A. The chromatogram shows the concentration profiles, or the detection of the separated components, at the exit of the column. Since A is the least retained component in the column, it is called raffinate, and will be the first component collected at the output of the column, while B receives the extract nomenclature and will be the last component to be presented at the chromatogram.

simultaneously interfere with the rates at which each component moves through the column and both can be manipulated by choosing the appropriate stationary and mobile phases.

Nowadays, chromatography is the main tool employed for purifying biopharmaceuticals [44], thanks to some advantages over other unit operations. To begin with, chromatography offers high separation efficiencies, enabling the use of mixtures with very similar molecular properties. A second factor is the high capacity of chromatographic adsorbents, allowing the capture of biomolecules from diluted solutions, which results in rapid product concentration or almost complete removal of contaminants present at low concentrations. Finally, chromatography can be employed in a nearly closed system and chromatographic media can be easily regenerated.

On the other hand, the restrictions imposed by the biopharmaceutical industry makes the scale-up of chromatographic processes a difficult achievement, making it a disadvantage for chromatography. However, this impasse can be solved and optimal columns for large-scale can be developed through the manipulation of engineering tools in conjunction with appropriate measurements [44]. For example, although there are still no products with such a demand, there are already adequate and viable (technically

and economically) chromatographic processes for the purification of proteins of 20 tons/year [140], showing that this unit operation is promising in view of the rapid growth of the biopharmaceuticals popularity.

Chromatography can have two different functions: preparative/production or analytical. While the purpose of preparative (or production) chromatography is the recovery of purified products, in analytical chromatography the main focus is to gain information about identification, purity and composition [206].

2.2.2 Types of Chromatography

Chromatography is attributed to a huge variety of applications, for qualitative and quantitative analysis, thanks to the several existing types of this method, defined by the mode of interaction of the various components with the mobile phase and stationary phase used. Regarding the mobile phase, the chromatography is categorized into two types, as shown in table 2.2. If the mobile phase is liquid it is called Liquid chromatography (LC), if it is gas then it is termed Gas Chromatography (GC); if the mobile phase is whole or partially a supercritical fluid then it is termed supercritical fluid chromatography.

Additionally, table 2.3 explains the main varieties of liquid chromatographic techniques commonly used, based on the specificity of the stationary phase.

2.2.2.1 Size Exclusion Chromatography (SEC)

Size Exclusion Chromatography (SEC), also called Gel Filtration (GF), is the simplest of all chromatography techniques. It is a highly flexible and multifunctional separation technique that uses as separation principle the different molecular weights as the sample passes through the resin [62]. In this method there is not any interaction, physical or chemical, between the analyte and the stationary phase, in other words, the molecules do not bind to the chromatographic resin, unlike the other types of chromatography, and consequently the composition of the buffer does not directly affect the final separation, or the resolution (i.e. the degree of separation between peaks) [109]. This implies a significant advantage of the SEC, where conditions may vary to suit the type of sample or requirements for further purification analysis or storage without altering the separation. In addition, since the composition of the buffer does not affect the final separation, SEC can be performed immediately after IEX, HIC, or AC. This technique is suitable for molecules sensitive to pH change, metal ion concentration and cofactors, or harsh environmental conditions, and can be operated within a wide temperature range (usually between 4-30 °C), covering the prerequisites for most of the experiments.

As shown in Figure 2.8, the SEC resin is constituted by a porous matrix of inert spherical particles [60]. The bed after being packed with the resin is equilibrated with buffer, which fills the pores of the matrix and the space between the particles. The liquid inside the pores, or stationary phase, is in equilibrium with the liquid (mobile phase) outside the particles. Larger molecules than the largest pores in the matrix can not enter

Table 2.2: Types of chromatography based on the differences in mobile phase.

Technique	Stationary phase	Mobile phase	Basis of separation	Specification	Applicability
Liquid Chromatography (LC)	Solid	Liquid	Polarity, size or ionic charge of the molecules, binding affinity between molecule of the analyte and molecule of the stationary phase, ...	Glass column is packed with different materials as stationary phase. The molecule of the liquid sample with lower affinity to the stationary phase leaves the column first.	Applied for thermal unstable, and non-volatile samples [204].
Gas Chromatography (GC)	Liquid or solid	Gas (inert gas like argon or helium)	Boiling point of the molecules.	Samples are volatilized and the molecule with lowest boiling point comes out of the column first. The molecule with the highest boiling point comes out of the column last.	Applied for gases, mixtures of volatile liquids and solid material [204].

Table 2.3: Principal types of Liquid Chromatography. The Mobile phase is *Liquid* and the Stationary phase is *Solid* for all chromatographies listed below.

Technique	Stationary phase	Basis of separation	Specification	Applicability
Size Exclusion Chromatography (SEC)	Microporous beads of silica or agarose.	Size	Small molecules get trapped into the adsorbent pores, while large molecules flow through the gaps between the beads and come out first.	Used to isolate components of a sample, to check the quality of the sample or to study biomolecule properties, and to decrease salt concentrations of solutions of proteins and enzymes, polysaccharides, nucleic acids, virus particles and other biological macromolecules.
Ion Exchange Chromatography (IEX)	Cationic or anionic resin.	Ionic charge of the molecules	Molecules with same resin charge flow through the column and elute out first, while molecules with opposite charge of the resin bind strongly to the resin.	Performed for separating and purifying proteins, peptides, nucleic acids, and other charged biomolecules.
Affinity Chromatography (AC)	Matrix of agarose, cellulose, dextran, etc., with a specific ligand attached.	Biorecognition (ligand specificity)	A component that is substrate for the ligand present on the matrix binds to it, while others unbound components flow through the column.	Applied to isolate pure molecules at low concentration in large sample volumes, to eliminate contaminants and to separate active biomolecules from functionally different or denatured forms. Required for purification of enzymes, hormones, antibodies, nucleic acids, and specific proteins.
Hydrophobic Interaction Chromatography (HIC)	Inert matrix of agarose, benzene, etc., with a hidrophobic ligand.	Hydrophobicity	Hydrophobic regions present on the surface of biomolecules bind to immobilized hydrophobic ligands on chromatographic matrix.	Applied for purification of proteins and other biomolecules, such as plasmid DNA. Widely used with analytical purposes, such as for monitoring and quality control, determination of folded proteins, etc.
Reversed Phase Chromatography (RPC)	Hydrophilic silica matrix covered by hydrophobic carbon chains, or a naked hydrophobic polymer matrix.	Hydrophobicity	Hydrophobic regions of biomolecules surface bind to hydrophobic carbon chains present on matrix or direct to a naked hydrophobic matrix.	Applied for purification and analysis of proteins, peptides and nucleic acids. Ideal for peptide mapping or purity checking and for polishing of peptides and nucleic acids. Still used to unleash and concentrate components of a sample.

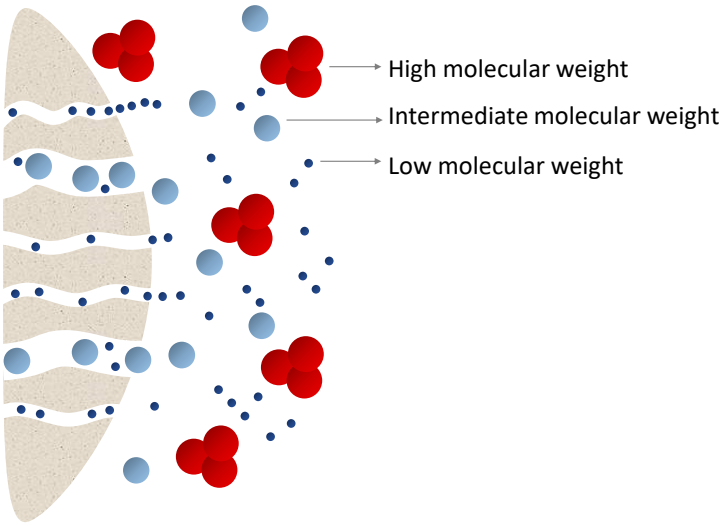

Figure 2.8: Separation principle of SEC. Biomolecules with higher size pass through the inter-particle spaces of the stationary phase and elute first, while smaller biomolecules enter inside the pores of the chromatographic media taking longer to elute.

the matrix, so they are the first molecules to exit the column having very low retention times, once they pass directly through the column. Next, the molecules with partial access to the matrix pores are eluted. Finally, the small molecules that have full access to the pores of the matrix are harvested at the exit of the column. Therefore, elution from the column occurs in decreasing order of size, and since there is no adsorption of molecules in the SEC, the elution is isocratic, i.e., the composition of the buffer remains the same during separation. However, at the end of the separation a washing step is usually proceeded using running buffer to remove molecules that may have been retained in the column at a nonideal behaviour, when interactions between the resin and the biomolecules occur, and to prepare for the next experiment.

A greater homogeneity in the distribution of the matrix grains inside the column, i.e. a smaller difference between the interparticular spaces, implies a greater uniformity with which the fluid crosses the column, and therefore increases the efficiency of this method [196].

The most regularly used SEC resins are based on agarose or silica [109], but there are also matrices from other materials such as dextran and polyacrylamide [62, 196].

Lastly, SEC is sectioned according to three main applications [109]:

i) **Preparative SEC:** Applied to isolate one or more components (such as proteins and enzymes, polysaccharides, nucleic acids, virus particles and other biological macromolecules) of a complex mixture.

ii) **Analytical SEC:** Apllied to evaluate the quality of the sample or to study the properties of a biomolecule, e.g. to determine molecular weights of the molecule. This

approach can also be used for rapid purity checks and screening.

iii) **Desalting and buffer exchange:** Approach to decrease salt concentrations. Applied to prepare samples for storage or for other chromatography techniques and assays.

2.2.2.2 Ion Exchange Chromatography (IEX)

Ion Exchange Chromatography (IEX) has as separation principle the electrostatic interactions between groups of charged biomolecules and the matrix [60]. The chromatography media has an ionic charge opposite to the biomolecule to be separated. Therefore, what characterizes the affinity between the biomolecule and the column are the ionic bonds. Since the molecules vary their charge properties, the degree of interaction with the charged matrix will be determined according to differences in overall charge, charge density, and surface charge distribution.

The chromatographic matrix can be porous or non-porous. The choice of the matrix is made by analyzing the degree of resolution, binding capacity and desired flow rate for the separation. Modern IEX media use polymer and agarose-based matrices to meet the requirements of high bonding capacity, chemical and physical stability, and to generate media with particle sizes satisfactory for a wide variety of applications [108]. The matrix surface is then replaced by functional groups. There are two types of IEX, according to the ion exchange media used, or, to be more specific, according to the functional groups that are linked to this matrix, determining the charge of the medium [131]:

i) **Anion exchange chromatography:** The matrix is positively charged, and adsorbs negatively charged biomolecules. Examples of functional groups: Quaternary ammonium (Q), Diethylaminoethyl (DEAE).

ii) **Cation exchange chromatography:** The matrix is negatively charged, and adsorbs positively charged biomolecules. Examples of functional groups: Sulfopropyl (SP), Methyl sulfonate (S).

Figure 2.9 shows the separation principle of IEX, separating biomolecules according to differences in their net surface charge. This procedure arose in 1960 and is one of the most commonly used tools for purifying proteins, peptides, nucleic acids, and other charged biomolecules. Such a technique is highly suitable for use in any of the steps of biomolecule purification (capture, intermediate purification and polishing steps), in addition, it is a mechanism used from micro-scale purification and analysis to purification of kilograms of product. This is because the IEX technique offers valuable qualities such as high resolution, group separations with high loading capacity, as well as being able to separate molecules that have only minimal differences in their charge properties, such as two proteins differing by one charged amino acid [108].

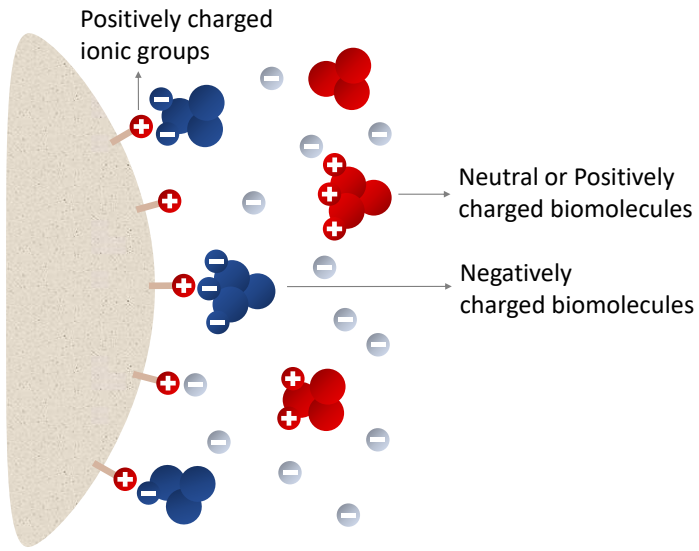

Figure 2.9: Separation principle of IEX. The adsorbent has positively (AEX) or negatively (CEX) charged functional groups. Biomolecules with opposite charge of the stationary phase bind to the functional groups, while the biomolecules with the same stationary phase charge flow through the column. In this case, AEX is illustrated.

To separate the components from the column matrix and elute out from the column, the pH or concentration of ion salts are changed, thus changing the ionic strength (ions concentration) of the buffer solution [134].

2.2.2.3 Affinity Chromatography (AC)

Affinity Chromatography (AC) uses as separation methodology the biorecognition (ligand specificity), i.e. highly specific biological interaction between the analyte molecule and the immobilized molecule present on the stationary phase (ligand) [265]. Thus, as seen in the Figure 2.10, a affinity ligand capable to make a complex with a specific biomolecule attaches to the chromatographic matrix (agarose, dextran, polyacrylamide, cellulose, etc.) to create a stationary phase [60]. Then, the specific protein present in the mobile phase binds to the stationary phase, remaining retained inside the column, while other components cross the column.

This method provides high resolution, high selectivity and high capacity. In addition, it generally exhibits very high purities and recoveries of the active substance [265]. As an advantage over other chromatography techniques, it is the only one that allows the purification of biomolecules based on their biological function and individual chemical structure. As a consequence, purities that would be time-consuming, difficult or even infeasible using other techniques can easily be performed with affinity chromatography [110].

This type of chromatography can be utilized whenever a appropriate ligand is available for the target biomolecule, and is applied to isolate existing pure molecules at low

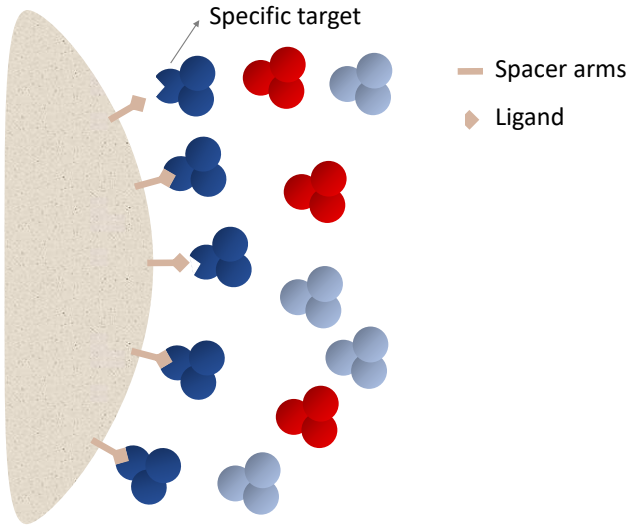

Figure 2.10: Separation principle of AC. The chromatographic media has a ligand specific to one biomolecule, and spacer arms to promote the bond between the matrix and the ligand. The specific biomolecules become attached as they pass through the column, while other biomolecules are collected at the output of the column.

concentration in large sample volumes, to eliminate contaminants and to separate active biomolecules from functionally different or denatured forms [110]. AC is required for the capture or intermediate step in a purification protocol of hormones, enzymes, nucleic acids, antibodies, and specific proteins [278], wherein the molecule(s) of interest is collected in a purified and concentrated form.

Biological interactions between the biomolecule of interest and the ligand is a consequence of Van der Waals forces, electrostatic or hydrophobic interactions, and/or hydrogen bonding [110]. The biomolecule that is attached to the ligand within the column will only be detached when the ionic strength changes, by altering the pH or adding salt solution, the polarity changes or when a competitive ligand is used [77].

2.2.2.4 Hydrophobic Interaction Chromatography (HIC)

Hydrophobic Interaction Chromatography (HIC) separates biomolecules based on the differences in their surface hydrophobicity using a reversible interaction between these biomolecules and the hydrophobic surface of the HIC stationary phase [212]. This interaction is influenced by the presence of salts in the mobile phase, in which high salt concentration in the sample increases the interaction between the hydrophobic biomolecules and the hydrophobic chromatographic medium, in contrast, the decrease of salt concentration weakens the interaction. Separation principle of this technique is demonstrated in Figure 2.11. Therefore, although this method can be used in all steps of the Capture, intermediate purification and polishing (CIPP) purification strategy [73], it is widely used as a complement to other chromatographic techniques, since the solution will already

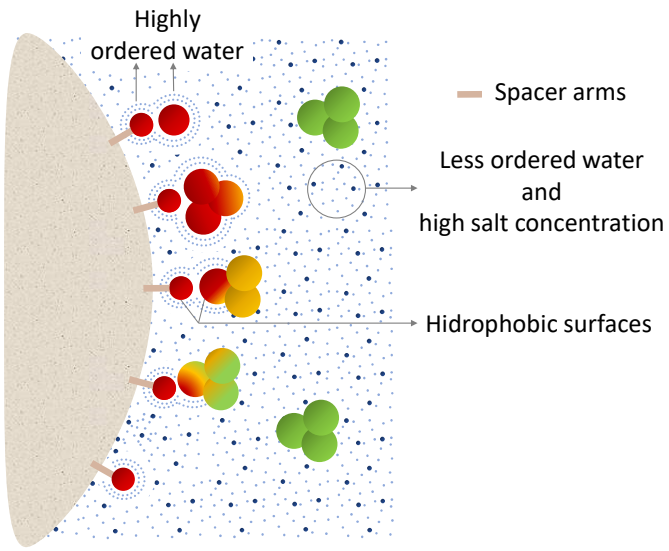

Figure 2.11: Separation principle of HIC. Hydrophobic binders are coupled to the matrix through spacer arms. Hydrophobic molecules of the analyte are retained at the stationary phase according to their level of hydrophobicity, and the presence of salts at the mobile phase favors interaction.

be at higher levels of salt concentration, and can be applied directly to the HIC column, without any or almost no additional preparation.

The elution principle uses the presence of salts in the running buffer to directly influence the hydrophobic interactions between the biomolecule and the stationary phase. At the same time that the salt concentration decreases, the interactions become weaker, so by reducing the ionic strength of the buffer the interaction is reversed and the biomolecule with the lowest level of hydrophobicity is eluted first [72]. Elution thus occurs in the order of hydrophobicity (from the less hydrophobic to the more hydrophobic biomolecule) as the concentration of salts in the buffer is gradually decreased, performed by linear gradient or step elution [170].

The stationary phase is formed by a immobilized ligand carrying alkyl or aryl groups, an inert support or spherical particles, and spacer arms to combine them [72]. The matrix material can be polystyrene/divinyl benzene, benzene, agarose, cellulose, dextran, chitosan, silica, methacrylate, etc [73, 88, 170].

Water plays an important role in this type of chromatography. Since water is a poor solvent for non-polar substances and their molecules are agglomerated (in liquid phase) through hydrogen bonds between themselves forming a highly ordered structure, water is unable to form hydrogen bonds with the hydrophobic surfaces and forms a highly organized shell around the hydrophobic ligand and the hydrophobic portion of the biomolecule surface. As thermodynamically it is favourable that the entropy (disorder between molecules) increases, the hydrophobic substances are forced to merge to decrease the extent of the water crown, leaving a greater number of water molecules dispersed

in the liquid medium, consequently increasing the entropy [170]. So the hydrophobic interaction depends more on the behaviour of the water molecules than on the direct attraction between the hydrophobic molecules [88].

HIC is therefore based on the interplay between the hydrophobicity of the stationary phase, the distribution of hydrophobic regions present on the surface of the target molecule (in the case of proteins, the hydrophobic residues are amino acids), the nature and constitution of the analyte, and the salt concentration used in the buffers [72].

This technique has the advantage of having weaker interactions in relation to the other techniques, which allows to preserve the biological activity of the biomolecule [247]. In addition, hydrophobic interactions are highly selective [73].

HIC is widely used in protein purification protocols, including monoclonal antibodies (antigen-antibody reactions), but also plays an important role in the purification of other biomolecules, such as plasmid DNA (pDNA) for gene therapy or DNA vaccines [73]. Additionally, because of its greater selectivity than in other techniques, HIC is widely performed for analytical purposes, for example, for monitoring and quality control, determination of folded proteins, separation and quantification of different isoforms or variants of proteins or pDNA, and evaluation of purity [65, 124, 153, 279].

2.2.2.5 Reversed Phase Chromatography (RPC)

Reversed Phase Chromatography (RPC) is a chromatographic technique that also uses the hydrophobicity differences of the molecules as separation principle, although it is a completely different technique from HIC. The surface of the RPC medium is more hydrophobic than the HIC medium, resulting in stronger interactions, and needing the use of non-polar elution, utilizing organic solvents (such as methanol, ethanol, propanol, acetonitrile, etc) [206], whereas the HIC adsorbent is more polar and has a less denaturing environment [88].

The nomenclature of this method comes from “normal phase chromatography” and the difference is explained as follow:

- Normal phase chromatography: The stationary phase is polar (hydrophilic) in nature and the mobile phase is non-polar (hydrophobic), consisting of organic solvents (e.g. hexane, methylene chloride);
- Reversed phase chromatography: The stationary phase is hydrophobic while the mobile phase is constituted by water/organic solvent.

In this procedure, the initial conditions are aqueous, which favors the formation of the highly structured water crown surrounding the biomolecule. Therefore, in order to obtain a "wetted"surface and avoid crown formation, a small portion of organic modifier (3-5%) [88] is usually placed in the mobile phase. The more hydrophobic molecules will bind more strongly to the chromatographic media.

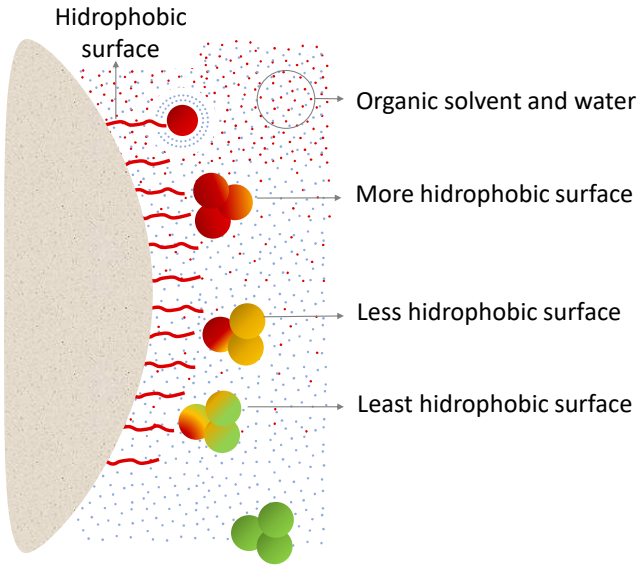

Figure 2.12: Separation principle of RPC. The interactions are also hydrophobic. However, in RPC the interactions are more hydrophobic than in HIC and, because of that, the elution uses organic solvents. As the amount of organic solvent in the column increases, biomolecules elution occurs in increasing order of hydrophobicity.

At elution, the percentage of organic solvent is increased, eluting the biomolecules in increasing order of hydrophobicity [206], as evidenced in Figure 2.12. The elution can be isocratic, but it is generally performed in gradient for reasons of reduced run time. For molecules with large differences in hydrophobicity, step elution can still be conducted.

The RPC stationary phase may be composed by a hydrophilic matrix of silica beads covered by hydrophobic carbon chains (n-alkyl or aromatic hydrocarbons) [206], or by a naked hydrophobic polymer matrix. For operations at high flow rates, it is recommended to use matrices with uniform particle size, and for high binding capacity highly porous matrices are recommended because of their large internal surface area [88].

An important feature of RPC is that it achieves extremely high-resolution separations, separating components that have a minimal difference in hydrophobicity. Because of this, this method is well suited for separation and analysis of small proteins, oligonucleotides and peptides, being required for peptide mapping or purity checking and for polishing step of peptides and nucleic acids, but it has limited utilization for the separation and characterization of large biomolecules [73]. Moreover, this technique is employed to desalt and concentrate hydrophobic components of a sample, being utilized for sample preparation and separations that require high selectivity [88].

2.2.3 Batch *versus* Continuous Chromatography

A chromatographic process can be operated in batch or continuous, being characterized according to the number of columns employed; this terminology is somewhat confusing

because some multicolumn processes can be discontinuous (that is, feed is not continuously inject into the system and/or product is not continuously collected).

In Batch Chromatography (BC) the process is designated by the use of a single column, and the injection of the feed mixture and the eluent is performed discontinuously on the same column [47]. In this system, the components are collected at the same side of the column, but at different periods of time due to the different speeds with which each component propagates (Figure 2.7). Since the component fractions are collected at the same end of the column, feed injection cannot be performed continuously. The optimization of BC consists at the discrimination of the pulse duration and the frequency with which it is injected into the column [100].

Meanwhile, in Continuous Chromatography (CC) the column is divided into a given number of smaller columns operated in series over a large number of cycles [47], with the feed being continuously or cyclically injected and the fractions of mixture are recycled internally.

Besides the various advantages achieved by a continuous system over batch operation already addressed in 2.1.4.4 (such as reduced equipment size, steady state operation, low cycle times, high volumetric productivity, more homogeneous product quality, improved controllability, and reduced economic costs), by allowing the simultaneous operation of several columns in the process, each performing different steps (i.e. feed, wash, elution, regeneration), the CC is more efficient in terms of resin and solvent usage [47]. This means that, switching from batch to continuous implies a reduction in solvent consumption, as well as an improvement in resin capacity utilization, achieved by continuously loading (overloading, in fact) the column, thus requiring less resin volume and, consequently, smaller columns, thereby saving cost and time.

The limitations faced by batch chromatography are explained by the existence of two trade-offs:

i) **Productivity vs Capacity Utilization:** In a purification process, e.g. mAbs processing, the capture is a loading or "saturation" adsorption process [248], with operating conditions rendering yields approximately of 100%, i.e. there is no mAb breakthrough [166]. For this case, the loading of bead-based stationary phase occurs under mass transfer limitation because of the low diffusivity of the mAbs, and once the flow rates increases, this becomes more evident, resulting in shallower breakthrough curves (concentration *vs* load volume). Thus, in batch mode there is a trade-off to be solved, since the high productivity originated from high loading flow rates face earlier breakthrough and therefore has the consequence of the decrease of eluate concentration and Capacity utilization (CU), which due to the high cost and limited lifetime of Protein A resins, this is a relevant parameter. To improve this factor, the loading flow rates can be reduced, which leads to a decrease in productivity. And so the trade-off between productivity and capacity utilization is in place. In order to solve it, it is expected to use countercurrent and internal recycling processes [267].

ii) **Purity vs Yield:** Unlike capture phase, the polishing phase in bind-elute mode is referred to as "elution separation" [266], in which different solutes must be resolved by step or linear gradient over the length of the column. In the case of antibody purification, the impurities elute before and after the target (mAbs), impurities being weakly and strongly adsorbed, respectively, representing a case of separation of three components. The point is that mAbs and impurities have a similar adsorptive behavior, implying low resolution (incomplete separation of chromatographic peaks), unless very low loadings and very flat gradients are chosen, which decreases the final productivity and concentration of the product. Therefore, it suggests another trade-off in batch processing, this time between purity and yield at a given productivity value [267]. With this, or a small section of the chromatrogram is collected as a high purity product, but low yield, or a large segment is extracted increasing yield but abdicating purity. This problem is repeated whenever the separation is difficult (low resolution) or if the column is not long enough.

Both trade-offs, in the capture and polishing steps, can be softened by continuous countercurrent chromatography, where the unresolved portions of the elution stream are recycled internally. For this, the first process that exploited these problems were the True Moving Bed (TMB) [136, 266] and SMB [41] processes.

2.3 Continuous Multicolumn Countercurrent Chromatographic Processes

2.3.1 True Moving Bed Process (TMB)

In batch chromatography it is impossible to feed the system continuously since product fractions are collected at the same end of the column, as shown in Figure 2.13a (case of binary separation). However, in countercurrent chromatography, Figure 2.13b, if the adsorbent is moving within the column and traveling in the opposite direction of the mobile phase, with an intermediate velocity between the migration velocities of the two solutes, the less retained solute (A) is carried by the mobile phase and collected at the liquid outlet, while the more retained component (B) is dragged with the adsorbent and collected at the other end of the column. After the total development of the concentration profiles (i.e., when the system reaches steady state operation), solutes A and B are collected purely at the extract and raffinate outlet, respectively.

Thus, since the components are collected at the extremes of the concentration profiles, even if the resolution of the peaks is not total, high purities are obtained with the moving bed, while in batch chromatography high purities are only achieved if the resolution is also high (complete separation of the peaks). Moreover, in the moving bed the adsorbent is more loaded with solute than in the fixed bed, this is because countercurrent operation

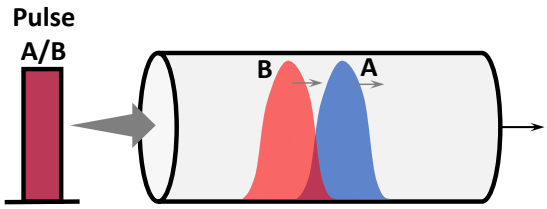

(a) Batch chromatography.

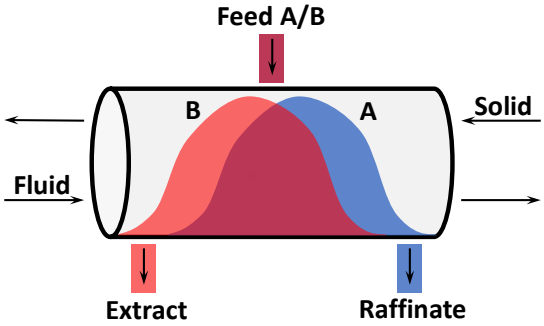

(b) Countercurrent chromatography.

Figure 2.13: Comparison between the principles of batch and countercurrent separations. At 2.13a, the two products exit at the same end of the column, which makes it impossible to continuously feed in the chromatographic column, while at 2.13b each component is collected at one end of the column, thanks to the movement of the stationary phase in countercurrent with the mobile phase movement, where the less retained bioproduct (A) is arrested with the fluid and the more retained compound (B) accompanies the solid phase.

maximizes the drive force for mass transfer, which increases the efficiency of use of the adsorbent [177]. This greater use of the adsorbent increases the productivity significantly.

The TMB was the first projected method of continuous countercurrent chromatography [230]. Its process is based on four chromatographic zones (groups of columns) countercurrently-operated, sequentially linked and in closed-circuit, each zone performing a different function [177]. Its working principle is illustrated in Figure 2.14. For a two-component separation, the mixture (A/B) is injected between sections II and III where separation of A and B occurs. Because B is the most retained, it is drawn by the chromatographic media to the outlet port of the extract stream, where it will be collected, between sections I and II. The less retained solute A, however, moves along with the mobile phase to the outlet port of the raffinate stream, being collected between sections III and IV. The input of zone I is fed with pure solvent to regenerate the adsorbent before it is recirculated to zone IV, whereas in zone IV the solvent is regenerated before being recirculated to zone I.

However, the countercurrent movement of the solid bed is never implemented in practice, as this causes some operational problems of friction and of particles mixing (dispersing the concentration profiles and therefore losing efficiency).

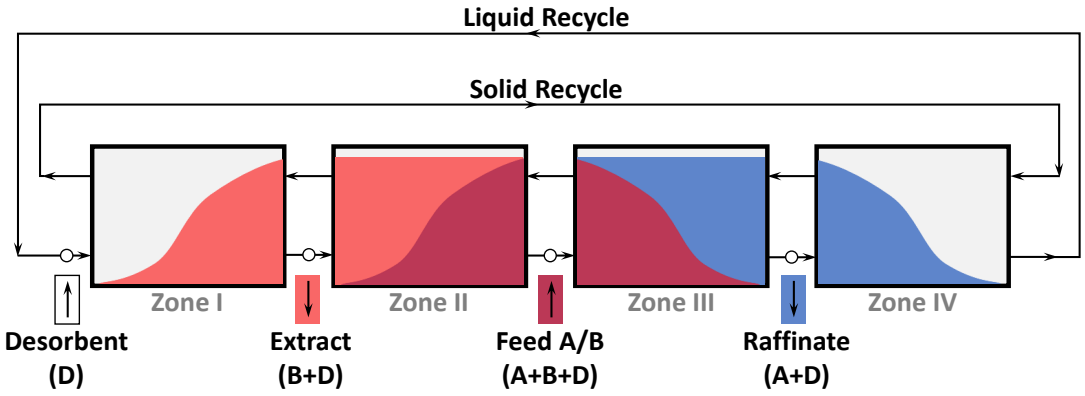

Figure 2.14: Functional principle of True Moving Bed process. The scheme is divided into four columns (sections), with the stationary phase moving countercurrently with respect to the mobile phase. Both phases (mobile and stationary) recirculate in the system, in order that, the operation happens in closed-loop. Feed is injected between zones II and III, extract is collected between zones I and II, raffinate is gathered between zones III and IV and desorbent is inserted at the entrance of zone I to promote the regeneration of the adsorbent. Adapted from [177].

2.3.2 Simulated Moving Bed Process (SMB)

To overcome the limitations of the TMB, rather the problems associated with the movement of the bed particles, the Simulated Moving Bed was developed. The SMB is a continuous process of multi-column chromatographic separation with countercurrent adsorption.

Its emergence occurred in 1961 [41] (with *Sorbex process* as commercially name), for first implementation in the petrochemical industry, for separation of hydrocarbons, and soon after in the refining of sugar. It was only in the early 1990s that the opportunity was seen to reduce the SMB scale for application in separations at the pharmaceutical and fine chemistry areas [133], due mainly to the appearance of new stationary phases, more economical and more stable [156, 190, 195]. Nowadays, the SMB process is widely used in different chromatographic separations in distinct steps of the development cycle of a new biopharmaceutical product, and one of the drivers for this is the variety of SMB models that have already been developed based on the conventional process [149, 239], approaching concepts such as asynchronous port switching (Varicol process) [8, 165, 262], time-variable manipulation of the flow rates (PowerFeed process) [139, 149, 283, 287, 288], cyclic modulation of feed concentration [236, 237], solvent-gradient operation [2, 15, 127], and several others.

The trend is new schemes using only few columns, as it decreases the amount of adsorbent, the units are more compact and more economical, in addition to being simpler and faster to switch between separations of different mixtures [227]. Nevertheless, this improvement in separation performance is achieved at the expense of increasing the

complexity and the sensitivity to procedural uncertainties and operative variability. Because of this, requirements like highly versatile equipment [281], advanced optimization tools [69, 137, 138, 261, 262] and robust automatic control procedures [3, 146, 147, 238] are strongly requested for this added complexity.

The conventional SMB is also divided into four zones of constant flow rates by the presence of four ports: two ports for addition of fresh feed and eluent, and two ports for product collection (extract and raffinate) [227]. The difference of SMB operation when compared to the TMB, as shown in Figure 2.15, is that the countercurrent movement between the fluid and the stationary phase is simulated/provided by switching the inlet and outlet ports in the same direction as the fluid flows at each completed switching interval, while the chromatographic media remains fixed in the column. SMB is, thus, a simulation of the continuous operation of TMB, through replacement of each TMB section (or column) by several identical chromatographic columns (or subsections) interconnected circularly to form a closed-loop. In closed-loop operation, zone IV is a zone for raffinate enrichment and solvent recirculation, so the outlet stream of zone IV is recirculated to zone I. This solvent recycle configuration reduces solvent consumption; on the other hand, it requires an extra pump to do the recycle.

Although traditional SMB has four zones, other schemes with fewer zones have been developed in recent years. There is, for example, the three-zone SMB scheme [171, 230, 284] obtained by removing zone IV from a typical SMB. Since without zone IV there is no solvent recirculation, the 3-zone configuration, as well as the open-loop operation, avoids any possibility of contamination of the extract. This type of configuration with reduced number of zones implies some advantages over the traditional configuration, such as reduction of the number of pumps, reduction of the residence time of the components that are collected in the raffinate stream (which can prevent aggregation and denaturation at chromatographic process for protein purification [184], for example), reduction of the total number of columns, reduction of the amount of adsorbent required (in some chromatographic separations, the resin may represent the dominant cost), and finally, the scheme is easier and simpler to control. As disadvantages, the three-zone configuration shows raffinate dilution and increased solvent consumption [177, 281].

The two-zone SMB has also been implemented with variations in the operation mode of each process, being able to have intermittent feed and partial withdrawal for binary separation [160]; continuous feeding and withdrawal for ternary separation [13]; partial feeding with implementation of a solvent collection tank, to reserve and subsequently use applied for binary [128, 129] or ternary separations [121, 122], but in the former case without use a storage tank; modulation of the port configurations and flow-rate during the cycle used for binary [227] or ternary separation [223] (the former, performed through the addition of a further withdrawal), among several others.

Finally, the limiting case of using only one column to reproduce the cyclic behaviour of multicolumn SMB chromatography, through delay in the recycle, has been proposed [4–7, 16, 17, 176, 209] and will be discussed further below since it fits into the main theme

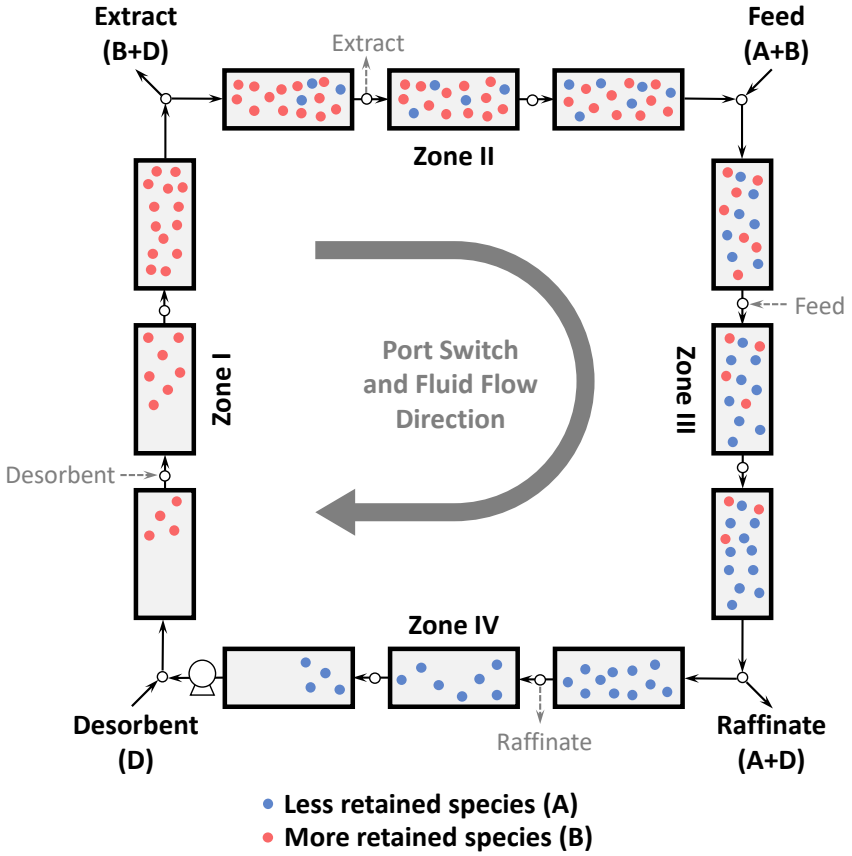

Figure 2.15: Schematic diagram of Simulated Moving Bed process. The conventional scheme has four zones as well as the TMB. The continuous movement of the adsorbent is simulated through the periodic switching of the inlet and outlet ports in the same direction as the fluid flow. In addition, each section is partitioned into several subsections (or columns) to approximate the discrete movement of the SMB to the continuous movement of the TMB, thereby increasing process efficiency. The system is composed by identical columns and operated at a constant flow rate. Adapted from [222].

of this thesis plan.

In general, SMB enjoys numerous advantages over other preparative chromatographic techniques, almost all have already been cited throughout the continuous (subsection 2.2.3) and countercurrent (subsection 2.3.1) chromatography approach. To summarize the advantages:

- The process is continuous, which dispenses manual intervention and facilitates the stabilization of product quality and controllability of the process, besides operating at steady state after a few cycles;

- The consumption of solvent is considerably reduced due to automatic solvent recycling;

- Resin capacity utilization, purity and specific productivity (i.e., per mass unit of stationary phase) are increased ;

- As a consequence of the last topic, less resin is necessary for the same product purity, implying in reduced equipment size and reduction of total costs and operating time.

2.3.3 Multicolumn Countercurrent Solvent Gradient Purification Process (MCSGP)

Multicolumn Countercurrent Solvent Gradient Purification (MCSGP) [24, 26, 155, 181, 250, 252, 253] is a continuous chromatographic separation process that has been particularly highlighted as a suitable process for bioseparations, enabling ternary (three fractions) separation and linear solvent gradient application, resolving the constraints of the traditional SMB, which has the limitations of performing only two components separations and elution by step [267], the SMB being then rarely used in the polishing step. With this, MCSGP encompasses the benefits of SMB, and even goes beyond SMB. This method has also received notoriety for mAb purification [178].

The process was first developed in 2006 [252] and there are already different versions with two to six chromatographic columns [25, 26, 154, 182, 200, 250], allowing continuous [24, 252] or cyclic [25, 154] feeding and elution, multiproduct separation [155], and different cleaning-in-place steps [183]. MCSGP can be applied to any bind-elute chromatographic mode (CEX, AEX, HIC, RPC, etc.), although for mAbs the CEX is the most commonly used [267].

Its method of operation is demonstrated in Figure 2.16 for the two-column version, and consists of collecting the pure portions of the chromatogram, while the others fractions (or unsolved portions) are recycled to a second column, allowing high purity and yield. This is achieved thanks to alternation of the state of the columns between interconnected and batch. Each switching interval consists of four steps, two interconnected and two in batch mode. After the end of each switch intervals, the column positions are interchanged and the steps are repeated. These four steps are crucial for controlling purity and yield more independently than possible in a traditional batch operation. For this reason, the MCSGP responds well to the trade-offs of batch chromatography.

In the first interconnected phase (I1), column 2 elutes and recycles to column 1 product (P) containing weakly adsorbing impurities (W). To bring the solutes into a binding state, inline dilution is applied. The next step, the first batch step (B1), only begins when the outlet product flow is sufficiently pure, and therefore product is collected from column 2, while column 1 is fed. Once strongly adsorbing impurities (S) contaminate the product to a certain level, the columns are again interconnected for recycling including inline dilution. After the entire product is eluted from column 2, the second batch phase (B2) comes into action, where column 2 is regenerated (strip, CIP, equilibration) and the gradient begins at column 1, eluting W.

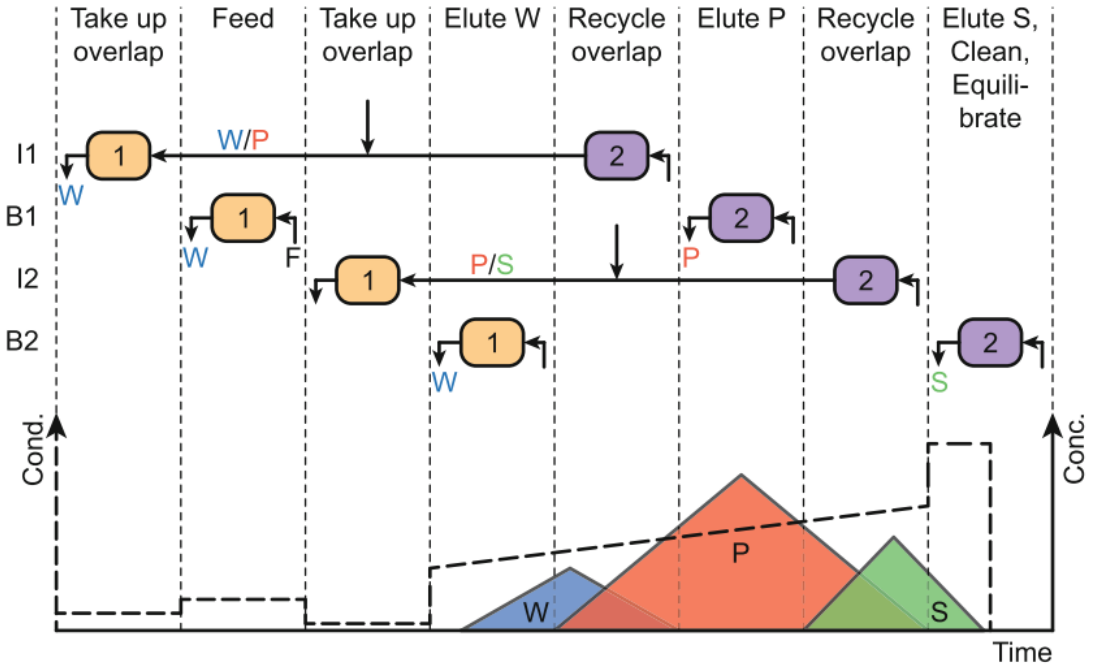

Figure 2.16: Schematic diagram of one switch interval of the two-column MCSGP process. The switch is divided into four steps, two interconnected (I1 and I2) and two batch (B1 and B2) modes, interspersed with each other. Phases I1 to B2 are performed sequentially. Source: [267].

MCSGP technology has low complexity and hardware demand, as well as high flexibility due to sequentially proceeded tasks [250]. In addition, the MCSGP has the advantage of, from complex mixtures, isolate and enrich single species in preparative amounts with a high resolution. This is attained by combining three factors: (i) use of high pressure, resulting in high separation resolution; (ii) use of chromatographic matrices with very low mesh size, which in preparative batch chromatography is not possible due to technical restrictions; (iii) and as a main factor, recycling of impurities containing product, resulting in high yields [253].

When comparing the principle of MCSGP process with batch chromatography, long process development times are generally solicited to achieve the required threshold product quality, whereas in the MCSGP this time is considerably reduced, reaching a faster higher product quality as can be seen in Figure 2.17. Furthermore, as the operating costs can be reduced because of lower maintenance cost and lower solvent consumption, while yield can be increased up to 50% for the same purity value, the Cost of goods (COG), at manufacturing field, can be significantly reduced, thus having a direct effect on profits [253]. COG is the expenses directly related to the production of a company's product.

In order to guide the decision of the most suitable chromatographic process to be used, a decision tree of chromatographic process has been proposed (shown in Figure 2.18), where it indicates that for problems of binary separation with great difficulty of separation

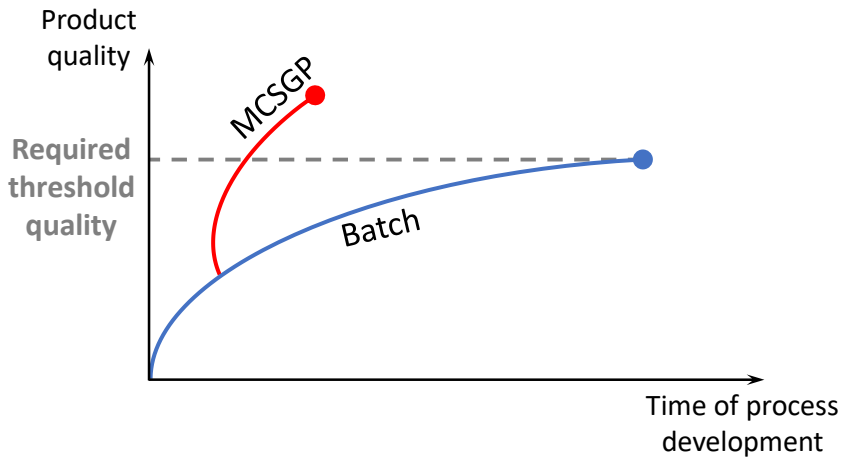

Figure 2.17: MCSGP *versus* batch with respect to process development time. Batch process generally requires a long process development time to reach the desired threshold quality, whereas through the MCSGP it is possible to abundantly decrease this time, achieving faster higher quality.

the SMB is the most suitable process, whereas for complicated ternary separations the most indicated process is the MCSGP.

2.4 One-Column Processes Similar to SMB

Nowadays, biomanufacturers demand agility and flexibility, so modern installations are expected to be increasingly efficient, capable of narrowing the ratio of produced volume and production time, without losing the quality of the product (purity and activity), through operating systems each simpler [199].

The way currently highlighted to achieve these benefits is through the transition from batch to continuous [267]. For the change to happen, the development and implementation of alternative continuous unit operations in the different production steps is required, as well as the robust connection between the steps and control of the different parts of the process. This modernization in the biopharmaceutical production process is so important that even the FDA has encouraged efforts in continuous bioprocessing and underscored its shocking potential in solving problems of flexibility, agility and robustness [162].

Concomitantly, there has been a tendency to decrease the number of chromatographic columns employed in a continuous process, thanks to advances in the development of cyclical operation policies [22], allowing the improvement of the performance of SMB operating units. By establishing units with a reduced number of chromatographic columns, benefits are outstripped, such as less stationary phase used, more economical set-up and reduction of overall pressure drop.

Therefore, working with the limit case of only one chromatographic column can be

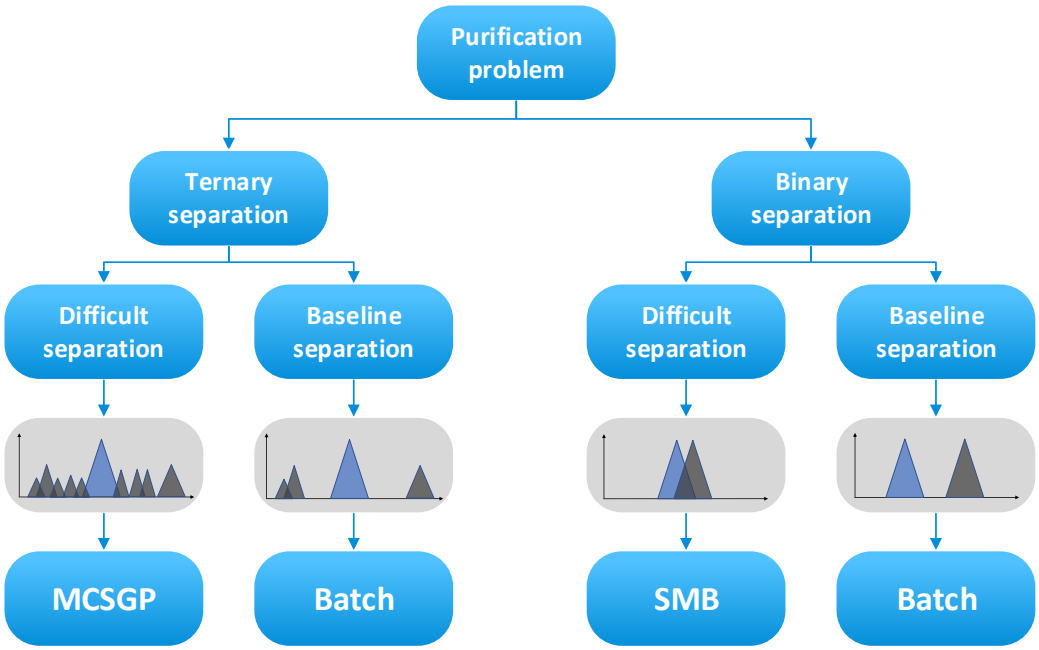

Figure 2.18: Chromatographic process decision tree. Scheme to aid in the selection of the chromatographic process to be applied in a purification problem. For separations where the product collection interval does not contain impurities, it is recommended to use batch chromatography. Meanwhile, for difficult binary separations SMB is the most recommended, and for more complicated ternary separations the MCSGP is indicated as more appropriate. Adapted from: [253].

very advantageous in some cases, since only one column needs to be repackaged, switching from one mixture to another tends to be easier and takes less time than in a SMB system [22], in addition to a simpler design bringing more flexibility [7]. One problem faced by SMB is the differences in separation when the columns are switched, because if the columns are not identically packaged, the purities are different, the pressure drop and/or flow rates in each zone may vary when switching happens, so the use of a single column is more stable to these fluctuations than the SMB [6].

Furthermore, when operating with only one chromatographic column, the total pressure drop decreases, which implies the reduction of the resistance to mass transfer and allows higher flow rates in the system. This may be a considerable benefit if smaller particles than those suitable to the equivalent SMB are used. And so, with higher flow rates, the specific productivity is also increased. An added consequence is that as the Péclet number is increased (due to increased flow rate), the hydrodynamic contribution to band broadening in the chromatographic column is reduced [176].

This limiting case of one-column process similar to SMB has been developed and studied by only two research groups in a recent past, one of which this thesis is embedded,

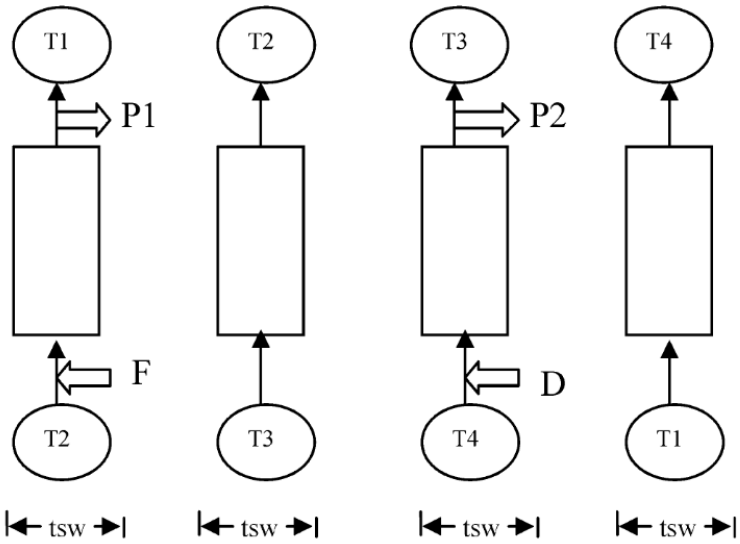

Figure 2.19: Complete cycle of the Analog mimicking a four-zone SMB with one column per zone. The system consists of one chromatographic column and mixed tanks in the same amount of columns used in the equivalent SMB. In the example shown above, four mixed tanks are used to reproduce the standard SMB. Its cycle is defined after studying the same column of the SMB during a complete cycle and then replacing the remaining columns with mixing tanks to procreate the recycle streams while maintaining constant specific productivity. F, D, P1, P2, t_{sw}, and T_i are feed, desorbent, raffinate, extract, switch time and the mixed tanks, respectively. Source: [7].

with variations in process design as well as in application purpose, and tested in different case studies. A brief literature review will be discussed below to explain the main differences between these processes, since this topic fits the main subject of this thesis.

2.4.1 The Analog

Abunasser et. al. [7] in 2003 were the first to address the idea of one-column chromatography with recycle to mimic the four-zone SMB, which they termed "the Analog." Its operating principle was based on one chromatographic column connected to a number of mixed tanks equal to the number of steps of an SMB cycle. For example, eight tanks are required by an Analog to mimic a four-zone SMB with two columns per zone. The schematic diagram of the Analog is presented in Figure 2.19. Case studies or proof-of-concepts were considered for linear systems, namely the separation of dextran T6-fructose and dextran T6-raffinose mixtures, as well as for nonlinear systems with the separation of binaphthol enantiomers. These separations were reproduced using the Analogs of four-zone SMB with one column per zone (under two different conditions: total-feed and partial-feed) and with two columns per zone. These applications were created and compared to the corresponding SMBs only at simulation level, using Aspen Chromatography.

A comparison of the different configurations showed there were no advantages of the basic Analog with partial-feed compared to the total-feed due to the mixing in the tank.

The Analog of the two-columns-per-zone SMB showed higher purities than the Analog of the one-column-per-zone SMB, since the former uses a larger number of tanks.

As an overall result, for the same values of specific productivity and desorbent-to-feed ratio (D/F), the Analog obtained less purity than the SMB due to mixing inside the tanks. The increase of product purity was achieved by dividing the tanks into several smaller tanks to approach plug flow. For the same specific productivity, equal values of purity to that of the SMB were achieved by the Analog through a modest increase of D/F from 1.0 to 2.6 (for one column per zone) or for 2.3 (for two columns per zone), which is a significantly smaller increase than that required for chromatography without recycle to obtain purities equal to an SMB. Therefore, the proposed analog showed to be a flexible (due to its simple design) and inexpensive alternative to elution chromatography and to SMB, reaching relatively high purities. The authors concluded that for high purity requirements, the SMB had advantages, but on the other hand, for frequent changes of the adsorbent, the Analog was advantageous.

Another theoretical case study was performed [144], this time considering the separation phenylalanine and tryptophan amino acids, in which a four-zone SMB with one column per zone was compared to a single Analog with four mixed tanks. The purity and yield results were very similar between the two systems, although the SMB obtained slightly higher values because the concentration profiles were destroyed in the fluid phase after mixing inside the collection tanks.

In 2004, Abunasser et. al. [6] provided further applications for the Analog, again in the framework of simulation and for binary separations. This time, these authors tried to solve the problems of purity existing in the basic design of the Analog due to the use of well-mixed tanks in the same amount of columns. For this, the tanks were replaced by an even larger number of smaller mixed tanks to approach a plug-flow behavior, using 4, 8, 16, 20 and even 28 tanks. Hence, the Analog obtained near-identical values of purities using 28 tanks over a four-zone SMB with one column per zone for linear dextran T6-fructose separation.

In addition, start-up and shutdown studies were performed using computational simulation to find the optimal operating conditions. It was showed that correct start-up conditions could reduce the time required to achieve steady state by 50%, while shutdown strategies could reduce the time and amount of desorbent needed to clean up the system.

Still in the same study, the scheme of the Analog was applied for the linear dextran T6-raffinose separation and compared to the three-zone SMB with partial-feed and selective withdrawal, and for the linear dextran T6-fructose separation and compared to the VARICOL system. The two Analogs had very similar purities to the compared systems, especially when additional tanks were used, concluding that the analogue concept was versatile and could successfully replicate several different configurations of the SMB for binary separations.

Detailed simulations were also used to investigate Analogs and SMBs with two-feeds in two different conditions: total feed and partial feed [143]. Analyzes showed that

Analogs obtained reasonable purities relative to SMBs, especially in the situation where total feed was performed.

2.4.2 The Single-column Analog with Recycle Lead

Two new concepts, the chromatograph with advance in recycle [22] and the chromatograph with delay in recycle [176], were developed by the research group in which this thesis was developed. In these concepts, the cyclic stationary state of the SMB, or of any other multicolumn chromatographic process that simulates countercurrent contact, can be reproduced by a one-column process with a recycle lag of $(N-1)\tau$ time units (in the case of chromatograph with delay in the recycle), N being the number of columns and τ the switching interval of the SMB mimicked, or with and advancement of τ units of time (in the case of the chromatograph with advance in the recycle); the recycle is the fraction of the output stream from the column that is not collected as product (extract or raffinate).

An SMB process can be pictured as N identical single-column processes operated with a lag of τ time units; if only the concentration profiles of the input and output streams of each column are analyzed, it is impossible to differentiate between these processes. Therefore, the operation of one-column chromatographs is performed by analyzing an arbitrary SMB column and following its operation over the complete cycle of operation, as can be seen in Figure 2.20. Therefore, the delay of $(N-1)\tau$ time units is consequence of the circular array of columns in the SMB and their periodic operation characteristics [177].

In practical terms, the chromatograph with advancement in the recycle, named "Single-column SMB Analog with Recycle Lead," is not physically feasible because it requires access to future events; however it was shown to be an efficient computational method (using gPROMS software) for direct determination of the cyclic stationary state of the SMB or any multicolumn chromatographic process that simulates countercurrent operation [18, 22].

2.4.3 The Single-column Analog with Recycle Lag

Differently from the chromatograph with advance in the recycle, the chromatogram with delay in the recycle, named "Single-column Analog with Recycle Lag," is physically achievable and can solve deficits of the Analog project. Although the Analog has succeeded in proving that it is possible to mimic an SMB system using only one chromatographic column and reduced number of two-way valves, the major drawback is that lower purities were obtained for the same specific productivity and D/F of the SMB mimicked, due to mixing in the tanks. This could be solved by increasing the amount of mixing tanks or increasing the D/F ratio, where the former brings increased volume and capital cost of the unit, while the latter brings increased separation cost.

Since it has been proven in previous studies with the Analog that by increasing the number of mixed tanks (to simulate plug-flow) the purity values have been increased, a

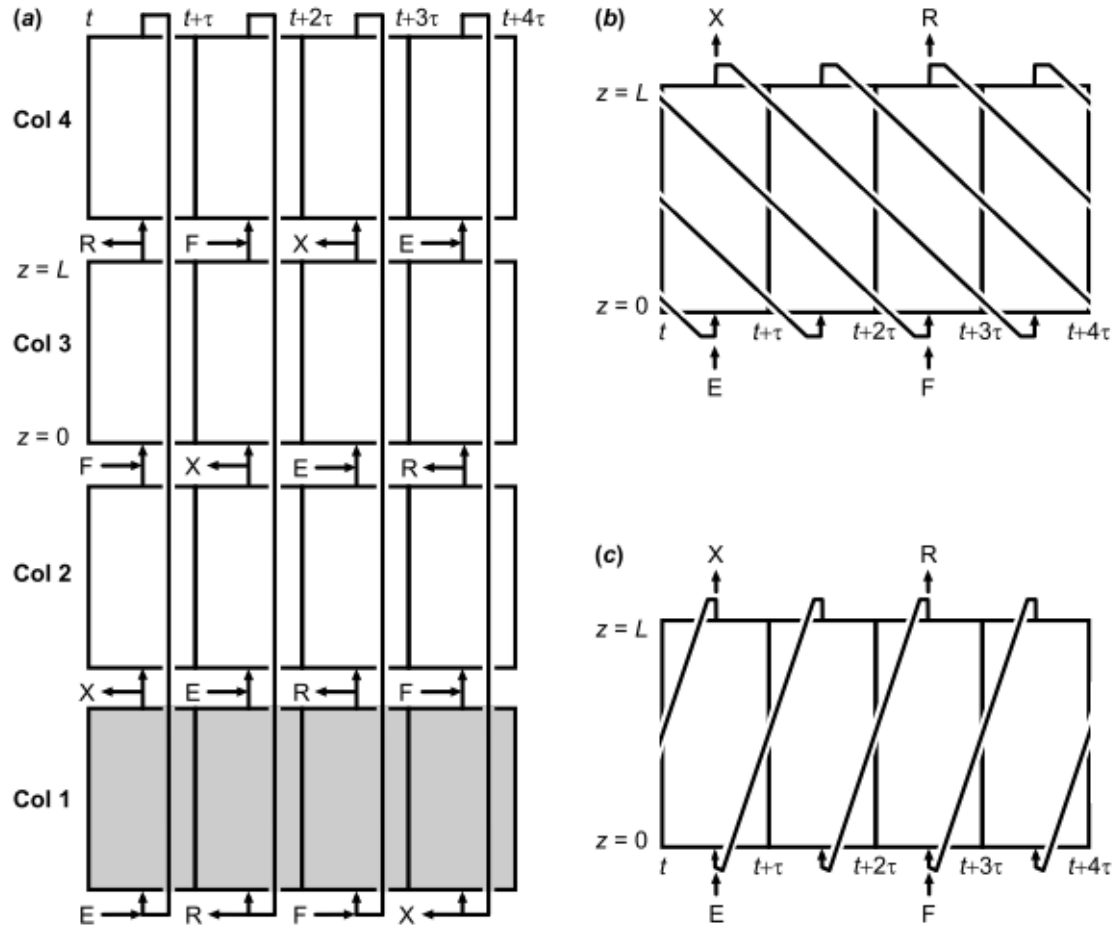

Figure 2.20: Schematic of a cycle of operation for (a) a classic SMB (4-zones, 1-column-per-zone), (b) its single-column analogue with recycle lag, and (c) its single-column analogue with recycle lead. The two monocolumn processes are obtained by selecting an arbitrary column of the classical SMB process, column 1 for example, and following its operation for a complete cycle. The recycle streams (i.e. the portion of the outlet stream of the column that is not withdrawn as product) is reinjected into the system with a time delay of $(N-1)\tau$ or time advance of τ. Source: [22].

new design was created to improve its performance using a single plug-flow (unmixed) reservoir connected to the chromatographic column [176], representing a promise due to the reduced number of equipment used (e.g. tanks, valves and tees), becoming less complex and expensive, while maintaining the flexibility of the Analog.

The scheme of the Single-column chromatographic process with recycle lag is illustrated in Figure 2.21. The project considered the use of a plug-flow device with an average residence time equal to the lag time [176]. This device was designed to solve the problem of the difference of flow rates between the column inlet and the column outlet fraction that is not collected as a product, which are not equivalent in some steps of the monocolumn chromatograph cycle, because the lag duration is not a multiple of the overall cycle duration ($N\tau$). Thus, the chromatographic column is connected to a plug-flow tube,

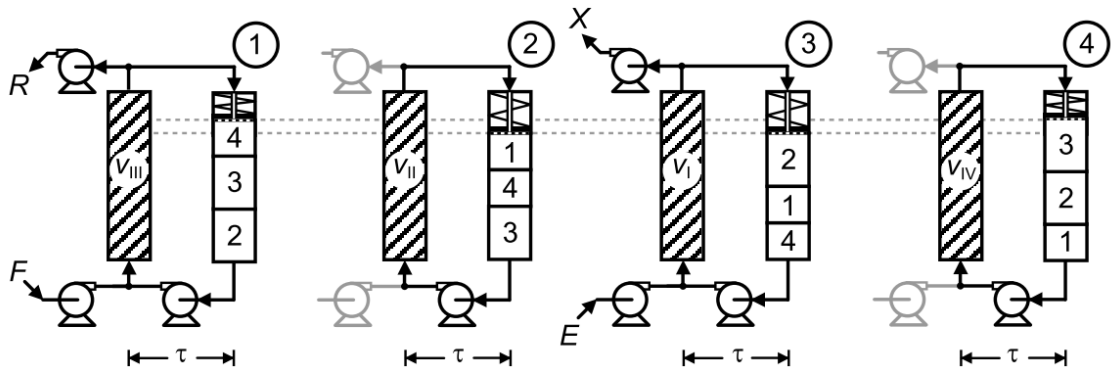

Figure 2.21: Single-column with recycle lag analogous to a classical four-zone SMB. A single plug-flow tube with a piston at one end is connected to the chromatographic column. The tube implements the recycle lag of $(N-1)\tau$ time units. The difference of flow rates at the inlet and outlet of the tube that occurs during some steps of the cycle is compensated by the movement of the piston. F, E, R, X are the feed, eluent, raffinate and extract streams, respectively. Source: [176].

which has a piston actuated with spring at one end, allowing the piston to be continuously pressed against the fluid, moving to compensate the difference between the inlet and outlet streams. At the design of the new scheme it was also assumed that there are internal elements or filler at the internal structure of the tube, to produce a flow as close as possible to plug-flow, which could be filling with high porosity and inert to the adsorption of solutes, grid structure, polymeric or metallic foam, among others [177].

In theory, under Cyclic steady-state (CSS) conditions, this single-column process is identical to the equivalent SMB, except for the discontinuous use of the input/output ports [17].

The scheme was used for the separation of binaphthol enantiomers as case study, and the efficiency of the process was compared with a four-zone SMB with one column per zone and two columns per zone, by simulation in gPROMS [176]. For reference, the comparison was also extended to the Analog [6, 7]. The system proposed, in addition to having the advantages of a single column system already mentioned in this section, it exceeds results found with the Analog system, since it could potentially achieve purities identical to the equivalent SMB while keeping the specific productivity constant, while reducing the costs and complexity of the system by using a single reservoir, fewer valves and less tees.

In a second study, presented by Araújo et. al. [17], the enantiomeric separation case study was used to demonstrate the applicability of the single-column process for asynchronous operation. The analysis was performed for four different port configurations of the SMB: one (1/1/1/1) and two (2/2/2/2) columns per zone, five columns (1/2/1/1) and seven columns (2/2/2/1); and three different port configurations of Varicol: five columns (1/1.5/1.5/1), six columns (1.5/1.5/1.5/1.5) and seven columns (1.5/2/1.5/2). Considering the same specific productivity for all systems, the purity results indicated

that, as the *Pe* was increased, the purity values also increased. For very high values of *Pe* (i.e. almost no hydrodynamic dispersion inside the tube), the purities of single-column processes approached to those of the analogous SMB and Varicol processes. Analogues to Varicol presented superior results than those SMB analogues, due to the compensation of the less-perfect operation of the recycle tube by the Varicol concept, improving the performance of the Single-column analog system. This study demonstrated not only that the single-column system is able to mimic different configurations of SMB, but mainly the need for an efficient plug-flow device.

Even so, there is a lot that can be done on this system. The output flow rate of the chromatographic column in this design, for example, is divided between product (*X* or *R*) and recycle through the bifurcation of the liquid stream. This means that throughout the τ that the output stream is flowing, some of the liquid is collected and another part goes into the recycle tube at the same time, which can result in impurities in the product stream as well as excess of pure component in the stream that goes to the recycle. Moreover, the validation tests studied involved only binary separations and were only performed at the theoretical level through simulations in gPROMS. As it was only approached the conceptual implementation of the process, no filler was tested to ensure a plug-flow behaviour inside the tube.

2.4.4 The Unmixed Analog

In order to develop a similar but simpler plug-flow device than Single-column Analog with Recycle Lag, Abunasser et. al. [4] proposed a new design for a one-column chromatograph called the "unmixed Analog". In this novel process, shown in Figure 2.22, a fixed-size unmixed tank is used, i.e. it does not contain a piston therein, and is packaged with inert packing (nonporous beads in this example). The unmixed tank is connected to the chromatographic column in closed-loop. Since the size of the tank is not variable, its volume is constant and the variation in flow rates entering and exiting the column are accounted by dividing the inlet and outlet streams into two different streams (so $F = F_1 + F_2$, $D = D_1 + D_2$, $E = E_1 + E_2$ and $R = R_1 + R_2$). For constant flow rates into and out of the reservoir,

$$T_1 + R_2 = T_4 + D_2 = T_3 + E_2 = T_2 + F_2 \tag{2.1}$$

where F, D, E, R are respectively, feed, desorbent, extract and raffinate flow rates. Subscript 1 indicates that the streams enters and leaves the chromatographic column; subscript 2 indicates that the stream enters and leaves the unmixed reservoir. T_i is the flow rate exiting the corresponding tank in the Analog with mixed tanks.

Binary separation of 1,1' bi-2-enantiomers was enforced to this analog for the classical SMB using simulations, run at Aspen Chromatography [4], which obtained higher purities than the Analog with mixed tank and values slightly lower than SMB due to dispersion in the device (a result similar to that achieved with the design developed earlier by Mota et. al [176]).

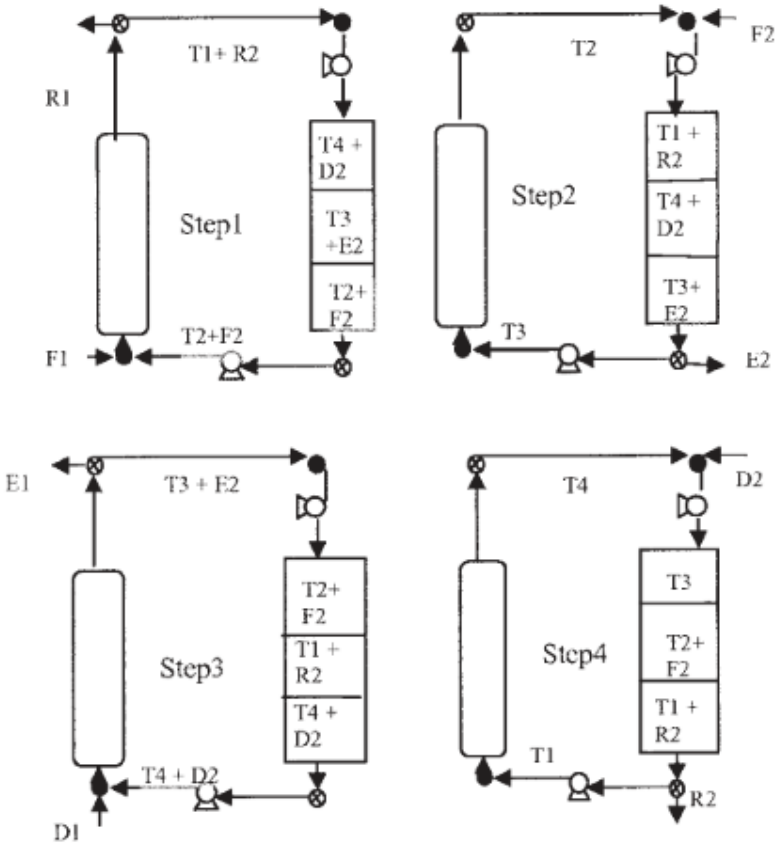

Figure 2.22: Schematic of the Unmixed Analog. The plug-flow reservoir has constant volume and is packaged with inert filler. To compensate for the variation of flow rates entering and leaving the column, the inlet and outlet streams are each separated into two distinct streams. F, D, R, E are respectively, feed, desorbent, raffinate and extract. Subscript 1 indicates that the streams enters and leaves the chromatographic column; subscript 2 indicates that the stream enters and leaves the unmixed reservoir. T_i is the flow rate exiting the corresponding tank in the Analog with mixed tanks. Source: [4].

As shown in the previous subsection 2.4.3, Mota and Araujo [17, 176] studies showed that decreasing the dispersion within the device (through the reduction of internal particles, for example) increases the purity values achieved by the system. Therefore, a second case study was addressed. Scaling rules were applied to the unmixed Analog for the separation of 1,1' bi-2-enantiomers [4]. The scaling rules are essentially identical to those used in SMB since Analog was designed to mimic a SMB [142]. For this, the Analog was first scaled to increase purities and match the SMB values by reducing the flow rates, and then the scaling rules were used a second time for each step operate at maximum pressure drop allowable (15 bar) with the aim of increasing productivity. With this, it was shown that if appropriate scaling is used, it can be matched to the standard SMB with productivity values 11 to 15% higher than standard SMB.

Subsequently, the versatility of the basic analog and unmixed Analog was extended for application at ternary separations, mimicking the following processes: a cascade of

two four-zone SMBs with one column per zone and a five-zone SMB with one column in each zone [5]. Simulations were performed at Aspen Chromatography for nucleosides separations (considered an easy separation, with linear isotherm at low concentrations). Analogs with mixed tanks showed lower purities than SMB due to mixing inside the tanks. For example, while the five-zone SMB achieved a *PI* of 88.3, the basic Analog with five mixed tanks had PI = 83.4 and the Analog with 10 smaller tanks (to consider the same specific productivities) had the PI of 85.4, where PI is defined as

$$\text{PI} = \frac{\%\text{-purity of less retained solute in raffinate} + \%\text{-purity of more retained solute in extract}}{2}. \quad (2.2)$$

However, the five-zone SMB is not robust for ternary separations, it can obtain pure products only if the separation is easy.

On that account, the unmixed Analog system was compared to the cascade of two four-zone SMBs with one column per zone, that is a more robust system for ternary separations [5]. As the reservoir reduces the mixing, the separation was improved, where the cascade of two four-zone SMB system had a PI of 86.7, the Analog with eight mixed tank obtained PI of 82.9, and the unmixed Analog reached PI of 84.6. Therefore, it has been shown that with the use of an unmixed reservoir it has still higher purities than the analogue with mixed tanks, but lower than the corresponding SMB due to the dispersion in the unmixed reservoir. The unmixed Analog could not be extended to the case of a cascade four-zone SMB with two columns per zone, since it can only mimic simple SMB configurations [5].

The design of the unmixed reservoir is limited to SMBs that have a small number of columns, because when the number of columns increases, there are not enough variables (input and output streams) to maintain equal the inlet and outlet flowrates of the unmixed tank [4]. Therefore, SMB configurations such as (1,1,1,1) and (1,2,1,1) can be imitated. Another point in question is that in practice, and in simulations, the reservoir is not perfectly plug-flow (as well as the design developed by Mota et. al. [176]), which leads to a deterioration of the purity values. One more situation commented by Abunasser [4] is that the device needs to be repackaged as well as the chromatographic column when new mixtures are used, although, when compared with SMB, this system is still simpler and more flexible since in the SMB a larger number of columns must be packaged and must have identical residence times. The authors further conclude [4, 5] that because extreme changes in flow rates are commonly required when new campaigns are conducted, the use of a plug-flow device with variable volume, like the proposed by Mota and Araujo [176], would be a gain to a one-column system.

2.4.5 Alternative Version of the Single-column Analog with Recycle Lag

In every SMB process, uncertainties in pump stability and calibration, temperature stability, dead volumes, isotherm parameters, band broadening, and reproducibility of packing, are unavoidable. It is therefore recommended that new operating schemes be developed

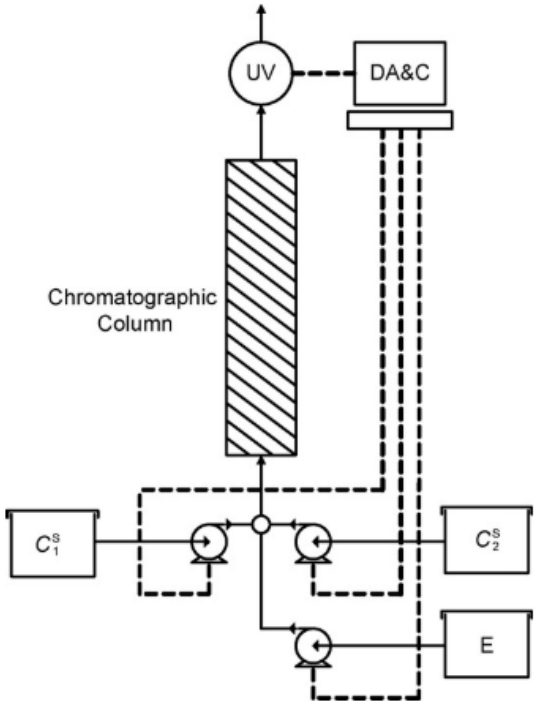

Figure 2.23: Schematic of the Alternative Version of the Single-column Analog with Recycle Lag. It is composed by a chromatographic column, three HPLC pumps, an UV detector to measure the outlet concentrations. Pumps and detector are coupled to a fully automated data acquisition and control system. Source: [226].

and validated on a small scale to identify possible operational bottlenecks and robust problems before executing them in large scale [225].

An alternative version to the system described in subsection 2.4.3 was designed and, unlike previous one-column systems, an experimental unit was created (Figure 2.23). Its purpose is not to separate components of mixtures, it is to quickly and economically reproduce the periodic behavior (i.e., cyclic steady state) of the SMB to not require the realization of experiments on the multicolumn unit. The same objective presented by Single-column Analog with Recycle Lead [22]. As shown in Figure 2.23, in this design there is no plug-flow tube with piston inside. The effluent stream from the chromatographic column has its composition monitored in-line and then this composition is artificially re-created by a multi-pump system and the stream resulting from that mixture is injected with a delay of $(N-1)\tau$ time units [225]. For this purpose, three variable speed pumps are used, where the flow rates are continuously manipulated according to the temporal profiles of the column output. For each pump a different solution: solute 1 concentrate, solute 2 concentrate and pure solvent; allowing the additive mixture to replicate the column inlet concentration and flow rate, as it is desired to simulate the concentration and flow rate collected at the outlet of the chromatographic column in previous steps, creating conditions similar to those experienced by the column if it were part of the SMB unit operating under stationary cyclic conditions.

This apparatus was validated experimentally [225, 226] and proved to be a simple, compact and fast method of experimentally reproducing the stationary cyclic state of different configurations of the SMB with a minimum consumption of solute and solvent. In addition, it may be useful in the early stages of development, optimization and validation of new multicolumn chromatographic separations. Several different configurations were tested for this system, including the classic SMB [225], the Varicol process (asynchronous port switching) [225, 226], the PowerFeed process (temporal modulation of flow rate) [226], and a hybrid process that combines Varicol and PowerFeed in the same unit [226].

A small disadvantage of this procedure is that it introduces solutions into the system through two separate solutes, which may represent a problem for separations in which pure components are expensive or difficult to obtain, such as enantiomeric separations. However, since the experiment is very short (one or two cycles) the amount of solute required is very low.

When analyzing all single-column processes already suggested in the literature, there are gaps for a design and (mainly) an efficient single-column experimental prototype. A single column system that combines all of the following benefits: able to mimic a wide variety of existing multi-column continuous systems (with varying levels of complexity), using only one volume-adaptable plug-flow reservoir, operating in closed-loop, and with practical purpose of carrying out the complete process of separation of binary or even ternary mixtures (which are considerably more complicated); was never designed, built its experimental unit and validated. Closed circuit operation, i.e. no need to re-create the output of the column through liquid pumps, and with as few equipment as possible would bring a more real, dynamic, faster and with less experimental error system. Gaps found in the literature will boost the current thesis to create an ingenious and efficient monocolumn system.

Chapter 3

Single-column Analog with Recycle Lag

3.1 Introduction and Objective

Currently, liquid chromatography (LC) is the best and most used technique to purify biopharmaceuticals, often used in downstream processing (DSP). The most common type of chromatography used by the industry, chosen specifically because of its simplicity of use and installation, is single-column batch chromatography. This process generates three fractions: (1) a pure product fraction that elutes first, (2) an impure fraction and (3) another highly pure product fraction that elutes last, like those shown in Figure 3.1. The main disadvantage is the product loss in the impure fraction, since the purity must meet the requirements established by government agencies or the company itself.

To solve this problem, some processes were developed, particularly the Simulated Moving Bed (SMB) process and allied variants, that implement multicolumn continuous chromatography. As demonstrated in Figure 3.2, the continuous process captures the impure fractions by internal recycling and purifies them until the purity desired is achieved, with new feed being continuously or cyclically injected. As easily seen, this gives higher yields of purer product while being able to process much more feed and use significantly less solvent, increasing the overall throughput relatively to batch chromatography [95, 132, 174, 254]. This process was first patented in the 1960s [41] as a practical approach to the True Moving Bed concept, and simulates the countercurrent contact of the stationary phase with the mobile phase by moving the inlets (feed and desorbent) and outlets (extract and raffinate) with the help of a system of valves, carefully placed among the system [27, 230, 251].

A standard SMB unit is made up of identical chromatographic columns, organized in-line, so that the output of one column is connected to the input of the next column. The columns are arranged into four sections or zones, each performing a different function

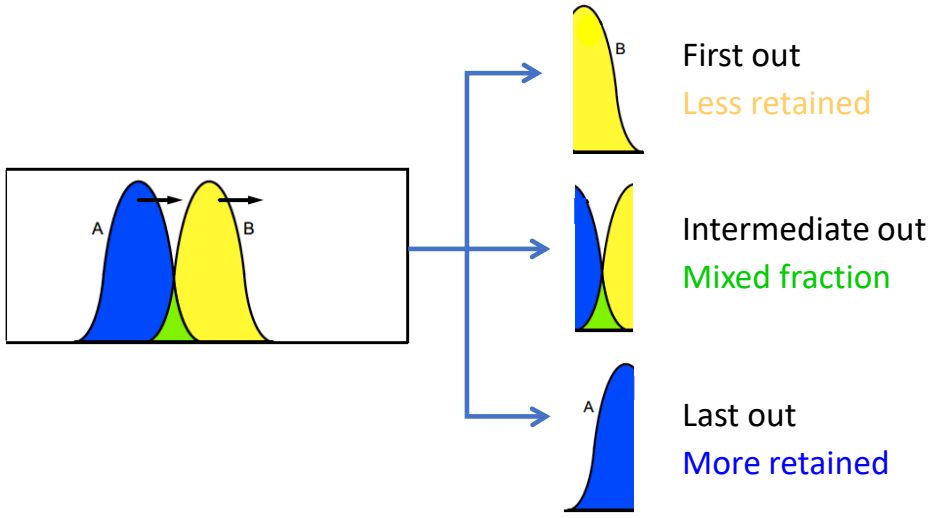

Figure 3.1: Outlet fractions of Single-column batch chromatography. The mixed fraction(s) is(are) taken out of the system.

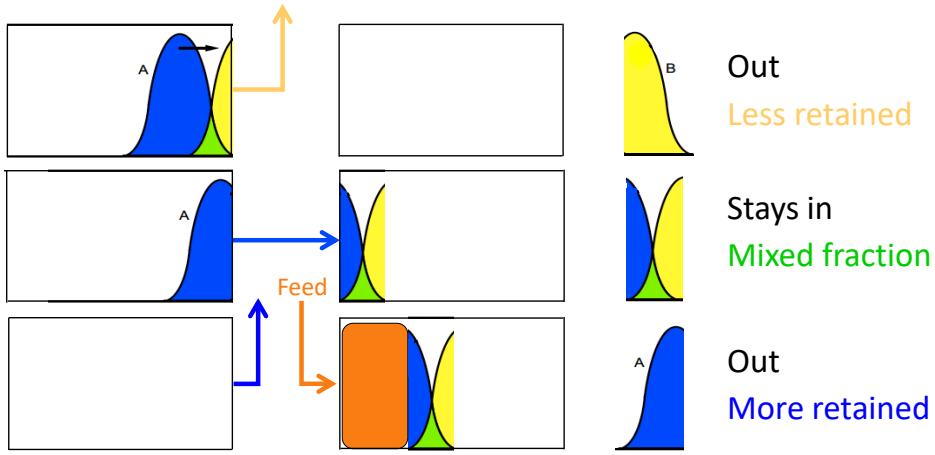

Figure 3.2: Output fluids of the Multicolumn continuous chromatography. The mixed fractions remain in the system, which move to the next downstream column.

and having one of two input streams at its upstream end and one of two output streams at its downstream end. Although the traditional process has four sections, there are other processes studied and presented in the literature with a reduced number of sections: for example, three sections [230, 281, 284], two sections [21, 128, 129, 161, 227, 228], or even systems similar to the SMB with only one chromatographic column [6, 7, 17, 176].

The SMB technology was first applied in the petrochemical and sugar industries, for large scale production [27]. However, as time passed, other areas started applying this process in their production lines, such as the fine chemistry and pharmaceutical industries, to separate and purify a wide variety of substances [133]. Especially in the pharmaceutical industry, SMB systems are used in a wide variety of steps, performing all kinds of separation in the production line in the development of a particular drug.

For the biopharmaceutical field, the two most important problems in operating an SMB process are: (1) assessing product quality and (2) mantaining a long-term, stable and controlled operation. For product quality, there are several strict constraints imposed by regulatory organizations, particularly the American FDA [74], which increased the necessity of having much better ways to control product quality. These ways usually pass through new configurations and operating schemes, much different from the conventional process [226], in order to obtain pure drugs [234]. Highly versatile SMB equipment is required for these new schemes [281], as well as advanced optimization tools [20, 68, 69, 132, 138, 261, 262] and robust control procedures [3, 146, 147, 150, 239]. With all of this in mind, a smaller number of columns is preferable, since less solid phase is required, less equipment is involved and the pressure drop is reduced. Therefore, although the SMB technology is traditionally defined as a system that comprises more than one column, it would be quite advantageous, practically and economically, to have a system analogous to a SMB process that has only one column.

For this to be possible, single-column batch chromatography could achieve many of the benefits of continuous chromatography through smart recycling of the mixed fractions. Actually, some works have been published regarding this theory [4, 7, 22, 176, 226] (Appendix A.1), but without any experimental exploitation of the analogy with the continuous multicolumn chromatography.

The explored concepts proved to be possible to mimic SMB processes with flexible systems using just a single chromatographic column obtaining relatively high purities, but many gaps exist on these concepts and there is still a lot to explore. Specifically, single-column systems were validated only through simulations (with the exception of one [225, 226]), i.e. without experimental proof-of-concept, and all reproduced binary or simple ternary separations (nucleosides separation) [5]. In addition to these gaps, the concepts that considered mixture between the impure fractions in the recycle tanks [6, 7, 143, 144] obtained processes with purity results still lower than the mimetized SMB and a large amount of equipment was necessary; while the concepts that considered to maintain the concentration profile of the fractions collected for recycle [4, 5, 17, 18, 22, 176, 225, 226] were only addressed through simulations, and/or limited to mimic only simple SMB processes, i.e. with few chromatographic columns [4, 5], or even without the objective of promoting separation of components from the mixture, but rather reproducing the cyclic stationary state of the mimetized SMB [18, 22, 225, 226].

The most comprehensive concept, proved to be capable of mimicking a wide range of SMB processes and that received greater relevance among the few single-column concepts already created was developed in 2005 by our research group [176]. This novel concept that comprises a novel single-column chromatography analogous to SMB demonstrated that by collecting the column outlet to a plug-flow device that produces a recycle lag of $(N-1)\tau$ time units, where N and τ are the number of columns and switch interval of the equivalent SMB process, the periodic state of the latter SMB can be reproduced. In theory, there is only one difference in comparison with the traditional SMB process, which is the

discontinuous use of the inlet/outlet ports. Although this has been approached in the literature, this concept was little explored, having been validated and studied only in the scope of simulation work.

3.1.1 Two-column Chromatography for Purification of Biopharmaceuticals

For a better understanding of the One-Column Analog system, it is convenient to work through an example, and the simplest one can think of in terms of number of columns is a two-column SMB. In chromatography, there are two modes of operation: positive and negative mode. In the first one, the product is retained in the stationary phase and the undesired impurities are eluted. One example of this operation is the mAb capture step on Protein A. On the other hand, in negative mode, the product flows through the stationary phase and impurities are retained on the resin. The intermediate flowthrough purification and polishing of virus and other large biomolecules on Capto Core 700 resin are examples of this operation mode.

These two operating modes can be applied to the basic cycle of a two-column SMB. Because the process has two columns, a full cycle can be divided into two equal half-cycles or switching intervals as they are known in the jargon. At the end of each half-cycle the column positions are exchanged and the steps are repeated all over. Hence, the process needs only to be explained by the first half-cycle, as shown in Figure 3.3. The plotted axial concentration profiles are those in the interparticle liquid phase inside the columns at the start of each step. The profiles have been normalized by the corresponding values in the feed.

Feed mixture is injected into the upstream column, which has been loaded with feed up to nearly breakthrough during the previous cycle. The outlet of the upstream column is directed to the inlet of the downstream column. The latter provides pure P2 (raffinate). At the end of step 1 the upstream column is fully loaded with mixture to a point where part of the mixture has broken through to the downstream column. In step 2 of the cycle buffer is injected to clean the interparticle fluid of the upstream column and displace it to the other column. The downstream column provides the P2 fraction. During step 3 of the cycle, P1 (extract) is started to be collected from the upstream column while at the same time feed starts to be injected into the other column. Thus, the upstream column provides pure P1, which can be purified mAb in the case of positive mode chromatography or viral impurities in the case of negative mode operation; during this step the downstream column still provides the P2 fraction. Finally, during steps 4 and 5 of the cycle the upstream column is washed and re-equilibrated while at the same time feed continues to be injected into the other column. The downstream column still provides the P2 fraction.

Steps 6 through 10 of the cycle make up the second half-cycle. They are the same as steps 1 through 5 of the first half-cycle but the positions of the columns are exchanged. At the end of these steps one full cycle is completed and the process is repeated.

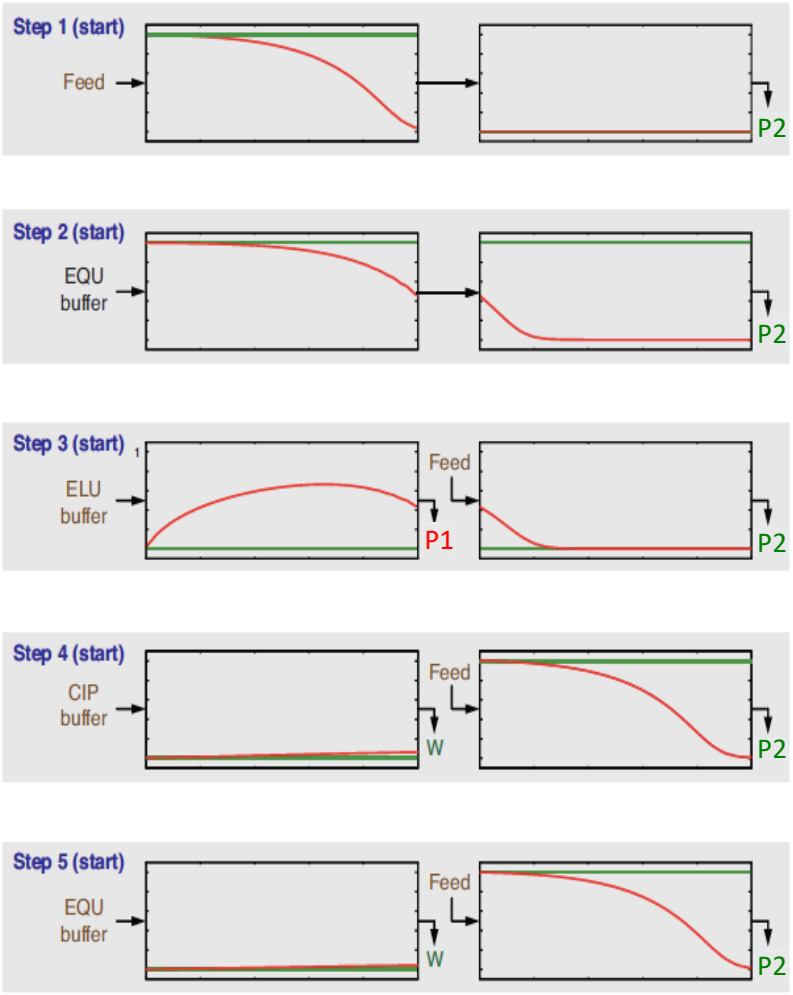

Figure 3.3: First half cycle of a two-column SMB process for capture or flowthrough mode. In positive mode: P1 (extract) = mAb (product), P2 (raffinate) = undesired impurities; In negative mode: P1 = undesired impurities, P2 = virus (product).

3.1.2 Objective

In this chapter we propose to implement the conceptual design of the chromatography unit for the "Single-column Analog with Recycle Lag" concept, the assembly of the respective laboratory prototype, and the study of the mathematical model of the proposed system. The objective is to fulfill the purpose of the concept previously developed [176] in order to develop a versatile setup for chromatographic processes using just one column, capable of mimicking the broadest range of SMB and derived processes, and to perform not only simple binary and ternary separations but also more complicated separations, i.e. those with overlapping peaks in the chromatogram.

3.2 Conceptual Design of the Purification Train

Our aim is to propose a significant change in the configuration of chromatographic processes, with the replacement of single-column discontinuous chromatography and multicolumn chromatography in continuous or semi-continuous operation by one-column chromatography in semi-continuous operation. To achieve this goal, the new purification process should combine the advantages of recycle chromatography, simulated countercurrent operation of the solid and fluid phases, and additional flexibility provided by the addition of solvent gradient.

The design for the new process was based on theoretical studies presented in the literature [17, 176], which demonstrated that the periodic state of the SMB process is reproduced by a single-column chromatographic process with a recycle lag of $(N-1)\times\tau$ time units, where N is the number of columns of the equivalent SMB unit and τ is the switching interval (time interval between consecutive switches of the inlet and outlet ports).

The operation of this ideal one-column process is formulated by drawing the schematic of the complete operating cycle of a multicolumn processes (say a process with N columns), then selecting an arbitrary column of the SMB and following its operation over a complete cycle. One important point to note is that, under cyclic steady state operation, the inlet stream of any given column of the multicolumn process, at an arbitrary instant t, can be reconstructed from its outlet stream at time $t-(N-1)\tau$. By cyclic steady state operation, we mean the periodic operation of the unit after the initial transient cycles have died out and the process behaviour is replicated from cycle to cycle. Finally, the mixed fractions exiting the single-column chromatography are saved and reused according to the following scheme: they are recycled with a lag in time of $(N-1)\tau$.

Figure 3.4 shows the basis for the one-column analog via the example of how to convert the process of the two-column SMB into the single-column process. The figure shows a complete cycle, with the steps of the first half-cycle shown on the left hand side and those of the second half-cycle shown on the right hand side. Firstly, one column needs to be selected at random (in this case, the first column was chosen) and its operation followed during a complete cycle. Then, it is required to track at each step of the cycle where the outlet stream of the column is required to reconstruct the inlet stream. For example, the outlet in step 1 of the cycle will be reinjected into the column in step 1 of the next half-cycle, and the same happens with the outlet of the column during the second step of the cycle where this fraction will be reinjected into the column during the second step of the next half-cycle. During the other steps of the cycle the outlet stream is collected as product or discarded as waste; so it will not be used later on in the process. Getting back to the beginning of the cycle, the fraction coming out of the column during the first step of the cycle is collected by the newly developed device, just like the fraction coming out of the column during the second step of the cycle, keeping in mind that there is a previous fraction that must be kept ahead of the one currently collecting. Next, steps

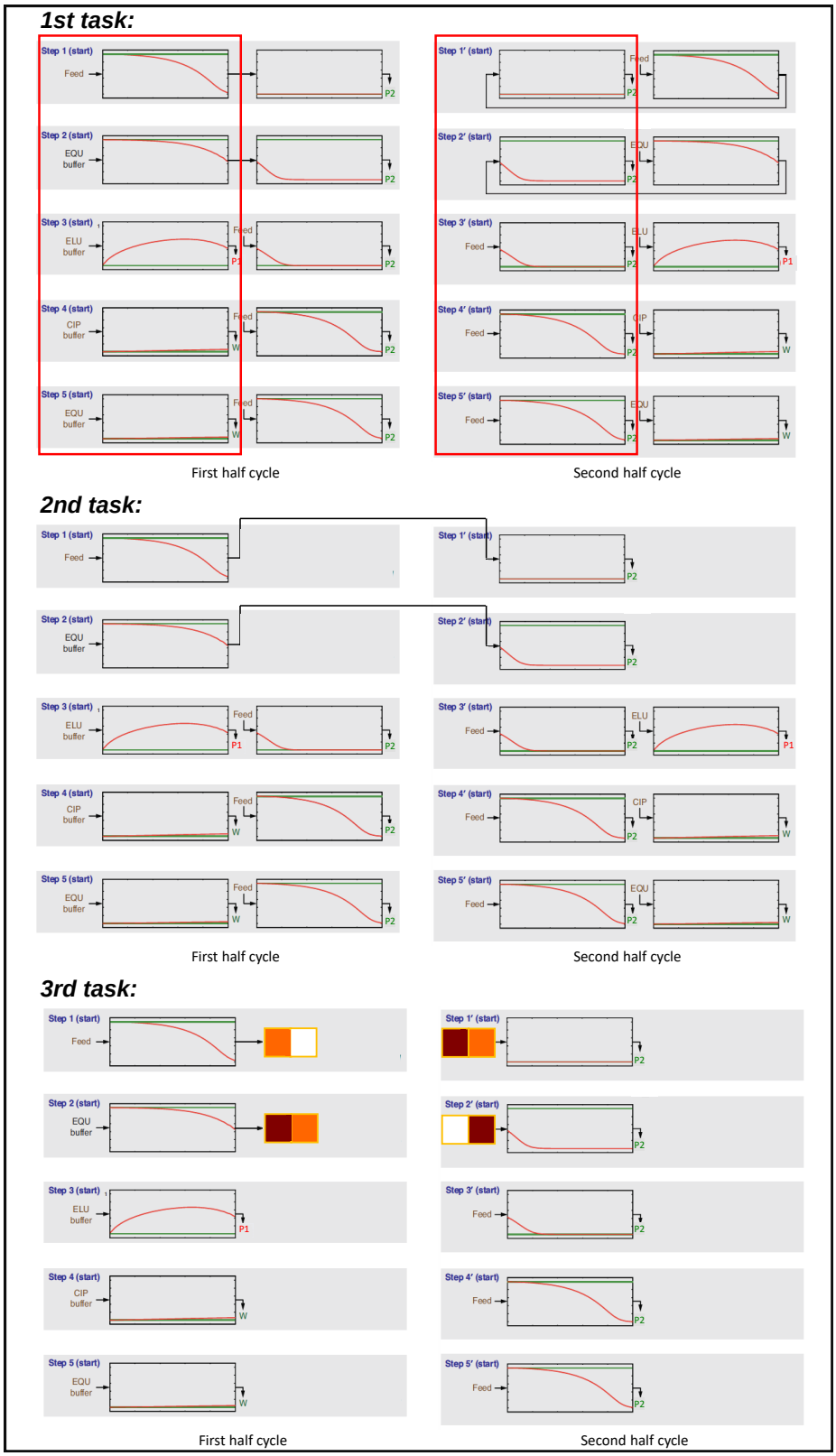

Figure 3.4: Recipe for the One-Column Analog. 1st task: A column is selected at random; 2nd task: The steps of the cycle where the outlet stream of the column is required to reconstruct the inlet stream are selected. 3rd task: The fraction coming out of the columns are collected in sequence and reinjected to the other columns at the same sequence.

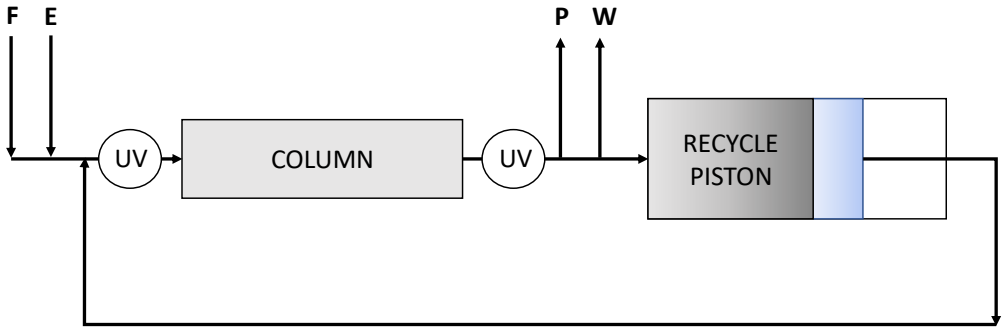

Figure 3.5: Conceptual sketch of the novel one-column analog system. The process has one chromatografic column with UV detectors immediately before and after it, and a recycle device to collect fractions from the column. The product and waste exit occurs between the column and the piston. F, E, P and W are, respectively, feed, eluent, product and waste streams.

3, 4, and 5 of the cycle are carried out, producing pure product and discarding the waste fractions. After this, the second half-cycle starts and the first fraction collected at the beginning of the previous half-cycle is reinjected into the column (in the figure this is the fraction colored in orange). During the second step of the half-cycle, the second fraction which was stored previously, is reinjected while the outlet of the column is discarded to waste. Lastly, these steps keep repeating as many times as necessary.

To summarize the procedure, the one-column process operates by recycling mixed fractions back to the inlet of the column with a lag in time. The conceptual sketch of the new process is represented in Figure 3.5, which consists of a chromatographic column and a new device to promote recycle, connected to each other by automatic valves, which also allow the entrance of feed and eluent and the exit of products and waste. In our experimental prototype the concentration profiles are obtained by measuring the absorbance values, thanks to the presence of in-line UV detectors right before and after the column.

The recycle lag is implemented, in practice, by means of a special type of plug-flow tube that includes a moving piston to compensate for the difference between inlet and outlet flow rates. The proper operation of the inlets and outlets of such device implements an approximate "first in, first out" method for organizing and manipulating the fractions of fluid collected from the chromatographic column, where the oldest (first) amount of fluid, or 'head' of the fraction, is the first to exit the plug-flow tube. This is necessary because the recycle lag is not a multiple of the overall cycle duration. This recycle device should avoid, as much as possible, fluid mixing and deviations from plug-flow of the fluid therein.

Several aspects regarding the new process should be highlighted before assembling it:

- The use of no more than one chromatographic column is a prerequisite to define the

system as innovative, since the conceptual design craved the substantial reduction of stationary phase volume for continuous systems, aiming at an economical set-up and allowing a reduction in overall pressure drop. The use of smaller number of chromatographic columns also makes easier and faster to clean the system and switch from one mixture to another, since only one column needs to be repacked;

- More and more compact installations are developed by the competitive market, so the new system should contain as few equipment as possible, having a compact and simpler design without losing its versatility (i.e. capability to mimic, with this design, different variations of the SMB and other countercurrent multicolumn processes existing in the literature). Therefore, the overall dead volumes must be reduced to the maximum and the amount of equipment (liquid pumps and valves) must be optimized in order to have the most compact and versatile set-up possible;
- The process must operate in a stable, reproducible manner. Although the reduction of the number of columns already helps in this respect, the process automation is crucial to carry out the experimental procedures, in order to instantly (in-line) measure the variables of the system;
- In order to successfully mimic different chromatographic processes, from simple to more complicated separations, as center-cut separation cases, a wide variety of operating steps is required and must be in perfect working order. Each step needs to be taken into account in order to build the apparatus;
- In order to increase system flexibility and avoid operational errors, the liquid pumps must be able to operate in continuous mode, doing recycle to the respective feed tank when the corresponding solution is not being injected into the operating system. In addition, the continuous operation of the eluent pump allows the operation of the device (piston) without the need to implement an extra pump in the setup.;
- As the recycle device should avoid as much as possible axial dispersion and mixing of the fluid inside it to ensure that the conceptual design is being applied, the "first in, first out" method is crucial to this process and experiments are required to ascertain the operation of this method.

3.3 Assembly of the Experimental Setup

3.3.1 Recycle Device

The device consists of a column with a fluid distribution system at the top, a closed end at the bottom with three inlets/outlets, and a movable piston with a fluid collector at the top surface. The fluid collector is connected to the closed end of the device by a flexible tube. It is important to emphasize that it is not the chromatographic column but rather the piston-type device that implements an approximate "first in, first out" method.

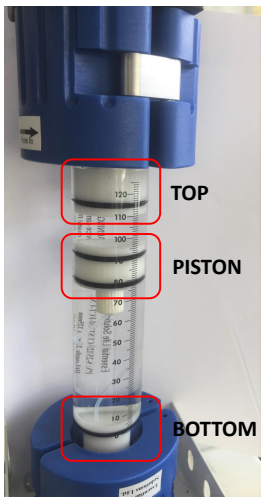

(a) Recycle device.

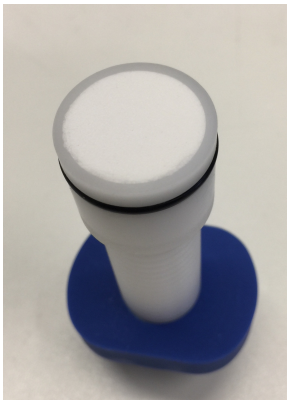

(b) Top with fluid distributor.

(c) Movable piston.

Figure 3.6: Piston-type device utilized for the One-column analog to SMB. (a) Complete recycle device. The device consists of a column with a fluid distribution system at the top, a closed end at the bottom with 3 inlets/outlets, and a movable piston with a fluid collector at the top surface. The fluid collector is connected to the closed end of the device by a flexible tube. (b) Top of recycle device with the distribution system made of polyethylene (porosity: 20μm). (c) Movable piston with polyethylene frit and a fluid collector at the top, and an outlet for the flexible tube (1/16") at its bottom.

The prototype (Figure 3.6) was built from a modified SNAP column from Essential Life Solutions Ltd (USA), made of borosillicate glass, with dimensions of 25 mm for internal diameter (ID), internal height range of 0–125 mm, maximum pressure of 24 bar, temperature range of 4–40°C and tubing connections of 1/16". The upper and lower cover, as well as the movable piston are in teflon, and the o-rings, which ensure the seal between the two internal sections of the piston, are made of ethylene propylene diene monomer (EPDM) material. The flexible tube that passes through this piston and connects to a 2-position-6-port valve has 35 cm, so that the length of the part that lies inside the piston is 12.5 cm. Two polyethylene frits, with external diameter (OD) of 25 mm and porosity of 20 μm, produced by YMC Europe GmbH (Dinslaken, Germany), are coupled at the top surface and up side of the movable piston, respectively, to ensure that there is radial distribution of the fluid concentration and to avoid possible preferred paths, while helping in decreasing the generation of pressure drop in the system.

The piston-type device has two main settings, as shown in Figure 3.7. In the left-hand side schematic fluid injected into the top of the device is stored in section A by forcing the piston to move downward and the excess fluid in section B is redirected to the tank from where it was first pumped. The pump that injects fluid into section B is typically an eluent pump that is used to inject the eluent into other parts of the process. Thus, no extra pump is required. In the configuration in the right-hand side, the fluid injected into section B by the pump forces the piston to move upward and the excess fluid in

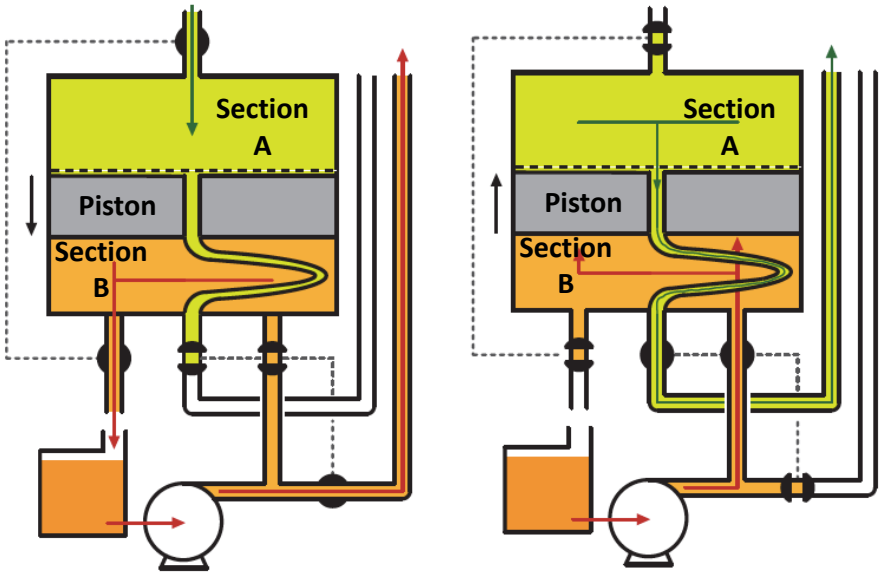

Figure 3.7: Main piston operating configurations. At left one, movable piston is moving down while collecting fractions from column. In configuration on the right, the movable piston is going up while the fluid is being reinjected to the column following the "first in, first out" method.

section A is redirected via the collector and flexible tube to the inlet of the column. This implements an approximate "first in, first out" method.

After the need to assemble and disassemble the piston several times, it was noted the need to create a protocol of the best way to assemble the piston, thus avoiding errors and difficulties. This protocol is described in Appendix A.2.

3.3.2 Purification Unit

After having mastered the process, the installation scheme was designed in several steps until the most appropriate prototype design, shown in Figure 3.8, was obtained. In this schematic F, E, P, W, R are the feed, eluent, product, waste, and recycle streams (it comes out of the piston in direction to the column inlet), respectively; COL, RP, UV_i, V_i refer, in this order, to the column, recycle piston, UV detector and on-off valve apparatus; The 2-position-6-port valves are represented by the circles with their fluid passage position inside, which can be A, B, IN (fluid injection to the column) or BY (fluid bypassing the column); COM_i is the communication port responsible for making each equipment to be identified by the computer.

The current prototype for the one-column analog to SMB was built with a series of instruments. It essentially contemplates three Knauer (Berlin, Germany) pumps: one V5010 S100 Smartline pump, denominated *Pump F*, for injecting fresh feed into the chromatographic column and two HPLC K501 pumps, one for injecting fresh eluent or solvent into the process, denominated *Pump E*, promoting elution of the separating mixture, and

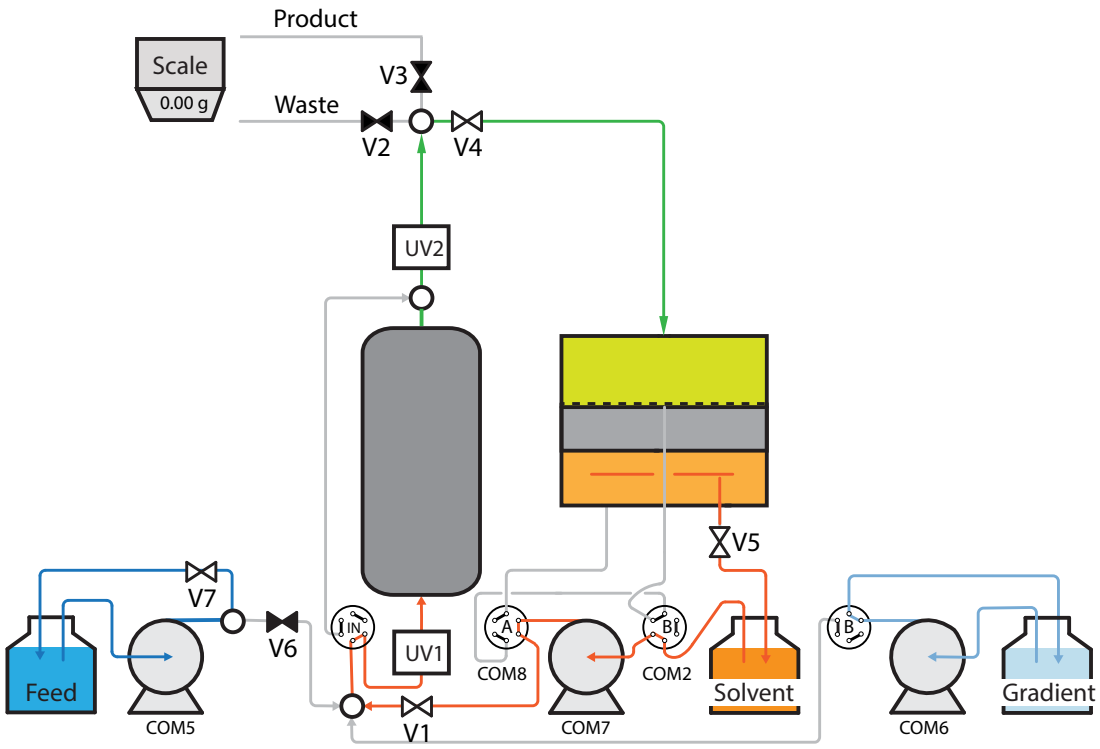

Figure 3.8: Schematic of the Single-column with Recycle Lag setup. The unit uses one chromatographic column, the recycle device, three liquid pumps, two UV detectors, seven one-way valves and three 2-pos/6-port valves, beyond an digital scale. The layouts were created in the Adobe Illustrator image editor.

another to generate concentration gradients in the process, if necessary, denominated *Pump G*; all with 10 mL pump heads, operating pressure range of 0–40 MPa (0–400 bar), and controlled via RS232 communication protocol. If required, the pumps can run continuously, even when they are not injecting the stream into the chromatographic column. This means that, when pumps are not pumping fluid into the system, they are promoting fluid recycling to their own source tank.

The setup still has two multi-wavelength UV detectors (two UV cells from Icon Sci., United Kingdom, each one linked to USB2000 or USB4000 Spectrometer from Ocean Optics, USA), located immediately before and after the chromatographic column, connected with a DH-2000-S-DUV light source (Micropack, Ostfildern, Germany), which has Deuterium and Halogen lamps, ensuring absorbance readings in a broad range of wavelengths. The presence of UVs provides the inline reading, instantaneously to the fluid passage, generating the chromatogram of the experiment, allowing to identify the cycle zones, or the time intervals, in which the compounds are separated and therefore to measure the purity of the flowing fluid.

The operation of the setup is manipulated via seven one-way (i.e., on/off) valves, one manually-actuated 2-position 6-port valve (VICI Valvo, Schenkon, Switzerland) to

manipulate the fluid path, by bypassing the chromatographic column or by passing through the column depending on the experiments to be performed. There are still two electrically-actuated, 2-position 6-port/3-channel-injection valves from Valco International (Schenkon, Switzerland). The one-way valves are model SFVO, with pneumatic actuation, and each valve is automated by means of a single computer-controlled three-way solenoid: application of 50 psi opens the valve; venting the air allows the spring to return the valve to the closed position [228].

Although the flow path configurations based on one-way valves are very flexible, their assembly tends to be bulky because an on-off valve has only two positions: open, which allows the fluid to flow through; and closed, which blocks the fluid flow. In this way, although the 2-position-6-port valves also switch between only two positions, each position is more flexible than those of the simpler one-way valve, allowing a combination of injection valves and thus making the feed and eluent pumps to operate continuously over the cycle. The simplest way to do this is to redirect the pumped fluid back to the feed and eluent tanks, respectively, during the sub-steps in which these pumps are supposed to be turned off.

Two OptoRLY88 relay boards (Robot Electronics, United Kingdom) are used to signal the pneumatic actuators of the different on-off valves of the setup. Each relay board supports eight valves, so although two boards are installed (connected to a total of sixteen on-off valves), only one is required to operate the seven pneumatic valves currently necessary by the setup. This allows, if necessary, possible future changes to the prototype scheme to be easily performed. The diagram explaining the relationship between relays and pneumatic valves is provided in Appendix A.3.

Since a generic process is desired, applicable to the purification of different biomolecules, the chromatographic column type used varies according to the separation to be processed with the setup. The recycling device has already been described in the previous section.

All equipments are connected through ETFE tubing (Upchurch Scientific, Germany), with 1/16"OD and 0.040"ID, through which mixtures and other solutions travel. ETFE capillaries support operating temperatures up to 80 ºC and are suitable for pressures up to 276 bar, being a highly resistant material for the application it was employed. The capillaries have been connected with care to minimize system dead volume, so the shortest possible tube lengths were used to assemble the prototype. The connectors used to link capillaries and equipments were PEEK finger-tight fittings (ACE, Scotland), with pressures rated to 350 bar.

Product and waste collection containers are positioned on a monolithic digital scale, model TE3102S (Sartorius AG, Germany), which allows to calibrate the pumps prior to the experiments, as well as to verify the real pump flow rates during the experiments, making the setup operating conditions more accurate, measuring the amount of raffinate and extract yielded during the separation process.

It is worth mentioning the use of 8-port RS-232 PCI board (Moxa, China) installed on

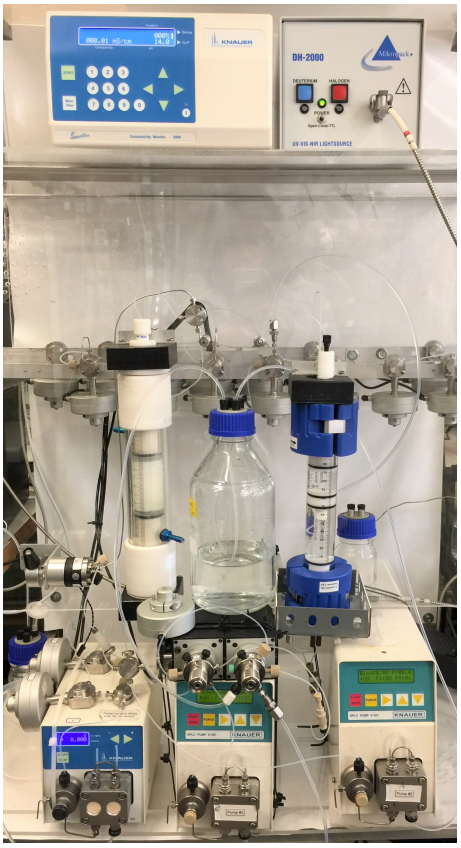

Figure 3.9: One-column with Recycle Lag prototype. Its installation was carried out in the Laboratory of Adsorption Technology and Process Engineering (Chemistry Department, FCT-UNL, Portugal).

the computer to allow communication with the RS232 connectors present on pumps and 2-position valves. The rest of the instruments, the OptoRLY88 relay boards and USB2000 and USB4000 Spectrometers, are linked with the computer via USB 2.0 B connectors.

The final result of the laboratory prototype is shown in Figure 3.9. The constituent components of the prototype, their respective technical specifications and drawings, the possible suppliers and the suggested prices are given in Appendix A.4. The estimated overall cost of the setup is around 33930.00 €, disregarding the chromatographic column and resin used, since these two items vary according to the separative process to be mimicked. Although not accounted for the budget, the column and resin data used for the next chapter are also present in the Appendix A.4.

3.3.3 Automation of Prototype Operation

Economic transformations require companies to adapt quickly to the market to keep their businesses competitive, and thus have to adapt to broad digital transformation policies, changing work tools and internal strategies [42]. For this reason, one of the most followed path is process automation, so when it comes to the development of new machinery, it is essential that its operation be as autonomous as possible, that is, that human intervention

during operation cycles be minimized to the extremely essential.

The creation of a computational interface of operation, that is, of process automation, brings several benefits, among them:

1. It allows you to streamline the process, saving time, so that there are no operating intervals between steps and therefore increases productivity;
2. It avoids human operational errors, as it is more accurate;
3. It reduces operating costs, as employees become more productive by taking advantage of process automation;
4. It integrates data, as all experimental information is concentrated in one place, allowing easy access to data;
5. It integrates systems, allowing easy transfer to other software, such as software for analyzing these data;
6. It also makes process reproducibility more reliable, as it substantially reduces the error rate.

Taking this in consideration, all the Single-column Analog setup is fully automated and driven by an in-house developed automation system using *Julia* software, initially written for version 0.7.0 and recently upgraded to version 1.2.0. *Julia* is a very powerful and versatile programmimg language for technical computing and is open-source. Because of that, special modules with different functions were created by J. Antunes and J.P.B Mota [16], later joined by T. Santos, specifically to work in the Laboratory of Adsorption Technology & Process Engineering (LATPE, FCT-UNL Lisbon, Portugal) with the new chromatographic system, aiming to facilitate the interaction between each instrument and for realization of experiments in an automatic way, selecting only the sequence of cycle operation, and for analysis of several experimental data. Thus, the prototype has In-Line & Real-Time bioprocess monitoring, with the following key features:

1. Real-time display of Chromatograms (Absorbance (AU) x Time (s)), Intensity Spectrum (Light intensity (pixels) x Wavelength (nm)) and Absorbance Spectrum (Absorbance (AU) x Wavelength (nm));
2. Easy calibration of pumps' flowrates, due to the presence of functions that take equipments information, in this case the weight information on the scale. The pumps calibration protocol is expressed in Appendix A.5;
3. Simplicity in setting instrument operating parameters, such as pump flowrate;
4. System protection against too high pressure drop. The computational program stops the operation of the pumps as soon as they reach unwanted pressure, previously indicated by the operator of the set-up, which ensures that the installation will not suffer damage;

5. Ease of operation through pre-implemented cycle steps, operating through easy-to-understand macros;

6. Easy data handling: acquisition/recording of experimental reference data for later data analysis in external software.

The command line interface (CLI) created and used to run the experiments is called *ChromatographyStudio.jl* (see Figure 3.10), a versatile program that allows process automation and data acquisition. This main module calls all the others programs required for this project (the explanation of each one can be found in [16]), assisting with the coordination between devices and different functions. Annex I shows a briefly diagram of the programs created to work with this interface.

The most commonly used macros, i.e. codes placed on the interface that serve as commands for system operation, as well as a brief exposition of their corresponding function, are present in Table 3.1, as a usage protocol format for potential users. The commands were designed (by the present author and interface's authors) to be clear, simple to understand, for any operator who needs to use them.

Table 3.1: Protocol of mostly used `macros` in *ChromatographyStudio.jl*. The action of each command is explained in this protocol, serving as a help to the program user. (E = Eluent; F = Feed; G = Gradient; R = Recycle Piston).

Command	**Action**
`julia7`	Starts *Julia* software, version 0.7.0.
`using ChromatographyStudio`	Starts the program created for the system's operation.
`cal=calibrate_pump (pump_Z,bal,[FLOW`$_1$`, FLOW`$_2$`, ...])`	Pumps the selected pump, collecting 5 measurements for each chosen flow. Z = E, F or G; $FLOW_i$ = pump flowrate (mL/min).
`cal.fit[4].p)`	Gets the four coefficients of the calibration equation (a fourth-degree polynomial function).
`cal.fit_inv[4].p`	Gets the four coefficients of the inverted calibration equation.

(Table 3.1 – continued on next page)

Command	Action
`@step Y=>COL=>Y'`	Sets the pathway of the system's fluid by turning valves ON/OFF and/or changing valves position A/B. Y = E, F, G, R or E+F; Y' = P, W or R.
`@pump Z = VALUE`	Sets the value of the flow for the selected pump. VALUE = flow rate (mL/min).
`@pump Z PMAX = VALUE`	Sets the maximum pressure for the selected pump. VALUE = max. pressure (bar)
`get_pump(pump_Z; :P)`	Gets the current pressure for the selected pump (bar).
`@valve +V`$_i$	Turns ON the selected valves. i = 1, 2, up to 7.
`@valve +all ;`	Turns ON all the valves.
`@valve -V`$_i$	Turns OFF the selected valves.
`@valve -all`	Turns OFF all the valves.
`uv1.uv.po.integration_time _micros(VALUE)`	Sets the integration time. VALUE = integration time (μs).
`@uvc A set=dark`	Sets the value of the UV when the Deuterium and Halogen lamps are closed. All `@uvc A` commands also work with the other UV cell, `@uvc B`.
`@uvc A set=ref`	Sets the reference value of the UV absorbance when the Deuterium lamp is open and passing the reference solution.
`@uvc A plot=[I]`	Plots the Intensity Spectrum (Light Intensity (-) x Wavelength (nm)).
`saveintensityspectrum(uv1, "Experimental Data\\FileName.tsv")`	Saves the Intensity Spectrum.

(Table 3.1 – continued on next page)

Command	Action
`@uvc A wavelengths=[VALUE$_1$, VALUE$_2$, ...]`	Sets the selected wavelengths whose absorbances will be measured and plotted. VALUE$_i$ = wavelengths (nm)
`@uvc A plot=[A]`	Plots the Absorbance Spectrum (Absorbance (AU) x Wavelength (nm)).
`save_absorbances(uv1, "Experimental Data\\FileName.tsv")`	Saves the absorbance spectrum.
`@uvc A monitor=all`	Measures and saves the absorbances values (AU) of all wavelengths vs time (s).
`monitorAbsorbance(uv1,"")`	Plots the Chromatogram with the selected wavelength(s) (Absorbance (AU) x Time (s)).
`@uvc A plot=all`	Plots three graphs: Intensity Spectrum; Absorbance Spectrum and Chromatogram .
`monitor_balance(bal,TIME)`	Measures, saves and plots the weight values (g) of the scale *vs* time(s), and plots the corresponding flow rate(mL/min) vs time(s). TIME = time interval (s) for each measurement.
`@monitor file = "Experimental Data\\FileName.mon"`	Monitors the complete experiment (@pump, @step, @valve, @uvc commands, Chromatogram values, Scale values), saving the acquired data in a created FileName.mon file.
`include ("Experimental Routines\\ FileName.jl")`	Runs a personalized script, executing every command with the desired time.
`@monitor stop`	Stops the monitorization of every command and data acquisition, finalizing the created FileName.mon file.

(Table 3.1 – continued on next page)

Command	Action
`@mon_to_tsv "Experimental Data\\FileName.mon"`	Changes the file extension of FileName.mon from .mon to .tsv, allowing the data analysis of all the data.
`exit()`	Shuts-down the Julia software, automatically setting all pump values to zero and closing all ON/OFF valves.

3.3.4 Implemented Steps

The setup implements a broad range of system configurations, demonstrated in Figure 3.11, that give rise to a lot of different steps: fresh feed, fresh solvent, and fresh gradient can be injected while storing the outlet fractions of the chromatographic column into the recycle device; fresh feed, solvent or gradient can be injected while producing one or more product fractions or waste fractions; steps can be done by admixing feed, solvent, or gradient with one or more fractions from the recycle device in open-loop or closed-loop operation; or the setup can even operate in completely closed-loop, i.e. with no solution added or fluid withdrawal, just recirculating system streams.

In conjunction with the definition of the steps to be implemented in the system, the positions of on-off and switching valves were rigorously studied in order to set up as few valves as possible for the system. The positions of the valves are described in Appendix A.6.

All steps have been implemented in *Julia*'s software so that it is not necessary to select which valves should be open or closed, i.e. when selecting the desired step, the path that fluid must travel is already determined. This noticeably facilitates the operation of process cycles, as well as avoiding human and experimental errors and saving time when performing experiments. The default settings do not limit prototype versatility as it is easily possible to implement new operating steps directly from the command prompt on the computer.

The implemented commands generate the following prototype responses, and the schematics for all these implemented configurations are presented in Appendix A.7, demonstrating the path that fluid should take in each step:

- `F+R => COL => R`: Feed (F) is pumped by pump F to the chromatographic column (COL). At the same time, the column is also receiving mixing fractions from the recycle device (R). The fluid at the column outlet is directed to the recycling device. As there is constantly flow entering the system and no fluid is being collected, the piston is forced down. This is only achieved because the section B outlet is open

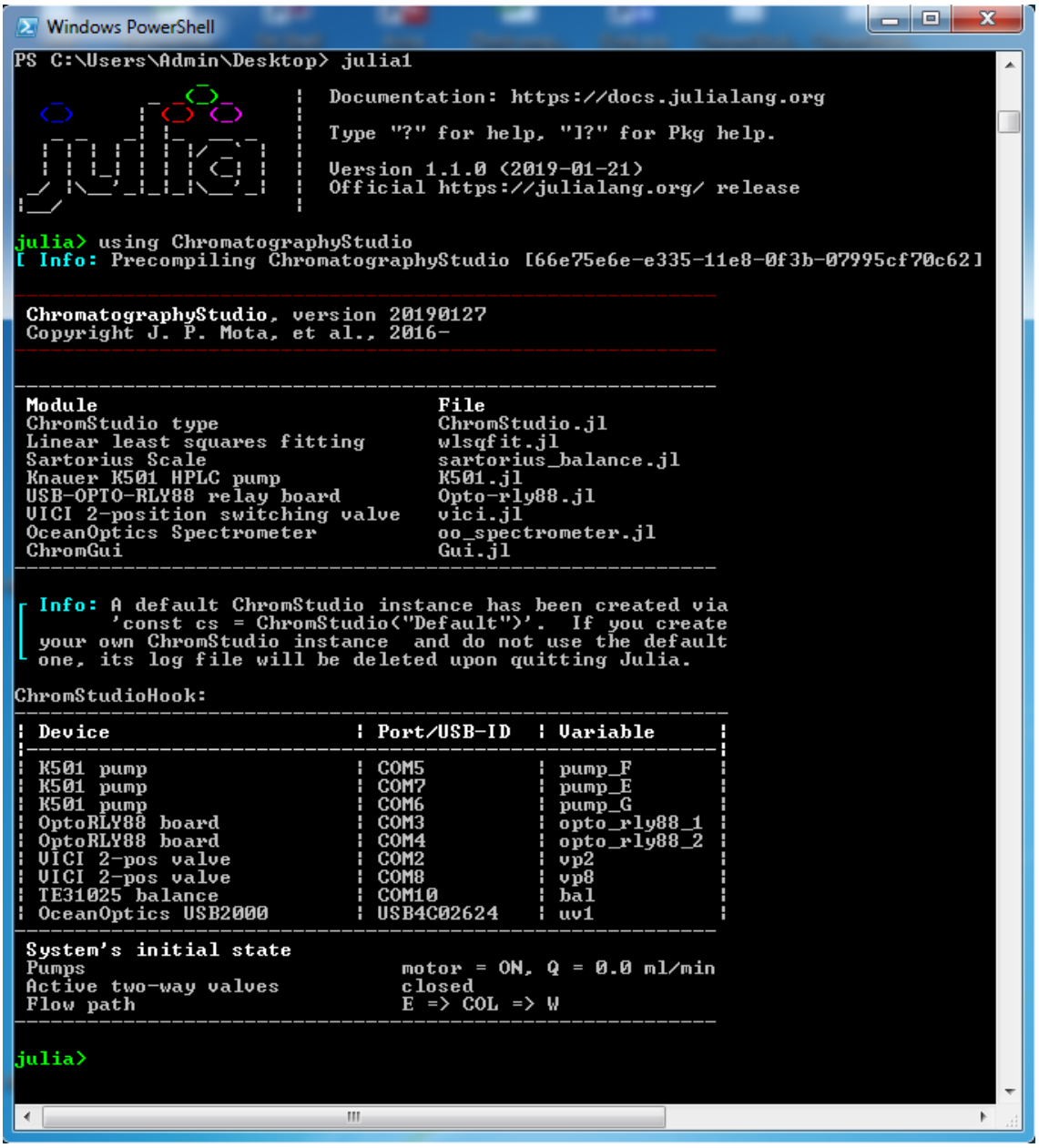

Figure 3.10: *ChromatographyStudio.jl* command line interface. Print-screen taken from the program as it starts, which shows the secondary modules that the main program calls, the devices controlled by this central module and their respective input ports, as well as the system's initial state.

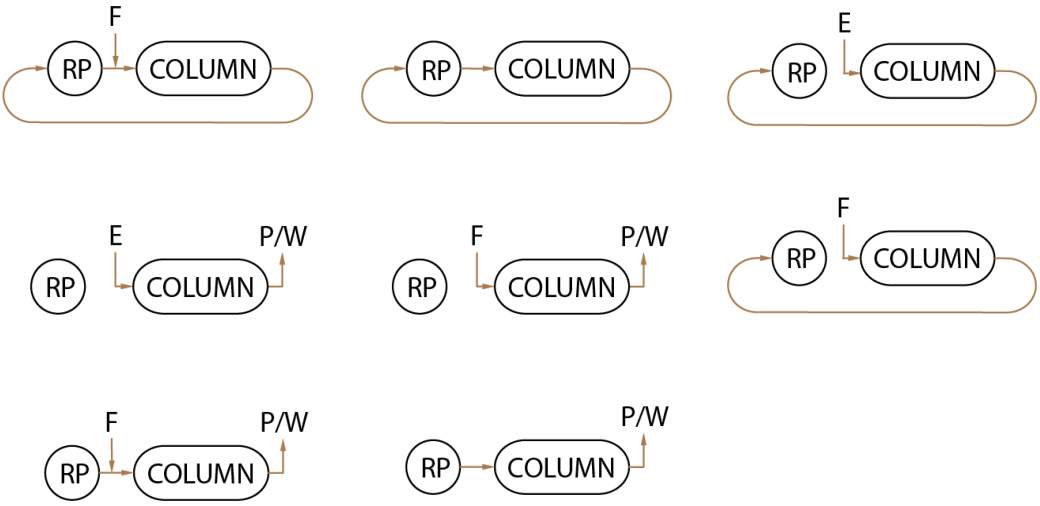

Figure 3.11: All implemented steps of the novel Single-column chromatographic process. The configurations were implemented on *Julia*'s software, allowing system automation.

allowing the eluent of this section to be redirected to the solvent tank. This is a case of closed-loop recycling with feed injection (Figure A.5);

- `R => COL => R`: The mixing fractions of the recycle device (R) are redirected to the chromatographic column (COL), and the column outlet fluid is again directed to the recycle device, providing a case of closed-loop operation, thanks to pump E operation. In this case, the piston is static (Figure A.6);

- `E => COL => R`: Eluent (E) is pumped by pump E into the chromatographic column (COL) until the recycling device (R), where fluid is stored, forcing the piston to go down as it receives the fluid fractions. For this to happen, while fluid is being received from section A of the device, the existing eluent from section B is redirected back to the eluent tank at the same flow rate (Figure A.7);

- `E => COL => P` or `E => COL => W`: Eluent (E) is pumped by pump E into the chromatographic column (COL) and the fluid is collected as product (P) or waste (W), with the collector located on top of the weight scale (Figure A.8);

- `F => COL =>P` or `F => COL =>W`: Feed (F) is pumped by pump F into the chromatographic column (COL) and the fluid is collected as product (P) or waste (W), with the collector located on top of the weight scale (Figure A.9);

- `F => COL => R`: Feed (F) is pumped by pump F into the chromatographic column (COL) until the recycling device (R), where fluid is stored, forcing the piston to go down as it receives the fluid fractions. Thus, the section B outlet is open to direct the eluent therein to its respective tank (Figure A.10);

- `F+R => COL => P` or `F+R => COL=> W`: Feed (F) is pumped by pump F to the chromatographic column (COL). At the same time, eluent is pumped by pump E to section B of the recycle device (R), while the inlet at the top of the device is closed, forcing the piston to rise and thus forcing fluid to flow from section A through the flexible tube to the chromatographic column . The fluid exiting the column is then collected as product (P) or waste (W) (Figure A.11);

- `R => COL => P` or `R => COL => W`: Eluent is pumped by pump E to section B of the recycle device (R), while the inlet at the top of the device is closed, forcing the piston to rise and thus forcing fluid to flow from section A through the flexible tube to the chromatographic column (COL). In this step product (P) or waste (W) is collected, with the collector on the digital scale (Figure A.12).

3.4 Revisiting the theory

Let Ω_j be the operator that advances over a switching interval the state of the chromatography column in position j relative to the locations of the inlet/outlet ports of the SMB unit. Consider, for example, what happens over the kth switching interval from instant $(k-1)\tau$ to $k\tau$, where τ is the duration of each switching interval. For this purpose let τ_k stand for $t = k\tau$, i.e., the end of the switching interval, and T_k the interval $(k-1)\tau < t \leq k\tau$, i.e., its duration; the start of the switching interval is simply τ_{k-1}.

Using this notation the operator Ω_j can be symbolically represented as

$$(C_j^{\text{start}}, C_{j-1}^{\text{out}})|_k \xrightarrow{\Omega_j} (C_j^{\text{end}}, C_j^{\text{out}})|_k. \tag{3.1}$$

That is, given initial conditions $C_j^{\text{start}}|_k$ for column C_j at τ_{k-1} and outlet conditions $C_{j-1}^{\text{out}}|_k$ for the upstream column connected to C_j during T_k, which together with other external inputs specific of Ω_j define the inlet conditions for C_j during T_k, Ω_j advances the state of C_j from $C_j^{\text{start}}|_k$ to $C_j^{\text{end}}|_k$ and computes the outlet conditions $C_j^{\text{out}}|_k$ for C during T_k.

Using Ω_j the operation of the SMB unit can be defined as follows:

$$C_j^{\text{start}}|_k = C_{j+1}^{\text{end}}|_{k-1}, \quad (C_j^{\text{start}}, C_{j-1}^{\text{out}})|_k \xrightarrow{\Omega_j} (C_j^{\text{end}}, C_j^{\text{out}})|_k. \tag{3.2}$$

This operation is represented in the schematic of Fig. 3.12.

Under cyclic steady-state (CSS) conditions C_j is τ-periodic, ie, its state is repeated every τ time units:

$$C_j|_k = C_j|_{k'} \quad \forall\, k, k' \in \text{CSS}. \tag{3.3}$$

Hence, under CSS conditions $C_{j+1}^{\text{end}}|_{k-1}$ in the previous equation can be replaced by $C_{j+1}^{\text{end}}|_k$ to yield the following equation:

$$C_j^{\text{start}}|_k = C_{j+1}^{\text{end}}|_k, \quad (C_j^{\text{start}}, C_{j-1}^{\text{out}})|_k \xrightarrow{\Omega_j} (C_j^{\text{end}}, C_j^{\text{out}})|_k \quad \forall\, k \in \text{CSS}. \tag{3.4}$$

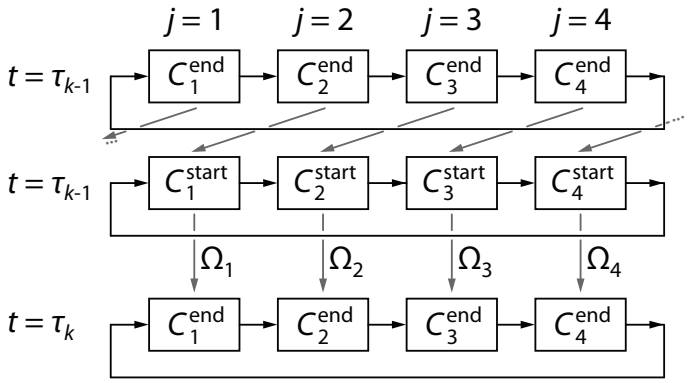

Figure 3.12: Schematic representation of SMB operation.

But given that under CSS conditions the dynamics of the switching intervals are all identical (they are τ-periodic), we can even drop the k subscript in the previous equation to get

$$C_j^{\text{start}} = C_{j+1}^{\text{end}}, \quad C_j^{\text{start}}, C_{j-1}^{\text{out}} \xrightarrow{\Omega_j} C_j^{\text{end}}, C_j^{\text{out}} \quad \text{(CSS)}, \tag{3.5}$$

or, enumerating for the N positions,

$$C_1^{\text{start}} = C_2^{\text{end}}, \qquad C_1^{\text{start}}, C_N^{\text{out}} \xrightarrow{\Omega_1} C_1^{\text{end}}, C_1^{\text{out}} \quad \text{(CSS)}, \tag{3.6}$$

$$\dots \tag{3.7}$$

$$C_j^{\text{start}} = C_{j+1}^{\text{end}}, \qquad C_j^{\text{start}}, C_{j-1}^{\text{out}} \xrightarrow{\Omega_j} C_j^{\text{end}}, C_j^{\text{out}} \quad \text{(CSS)}, \tag{3.8}$$

$$\dots \tag{3.9}$$

$$C_N^{\text{start}} = C_1^{\text{end}}, \qquad C_N^{\text{start}}, C_{N-1}^{\text{out}} \xrightarrow{\Omega_N} C_N^{\text{end}}, C_N^{\text{out}} \quad \text{(CSS)}. \tag{3.10}$$

This set of equations is perhaps the best to define the CSS behavior of an SMB unit.

If a particular column, say the one that happens to be in position N at the start of a cycle—a sequence of N consecutive switching intervals—is followed over a complete cycle, it will got through positions $j = N$ at switching interval k, $j = N-1$ at $k+1$, ..., $j = 1$ at $k+N-1$. Its operation can be defined as follows:

$$C^{\text{start}}|_k = C^{\text{end}}|_{k-1} \quad , \quad (C^{\text{start}}, C_{N-1}^{\text{out}})|_k \xrightarrow{\Omega_N} (C^{\text{end}}, C^{\text{out}})|_k, \tag{3.11}$$

$$C^{\text{start}}|_{k+1} = C^{\text{end}}|_k \quad , \quad (C^{\text{start}}, C_{N-2}^{\text{out}})|_{k+1} \xrightarrow{\Omega_{N-1}} (C^{\text{end}}, C^{\text{out}})|_{k+1}, \tag{3.12}$$

$$\dots$$

$$C^{\text{start}}|_{k+N-2} = C^{\text{end}}|_{k+N-3}, \quad (C^{\text{start}}, C_1^{\text{out}})|_{k+N-2} \xrightarrow{\Omega_2} (C^{\text{end}}, C^{\text{out}})|_{k+N-2}, \tag{3.13}$$

$$C^{\text{start}}|_{k+N-1} = C^{\text{end}}|_{k+N-2}, \quad (C^{\text{start}}, C_N^{\text{out}})|_{k+N-1} \xrightarrow{\Omega_1} (C^{\text{end}}, C^{\text{out}})|_{k+N-1}. \tag{3.14}$$

To derive a one-column process analogous to the N-column process it is necessary to replace the references to $C_N^{\text{out}}, \dots, C_1^{\text{out}}$ in the equations above by references to C^{out} that are equivalent to the former under CSS conditions. For example, given that under CSS conditions

$$C_j|_k = C_{j-1}|_{k+1} \quad \forall\, k \in \text{CSS}, \tag{3.15}$$

the equations above could be rewritten for the CSS as follows:

$$C^{\text{start}}|_k = C^{\text{end}}|_{k-1}, \quad C^{\text{start}}|_k, C^{\text{out}}|_{k+1} \xrightarrow{\Omega_N} (C^{\text{end}}, C^{\text{out}})|_k, \tag{3.16}$$

$$C^{\text{start}}|_{k+1} = C^{\text{end}}|_k, \quad C^{\text{start}}|_{k+1}, C^{\text{out}}|_{k+2} \xrightarrow{\Omega_{N-1}} (C^{\text{end}}, C^{\text{out}})|_{k+1}, \tag{3.17}$$

$$\cdots$$

$$C^{\text{start}}|_{k+N-2} = C^{\text{end}}|_{k+N-3}, \quad C^{\text{start}}|_{k+N-2}, C^{\text{out}}|_{k+N-1} \xrightarrow{\Omega_2} (C^{\text{end}}, C^{\text{out}})|_{k+N-2}, \tag{3.18}$$

$$C^{\text{start}}|_{k+N-1} = C^{\text{end}}|_{k+N-2}, \quad C^{\text{start}}|_{k+N-1}, C^{\text{out}}|_{k+N} \xrightarrow{\Omega_1} (C^{\text{end}}, C^{\text{out}})|_{k+N-1}. \tag{3.19}$$

Unfortunately, these equations as they stand describe a process that is physically impossible to realize because C^{out} in each of them is specified for one switching interval ahead in time (into the future) of that for C. But under CSS conditions any given column goes through the same state every $N\tau$ time units (it is $N\tau$-periodic), that is

$$C_j|_k = C_j|_{k-N} \quad \text{hence} \quad C^{\text{out}}|_k = C^{\text{out}}|_{k-N}, \tag{3.20}$$

and this allows us to rewrite the equations for the one-column analog as follows:

$$C^{\text{start}}|_k = C^{\text{end}}|_{k-1}, \quad C^{\text{start}}|_k, C^{\text{out}}|_{k+1-N} \xrightarrow{\Omega_N} (C^{\text{end}}, C^{\text{out}})|_k, \tag{3.21}$$

$$C^{\text{start}}|_{k+1} = C^{\text{end}}|_k, \quad C^{\text{start}}|_{k+1}, C^{\text{out}}|_{k+2-N} \xrightarrow{\Omega_{N-1}} (C^{\text{end}}, C^{\text{out}})|_{k+1}, \tag{3.22}$$

$$\cdots$$

$$C^{\text{start}}|_{k+N-2} = C^{\text{end}}|_{k+N-3}, \quad C^{\text{start}}|_{k+N-2}, C^{\text{out}}|_{k-1} \xrightarrow{\Omega_2} (C^{\text{end}}, C^{\text{out}})|_{k+N-2}, \tag{3.23}$$

$$C^{\text{start}}|_{k+N-1} = C^{\text{end}}|_{k+N-2}, \quad C^{\text{start}}|_{k+N-1}, C^{\text{out}}|_k \xrightarrow{\Omega_1} (C^{\text{end}}, C^{\text{out}})|_{k+N-1}. \tag{3.24}$$

These equations show that Ω_j uses $C^{\text{out}}|_{k-N+1}$ to define the inlet conditions for C at switching interval k, ie, the outlet fractions of C that are neither collected as product nor discarded are recycled back to its inlet with a lag in time of $(N-1)\tau$ time units.

It is important to notice that although the governing equations for the one-column analog were derived from eq. 3.25 rewritten here as

$$(C_j^{\text{start}}, C_{j-p}^{\text{out}})|_k \xrightarrow{\Omega_j} (C_j^{\text{end}}, C_j^{\text{out}})|_k, \quad p = 1, \tag{3.25}$$

they are still valid for other integer values of $p \geq 1$ as long as p is independent of j and does not change over the course of the switching interval. This will always be the case for two-column processes.

If $N \geq 3$, there will be nonstandard SMB processes for $p > 1$ that cannot be mimicked by the one-column analog either because $p = p(j)$ or/and p changes over the course of the switching interval. But a little reasoning shows that even in cases when $p = p(j)$ changes over the course of the switching interval, the one-column analog will still work if there at most two different column connections per switching interval.

For example, consider GE Health Care's three-column periodic counter-current (PCC) chromatography (3C-PCC) setup for the mAb capture step using protein A resin. Fig. 3.13

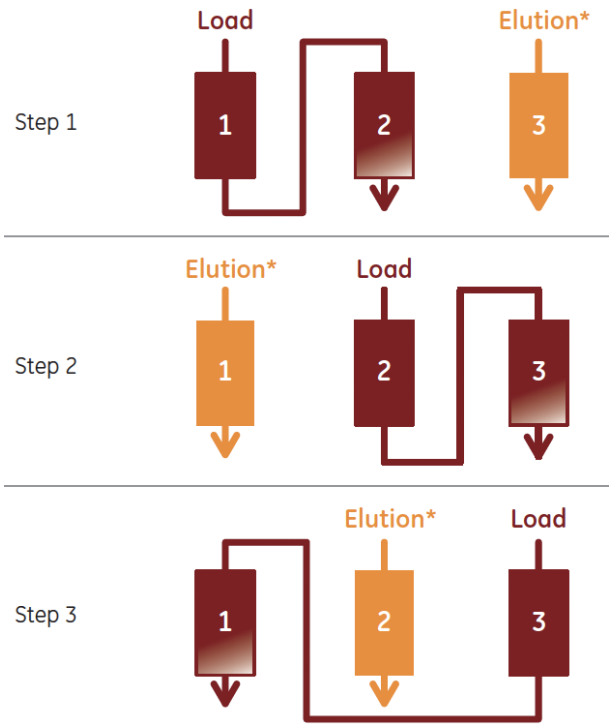

Figure 3.13: The principle of 3C-PCC chromatography (adapted from GE Healthcare's open literature). Step 1: columns 1 and 2 are loaded with clarified cell culture supernatant (red). Step 2: column 1 has reached the determined level of breakthrough and column 2 becomes the first column in the loading zone. In step 2, column 3 becomes the second column in the loading zone, while column 1 is subjected to wash, elution, strip, CIP, and re-equilibration (yellow). Step 3: column 2 has been loaded to the determined level of breakthrough and is disconnected from the loading zone and column 3 becomes the first column in the loading zone. In step 3, column 1 is now ready for the next cycle and becomes the second column in the loading zone. This procedure is repeated in a cyclic manner to achieve a continuous operation. *The elution phase in this figure includes wash, elution, strip, CIP, and re-equilibration.

shows a schematic of the basic process. In a PCC setup, columns are switched between the loading step and non-loading steps comprising column wash, elution, cleaning in place (CIP), and equilibration. At a predefined level of breakthrough, the primary column in the loading zone is disconnected from the loading zone and the load is redirected to the next column. In parallel, the disconnected, saturated column will be washed, eluted, and regenerated. To fully utilize the potential of this setup, the non-loading steps should be shorter or equal to the time for loading of a column. One cycle equals three loadings, one on each column.

As shown in Fig. 3.13, the basic 3C-PCC process is a three-column SMB process with $p = 1$ (standard) and hence can be mimicked by the one-column analog with recycle lag. This process, however, has yield losses associated with the wash step (with product either in void or loosely bound to the chromatography medium), which can be minimized by the wash strategy described in Fig. 3.14. The content of column 1 (saturated column) is

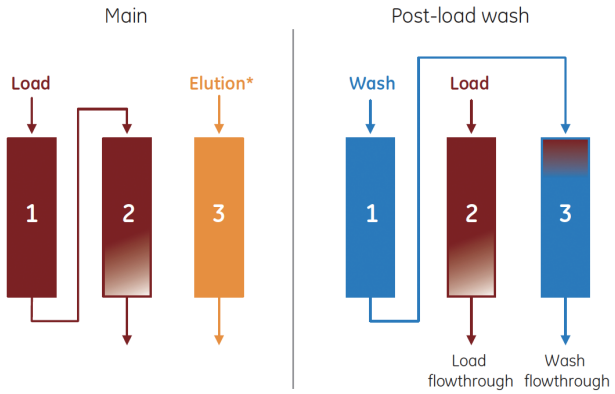

Figure 3.14: Wash strategy in 3C-PCC (adapted from GE Healthcare's open literature). This strategy is used to avoid yield losses associated with the post-load wash step: column 1 (saturated column) is washed into column 3 (regenerated column) before column 3 is added into the loading zone. *Includes wash, elution, strip, CIP, re-equilibration.

washed and bound in column 3 (regenerated column) before column 3 is placed as second in the loading zone.

When this enhanced variant of the 3C-PCC process is drawn over a full cycle (three switching intervals), as in Fig. 3.15a, it is seen that $p = 1$ for connection A whereas $p = 2$ for connection B. But given that this process has only two different column interconnections, A and B, per switching interval, it is possible to devise a one-column with recycle lag that mimics its operation. Fig. 3.15c shows the one-column process derived from the operation of column 3 over a complete cycle (Fig. 3.15b). The first two cycles correspond to the start-up of the process whereas from the third cycle onwards the process is fully periodic. Note that, and this is extremely important, in the second cycle fraction B is replaced by washing buffer to stagger the ABAB sequence from cycle three onwards.

Consider now the hypothetical three-column process depicted in the schematic of Fig. 3.16. This process was obtained by adding an extra step to the one in Fig. 3.15a. The one-column analog derived by following the operation of column 3 over a full cycle (Fig. 3.16b) is shown in Fig. 3.16c. It is seen that for the new process $p = 1$ for connections A and C whereas $p = 2$ for connection B. We now have $p = p(j)$ and more than two different column interconnections per switching interval. The resulting one-column analog is not physically realizable because the sequences of inlet and outlet fraction histories are incompatible as shown in Fig. 3.16d.

As another example, consider Novasep's Sequential Multicolumn Chromatography (SMCC) commercialized as BioSC. Fig. 3.17 shows a schematic of a full SMCC switching interval with five steps applied to a four-column BioSC. At the start of cycle the highly loaded layers are contained in the first column (1), which is isolated from the process, and the latter steps of the chromatographic method are applied independently. A washing step, of appropriate volume for this first column, pushes unbound target product contained in the liquid phase of the first column to the second (2) column, thus preventing product loss and maximum buffer usage. The first column is now eluted while loading

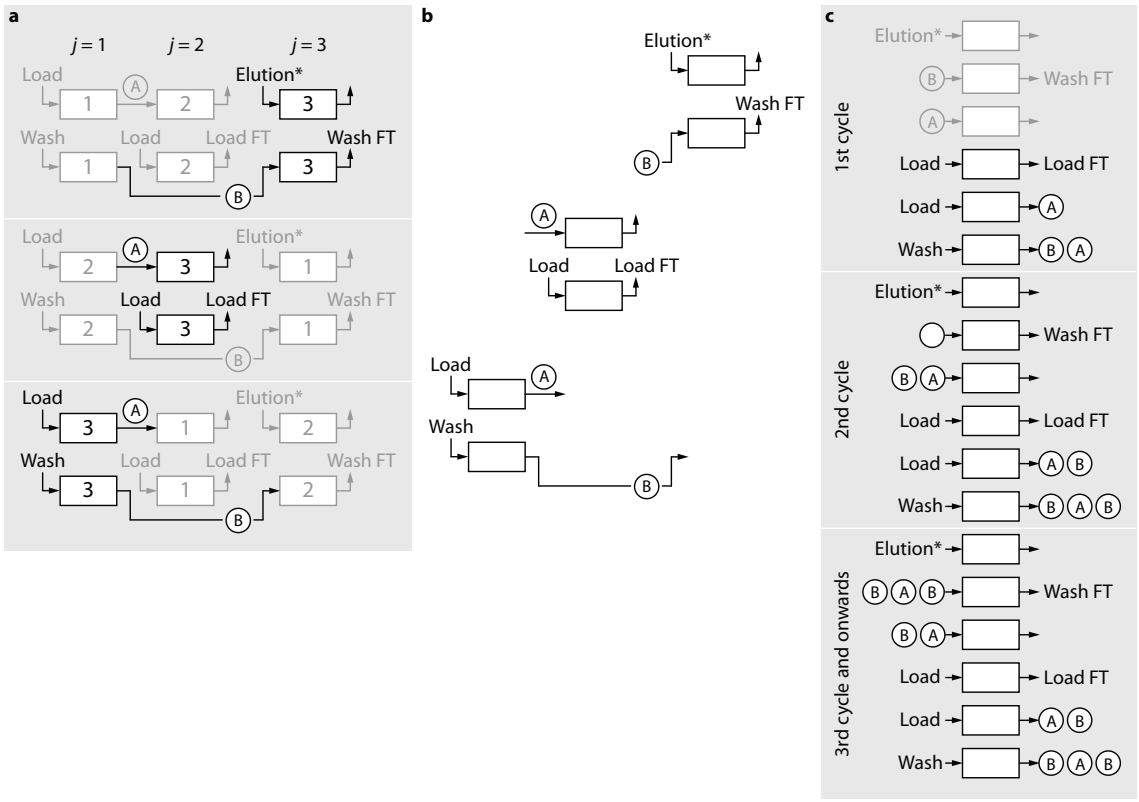

Figure 3.15: (a) Full cycle of 3C-PCC with wash strategy (FT stands for flowthrough; *includes wash, elution, strip, CIP, re-equilibration). (b) Isolation of the operation of column 3 over a full cycle. (c) Corresponding one-column analog with recycle lag (◯→ stands for injection of wash buffer).

restarts in linear sequence through partially loaded columns (3). The second column will reach a highly loaded state as the first column described before and the process repeats for each column completing a full SMCC cycle. At the end of one cycle, each column is exposed to the same quantity of product and buffers.

This process is an SMB with constant $p = 1$ and can thus be mimicked by a one-column analog with recycle lag. Figure 3.18a shows a schematic of a full SMCC cycle with any given column, say column 4, targeted for emulation. To generate the one-column analog, the operation of the targeted column is followed over a complete cycle, as illustrated in Fig.3.18. The fractions exiting the one-column analog that are neither recovered as product nor discarded—fractions A–H in this case—are recycled back to the inlet of the one-column analog with a lag of 3τ time units (Fig. 3.18c). Figure 3.18d shows a simplified schematic of the full cycle of the one-column after merging identical, sequential steps.

Figure 3.18 illustrates another important feature of the single-column analog with recycle lag. It is that any multicolumn process with steps involving sequences such as

$$\rightarrow\square\rightarrow\square\rightarrow\square\rightarrow \quad \text{or} \quad \overleftarrow{\rightarrow\square\rightarrow\square\rightarrow}$$

(the latter for the case of a two-column unit) gives rise to a one-column analog with steps

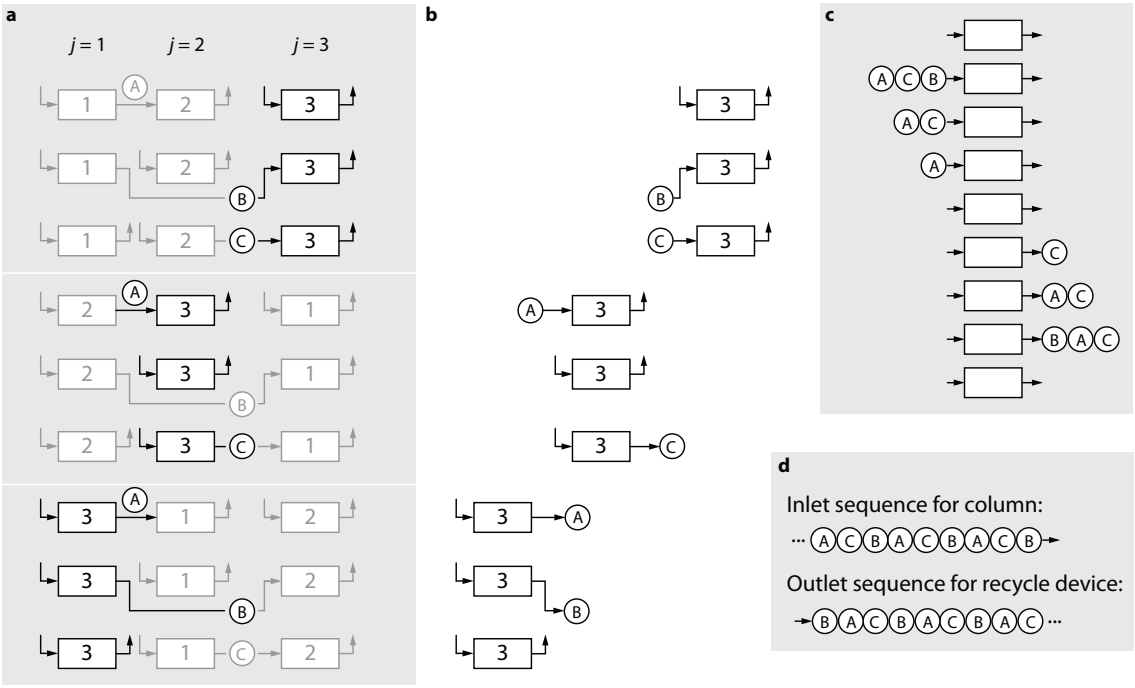

Figure 3.16: One-column analog of an hypothetical variant of the 3C-PCC process. (a) Schematic of a full cycle with column 3 targeted for emulation. (b) following-up of column 3 over of a full cycle. (c) Full cycle of the one-column analog. (d) Expected inlet sequence of fractions for the chromatographic column and outlet sequence of fractions obtained from the recycle device.

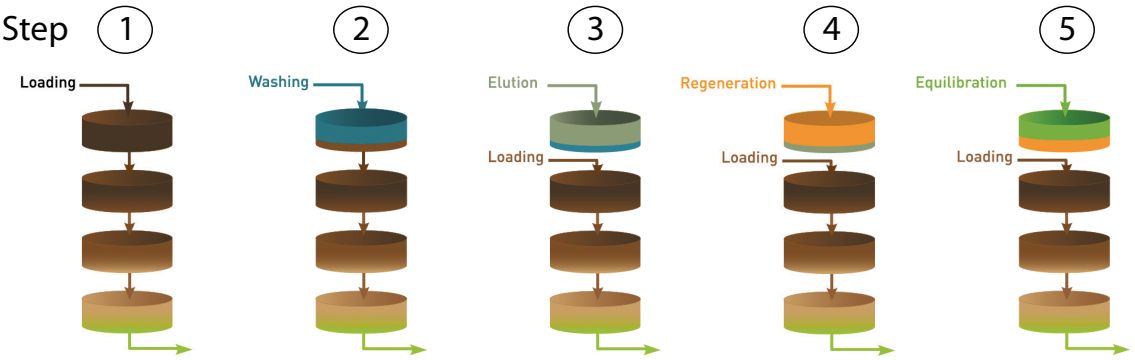

Figure 3.17: Example of a full SMCC switching interval with five steps applied to a four-column BioSC (adapted from Novasep's open litterature).

such as the second one in Fig. 3.18d in which the one-column chromatograph operates in closed-loop recycle, ie, the outlet of the chromatography column is directed to the recycle device while at the same time the outlet of the recycle device is directed to the inlet of the chromatography column.

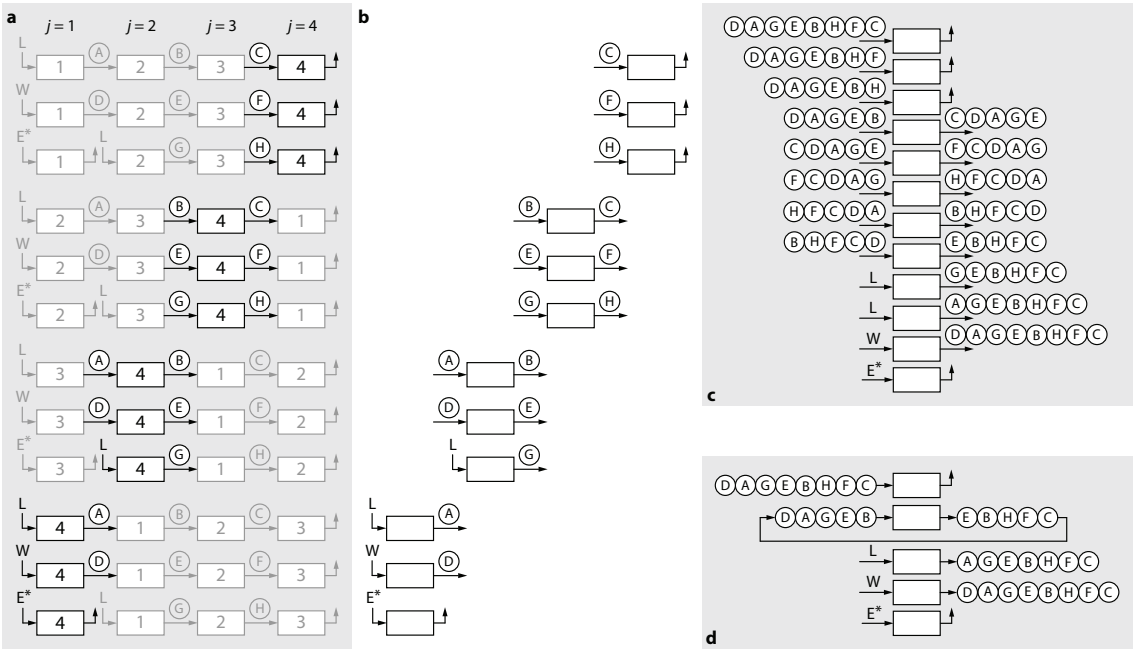

Figure 3.18: One-column analog of a four-column SMCC BioSC with five steps per switching interval (*includes elution, regeneration, and equilibration.). (a) Schematic of a full cycle with column 4 target for emulation. (b) following-up of column 4 over of a full cycle. (c) Full cycle of the one-column analog. (d) Full cycle of the one-column analog after merging identical, sequential steps.

3.5 Mathematical Modelling of the Proposed System

In a dynamic system, the values of the variables change with time. In this section, it will be considered the dynamic modelling for the setup, detailing the role that each equipment prints to the model. The mathematical model were divided in four steps.

3.5.1 Recycle Piston

Solute transport through the recycle piston lies between two limiting cases: the best case scenario—that of plug flow—and the worst case scenario—that of a perfectly mixed tank. A detailed analysis of the flow pattern inside the piston would require solution of the dispersed-flow equation for an inert scalar coupled to the Navier Stokes equation for laminar flow of an incompressible Newtonian fluid, subject to inlet and outlet conditions defined by the geometries of the distributor and fluid collector, a task that is beyond the scope of this work. Instead, we consider the simpler intermediate case of axially-dispersed plug flow [23, 257, 258] inside the piston:

$$\frac{\partial c_i}{\partial t} = D_{\mathrm{L}} \frac{\partial^2 c_i}{\partial z^2} - v_0 \frac{\partial c_i}{\partial z}, \qquad \forall t > 0,\ 0 < z < L(t), \tag{3.26}$$

where $c_i(z,t)$ is the concentration of solute i in the fluid inside the piston, t the time coordinate, z the axial coordinate along the piston, v_0 the inlet fluid velocity, and D_{L} the axial dispersion coefficient. The inlet is at a fixed spatial position, $z_0 = 0$, whereas the

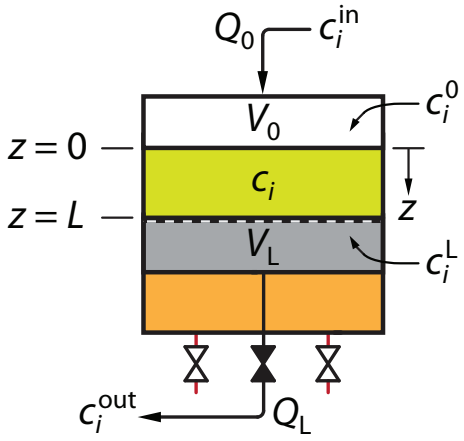

Figure 3.19: Schematic of the recycle piston with dead volumes. V_0 and V_L are the dead volumes at the piston inlet and outlet, respectively.

axial position of the outlet, $z_L = L$, can vary depending on whether the piston is steady or moving (Figure 3.19). If $D_L \to \infty$, the model describes the worst case scenario (perfect mixing); if $D_L \to 0$, the model describes the best case scenario (pure plug flow).

If v_L is the outlet fluid velocity then the difference $v_L - v_0$ gives the velocity at which the piston is displaced, that is,

$$\frac{dL}{dt} = v_0 - v_L. \tag{3.27}$$

For example, if the piston is being filled, $v_0 > 0$ and $v_L = 0$, and the piston moves with velocity v_0. If the piston is being emptied, $v_0 = 0$ and $v_L > 0$, and the piston moves with velocity $-v_L$.

Eq. (3.26) is subjected to the following (Danckwerts) boundary conditions:

$$\begin{aligned} v_0 c_i - D_L \frac{\partial c_i}{\partial z} &= v_0 c_i^{in} \quad \text{for } z = 0 \\ \frac{\partial c_i}{\partial z} &= 0 \qquad\quad \text{for } z = L(t) \end{aligned}, \tag{3.28}$$

where c_i^{in} is the inlet solute concentration; henceforth we shall also use the shorthand notation $c_i^{out} \equiv c_i(L,t)$ to denote the outlet solute concentration.

Eqs. (3.26) and (3.28) are easier to solve numerically if the moving boundary condition is replaced by a fixed one. To achieve this we introduce a change of variable that maps the spatial domain $z \in [0, L(t)]$ onto a dimensionless domain $x \in [0,1]$, of fixed length, through the transformation

$$x(z,t) = \frac{z}{L(t)} \quad \text{or} \quad z(x,t) = xL(t). \tag{3.29}$$

where, the partial derivative of $z(x,t)$ is

$$\frac{\partial z(x,t)}{\partial t} = x\frac{dL(t)}{dt} = x(v_0 - v_L). \tag{3.30}$$

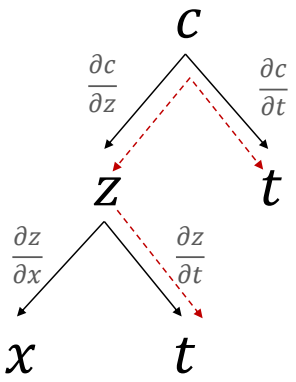

Figure 3.20: Chain Rule.

Moreover,

$$\frac{\partial c_i}{\partial z} = \frac{\partial c_i}{\partial x}\frac{\partial x}{\partial z} = \frac{1}{L}\frac{\partial c_i}{\partial x} \quad \text{and} \quad \frac{\partial^2 c_i}{\partial z^2} = \frac{1}{L^2}\frac{\partial^2 c_i}{\partial x^2}. \tag{3.31}$$

Using the chain rule (Figure 3.20) we obtain:

$$\frac{\partial c_i(x,t)}{\partial t} = \frac{\partial c_i(z,t)}{\partial t} + \frac{\partial c_i(z,t)}{\partial z}\frac{\partial z(x,t)}{\partial t}. \tag{3.32}$$

Replacing z by x, using eqs. 3.28, 3.30 and 3.31, gives the following transformed equation:

$$\frac{\partial c_i}{\partial t} = \frac{D_L}{L^2}\frac{\partial^2 c_i}{\partial x^2} - \frac{v_0}{L}\frac{\partial c_i}{\partial x} + \frac{1}{L}\frac{\partial c_i}{\partial x}x(v_0 - v_L), \tag{3.33}$$

or, simplifying

$$\frac{\partial c_i}{\partial t} = \frac{D_L}{L^2}\left(\frac{\partial^2 c_i}{\partial x^2}\right) - \frac{v_0 - (v_0 - v_L)x}{L}\left(\frac{\partial c_i}{\partial x}\right), \qquad \forall t > 0,\ 0 < x < 1, \tag{3.34}$$

subject to the boundary conditions

$$\begin{aligned} v_0 c_i - \frac{D_L}{L}\frac{\partial c_i}{\partial x} &= v_0 c_i^{\text{in}} \quad \text{for } x = 0 \\ \frac{\partial c_i}{\partial x} &= 0 \quad \text{for } x = 1 \end{aligned}. \tag{3.35}$$

At any time the volume of fluid in the piston is $V_P(t) = A_P L(t)$, where A_P is the cross-sectional area of the piston. Moreover, the flow rate at the piston's inlet is $Q_0 = A_P v_0$ and the flow rate at the piston's outlet is $Q_L = A_P v_L$. Rearranging these equations gives $A_P = \frac{V_P(t)}{L(t)}$ and $v_0 = \frac{Q_0}{A_P} = \frac{Q_0}{\frac{V_P(t)}{L(t)}}$.

Thus, the above equations can also be written as a function of the inlet and outlet flow rates:

$$\frac{\partial c_i}{\partial t} = \frac{D_L}{L^2}\left(\frac{\partial^2 c_i}{\partial x^2}\right) - \frac{\frac{Q_0}{\frac{V_P}{L}} - \left(\frac{Q_0}{\frac{V_P}{L}} - \frac{Q_L}{\frac{V_P}{L}}\right)x}{L}\left(\frac{\partial c_i}{\partial x}\right), \qquad \text{or}$$

$$\frac{\partial c_i}{\partial t} = \frac{D_L}{L^2}\left(\frac{\partial^2 c_i}{\partial x^2}\right) - \frac{\frac{Q_0 - (Q_0 - Q_L)x}{\frac{V_P}{L}}}{L}\left(\frac{\partial c_i}{\partial x}\right), \qquad \text{or}$$

$$V_{\mathrm{P}}\frac{\partial c_i}{\partial t} = \frac{V_{\mathrm{P}}D_{\mathrm{L}}}{L^2}\left(\frac{\partial^2 c_i}{\partial x^2}\right) - \left[Q_0 - (Q_0 - Q_{\mathrm{L}})\,x\right]\left(\frac{\partial c_i}{\partial x}\right), \qquad \forall t > 0,\ 0 < x < 1, \tag{3.36}$$

$$\begin{aligned} \frac{Q_0}{\frac{V_{\mathrm{P}}}{L}}c_i - \frac{D_{\mathrm{L}}}{L}\frac{\partial c_i}{\partial x} &= \frac{Q_0}{\frac{V_{\mathrm{P}}}{L}}c_i^{\mathrm{in}} \quad \text{for } x = 0, \qquad \text{or} \\ Q_0 c_i - \frac{V_{\mathrm{P}}D_{\mathrm{L}}}{L^2}\frac{\partial c_i}{\partial x} &= Q_0 c_i^{\mathrm{in}} \quad \text{for } x = 0 \qquad . \\ \frac{\partial c_i}{\partial x} &= 0 \qquad \text{for } x = 1 \end{aligned} \tag{3.37}$$

It is also more convenient to quantify the effect of the axial dispersion by means of a Péclet number than via D_{L} directly. If dispersion in the piston is assumed to be proportional to the fluid velocity then

$$D_{\mathrm{L}} \approx D_{\mathrm{m}}\,(1 + \gamma \mathrm{Pe_d}) = D_{\mathrm{m}} + \gamma D_{\mathrm{P}} v_0 = D_{\mathrm{m}} + \gamma \frac{D_{\mathrm{P}}Q_0}{A_{\mathrm{P}}}. \tag{3.38}$$

where D_{m} is the molecular diffusivity, γ should be regarded as an empirical constant whose value is much smaller than 1/192, and $\mathrm{Pe_d} = v_0 D_{\mathrm{P}}/D_{\mathrm{m}}$ is the Péclet number based on the diameter, D_{P}, of the piston. If the dispersion within the piston was assumed to be approximated by Taylor dispersion, then $\gamma \approx 1/192$, but this consideration is only valid for fully developed laminar flow in an infinitely long tube, which is certainly not the case.

Thus, the reciprocal of the Péclet number based on the piston length is

$$\frac{1}{\mathrm{Pe_0}} = \frac{D_{\mathrm{L}}}{v_0 L} = \frac{D_{\mathrm{m}}}{v_0 L} + \frac{\gamma D_{\mathrm{P}}}{L} = \frac{1}{\mathrm{Pe_m}} + \frac{1}{\mathrm{Pe_h}}. \tag{3.39}$$

where $\mathrm{Pe_m} = v_0 L/D_{\mathrm{m}}$ is the molecular Péclet number and $\mathrm{Pe_h} = L/\gamma D_{\mathrm{P}}$ is the hydraulic Péclet number.

Hence, multiplying the eq. 3.38 by $\frac{A_{\mathrm{P}}^2}{V_{\mathrm{P}}}$, results:

$$\frac{A_{\mathrm{P}}^2}{V_{\mathrm{P}}}D_{\mathrm{L}} = \frac{A_{\mathrm{P}}^2}{V_{\mathrm{P}}}D_{\mathrm{m}} + \frac{A_{\mathrm{P}}^2}{V_{\mathrm{P}}}\gamma\frac{D_{\mathrm{P}}Q_0}{A_{\mathrm{P}}}, \qquad \text{or}$$

$$\frac{V_{\mathrm{P}}^2}{L^2}\frac{1}{V_{\mathrm{P}}}D_{\mathrm{L}} = \frac{A_{\mathrm{P}}^2 D_{\mathrm{m}} + A_{\mathrm{P}}\gamma D_{\mathrm{P}}Q_0}{V_{\mathrm{P}}}, \qquad \text{or}$$

$$\frac{V_{\mathrm{P}}D_{\mathrm{L}}}{L^2} = \frac{\gamma_{\mathrm{m}} + \gamma_{\mathrm{h}}Q_0}{V_{\mathrm{P}}}, \quad \gamma_{\mathrm{m}} = A_{\mathrm{P}}^2 D_{\mathrm{m}},\ \gamma_{\mathrm{h}} = \gamma A_{\mathrm{P}} D_{\mathrm{P}}, \tag{3.40}$$

We can finally write our model as follows.

$$\frac{dV_{\mathrm{P}}}{dt} = Q_0 - Q_{\mathrm{L}}, \tag{3.41}$$

$$V_{\mathrm{P}}^2\frac{\partial c_i}{\partial t} = (\gamma_{\mathrm{m}} + \gamma_{\mathrm{h}}Q_0)\left(\frac{\partial^2 c_i}{\partial x^2}\right) - V_{\mathrm{P}}\left[Q_0 - (Q_0 - Q_{\mathrm{L}})\,x\right]\left(\frac{\partial c_i}{\partial x}\right), \tag{3.42}$$

$$\begin{aligned} V_{\mathrm{P}}Q_0 c_i - (\gamma_{\mathrm{m}} + \gamma_{\mathrm{h}}Q_0)\left(\frac{\partial c_i}{\partial x}\right) &= V_{\mathrm{P}}Q_0 c_i^{\mathrm{in}} \quad \text{for } x = 0 \\ \left(\frac{\partial c_i}{\partial x}\right) &= 0 \qquad \text{for } x = 1 \end{aligned} \quad , \tag{3.43}$$

$$\gamma_{\mathrm{m}} = A_{\mathrm{P}}^2 D_{\mathrm{m}}, \quad \gamma_{\mathrm{h}} = \gamma A_{\mathrm{P}} D_{\mathrm{P}}. \tag{3.44}$$

The last consideration is the time scaling. If we decide to replace t by $\theta = t/\tau$, a reduced time coordinate scaled by a reference time τ, the corresponding model equations are as follows.

$$\frac{dV_{\mathrm{P}}}{d\theta} = \tau(Q_0 - Q_{\mathrm{L}}), \tag{3.45}$$

$$V_{\mathrm{P}}^2 \frac{\partial c_i}{\partial \theta} = \tau(\gamma_{\mathrm{m}} + \gamma_{\mathrm{h}} Q_0)\left(\frac{\partial^2 c_i}{\partial x^2}\right) - \tau V_{\mathrm{P}}\left[Q_0 - (Q_0 - Q_{\mathrm{L}})x\right]\left(\frac{\partial c_i}{\partial x}\right), \tag{3.46}$$

$$\begin{aligned} V_{\mathrm{P}} Q_0 c_i - (\gamma_{\mathrm{m}} + \gamma_{\mathrm{h}} Q_0)\frac{\partial c_i}{\partial x} &= V_{\mathrm{P}} Q_0 c_i^{\mathrm{in}} \quad \text{for } x = 0 \\ \frac{\partial c_i}{\partial x} &= 0 \qquad\qquad\quad \text{for } x = 1 \end{aligned}. \tag{3.47}$$

Finally, if the flow rates are replaced by volumes of fluid, $W = \tau Q$, the equations are expressed as follows.

(*Dynamic volumetric balance*)

$$\frac{dV_{\mathrm{P}}}{d\theta} = W_0 - W_{\mathrm{L}}, \tag{3.48}$$

(*Dynamic component balance*)

$$V_{\mathrm{P}}^2 \frac{\partial c_i}{\partial \theta} = (\gamma_{\mathrm{m}}\tau + \gamma_{\mathrm{h}} W_0)\left(\frac{\partial^2 c_i}{\partial x^2}\right) - V_{\mathrm{P}}\left[W_0 - (W_0 - W_{\mathrm{L}})x\right]\left(\frac{\partial c_i}{\partial x}\right), \tag{3.49}$$

(*Boundary conditions*)

$$\begin{aligned} V_{\mathrm{P}} W_0 c_i - (\gamma_{\mathrm{m}}\tau + \gamma_{\mathrm{h}} W_0)\frac{\partial c_i}{\partial x} &= V_{\mathrm{P}} W_0 c_i^{\mathrm{in}} \quad \text{for } x = 0 \\ \frac{\partial c_i}{\partial x} &= 0 \qquad\qquad\quad \text{for } x = 1 \end{aligned}. \tag{3.50}$$

It is interesting to analyze the previous equations and compare them against the usual ones for dispersed-plug flow in an inert porous medium or empty tube:

$$\frac{\partial c_i}{\partial \theta} = \frac{\tau Q}{V_{\mathrm{P}}}\left(\frac{1}{\mathrm{Pe}_i}\frac{\partial^2 c_i}{\partial x^2} - \frac{\partial c_i}{\partial x}\right), \tag{3.51}$$

$$c_i - \frac{1}{\mathrm{Pe}_i}\frac{\partial c_i}{\partial x} = c_i^{\mathrm{in}}. \tag{3.52}$$

The equations are identical, the equivalence rules being

$$Q = Q_0 - (Q_0 - Q_{\mathrm{L}})x, \quad \frac{1}{\mathrm{Pe}} = \frac{\gamma_{\mathrm{m}} + \gamma_{\mathrm{h}} Q_0}{V_{\mathrm{P}} Q} \tag{3.53}$$

Notice that

$$Q = Q_0 - (Q_0 - Q_{\mathrm{L}})x = (1 - x)Q_0 + xQ_{\mathrm{L}}, \tag{3.54}$$

is a weighted average of Q_0 and Q_{L} and, moreover, $Q \geq 0$ for all $Q_0, Q_{\mathrm{L}} \geq 0$.

3.5.2 Perfectly Mixed Chamber

It is of interest to consider the model of the worst case scenario, that of perfect mixing in the piston chamber. The ideal Continuous Stirred Tank (CST) model [244], or Perfect Mixed Tank model, is very simple:

(*Dynamic volumetric balance*)

$$\frac{dV_P}{dt} = Q_0 - Q_L, \tag{3.55}$$

(*Dynamic component balance*)

$$\text{In} - \text{Out} = \text{Accumulation} - \text{Generation},$$

$$c_i^{in} Q_0 - c_i^{out} Q_0 = V_P \frac{dc_i^{out}}{dt} - 0, \qquad or$$

$$V_P \frac{dc_i^{out}}{dt} = Q_0 (c_i^{in} - c_i^{out}), \tag{3.56}$$

where V_P is the piston volume, Q_0 and Q_L are respectively the volumetric flow rates at inlet and outlet of the piston, and c_i^{in} and c_i^{out} are respectively the piston inlet and outlet concentrations of component i.

The time-scaled model is very simple:

$$\frac{dV_P}{d\theta} = \tau(Q_0 - Q_L) = W_0 - W_L, \tag{3.57}$$

$$V_P \frac{dc_i^{out}}{d\theta} = \tau Q_0 (c_i^{in} - c_i^{out}) = W_0 (c_i^{in} - c_i^{out}). \tag{3.58}$$

Notice that during the emptying of the recycle piston, $Q_0 = 0$ and $Q_L > 0$, and thus $dc_i^{out}/dt = 0 \rightarrow c_i^{out} = \text{const}$, as it should be.

To avoid numerical errors when $V_P \approx 0$ it is probably safer to replace eq. (3.58) by

$$(\delta + |V_P|) \frac{dc_i^{out}}{d\theta} = \tau Q_0 (c_i^{in} - c_i^{out}) = W_0 (c_i^{in} - c_i^{out}), \tag{3.59}$$

where δ is a small positive real, say 10^{-4}. This does not change the results and avoids the singularity

$$0 \times \frac{dc_i^{out}}{d\theta} = 0 \tag{3.60}$$

when $V_P \approx 0$ and $Q_0 = 0$.

3.5.3 Dead Volumes

It is of interest to consider the implications of the existence of non-negligible dead volumes in the recycle piston. For the purpose of the present discussion we considered the schematic shown in Figure 3.19. Two dead volumes are considered for this set-up. V_0 and V_L are the dead volumes at the piston inlet and outlet, respectively.

The equation for the dead volumes was taken from the usual axially-dispersed plug flow model (eq. 3.26), where, when applying the chain rule (eq. 3.32) to put c_i as a function of (x,t), the term $\frac{\partial z(x,t)}{\partial t}$ is null, since the dead volume has a fixed position, with no change of z over time. Hence:

$$\frac{\partial c_i}{\partial t} = \frac{D_\mathrm{L}}{L^2}\frac{\partial^2 c_i}{\partial x^2} - \frac{v}{L}\frac{\partial c_i}{\partial x}, \qquad or \tag{3.61}$$

$$\frac{\partial c_i}{\partial t} = \frac{v}{L}\left(\frac{D_\mathrm{L}}{vL}\frac{\partial^2 c_i}{\partial x^2} - \frac{\partial c_i}{\partial x}\right), \tag{3.62}$$

Remembering that $Q = vA$, $V = LA$ and $\mathrm{Pe_i} = \frac{Lv}{D_\mathrm{L}}$:

$$\frac{\partial c_i}{\partial t} = \frac{Q}{V}\left(\frac{1}{\mathrm{Pe_i}}\frac{\partial^2 c_i}{\partial x^2} - \frac{\partial c_i}{\partial x}\right), \tag{3.63}$$

where $x = z/L$ is the dimensionless axial position along the column (L is the column length), and $\mathrm{Pe_i}$ is a Péclet number for axial dispersion in the column. Here, V can be V_0 or V_L depending on which dead volume is being referenced.

Thus, the time-scaled model is:

(*Inlet dead volume*)

$$\frac{\partial c_i^0}{\partial \theta} = \frac{W_0}{V_0}\left(\frac{1}{\mathrm{Pe}_0}\frac{\partial^2 c_i^0}{\partial x^2} - \frac{\partial c_i^0}{\partial x}\right), \quad W_0 = \tau Q_0, \quad (c_i^0)^{\mathrm{out}}(\theta) \equiv c_i^0(x=1,\theta), \tag{3.64}$$

$$\begin{aligned} c_i^0 - \frac{1}{\mathrm{Pe}_0}\frac{\partial c_i^0}{\partial x} &= (c_i^0)^{\mathrm{in}} \quad \text{for } x = 0, \\ \frac{\partial c_i^0}{\partial x} &= 0 \qquad\quad \text{for } x = 1. \end{aligned} \tag{3.65}$$

(*Outlet dead volume*)

$$\frac{\partial c_i^\mathrm{L}}{\partial \theta} = \frac{W_\mathrm{L}}{V_\mathrm{L}}\left(\frac{1}{\mathrm{Pe_L}}\frac{\partial^2 c_i^\mathrm{L}}{\partial x^2} - \frac{\partial c_i^\mathrm{L}}{\partial x}\right), \quad W_\mathrm{L} = \tau Q_\mathrm{L}, \quad (c_i^\mathrm{L})^{\mathrm{out}}(\theta) \equiv c_i^\mathrm{L}(x=1,\theta), \tag{3.66}$$

$$\begin{aligned} c_i^\mathrm{L} - \frac{1}{\mathrm{Pe_L}}\frac{\partial c_i^\mathrm{L}}{\partial x} &= (c_i^\mathrm{L})^{\mathrm{in}} \quad \text{for } x = 0, \\ \frac{\partial c_i^\mathrm{L}}{\partial x} &= 0 \qquad\quad \text{for } x = 1. \end{aligned} \tag{3.67}$$

(*Piston outlet*)

$$c_i^{\mathrm{out}} = c_i^\mathrm{L}|_{x=1}. \tag{3.68}$$

3.5.4 Chromatographic Column

The differential material balances in preparative chromatography are based on several important considerations. It is assumed that: (1) the column is radially homogeneous; (2) the mobile phase is incompressible (then the velocity of the mobile phase can be considered constant along the column); (3) the axial dispersion coefficient is constant (it

is not dependent on the solute concentration); (4) the partial molar volumes of sample components are the same in both phases; (5) the solvent is not adsorbed; and (6) there are no thermal effects and there is no influence of the heat of adsorption [100].

It is well known that a chromatographic column with isothermal operation is satisfactorily defined by a dispersed-plug-flow model, with Linear-driving-force (LDF) approximation for mass transfer under the form of a lumped solid-diffusion model. These are sufficiently general to provide a realistic representation of preparative chromatography and SMB modeling [61, 101].

Furthermore, the LDF model can be fairly well approximated by an equilibrium-dispersed model with dispersion coefficients dependent on the local slopes of the adsorption isotherms [61].

For a linear adsorption system the material balance of the ith solute can be written by an equilibrium dispersed plug-flow model. To arrive at this model, we start from the transport equation for a solute dissolved in a liquid with dispersed plug-flow through a fixed bed of adsorbent:

$$\frac{\partial c_i}{\partial t} = D_{\mathrm{L}} \frac{\partial^2 c_i}{\partial z^2} - v_\epsilon \frac{\partial c_i}{\partial z} - \frac{(1-\epsilon)}{\epsilon} \frac{\partial q_i}{\partial t}, \qquad \forall t > 0,\ 0 < z < L(t), \tag{3.69}$$

where ϵ is the interparticle void fraction (i.e. interparticle porosity of the fixed bed), q the amount of solute adsorbed at any given time (i.e. concentration of adsorbed solute), $D_{\mathrm{L}} = v_\epsilon L/\mathrm{Pe_i}$ the axial dispersion coefficient ($v_\epsilon = Q/\epsilon A$ is the interstitial velocity of the liquid [30], i.e. liquid velocity between the particles and between the particles pores) and Pe_i the Péclet number for axial dispersion at adsorbent fixed bed. In this equation the concentration of solute adsorbed is expressed per unit of apparent volume of solid: ϵV_c is the column volume occupied by interparticular fluid, $(1-\epsilon)V_c$ is the column volume occupied by the solid and intraparticular liquid.

Introducing the chnage of variable $x = z/L$ gives

$$\frac{\partial c_i}{\partial t} = \frac{D_{\mathrm{L}}}{L^2} \frac{\partial^2 c_i}{\partial x^2} - \frac{v_\epsilon}{L} \frac{\partial c_i}{\partial x} - \frac{(1-\epsilon)}{\epsilon} \frac{\partial q_i}{\partial t}, \qquad \forall t > 0,\ 0 < x < 1. \tag{3.70}$$

It is important to note that this equation presupposes local equilibrium between liquid and adsorbed phase (mass transfer between interparticular fluid and the adsorbent interior is infinitely rapid).

Given that local thermodynamic equilibrium is assumed:

$$\frac{\partial q_i}{\partial t} = \frac{\partial q_i^*}{\partial t}, \tag{3.71}$$

where q^* is the solute concentration at solid phase in equilibrium with the solute concentration at liquid phase.

For linear adsorption isotherms [100]

$$q_i = H_i c_i \tag{3.72}$$

where H_i is the slope of the isotherm (Henry's constant of adsorption). It's worth noting that this is an apparent constant ($H_i = H_i^{app}$), which covers the intraparticle porosity (ϵ_p) and the real Henry's constant (H_i^r). Hence, $H_i = \epsilon_p + H_i^r$ [242]. Thus,

$$\frac{\partial q_i^*}{\partial t} = \frac{\partial q_i^*}{\partial c_i}\frac{\partial c_i}{\partial t} = \frac{\partial (H_i c_i)}{\partial c_i}\frac{\partial c_i}{\partial t} = H_i \frac{\partial c_i}{\partial t}, \tag{3.73}$$

where q^* is the concentration of solute adsorbed in equilibrium with the concentration of solute in mobile phase, c.

Substituting eq. 3.73 and D_L at eq. 3.70, the transport equation takes the following form:

$$\frac{\partial c_i}{\partial t} = \frac{v_\epsilon L}{\mathrm{Pe}_i L^2}\frac{\partial^2 c_i}{\partial x^2} - \frac{v_\epsilon}{L}\frac{\partial c_i}{\partial x} - \frac{(1-\epsilon)}{\epsilon}H_i\frac{\partial c_i}{\partial t}, \qquad \text{or} \tag{3.74}$$

$$\left(1 + \frac{(1-\epsilon)}{\epsilon}H_i\right)\frac{\partial c_i}{\partial t} = \frac{v_\epsilon}{L}\left(\frac{1}{\mathrm{Pe}_i}\frac{\partial^2 c_i}{\partial x^2} - \frac{\partial c_i}{\partial x}\right), \qquad \text{multiplying by}\left(\frac{\epsilon A}{\epsilon A}\right) \tag{3.75}$$

$$\left(\frac{\epsilon + (1-\epsilon)H_i}{\epsilon}\right)\frac{\partial c_i}{\partial t} = \frac{Q}{\epsilon V_c}\left(\frac{1}{\mathrm{Pe}_i}\frac{\partial^2 c_i}{\partial x^2} - \frac{\partial c_i}{\partial x}\right), \tag{3.76}$$

Finally, the equilibrium dispersed plug-flow model is

$$\frac{\partial c_i}{\partial t} = \frac{Q}{[\epsilon + (1-\epsilon)H_i]\,V_c}\left(\frac{1}{\mathrm{Pe}_i}\frac{\partial^2 c_i}{\partial x^2} - \frac{\partial c_i}{\partial x}\right), \qquad \text{or} \tag{3.77}$$

$$\frac{\partial c_i}{\partial t} = \frac{Q}{V_i}\left(\frac{1}{\mathrm{Pe_i}}\frac{\partial^2 c_i}{\partial x^2} - \frac{\partial c_i}{\partial x}\right), \quad V_i \equiv [\epsilon + (1-\epsilon)H_i]V_\mathrm{c}. \tag{3.78}$$

The time-scaled version of this model is

$$\frac{\partial c_i}{\partial \theta} = \frac{W}{V_i}\left(\frac{1}{\mathrm{Pe_i}}\frac{\partial^2 c_i}{\partial x^2} - \frac{\partial c_i}{\partial x}\right), \quad V_i \equiv [\epsilon + (1-\epsilon)H_i]V_\mathrm{c}, \quad W = \tau Q, \tag{3.79}$$

where V_c is the column volume and V_i is the apparent volume for solute i.

Some authors prefer to use the dimensionless plate height, h, instead of Pe; the relationship between them is simple: $h = 2/\mathrm{Pe}$. Replacing Pe by h in the previous equation gives

$$\frac{\partial c_i}{\partial \theta} = \frac{W}{V_i}\left(\frac{h}{2}\frac{\partial^2 c_i}{\partial x^2} - \frac{\partial c_i}{\partial x}\right). \tag{3.80}$$

Returning to equation 3.79, $\mathrm{Pe_i}$ can be expressed as the sum of two components:

$$\frac{1}{\mathrm{Pe_i}} = \alpha_i + \beta_i Q, \quad \alpha_i = \frac{1}{(\mathrm{Pe_h})_i}, \quad \beta_i = \frac{V_i - \epsilon V_\mathrm{c}}{k_i V_i^2}, \tag{3.81}$$

where $(\mathrm{Pe_h})_i$ is the hydraulic Péclet number and k_i is the LDF mass transfer coefficient. This equation shows that the k_i is represented (masked) by the axial dispersion coefficient (D_L), or more properly, by Pe, which symbolizes the lumped solid-diffusion model.

Thus, the differential material balance can be expressed as

$$\frac{\partial c_i}{\partial \theta} = \frac{W}{V_i}\left[\left(\alpha_i + \frac{\beta_i W}{\tau}\right)\frac{\partial^2 c_i}{\partial x^2} - \frac{\partial c_i}{\partial x}\right], \tag{3.82}$$

subject to the usual Danckwerts boundary conditions

$$\begin{aligned} W\left[c_i - \left(\alpha_i + \frac{\beta_i W}{\tau}\right)\frac{\partial c_i}{\partial x}\right] &= (W c_i)^{\text{in}} \quad \text{for } x = 0, \\ \frac{\partial c_i}{\partial x} &= 0 \qquad\qquad \text{for } x = 1. \end{aligned} \tag{3.83}$$

We shall also employ the following shorthand notation: $c_i^{\text{out}}(\theta) \equiv c_i(x = 1, \theta)$.

Although there are several boundary conditions, the conditions of Danckwerts are more realistic, since they consider the continuity of the system, contrary to what occurs with changes in pulse [78].

3.6 Final Outlook

Based on the analysis that single-column batch chromatography can potentially achieve many of the benefits of continuous chromatography through smart recycling of the mixed fractions, the purpose of this chapter was to describe the most efficient way of mimicking the behaviour and performance of continuous multicolumn chromatography with a single-column apparatus for the purification of biopharmaceuticals. Hopefully, this single-column process can achieve the same specific productivity (feed processed per unit time per resin volume or feed processed per unit time per column) as the multicolumn process mimicked.

To fulfill the purposes of the work, as first step, the basis for single-column analog and a brief explanation of how to replace multicolumn continuous chromatographic systems was given. The conceptual prototype design of the biomolecule purification train, using only one chromatographic column, was developed to work in a broad range of configurations (including a fully continuous way). To define the best project, results obtained in previous studies [17, 176] carried out by the research group from which the thesis project is inserted was taken as reference. In order to show that the outlined design is feasible, the operation of the recycle piston was depicted and the experimental prototype was described and assembled with attention to minimize dead volumes, quantity of equipment required and size of the installation in general, as well as to operate with the least possible human intervention. A full automated system, controlled by *Julia*, was obtained. The automation of the entire structure avoids operating errors during the capture or purification process of a biomolecule. The mathematical model of the new system was described and discussed, being divided in four sections: recycle device, perfectly mixed tank, dead volumes and chromatographic column.

This out-of-the-box process has the potential to entirely revolutionize the field of continuous chromatography, once the newly developed platform shares the benefits of SMB chromatography in that it not only gives significantly higher yields of purer product, but also enables processing more feed and thereby increasing the overall throughput comparing to batch chromatography. However, the novel single-column analog to SMB

process uses just a single chromatographic column, which implies a great added value: a smaller number of columns is preferable, less solid phase is required, less equipment is involved and the pressure drop is reduced. The only thing that can compromise the product purity and productivity of this process comparing to the analogous SMB is the efficiency of the plug-flow device.

The built prototype was used to validate the new method, the Single-column Analog with Recycle Lag, in the following chapters of the thesis.

Chapter 4

Experimental Validation of the Adsorption Unit: Nucleosides Separation by Reversed-phase

4.1 Introduction and Objective

4.1.1 Validation of Chromatographic Methods

Analytical chromatography is a method commonly used for quantitative and qualitative analysis of drugs substances and compounds in biological fluids. Preparative chromatography is used for the separation and/or purification of these compounds under undiluted conditions. When it comes to a new chromatographic method, validating this process is a key requirement [232]. Method validation is defined as the process by which the method is tested by the developer for accuracy, reliability and reproducibility of its intended purpose, as well as to ensure process robustness and product quality.

In addition, testing a new method should ensure that it is reproducible when used by other users on other equivalent equipment, on other day or location. The validation process should also be a work in progress, open to method changes, with the possibility of re-validation if required. Therefore, design and validation is the starting point for using a new method before generating important results.

The Analytical Methods Technical Committee of the Chemistry Manufacturing Controls Coordinating Committee (CMCCC), at FDA, published a Technical Reviewer Guidance for the validation of new chromatographic methods, presenting the issues to consider when evaluating chromatographic methods from a regulatory perspective, discussing the weaknesses of chromatography that must be taken into account to ensure good performance of the method [45]. Although not all parameters of validation are applicable for all types of tests, the typical validation characteristics are [46]:

- **Accuracy:** Measure of how close the experimental value is to the true value;
- **Detection Limit:** The lowest analyte concentration in a sample capable to be detected, although not inevitably quantified, under the established experimental conditions;
- **Quantitation limit:** The lowest analyte concentration in a sample capable to be quantitated with precision under the established experimental conditions;
- **Linearity:** The working sample concentration and samples tested for accuracy should be in the linear range (UV response x concentration at a linear relationship). The linear range of detectability is dependent on the detector and compound utilized;
- **Precision (Repeatability or reproducibility):** Measure of how close the data values are to each other for a number of measurements under the same analytical conditions;
- **Range:** Interval between the low and high concentrations of analyte studied;
- **Recovery:** Amount of the compound of interest at the product as percentage of the theoretical amount present in the analyte;
- **Robustness:** Measure of the method's capability to persist unaltered by little variations in method parameters, e.g. column type, column temperature, age of columns, reagents, pH of buffer in mobile phase;
- **Specificity/selectivity:** The analyte must not have interference from other foreign components. Therefore, a representative chromatogram should be generated showing that the extraneous peaks are well resolved from the main analyte.
- **System suitability specifications and tests:** Parameters that provide assistance in achieving a well-behaved chromatographic system. The parameters can be capacity factor, precision/injection repeatability, relative retention, resolution, tailing factor, theoretical plate number, among others.

4.1.2 Two-column SMB for Binary Separation

In 2010 our research group developed and validated experimentally a streamlined, two-column SMB process for two-fraction separation [228]. As the name suggests, this system uses two identical chromatography columns and the fluid is injected and circulated into the system through two liquid pumps. The feasibility and effectiveness of the reported two-column process were verified experimentally using the linear separation of uridine and guanosine by reversed phase chromatography, operating in an open-loop configuration, as case study. The schematic of one full operating cycle is shown in Figure 4.1. This semi-continuous, two-column process implements pulsed feed injection and selective

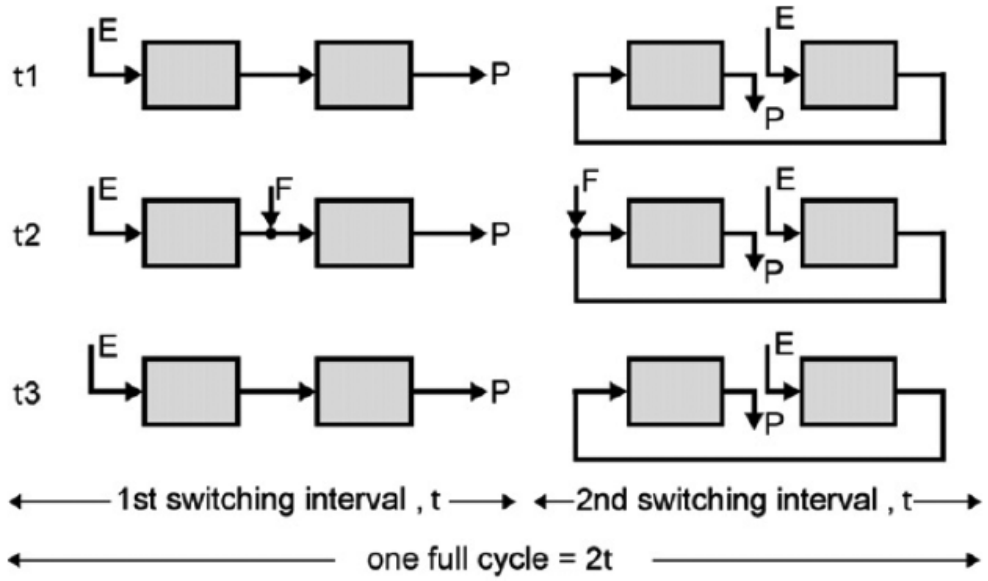

Figure 4.1: Schematic of one full operating cycle for the two-column, semi-continuous, open-loop process. E = eluent inlet, F = feed inlet, and P = product outlet, which can be either the less or more retained compound depending on the separation [228].

product withdrawal, representing a compromise between continuous, multi-column SMB and traditional batch chromatography.

Because the process has two columns, a full cycle can be divided into two equal half-cycles, or switching intervals as they are known in the jargon. At the end of each half-cycle the column positions are exchanged or, alternatively, the columns are fixed in space and instead the inlet and outlet ports [192] are moved, and the steps are repeated all over. Therefore, the process can be explained by the first half cycle only. The upstream column outlet is continuously eluted, feed is periodically injected into the fluid stream between the two columns, and the two components are selectively collected in the downstream end.

Experimental results were compared to simulated data generated from a dynamic model implemented in gPROMS and a very satisfactory agreement between was obtained. Steady-state operation was reached after six operating cycles, while the minimum purities of extract and raffinate were set at 99% each. The performance of the two-column, semi-continuous, open-loop scheme was compared to single-column batch chromatography and its enhanced version with ideal steady-state recycling (SSR) technique, but also with the closed- and open-loop versions of a classical, four-column SMB, taking into consideration that the total amount of stationary phase was the same on all processes. As result, the two-column process obtained the best performance, with lower eluent consumption (Eluent-to-Feed flow rate ratio) for the same feed flow rate in comparison with the batch systems, and very similar compared with the two four-column SMBs; however the developed process has less equipment and half the number of columns than the two

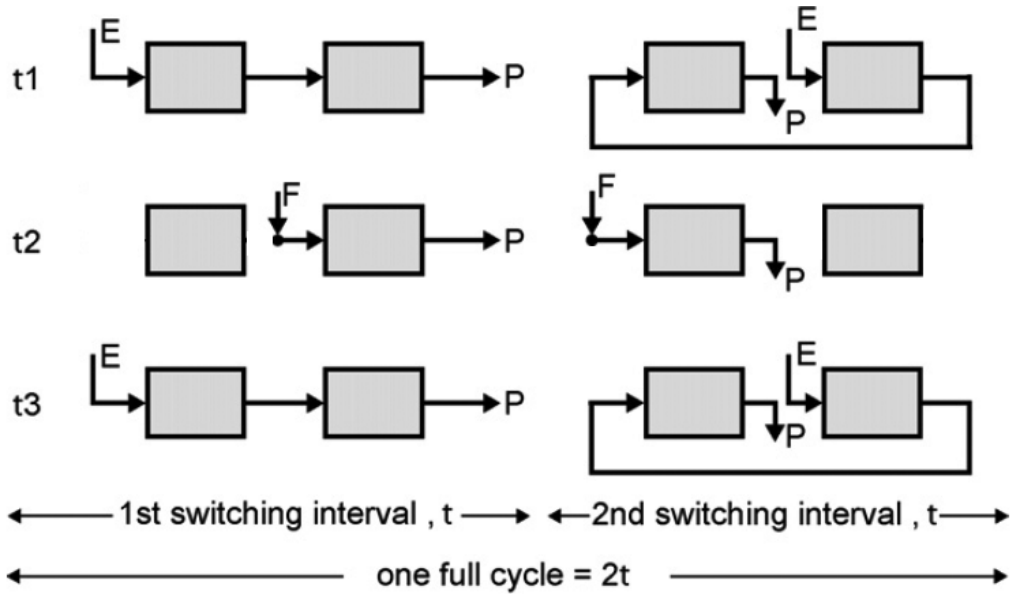

Figure 4.2: Schematic of one full operating cycle for the two-column, semi-continuous, open-loop process with discontinuous elution. E = eluent inlet, F = feed inlet and P = product outlet, which can be either the less or more retained compound.

SMB systems [224].

Actually, there is also a variant of the same process that was not explored in that paper. In this second process the elution is stopped at the upstream column during the step in which fresh feed is injected into the downstream column. The schematic of this variant is shown in Fig. 4.2. The two processes have about the same performance.

This two-column system presents itself as a promising alternative to single-column batch chromatography due to its increased performance, simplicity of operation and implementation, and ease of scaling-up. Therefore, the two-column SMB proved to be a combination of simplicity and flexibility of the batch process and the increased productivity of multi-column chromatography. Because of these qualities, this system was chosen as reference for the experimental validation of the Single-column Analog to SMB.

4.1.3 Objective

The purpose of this chapter is to validate the single-column process developed in this thesis, proving the effectiveness of its operation. For this, a two-column SMB process already developed in the past for linear binary nucleoside separation is used as reference for the Single-column Analog to SMB and, moreover, the general techno-economic challenges are evaluated and discussed, specifically data of purity, recovery, solvent consumption, complexity, cost, maintenance, dimensions and reproducibility. Some secondary objectives arise to achieve the main objective; they are: preliminary tests of piston operation evaluation and the characterization of the system; experiments previously necessary to be able to proceed to the separation of biomolecules.

Table 4.1: Reagents used in the execution of the activities of Chapter 4.

Reagent	Molecular formula	Manufacturer
Blue Dextran (from dextran w/ MW 2x10^6)	$C_6H_{10}O_5$	Sigma-Aldrich
Ethanol absolute	CH_3CH_2OH	Panreac
Uridine (99%)	$C_9H_{12}N_2O_6$	Sigma-Aldrich
Guanosine (98%)	$C_{10}H_{13}N_5O_5$	Sigma-Aldrich

4.2 Materials and Methods

4.2.1 Materials

The reagents are listed and described in Table 4.1.

4.2.2 Preliminary Tests: Piston Proof-of-Concept

Preliminary experiments (Figure 4.3) to test the operation of the recycle device were carried out. The first two experiments were ran even before coupling the device to the setup structure with the rest of the setup equipments. An isocratic pump K501 (Knauer, Germany) was connected to the inlet capillary of section A of the device, while another similar liquid pump was connected to the inlet of section B of the recycle equipment.

First, isocratic injection of blue dextran solution, at 0.08 g/L, was done into the recycle bin at a flow rate of 5 mL/min until 10 cm of heigh in section A, while the section B outlet was open. Soon after, the pump connected to the section B inlet was started with deionized water at the same flow rate of 5 mL/min up to full piston closure, while the section A inlet was closed and the section A outlet was open, fluid coming out of the equipment through the flexible tube that connect section A outlet to the bottom of the recycle device.

The second piston function test consisted of gradient injection using blue dextran solution, at c = 0.24 g/L, and performing the experiment in the same two configurations as the previous one: solution injection in section A and later deionized water injection in section B. A third pump was used with deionized water to promote the gradient. A connector was placed in the piston inlet capillary to receive fluid from the two pumps and promote mixing before it enters in section A. The gradient was performed from highest to lowest concentration. To achieve the flow rate of 5 mL/min, the flow rate of each pump changes over time, starting with the pump responsible for the dye solution at maximum flow rate down to 0 mL/min, while the other pump starts at flow rate 0 mL/min up to 5 mL/min. Approximately 6 mL fluid fractions were collected in small glass vials whereas the piston was returning to original position (closed).

In a third experiment, it was tested if there was mixture between sections A and B of the piston. This time, the piston was already connected to the system, with possibility of

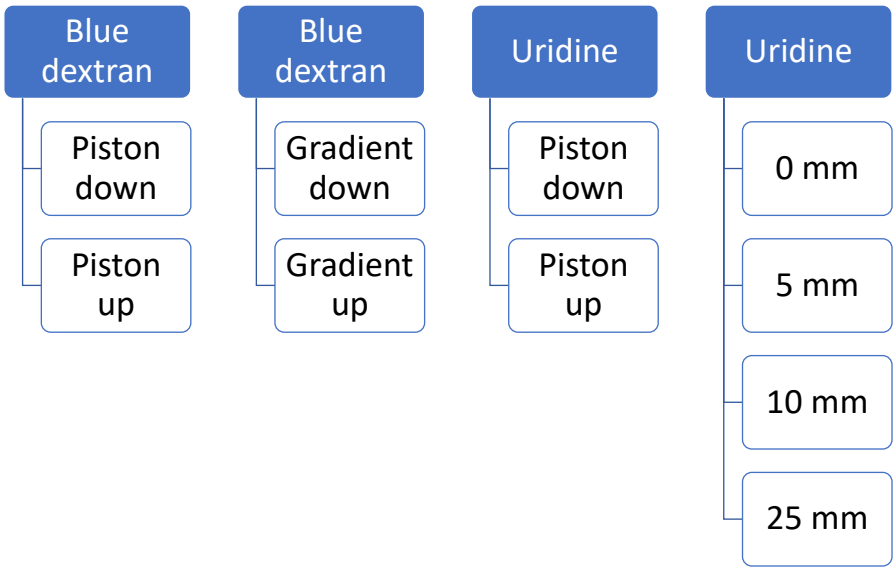

Figure 4.3: Four preliminary tests for piston proof-of-concept. The first consist of isocratic injection, in the second gradient injection was performed, while in the third fluid mixture between section A and B were tested, and finally, in the fourth experiment, the hydrodynamic behaviour inside the piston was tested for different heights.

UV reading. The test consisted of injecting uridine solution to the piston, in order to put the movable part down, and then remove this solution from the piston, so that the mobile piston touches the top of the piston. This test was conducted with 0.05 g/L uridine in 5%-v/v ethanol solution. The solvent used as reference for the UV reader was 5%-v/v ethanol in deionized water. The flow rate of each the pump was 2 mL/min. The UV absorbance was read at the entrance of the piston during the injection and at the output of the same during the closing, with sampling intervals of 0.5 s, with absorbance reading at 260 nm, using the USB2000 spectrometer, only Deuterium lamp turned on, integration time of 15000 μs.

To characterize the piston, in order to determine the hydrodynamic behaviour within the piston, the fourth preliminary experiment was conducted. Uridine injections, up to UV signal saturation, were performed for different heights of the movable piston, 0, 5, 10, and 25 mm, which remained static throughout the experiment. For each height, the experiments were performed in triplicate. Furthermore, for these experiments, the absorbance detector was placed after the piston. All other operating conditions were similar to the previous experiment. The *Julia*'s command script, used for this experiment, is listed in Appendix B.1.

4.2.3 System Characterization

The characterization of the system consists in determining the parameters of the chromatographic column, piston and capillaries of the setup.

4.2.3.1 Column Packaging and Interparticle Porosity (ϵ)

The chromatographic column used for the nucleosides separation was a Superformance 26 mm i.d. thermojacketed glass column (Götec Labortechnik, Germany). The resin utilized was Source30 RPC (GE Healthcare Amersham Biosciences, Uppsala, Sweden). The stationary phase was slurry packed into the column, as described elsewhere [228], to a bed height $L = 6.0$ cm, using mobile phase at 25 mL/min, back-pressure of 30 bar and 30 min packing time.

The interparticle porosity of the resin packed into the column (interparticle void fraction, ϵ) was determined from the difference of retention volumes of step injections of blue dextran ($c = 0.24$ g/L) in an aqueous solution of 5%-v/v ethanol eluting through the column ($t_{injection} \approx 1000$ s) and bypassing the column ($t_{injection} = 60$ s). The flow rates were set at 1 mL/min for each pump. The wavelength of 620 nm was used to measure the absorbances at bypass and column. The choice for wavelength is discussed in Appendix B.2. The UV sampling time was 1.0 s. The experiments were performed in triplicate.

The retention volume (θ_R) is defined by

$$\theta_R = t_R Q, \tag{4.1}$$

where Q is the volumetric flow rate and t_R the retention time, ie, the time that the solute takes to travel the entire column and elute. The retention volumes for bypass (θ_R^{bp}) and column (θ_R^{col}) were calculated using the Equal-Area Method (EAM) (see Figure 4.4), that is, the point in the graph giving the retention volume is found when the area between the reference and the point is equal to the area between the same curve point and the plateau (UV signal for saturation absorbance, or saturation concentration).

Hence, the interparticle porosity is

$$\epsilon = \frac{\theta_R^{\text{col}} - \theta_R^{\text{bp}}}{V_{\text{c}}}, \tag{4.2}$$

where V_{c} is the empty column volume. Figure 4.5 illustrates the calculation method for the porosity of a packed chromatography column.

For each set of experiments done in triplicate the results were averaged and the error was calculated. An error of up to 5% was deemed acceptable to take the average as the final result. All experiments in triplicate or duplicate hereinafter were treated as such.

For the error determination, first the standard deviation was calculated:

$$\sigma = \sqrt{\frac{\sum_{i=1}^{N}(x_i - \mu)^2}{N}}, \tag{4.3}$$

where σ is the standard deviation, x_i is the ith experimental value, N is the number of experimental data, and μ is the arithmetic mean of the values.

Thus, the error is

$$error \text{ or } \sigma_{relative}(\%) = 100 \times \frac{\sigma}{\mu}. \tag{4.4}$$

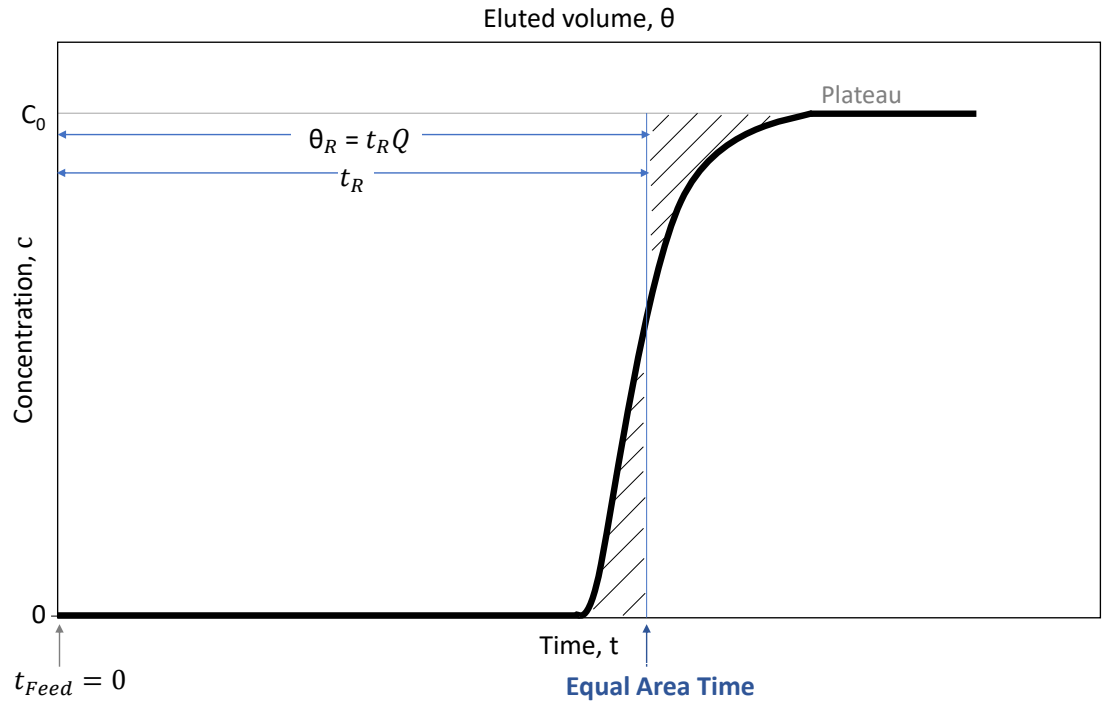

Figure 4.4: Scheme for Equal Area Method. The point is determined when the areas below the curve and above the curve are equal. $t_{Feed} = 0$ is the time when blue dextran solution (feed) begins to be injected.

4.2.3.2 Henry's Constant (H)

If the concentration c_i of a solute i in a fluid phase in thermodynamic equilibrium with an adsorbent is sufficiently diluted, the solute concentration in the adsorbed phase, q_i, will be directly proportional to c_i, ie,

$$\lim_{c_i \to 0} q_i = H_i c_i, \tag{4.5}$$

where H_i is known as the Henry constant. The solute concentration c_i is commonly expressed as a molar or mass concentration (amount of solute per volume of fluid, but sometimes per column volume) and seldomly as molar, mass or volumetric fraction in the solvent. For example, if c_i is expressed as amount of solute per unit volume of mobile phase, which is the convention adopted in this work, the amount of solute in the interparticle fluid per unit volume of packed column will be simply given by ϵc_i.

The solute concentration in the adsorbed phase is usually expressed as amount of solute (moles or mass) per unit amount of solid, which can be mass, number of moles, volume of solid, or even column volume. If q_i is expressed as amount of solute per unit volume of solid, which is the convention adopted in this work, the amount of adsorbed solute per unit volume of packed column will be simply given by $(1 - \epsilon)q_i$.

Experimentally the Henry constants were determined from the difference of retention volumes of diluted pulses (40 s) of each component of the mixture (guanosine and

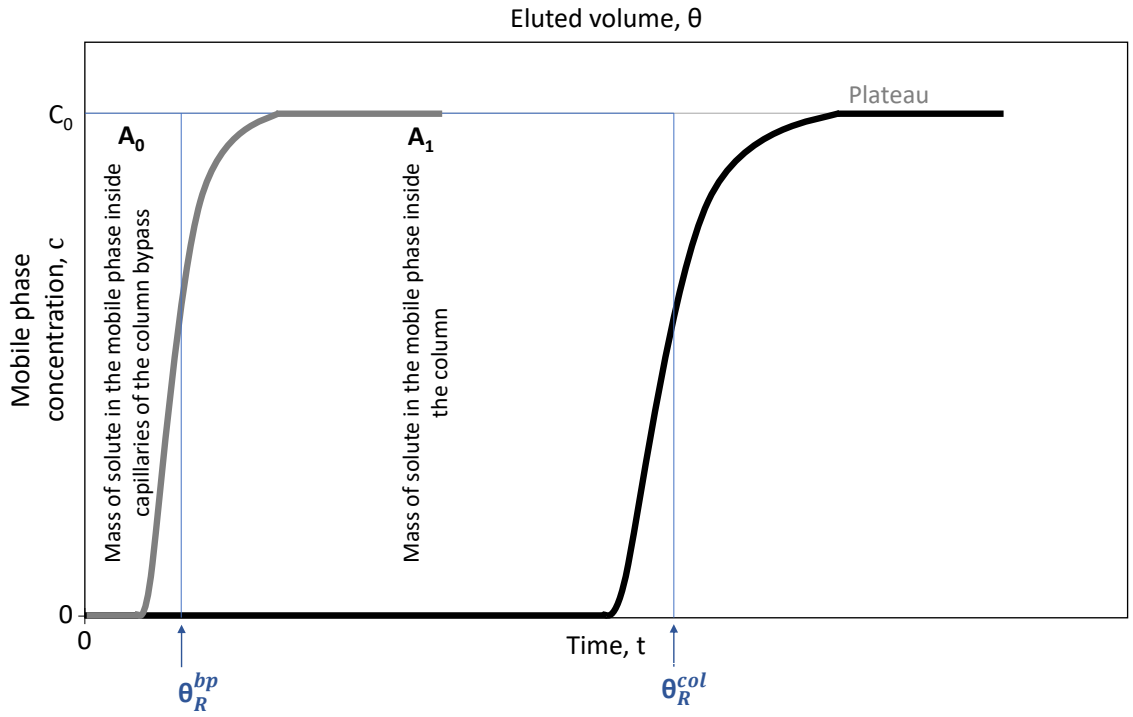

Figure 4.5: Calculation method for the interparticle porosity of the chromatographic bed. θ_R^{bp} is the retention volume of fluid bypassing the chromatographic column and θ_R^{col} is the retention volume of blue dextran passing through the column.

uridine), at $c_i = 0.05$ g/L, passing through ($\theta_{R,i}^{col}$) and bypassing ($\theta_{R,i}^{bp}$) the column, where $\theta_{R,i} = Qt_R$ and Q is the volumetric flow rate. It was known beforehand that the two nucleosides exhibit linear adsorption behavior for concentrations well above 0.05 g/L. The Henry constant is related to $\theta_{R,i}^{col}$ and $\theta_{R,i}^{bp}$ as follows:

$$\theta_{R,i}^{col} - \theta_{R,i}^{bp} = [\epsilon + (1-\epsilon)H_i]V_c \quad or \quad H_i = \frac{\theta_{R,i}^{col} - \theta_{R,i}^{bp}}{(1-\epsilon)V_c} - \frac{\epsilon}{1-\epsilon}. \tag{4.6}$$

Here, the retention volumes for bypass (θ_R^{bp}) and column (θ_R^{col}) are the intervals measured between half of the peak of their respective detections and half of injected pulse peak (see Figure 4.6).

Five flow rates were utilized, with the experiment performed in triplicate for each flow rate: 1, 2, 3, 4 and 5 mL/min. The experimental chromatograms were monitored using a USB2000 spectrometer at a wavelength of 260 nm, integration time of 37000 μs and 1 s sampling rate.

Figure 4.7 illustrates the calculation method for the Henry constant of each component. Appendix B.3 contains the sequence used in *Julia*. Appendix B.4 shows the absorbance spectrum of uridine and guanosine, previously analyzed to decide the ideal wavelength to work with the components.

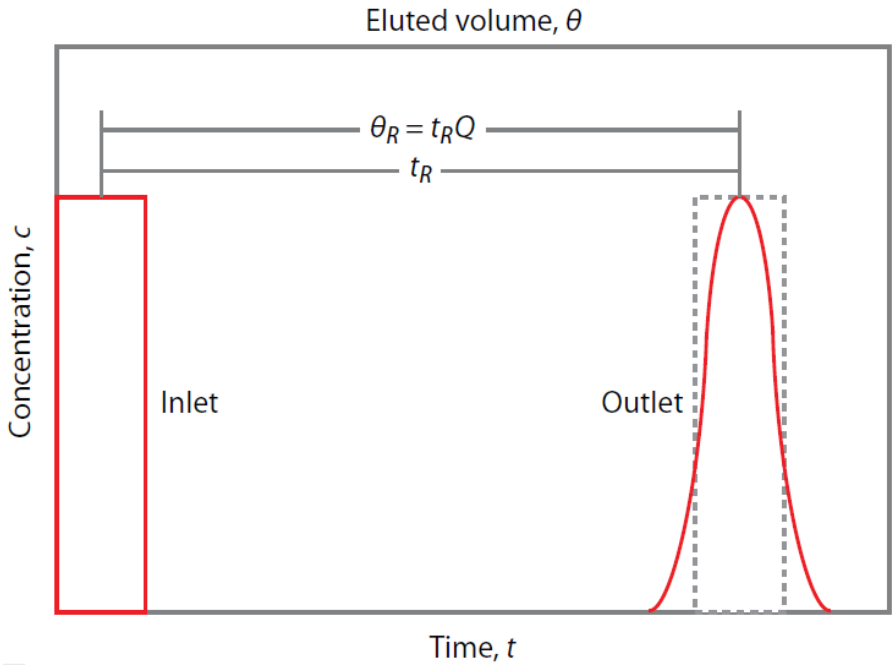

Figure 4.6: Scheme for the test of solute pulse injection at dispersion plug flow.

4.2.3.3 Adsorption Isotherms

Adsorption isotherms were determined by step injection (1080 s, or 18 min) at five different concentrations for each solute. The experiment was performed in duplicate. The stock solution had c_i = 0.2 g/L, and the operating flow rate was set at 5 mL/min. The concentrations were obtained through the effect of solution gradient, thanks to the use of two pumps, promoted by the operation script presented in Appendix B.5, so that the total flow rate always remained constant. USB2000 spectrometer was used, IT = 37000 μs, with a UV measurement range of 1 s, and λ_{uri} = 287.25 nm and λ_{gua} = 293.20 nm.

For the concentrations to be used in the case studies of this thesis, linear isotherm is expected, therefore:

$$q^* = Hc, \tag{4.7}$$

where q^* is the concentration of solute adsorbed in equilibrium with the liquid phase and c is the concentration of solute in the mobile phase.

Therefore, with this procedure, the adsorption isotherm is verified and the Henry constant for each compound is also obtained by the curve slope, which can be compared to that determined in the previous section.

4.2.3.4 Column Dynamic Behaviour: Péclet Number (Pe)

The Péclet number, Pe, is a measure of band broadening (ie, smearing or smoothing of a concentration font in the fluid phase) or axial dispersion as a solute percolates through a packed column by the action of a mobile phase. The phenomena lumped into Pe can

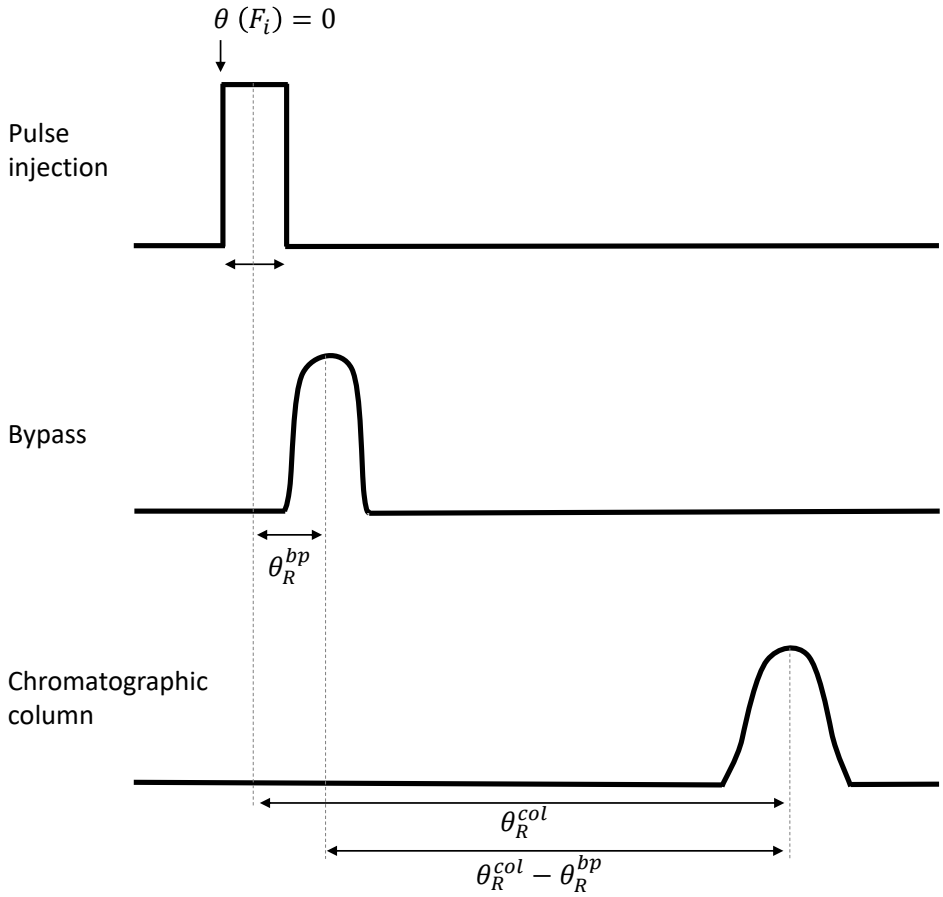

Figure 4.7: Calculation method for the Henry constant for each component. $\theta(F_i) = 0$ is the eluted volume when compound solution (feed) begins to be injected, θ_R^{bp} is the retention volume of fluid bypassing the chromatographic column and θ_R^{col} is the retention volume of the same compound passing through the column.

range from the simplest case of the combined effect of molecular diffusion and hydrodynamic dispersion to cases which also account for external film mass transfer, intraparticle (molecular and surface) diffusion and, in some rare cases, even adsorption kinetics. A related measure of band broadening is the plate height, hL, defined as

$$h = \frac{2}{\mathrm{Pe}}, \tag{4.8}$$

where h is the dimensionless plate height and L the column length; the number of theoretical plates is $1/h$.

In the present study of nucleosides Pe is taken as a measure of the lumped contributions of molecular diffusion and hydrodynamic dispersion of the solid in the interparticle fluid and intraparticle solute mass transfer. For the range of flow rates commonly used in preparative chromatography the dependence of h (or 1/Pe) on the flow rate is usually well approximated by a straight line with negative slope.

The Péclet number was determined from the same chromatograms used to determine

the Henry constant, fitting the experimental dependence of the plate height on flow rate for diluted pulses of the solutes. For this purpose the experimental absorbance data as a function of time (ie, the chromatogram) obtained at the various flow rates (1, 2, 3, 4, 5 mL/min) were fitted in gPROMS software to a dispersed plug-flow model to estimate Pe for uridine and guanosine.

4.2.3.5 Characterization of the Recycle Device: Dead Volumes (V_0 and V_L)

The dead volumes at piston inlet (V_0) and outlet (V_L) due to the presence of frits at the ends of piston were determined by step injection of blue dextran solution (c = 0.24 g/L in 5%-v/v ethanol) until saturation in UV detector at Q = 1 mL/min, as was proceeded in the column porosity experiment. The reference solution was ethanol 5% (v/v) in water, at c = 0.05 g/L. The absorbances were measured at λ = 620 nm and the UV sampling interval was 1.0 s.

The difference here is the UV detector position, which is located, in this experiment, at the capillary immediately after the piston. The piston is kept closed and the fluid flow is always bypassing the column. The total dead volume is divided by two to obtain values of V_0 and V_L, given that the two frits are identical.

Two different setup settings are required for piston dead volumes determination:

1. Feed stream flows through the closed piston, obtaining θ_R^{RP}. Feed injection time, $t_{injection}$ = 350 s;

2. Feed stream bypasses the piston, with a capillary of L = 35 cm replacing the piston, obtaining $\theta_R^{RP_{bp}}$. The 35 cm represents the flexible capillary that is contained within the piston and must be accounted for when calculating the eluted volume. Feed injection time, $t_{injection}$ = 200 s.

Therefore, the frits dead volumes are:

$$V_0 = V_L = \frac{\theta_R^{RP} - \theta_R^{RP_{bp}}}{2}, \tag{4.9}$$

The calculation of the eluted volume is done exactly as explained in section 4.2.3.1, through EAM calculation.

4.2.4 Experimental Validation

4.2.4.1 Cycle Determination

The experimental proof of concept of the single-column process with recycle lag, that uses a simplified version of the plug-flow device, uses the linear separation of two nucleosides, uridine and guanosine, by reversed phase Source30 RPC, as case study to demonstrate the effectiveness of the proposed chromatography apparatus to mimic the behaviour of two-column continuous chromatography. An optimized two-column chromatographic process

for nucleosides separation has been previously addressed by our research group [228]. For this reason, this process was selected to be mimicked by the new apparatus presented in this thesis.

To convert the multicolumn process into a one-column process with recycle lag, it is necessary to select a column at random from the two-column process, say column 2, and follow its operation over a full cycle. The fractions of its effluent that are directed to the other column are, instead, diverted to the recycle piston to be reinjected later in the cycle. This procedure was applied to the two-column process whose cycle is depicted in Figure 4.2.

4.2.4.2 Steps Duration

Using the column parameters determined experimentally (Section 4.2.3) and the resulting single-column process (Section 4.2.4.1), the cycle parameters were determined using model-based optimization in AMPL, achieving the ideal times for each step of the cycle. This procedure is explained in detail later on.

4.2.4.3 Experimental Procedure

The linear separation of two nucleosides, uridine (Figure 4.8a) and guanosine (Figure 4.8b), by reversed phase Source 30 RPC, was performed isotermically at 30ºC. To give adequate retention and separation factors, 5% (v/v) ethanol in water was fixed as mobile phase [3]. The organic solvent is added to lower the polarity of the aqueous mobile phase, and thereby improve the eluting strength in reversed phase chromatography. In addition, the organic solvent (modifier) should not have high viscosity (such as isopropanol), in order to avoid low column efficiencies and high back-pressures [10].

Uridine (99%) and guanosine (98%) were purchased from Sigma-Aldrich (Steinheim, Germany), and HPLC-grade ethanol from Panreac (Spain). The solvents were mixed in the appropriate volumetric proportions. Feed solution was prepared with $c_i = 0.05$ g/L ($i = 1$ for uridine and $i = 2$ for guanosine) in ethanol 5% (v/v), and subsequently subjected to an ultrasound bath, to remove possible dissolved air. These concentrations were selected to ensure linear calibration curves. Therefore, the deconvolution of the UV measurements taken at several, suitably chosen, wavelengths results in the individual nucleoside concentration. Only one UV detector is used in this experiment placed right after the chromatographic column. As monitoring scheme, the sampling rate of the UV was fixed at 0.5 s, monitoring the outlet effluent composition of the chromatography column. Absorbance measurements were made using the USB2000 spectrometer, integration time 15000 μs, and λ in the range 260–300 nm. The pumps of the system were calibrated using *Julia*'s software, and both pumps, for feed and eluent, were operated at constant flow rate. The flow rates were set at $Q_E = Q_F = 4$ mL/min. The experimental script performed in *Julia* for this procedure, "ColExps.jl", is described in Appendix B.6.

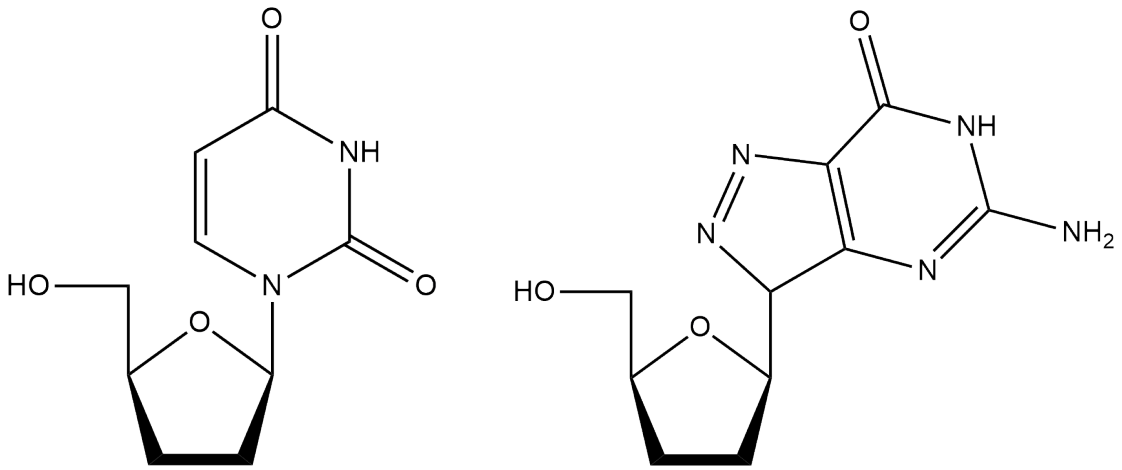

(a) Uridine molecule. (b) Guanosine molecule.

Figure 4.8: Biomolecules utilized at experimental procedure. Guanosine is a purine nucleoside in which guanine is attached to a ribose (ribofuranose) ring via a β-N(9)-glycosidic bond, and is essential for metabolism [53, 67]. Uridine is a ribonucleoside consisting of a molecule of uracil attached to a ribofuranose moiety via a β-N(1)-glycosidic bond, and as guanosine, it also has a function as a human metabolite [54]. Images source: [209].

The mode of operation performed for the experimental validation is the open-loop configuration. For this, the cycle design for this configuration was established before each experiment is performed.

The process takes a few cycles to attain what is called the cyclic steady state when the concentration profiles are identical from cycle to cycle. Therefore, for this experiment it was decided to produce thirteen cycles.

The choice of the mixture to be used for this experimental validation, as well as the concentrations of the mobile phase and the desorbent were based on previous studies [228] carried out by the group in which the present thesis is inserted, where the validation of another chromatographic system, a two-column SMB process, was carried out for binary separation.

The experiments were evaluated in terms of purity, recovery, and solvent consumption. The calculations of purity (*Pur*) and recovery (*Rec*) of the extract and the raffinate are based on the following equations:

$$Pur_R = \frac{\int_{t_n}^{t_n+\tau} c_1^{out} Q_R \, dt}{\int_{t_n}^{t_n+\tau} (c_1^{out} + c_2^{out}) Q_R \, dt}, \quad Pur_X = \frac{\int_{t_n}^{t_n+\tau} c_2^{out} Q_X \, dt}{\int_{t_n}^{t_n+\tau} (c_1^{out} + c_2^{out}) Q_X \, dt}, \tag{4.10}$$

$$Rec_R = \frac{\int_{t_n}^{t_n+\tau} c_1^{out} Q_R \, dt}{c_1^F \int_{t_n}^{t_n+\tau} Q_F \, dt}, \quad Rec_X = \frac{\int_{t_n}^{t_n+\tau} c_2^{out} Q_X \, dt}{c_2^F \int_{t_n}^{t_n+\tau} Q_F \, dt}, \tag{4.11}$$

where indices 1 and 2 denote the less (uridine) and more (guanosine) retained solute, respectively, $\tau = \sum_k \tau_k$ is cycle duration (τ_k is the duration of the kth step of the cycle), and $t \in (t_n, t_n + \tau)$ the time interval during which the nth cycle takes place.

Figure 4.9: gPROMS logo. Source: [218].

The productivity (mL/min), specific productivity (min^{-1}), and solvent consumption (–) are defined as

$$Productivity = \overline{Q_F}, \quad \overline{Q_F} = \frac{Q_F \tau_F}{\tau}, \tag{4.12}$$

$$Specific\ productivity = \frac{\overline{Q_F}}{V_c}, \tag{4.13}$$

$$Solvent\ consumption = \frac{\overline{Q_E}}{\overline{Q_F}}, \quad \overline{Q_E} = \frac{Q_E \tau_E}{\tau}, \tag{4.14}$$

where Q_j is the volumetric flow rate, $j = R$, X, F or E, being the raffinate, extract, feed and eluent, respectively. τ_F is the step duration of the cycle during which feed is injected into the process, τ_E the step duration of the cycle during which fresh eluent is injected into the process, and τ the overall cycle duration.

4.2.5 Data Simulation

Two distinct simulations were developed for the separation of uridine and guanosine using the single-column apparatus. Both used the same experimental cycle (section 4.2.4.1) and system and cycle parameters (sections4.2.3 and 4.2.4.2, respectively) experimentally obtained; however one simulation considered the piston as a dispersed plug-flow device and another one considered it as a perfectly stirred tank.

The simulations were implemented in the process modelling platform, gPROMS Model Builder, version 4.0.0 (Figure 4.9). The simulation was performed to ensure consistency of the new process and to evaluate which fluid behaviour corresponded within the recycling device when the experimental data is compared with these two distinct simulation conditions: the best scenario, dispersive piston flow behaviour, or the worst scenario, tank with perfect agitation.

4.3 Results and Discussions

4.3.1 Piston Proof-of-Concept

The initial experiments performed on the recycle device allowed analysing not only if the design of the equipment was well established through the operation of the movable piston, but also the pressure reached when the piston is operating and also the behaviour of the fluid inside it. Thanks to the dark blue colour of the blue dextran solution, serving

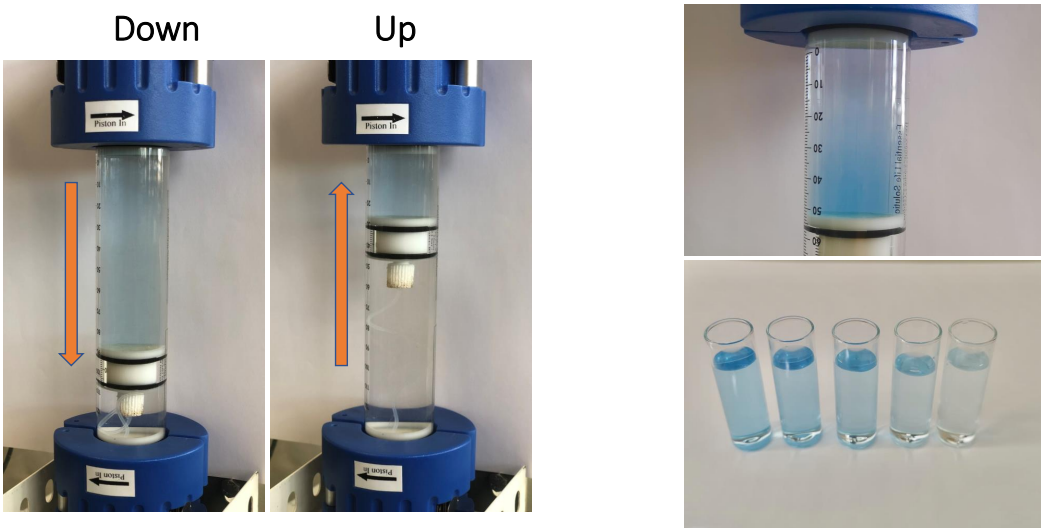

(a) Isocratic injection.

(b) Gradient injection.

Figure 4.10: Proof-of-concept of the piston-type device. Fig. 4.10a proved that the design of the recycle device really works, making the movement of the mobile plunger, while in Fig. 4.10b the gradient was done from the more concentrated solution of blue dextran to the less concentrated, successfully collected in fractions.

as a dye, the analysis of this proof of concept could be performed with the naked eye for the proper purpose. The operating configurations chosen promoted piston movement. Injection of solution in section A with the open section B outlet promoted lowering of the piston, and subsequent injection of deionized water in section B with the output of the device opened, forced the piston to rise. The chosen height of 10 cm is long enough to cover almost the full length of the recycle column, which allowed to analyse the pressure drop differences for different piston heights.

When the newly designed piston was tested for isocratic injection, results showed that its mechanical operation is very good and the design was successful (see Figure 4.10a). The maximum pressure reached on the piston was 6 bar, which gives a satisfactory low pressure, considering that the piston would still be inserted in the setup and, when in operation with other equipments (valves, UV detectors, capillaries and chromatographic column), the total system pressure would increase. The main responsible for the maximum pressure values achieved are the o-rings (two, in total) of the piston, which provide resistance when moving due to friction with the column glass. Thus, when operating only the piston, the resistance offered by the piston o-rings cannot be too high, given that the maximum pressure recommended by the manufacturers is 24 bar for recycle device and 60 bar for the chromatographic column used in this chapter, so the total system pressure must not exceed 20 bar to work with a safety margin.

In the second experiment, the gradient promoted on the piston was well identified, as shown in Figure 4.10b, where over the length of section A (from inlet to outlet), whereas the piston was descending, the gradient was clearly maintained. Since fluid collection

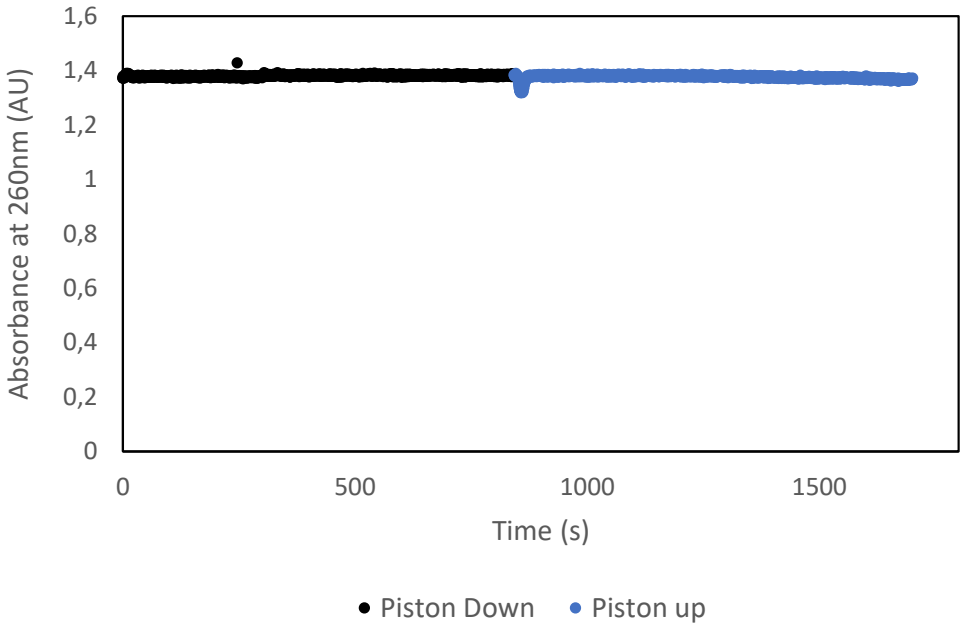

Figure 4.11: Graph of the mixing evaluation between the sections, A and B, of the piston. Uridine injection, 0.5 g/L v/v in ethanol 5%, was made by triggering the piston filler (UV at the piston inlet), and shortly after the piston closure (UV at the piston output. The graph shows the good sealing of the o-rings, that is, there is no fluid passing between the sections.

occurs as the piston is placed to rise, the collected fractions showed that the hydrodynamic behaviour of the piston matched the design presented in the previous chapter, keeping the concentration profile inside, not only in the descent as in the ascent of the mobile plunger, which gave, at first instance, the validity of the "first in, first out" method.

The third experiment proved that there was no mixture between the upper and lower part of the piston's movable plunger, indicating that the o-rings are fulfilling the function well. The result can be seen through the graph in Figure 4.11. After conducting these base experiments, the piston is ready to operate in processes of biomolecules separation.

The piston fluid characterization experiments were performed with the piston closed and with heights of 5, 15 and 25 mm inside the piston. Before the injection of uridine, the piston was only eluted; after saturation, the eluent was again injected until the piston was completely cleaned. It is important to mention that the injection times were different for each height, since they needed different times to reach saturation. From graph of Figure 4.12, it is envisaged that the hydrodynamic behaviour within the piston approached a dispersed plug flow, being acceptable and valid for the continued experiments. More detailed experiments on the fluid performance inside the recycle device were carried out in subsequent units of this chapter.

After conducting these base experiments, the piston is ready to operate in processes of biomolecules separation.

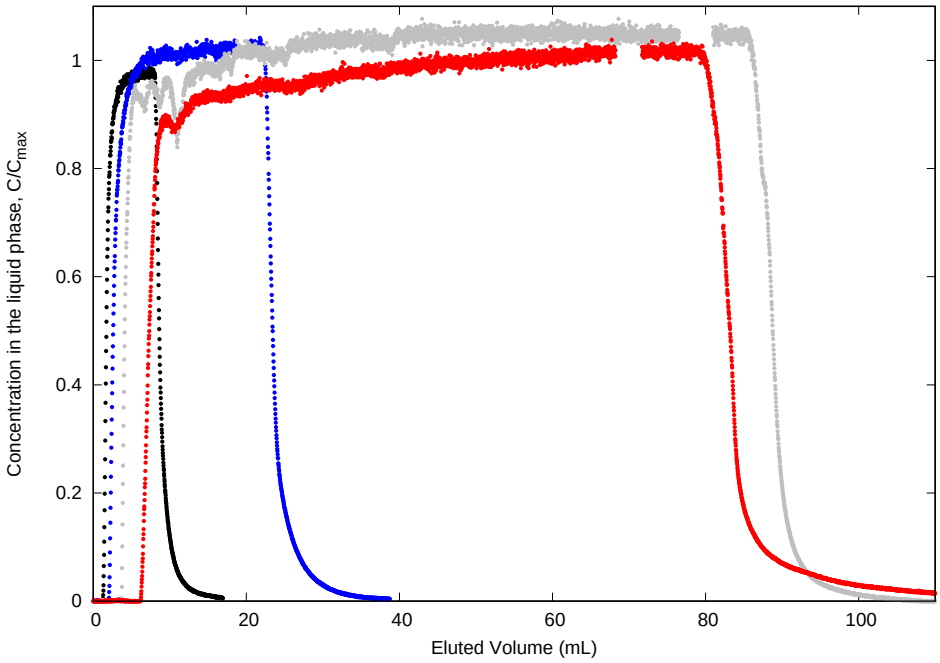

Figure 4.12: Hydrodynamic behaviour inside static piston, with uridine 0.05 g/L injection until saturation and subsequent cleaning with ethanol 5% v/v for piston heights of 0 mm (black), 5mm (blue), 10 mm (gray) and 25 mm (red). The piston presented similar behaviour to a dispersed plug flow for all different conditions.

4.3.2 System Characterization

4.3.2.1 Packaging and Interparticle Porosity (ϵ) of the Chromatographic Column

The chosen matrix, Source 30RPC, is a naked hydrophobic matrix, composed by mono-sized and spherical polystyrene/divinyl benzene particles, properly used for reversed-phase chromatography. With this resin, the components of the feed mixture bind to the stationary phase by order of hydrophobicity. The most hydrophobic compounds are adhered more strongly, while the less hydrophobic compounds are the first to leave the column when the elution is performed. The matrix and column used were exactly the same utilized in the two-column process already validated [228] for nucleosides separation. In this way, the imitation of the multicolumn process is subjected to more realistic conditions, that is, less experimental errors, considering that one of the major problems addressed by multicolumn processes is the fact that it is very difficult to obtain exactly the same fixed bed columns, even when they are subject to the same conditions of packaging. The column colume is $V_c = 31.86$ cm^3, since the column has $L = 6.0$ cm and i.d. = 2.6 cm.

To calculate the column's interparticle porosity (ϵ), a blue dextran solution was used.

Blue dextran is commonly utilized for void volume calculations in chromatographic columns, since it does not adsorb nor penetrates in resin particles [98]. The experimental data for the proper calculation are shown in Figure 4.13. The moment when the step of 60 s begins to be injected is the starting point of the data ($\theta_{Feed} = 0$). The retention volume for bypass was $\theta_R^{\text{bp}} = 0.180$ cm^3, while for column it was $\theta_R^{\text{col}} = 10.302$ cm^3. The difference between the retention volumes of the Blue Dextran solution passing through the chromatographic column and bypass the column allowed to calculate the interparticle porosity of the fixed bed, resulting $\epsilon = 0.318$. Since the column is the same used by the chromatographic process mimicked in this chapter, when comparing with the result, $\epsilon = 0.318$, obtained in the literature [228], the values present total concordance. Thus, the interparticle porosity calculated by the present doctoral student was used hereafter.

It is important to note that the column bypass retention volume also represents the dead volume of the setup up to the first UV, printed by the existing capillaries between the connector that joins the input streams of the system (Feed and Eluent) and the UV2 detector.

4.3.2.2 Henry's Constant (H)

The graphs used to calculate Henry's constants are shown in Figures 4.14 to uridine component, and Figure 4.15 to guanosine component. The difference between the retention volumes of the component passing through the column and bypassing ($\theta_{R,i}^{col} - \theta_{R,i}^{bp}$), and consequently the Henry's constant (H_i) were calculated for each flow rate. This difference must remain constant with the flow variation, as it is equal to the apparent column volume (V_i). The θ value considered for each graph was the average triplicate value.

The results obtained are expressed in Table 4.2. $H_1 = 1.264$ and $H_2 = 1.896$ are Henry's final values for uridine and guanosine, respectively, calculated by averaging H_i between the flow rates. As Henry does not change with the flow rate, it was expected that the H_i values for the different flow rates would be very similar. The low relative standard deviations obtained for H presented in the table prove the theory's agreement with the experimental results.

Moreover, it is noteworthy that the calculated values are very similar when compared with the values present in the literature [228], where was obtained $H_1 = 1.275$ (uridine) and $H_2 = 1.9$ (guanosine). Therefore, the parameters calculated in this section were used hereinafter.

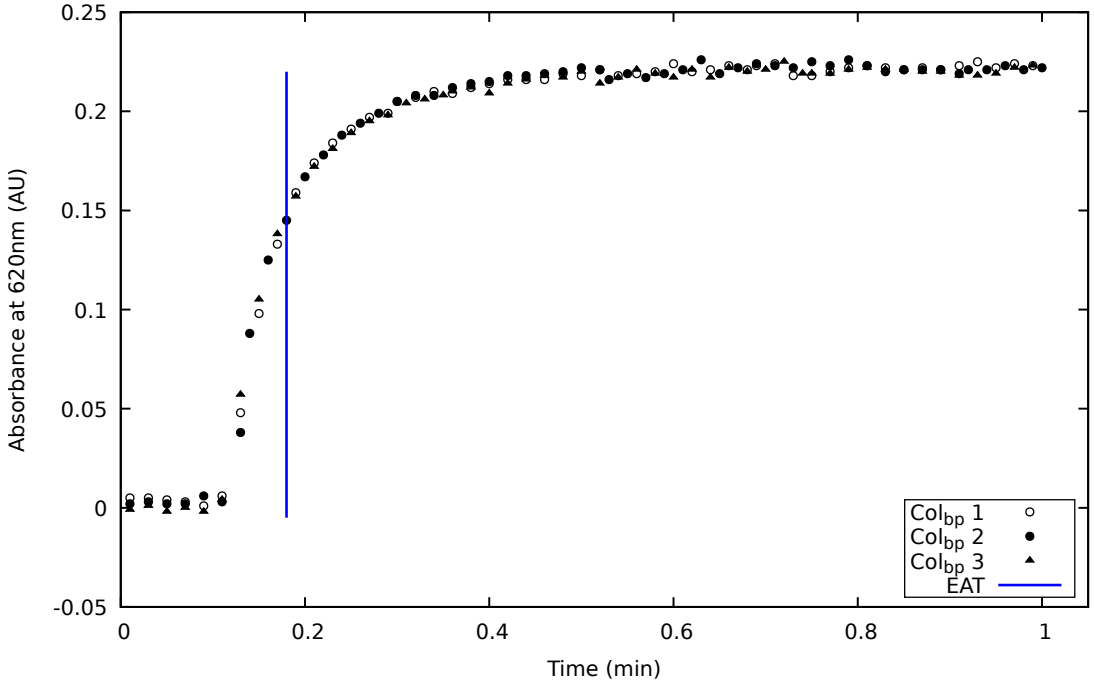

(a) Step injection (60 s) of blue dextran bypassing the column. The retention volume was $\theta_R^{bp} = 0.180$ cm^3.

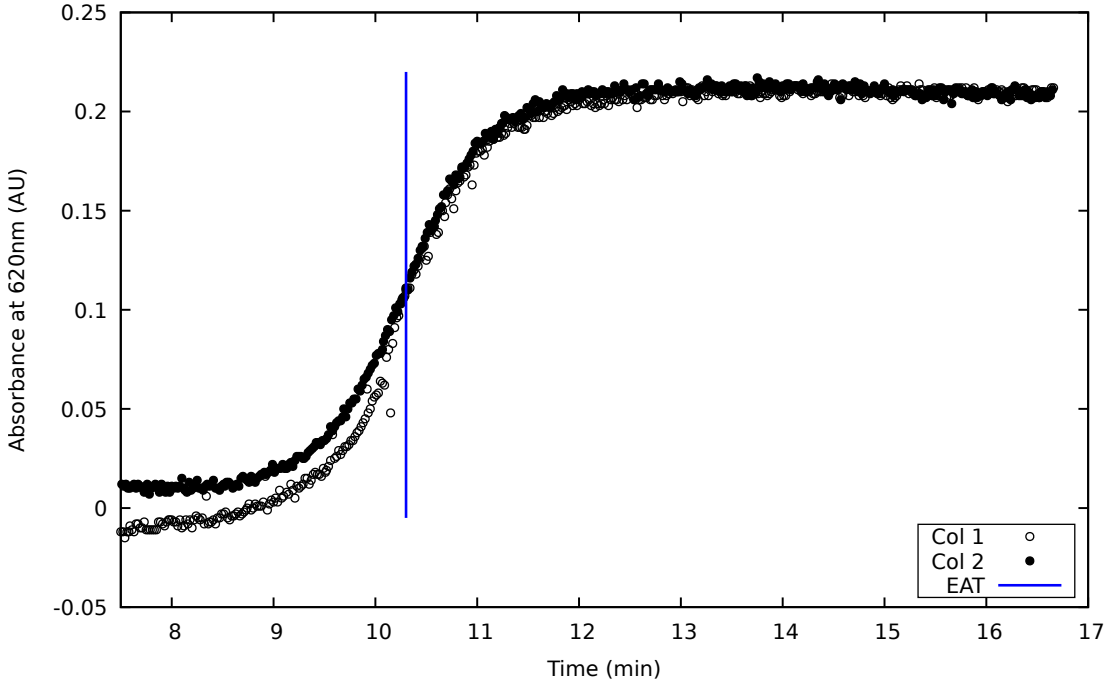

(b) Step injection (≈ 1000 s) of blue dextran passing through the column. The retention volume was $\theta_R^{col} = 10.302$ cm^3.

Figure 4.13: Blue dextran step injection curves for interparticle porosity calculation of the chromatographic column. The differences between the retention volumes of the Blue Dextran solution, bypassing (θ_R^{bp}) and passing through the column (θ_R^{col}), allow to calculate the void volume between the fixed bed particles. Since the experiments were performed at a flow rate of 1 mL/min, the time (min) shown in the graph also represents θ (cm^3). The experiments were performed in triplicate for the bypass and duplicate for the column.

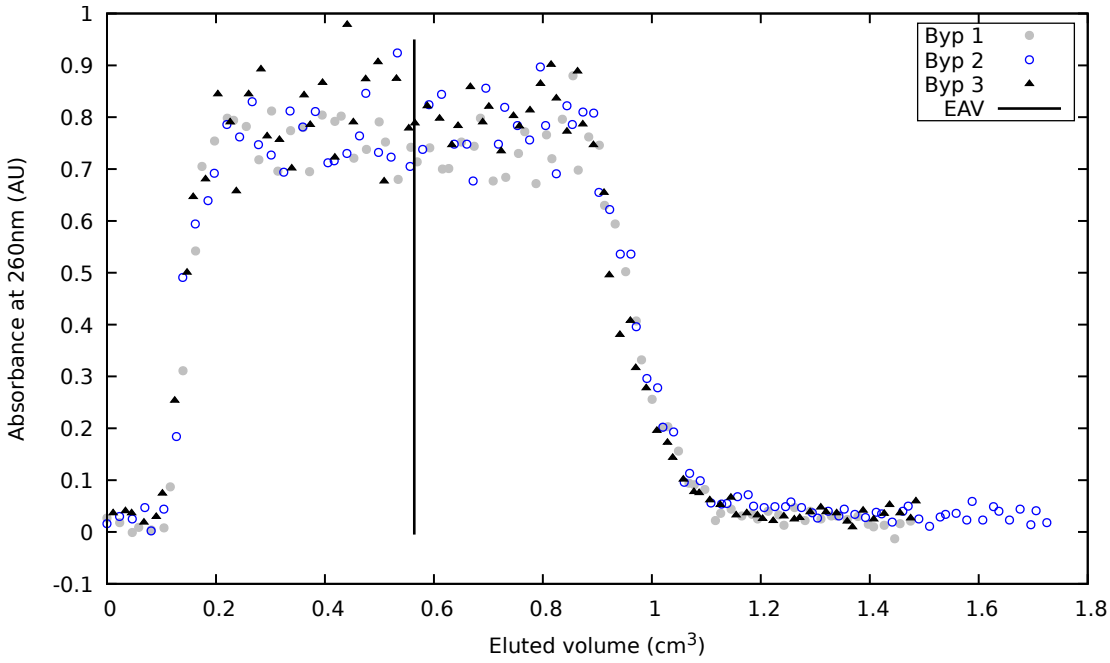

(a.1) Bypass, $Q = 1mL/min$.

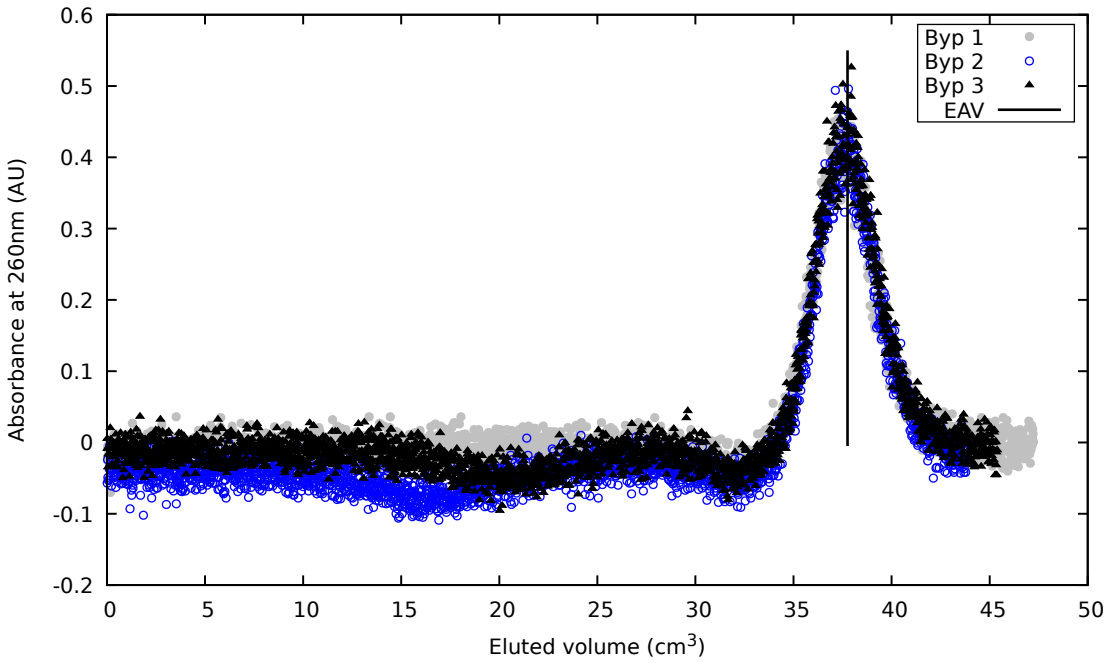

(a.2) Column, $Q = 1mL/min$.

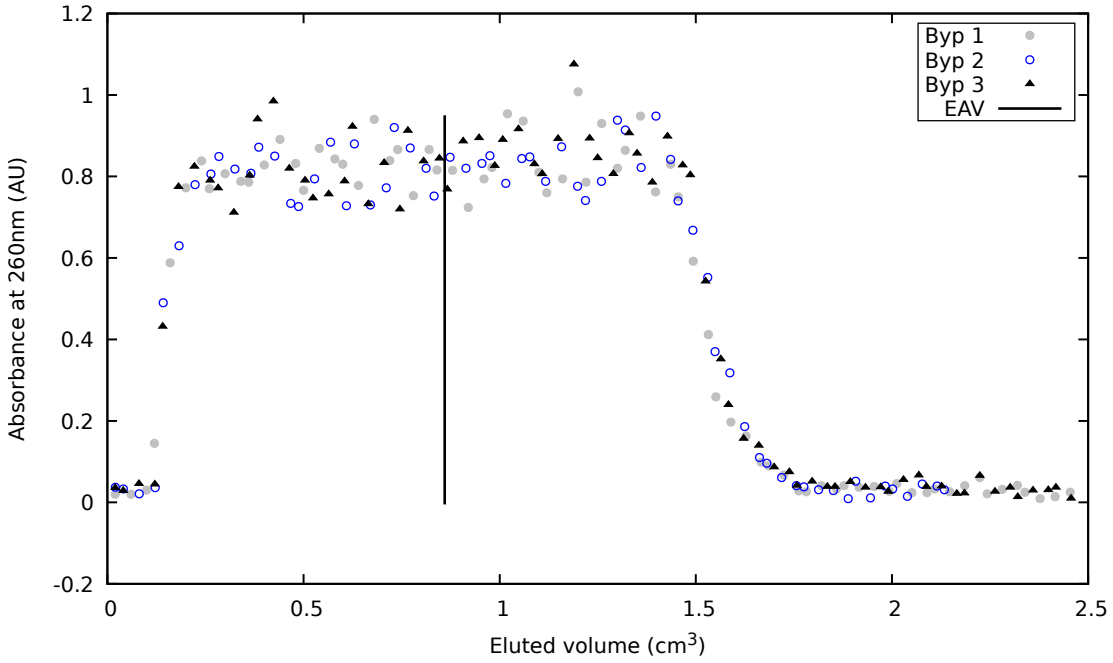

(b.1) Bypass, $Q = 2mL/min$.

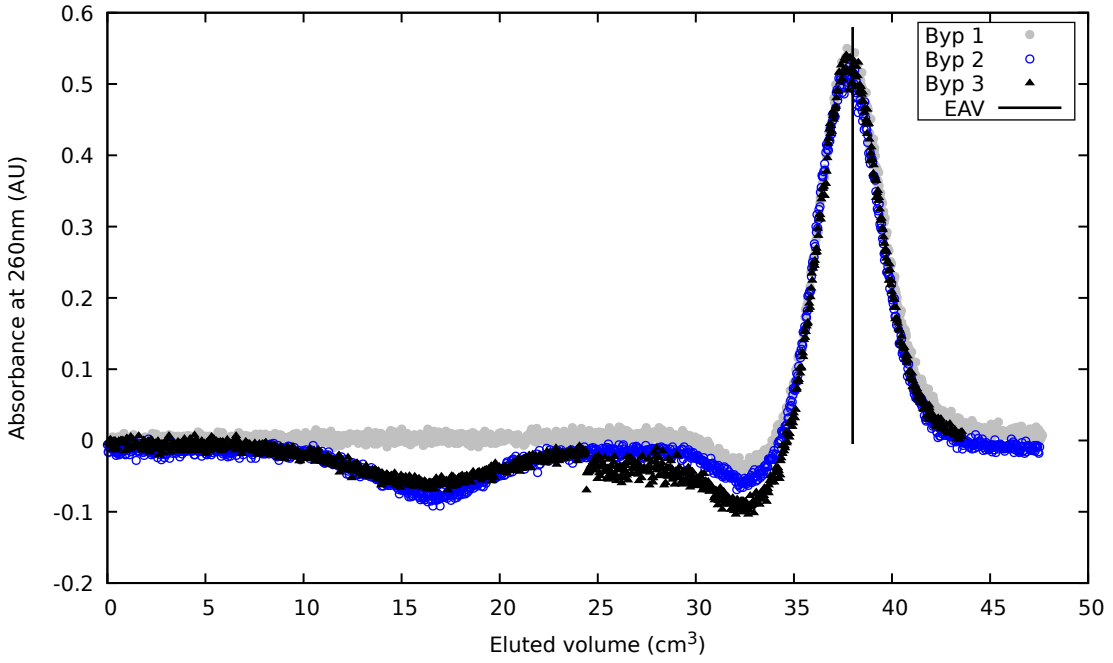

(b.2) Column, $Q = 2mL/min$.

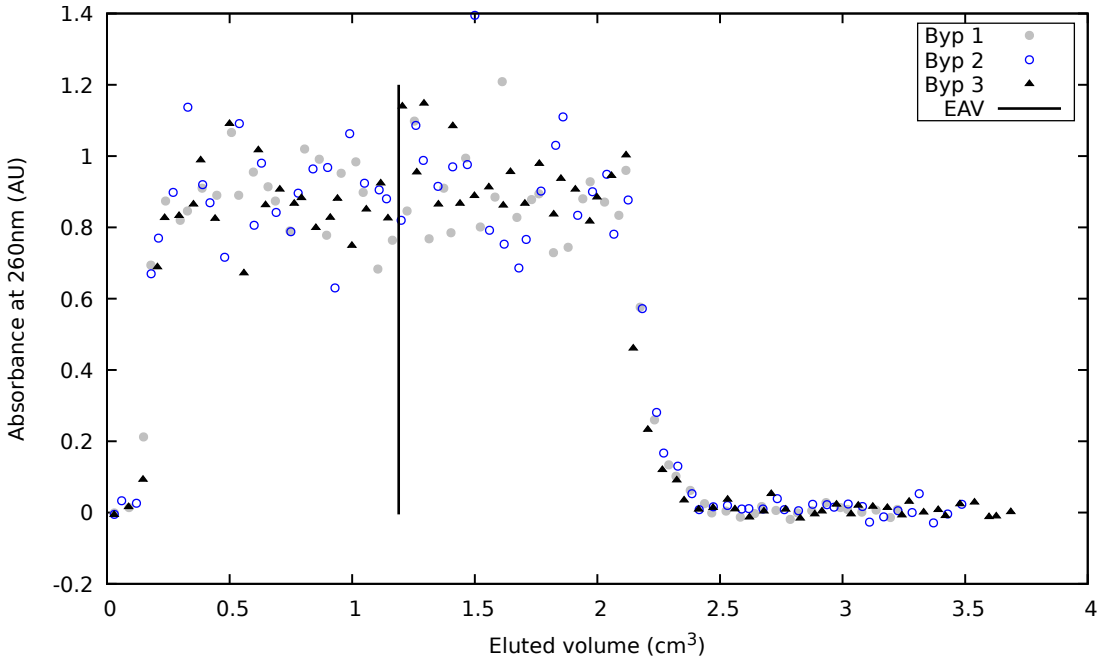

(c.1) Bypass, $Q = 3mL/min$.

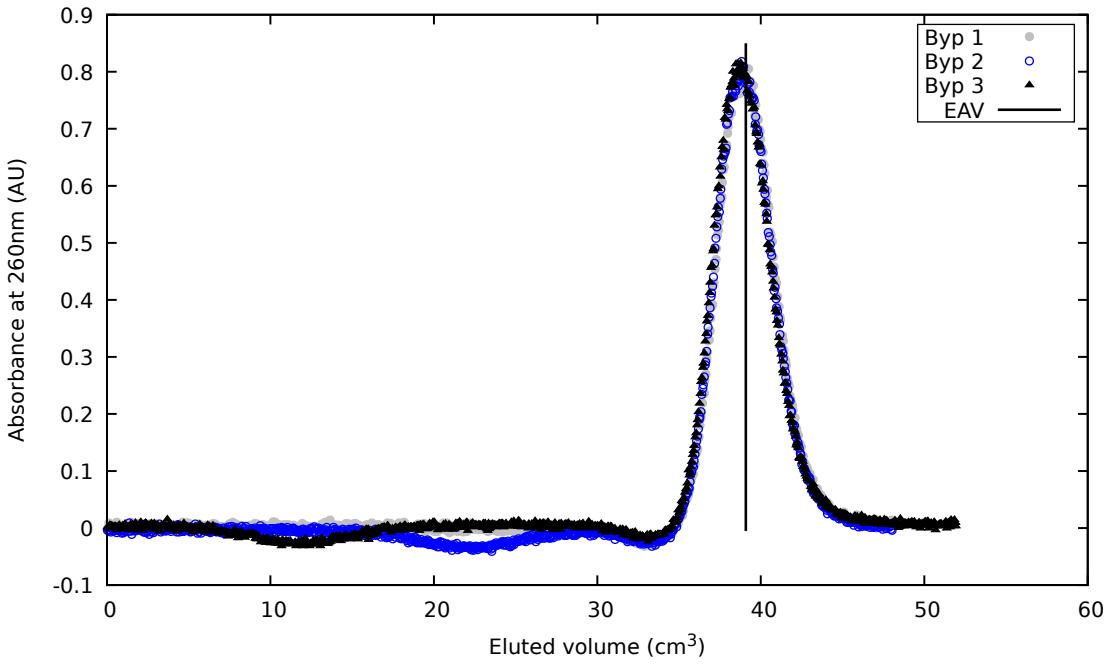

(c.2) Column, $Q = 3mL/min$.

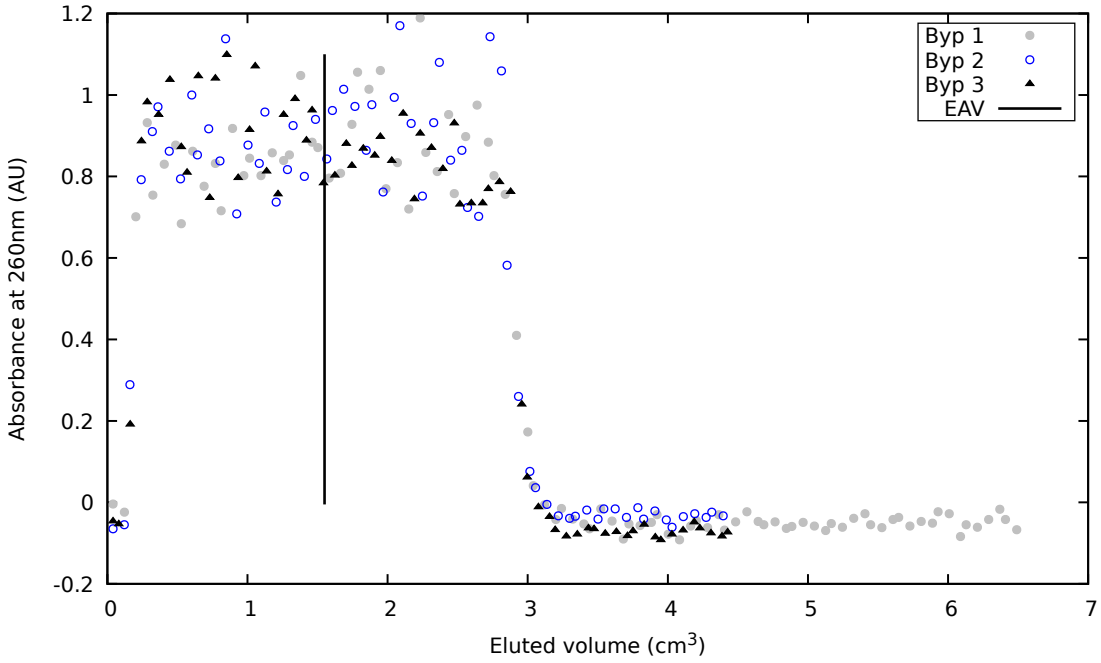

(d.1) Bypass, $Q = 4mL/min$.

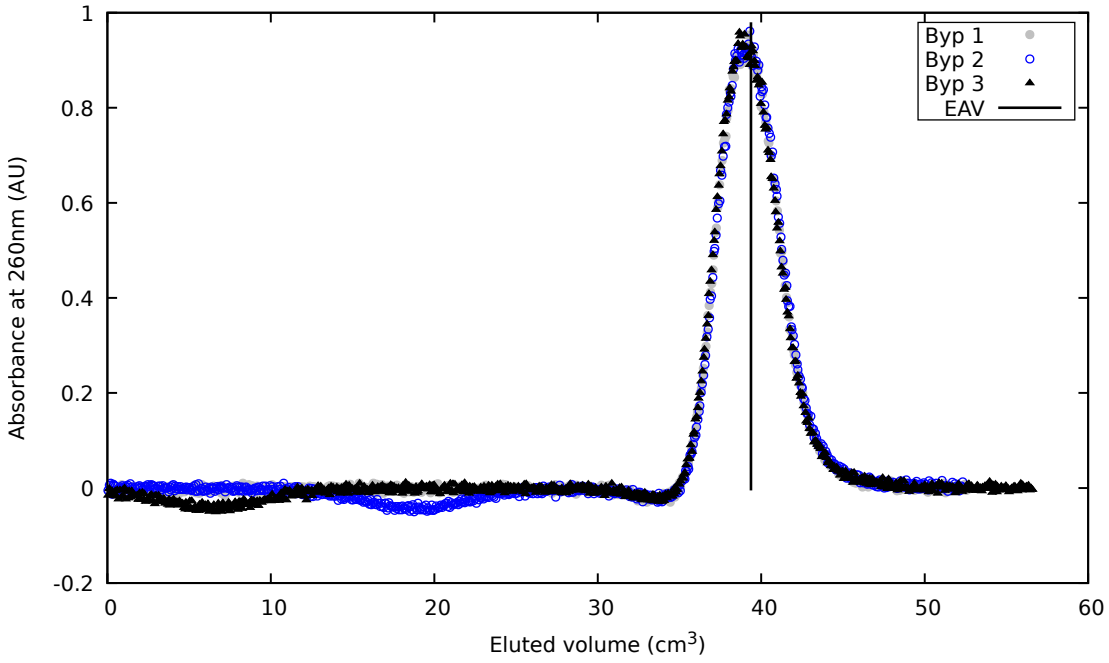

(d.2) Column, $Q = 4mL/min$.

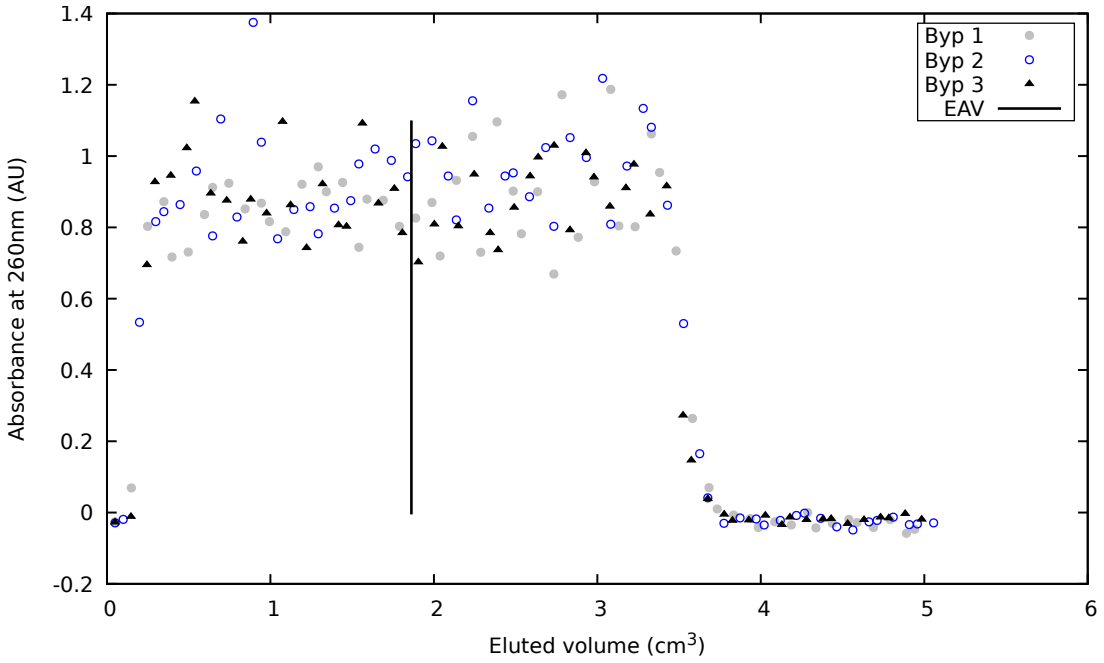

(e.1) Bypass, $Q = 5mL/min$.

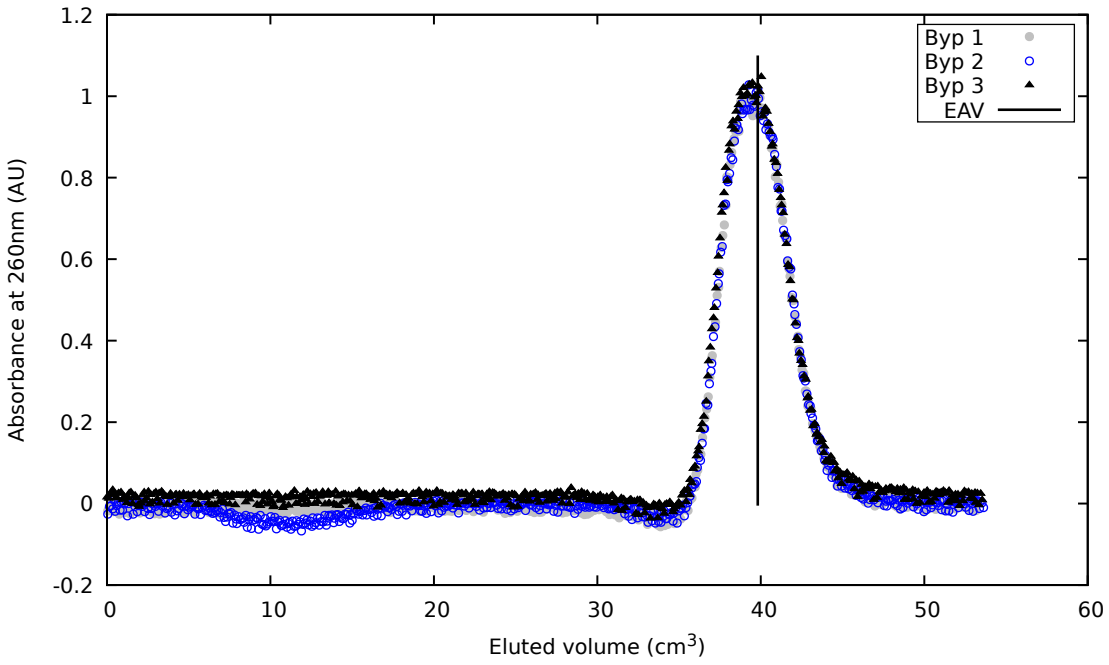

(e.2) Column, $Q = 5mL/min$.

Figure 4.14: Pulse injection (40 s) of Uridine (c = 0.05 g/L) at five different flow rates: 1, 2, 3, 4, 5 mL/min; and two paths: bypassing the column and passing through the column. The θ_R calculated from these curves are used to find Henry's constant and Peclet number.

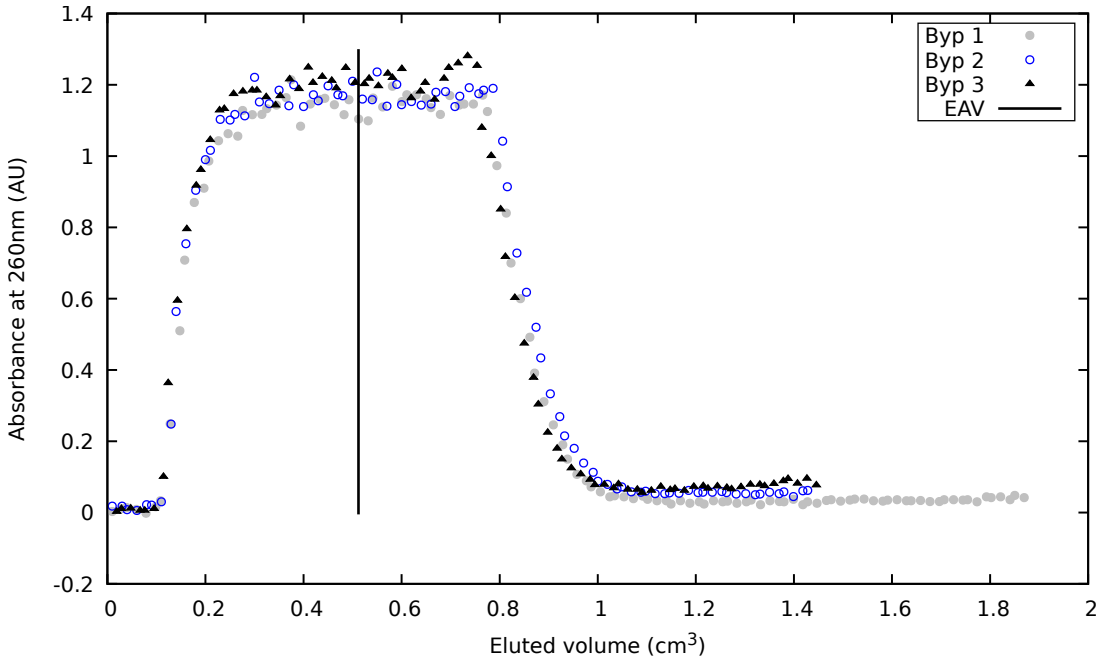

(a.1) Bypass, $Q = 1mL/min$.

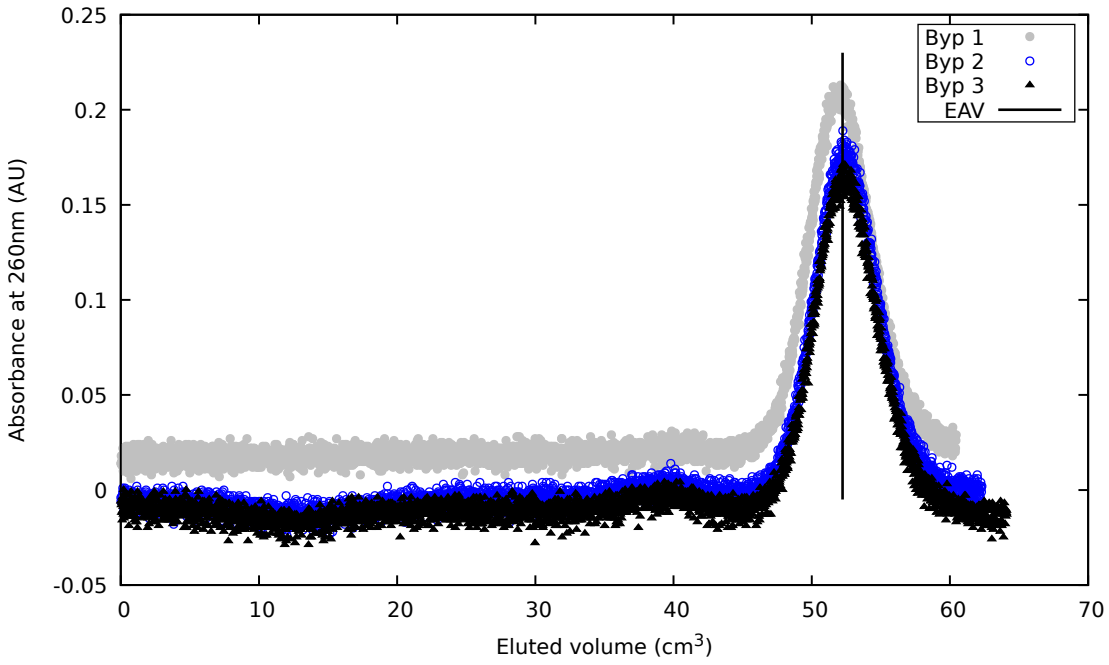

(a.2) Column, $Q = 1mL/min$.

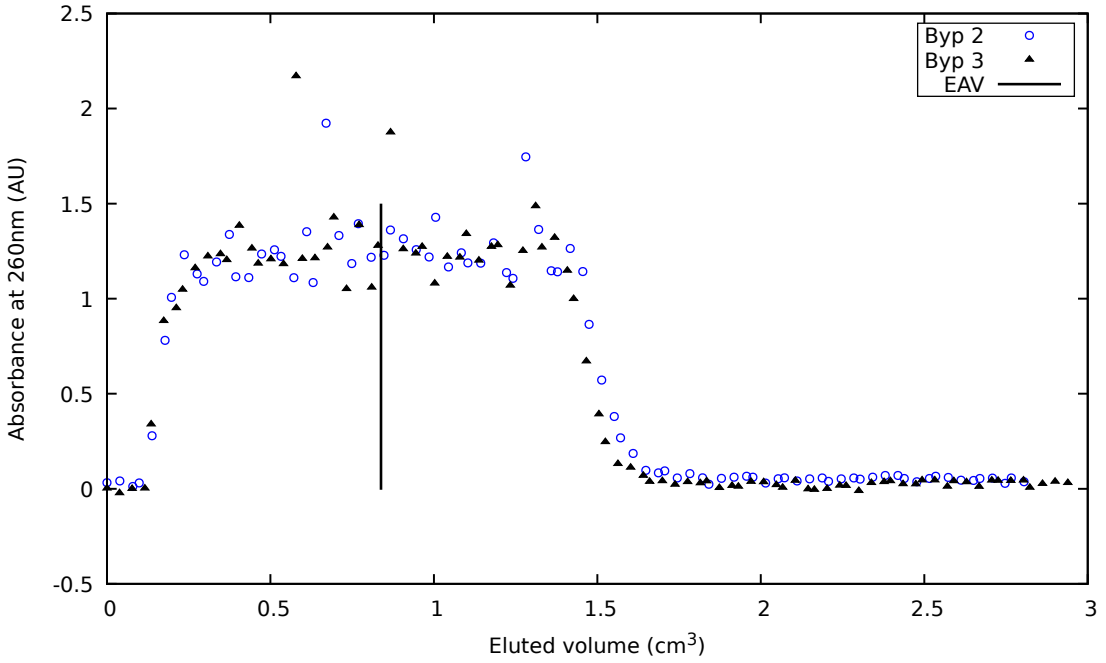

(b.1) Bypass, $Q = 2mL/min$.

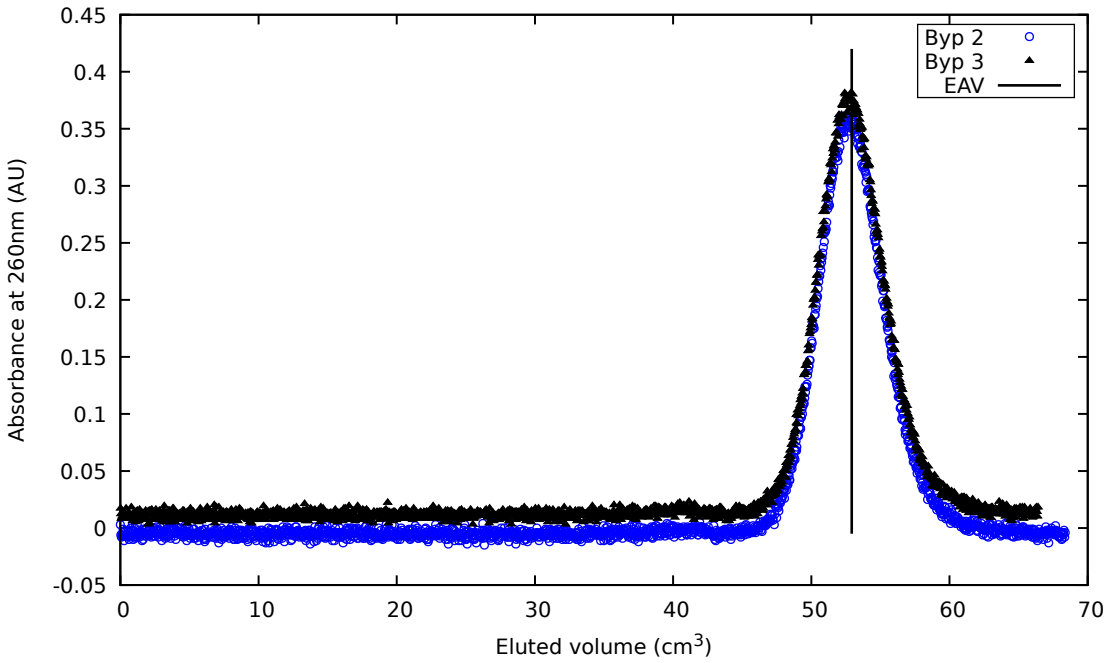

(b.2) Column, $Q = 2mL/min$.

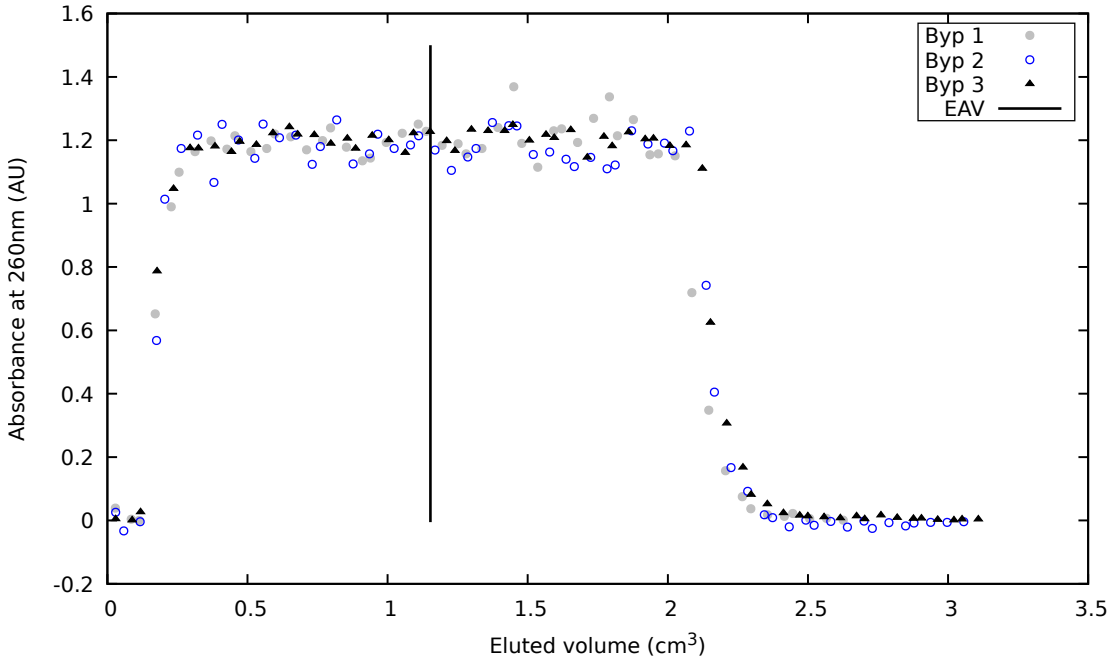

(c.1) Bypass, $Q = 3mL/min$.

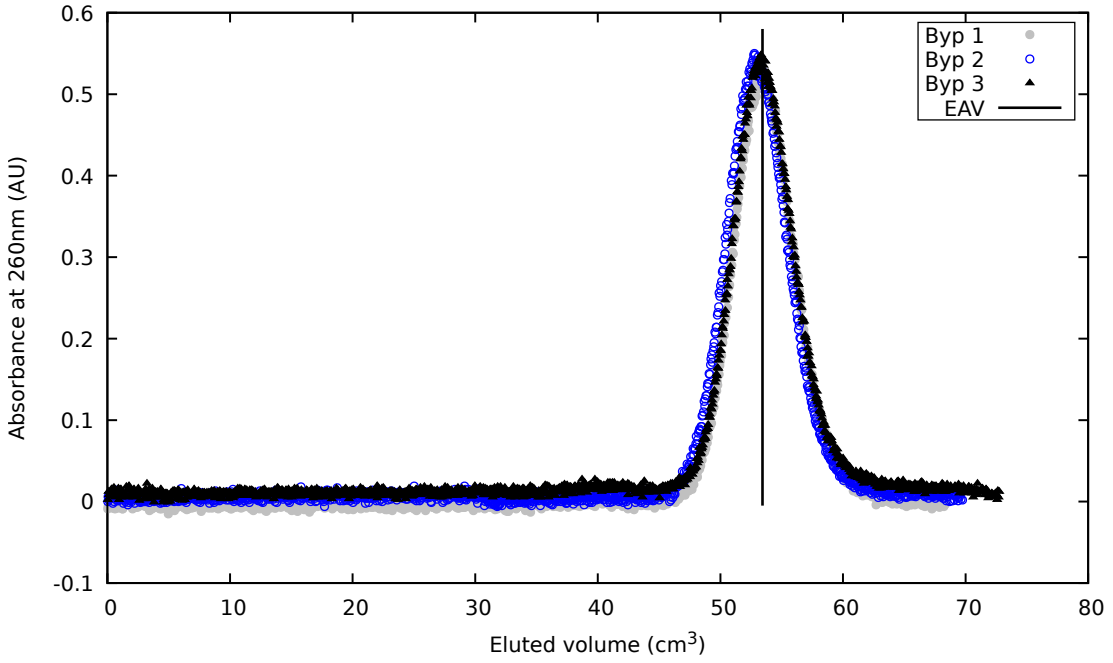

(c.2) Column, $Q = 3mL/min$.

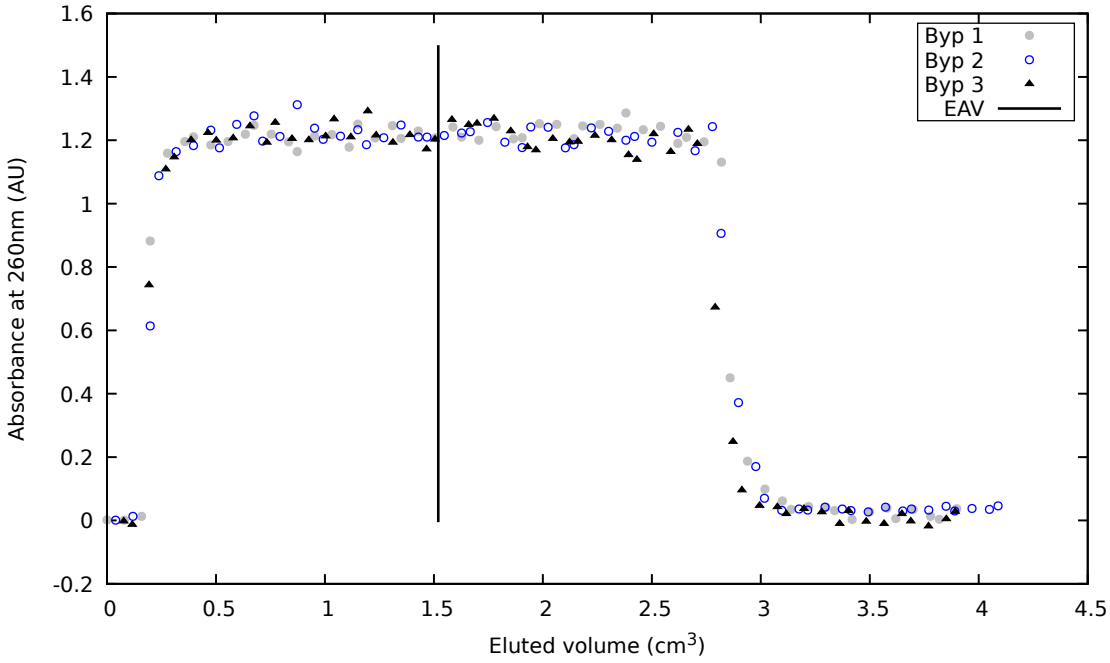

(d.1) Bypass, $Q = 4mL/min$.

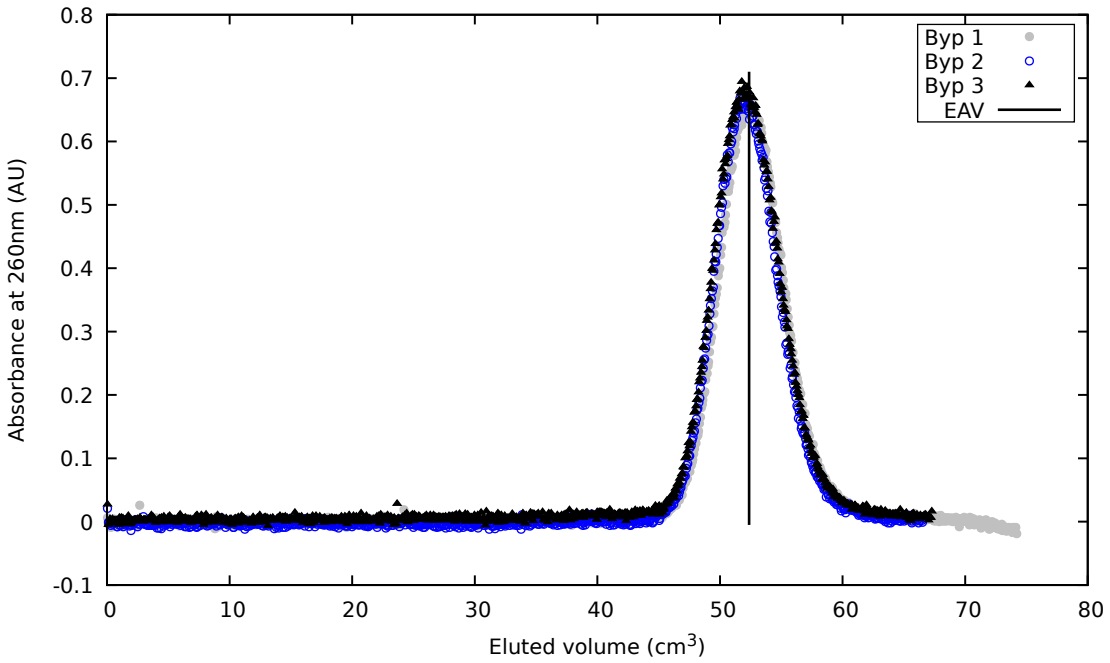

(d.2) Column, $Q = 4mL/min$.

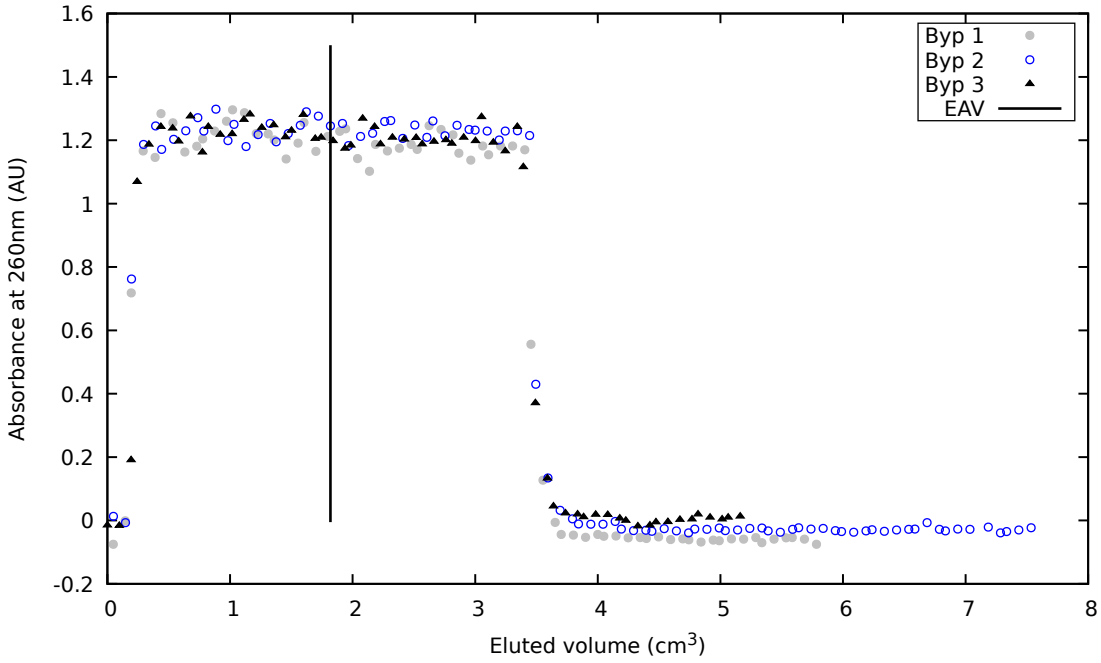

(e.1) Bypass, $Q = 5mL/min$.

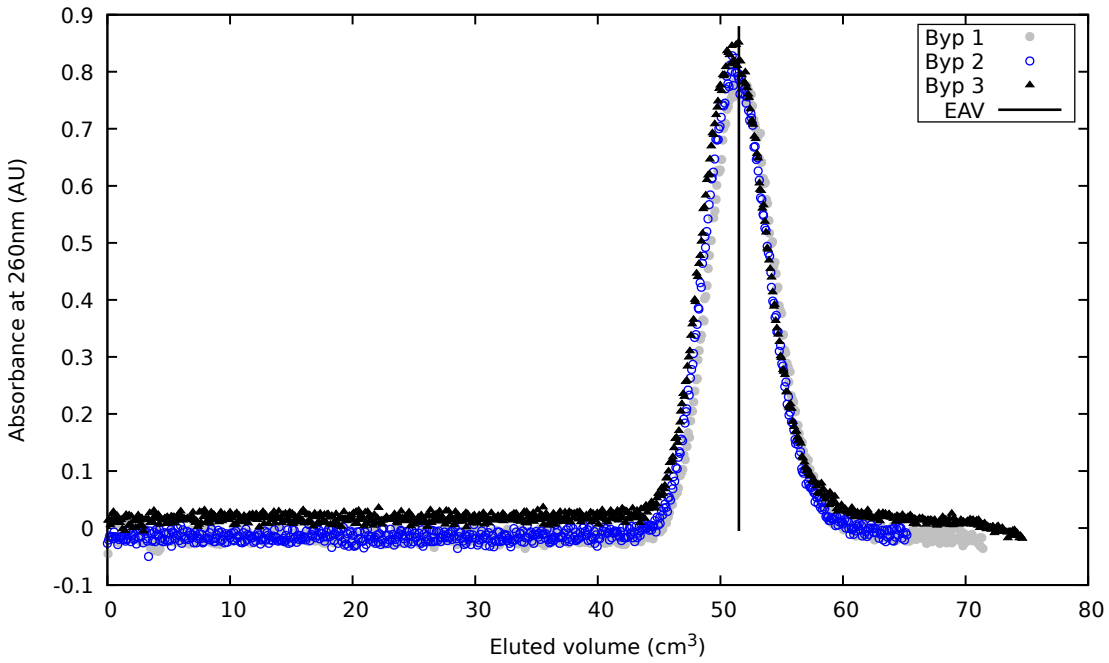

(e.2) Column, $Q = 5mL/min$.

Figure 4.15: Pulse injection (40 s) of Guanosine (c = 0.05 g/L) at five different flow rates: 1, 2, 3, 4, 5 mL/min; and two paths: bypassing the column and passing through the column. The θ_R calculated from these curves are used to find Henry's constant and Peclet number.

Table 4.2: Experimentally calculated Henry's constants. The retention volumes expressed here are the mean values taken from triplicate experiments. The final H_i is the mean value from experiments at five different flow rates, as Henry constant must not change with variations in flow rate. The equation used for Henry's constant determination was $H_i = (\theta_{R,i}^{col} - \theta_{R,i}^{bp})/[(1-\epsilon)V_c] - \epsilon/(1-\epsilon)$.

	Uridine			**Guanosine**		
Q (mL/min)	$\theta_{R,1}^{bp}$ (cm^3)	$\theta_{R,1}^{col}$ (cm^3)	H_1	$\theta_{R,2}^{bp}$ (cm^3)	$\theta_{R,2}^{col}$ (cm^3)	H_2
1	0.564	37.75	1.245	0.512	52.23	1.914
2	0.860	37.99	1.243	0.838	52.92	1.931
3	1.190	39.08	1.278	1.153	53.44	1.940
4	1.550	39.37	1.275	1.520	52.38	1.874
5	1.862	39.81	1.281	1.172	51.51	1.821
		$\overline{H_1}$	**1.264**		$\overline{H_2}$	**1.896**
		$\sigma_{relative,1}$ (%)	1.469		$\sigma_{relative,2}$	2.589

4.3.2.3 Adsorption Isotherms

The adsorption isotherm, which is dependent on the compound and the chromatographic column used, determines the relationship between the concentration of adsorbed solute in the stationary phase in equilibrium with the mobile phase and the concentration of the same solute in the mobile fluid. The nucleosides separation, uridine and guanosine, can be described by linear adsorption isotherms (eq. 4.7) for low solute concentration range [228]. The linear isotherm is widely used in validation process of new chromatographic systems [19].

Therefore, to prove the linearity of the isotherm curves, the experiment was performed with a very low concentration range, so that the 0.05 g/L concentration would be covered by the curve, since it is the concentration used for the nucleosides separation case study. The $c_{i_{max}}$ = 0.2 g/L was chosen based on the solubility of each compound in water, 0.75 g/L (25 °C) for guanosine [52] and 50 g/L for uridine [241]. Since the uridine and guanosine solutions used in the separative process are prepared with 5% (v/v) ethanol, these solubilities should subtly reduce; or temperature variations may occur, contributing to slightly changes in solubility; and furthermore, it is noteworthy that it is not recommended to use concentrations above 80% solubility, to not subject the system to the no risk of precipitation within the column. Taking this into account, the maximum concentration of 0.2 g/L is a safe margin of concentration for the ongoing experiment.

Since the experiment was performed on five different steps, equally sparse between concentration values, the steps corresponded to the concentrations is shown in Table 4.3.

The chromatograms of Figure 4.16 were obtained at the outlet of the chromatographic

Table 4.3: Solute concentrations used at adsorption isotherms experiments. Diluted solution ($c_{i_{max}}$ = 0.2 g/L) was used as bulk solution, a considerably low concentration compared to the solubility of each compound, i.

Stair, j	c_i (g/L)
1	0.04
2	0.08
3	0.12
4	0.16
5	0.2

column. It can be seen that the injection time, t_{inj} = 1080 s, was sufficient to achieve equilibrium saturation in the chromatographic column for both components.

Since the duplicate curves are almost the same, henceforth the graphs will be plotted for Exp 2 only, although calculations were made for both curves of each compound. With the five concentration values already set, and together with the obtained absorbances, the calibration curves were determined, for uridine and guanosine. The trend line drawn on the experimental points that best represented the relationship between the axes was a cubic type curve.

To facilitate the analysis, the eluted volume ($\theta = Qt$) was used instead of experimental time (t). Then the concentration *versus* eluted volume graph was plotted (see Figure 4.17).

The adsorbed volume on the chromatographic column (θ_{ads}), for each component i and for each concentration (or step injection, j), was calculated:

$$\theta_{ads_{i,j}} = \theta_{EAM_{i,j}} - \theta_{0_{i,j}}, \tag{4.15}$$

where $\theta_{EAM_{i,j}}$ is the retention volume of compound i (uridine or guanosine) passing through the chromatographic column, at step j, added to the eluted volume of the previous steps. This term is taken from the graph x-axis, through EAM calculation. While $\theta_{0_{i,j}}$ is:

$$\theta_{0_{i,j}} = \theta_R^{\text{col}} + (j-1)\theta_{inj}, \tag{4.16}$$

where $\theta_{0_{i,j}}$ is the eluted volume when accounting for: the bypass to the column plus the internal column volume occupied by the mobile phase, the θ_R^{col} (this value was already determined by the blue dextran passing through the column, θ_R^{col} = 10.302 cm^3); and the θ_{inj} = 90 cm^3 is the injection volume of one step.

The adsorbed mass ($m_{ads_{i,j}}$) could then be determined:

$$m_{ads_{i,j}} = c_{i,j}\theta_{ads_{i,j}} + \sum_{j=1}^{j-1} m_{ads_{i,j}}. \tag{4.17}$$

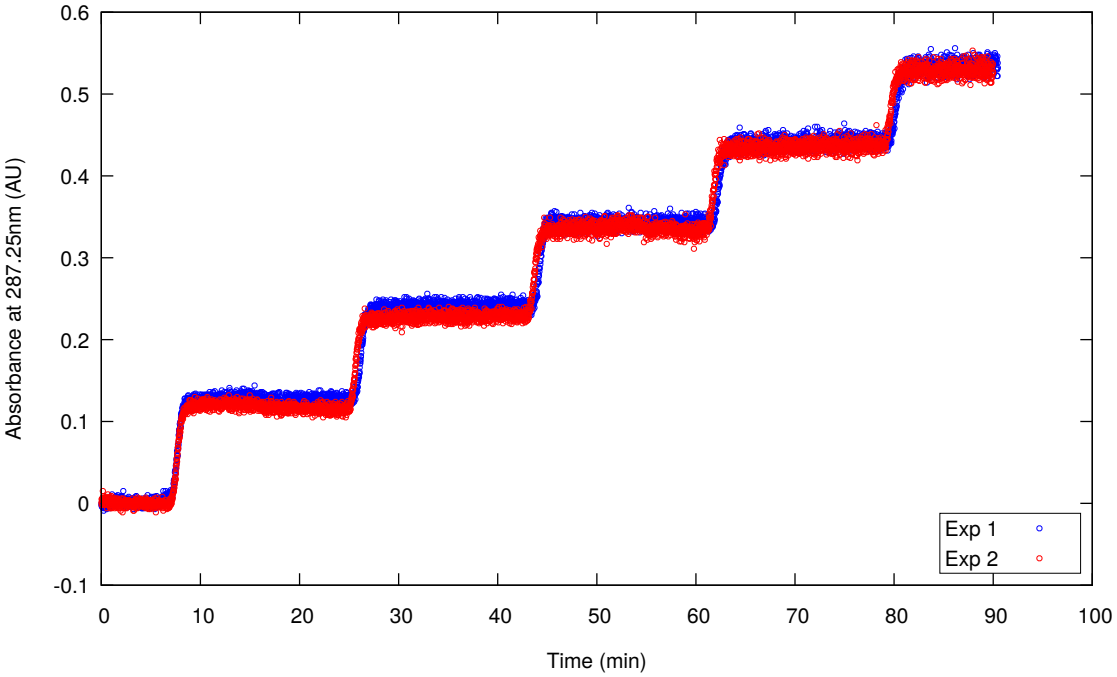

(a) Step injections (1080 s) of uridine.

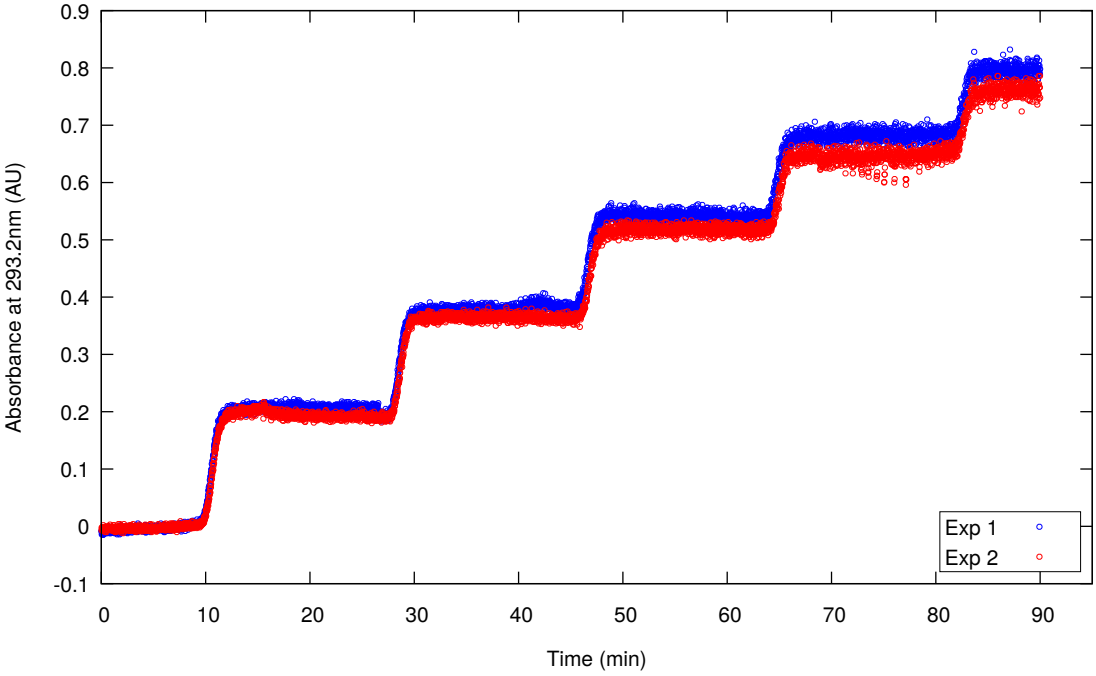

(b) Step injections (1080 s) of guanosine.

Figure 4.16: Step injections of the nucleosides, at different concentrations, to determine the adsorption isotherm. The highest concentration solution was 0.2 g/L, a value substantially far from each component solubility. The UV reading was performed at the exit of the chromatographic column. The experiments are shown in duplicate.

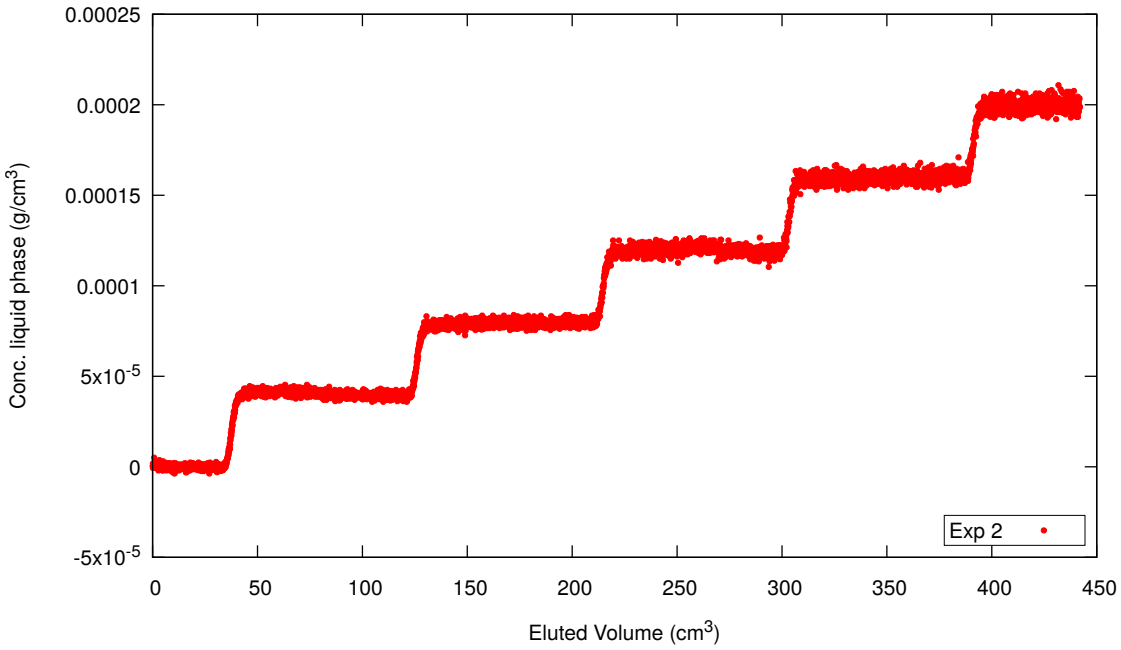

(a) Uridine.

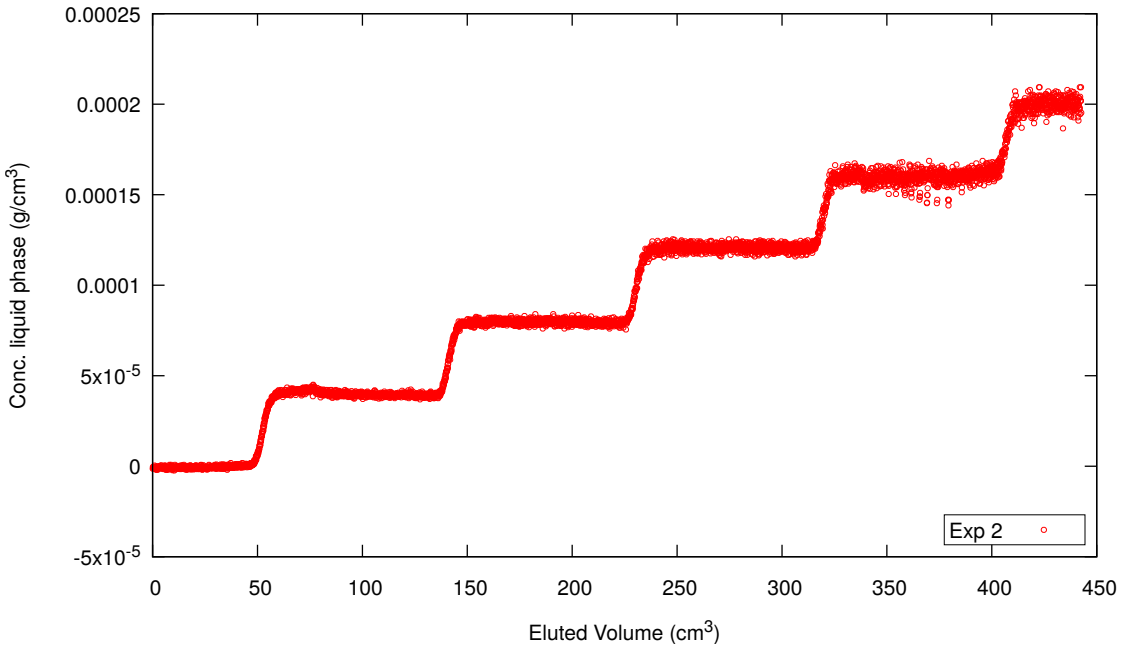

(b) Guanosine.

Figure 4.17: Relationship between concentration and corresponding eluted volume for each component i (uridine and guanosine). The eluted volumes were taken from this graph to calculate q^*.

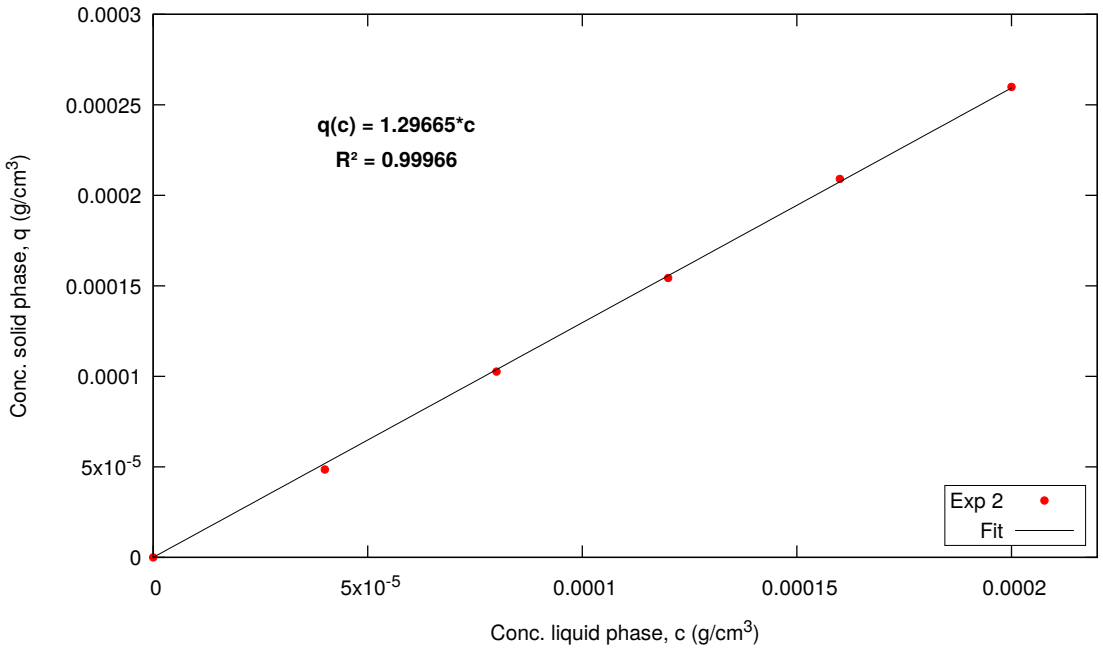

(a) Uridine.

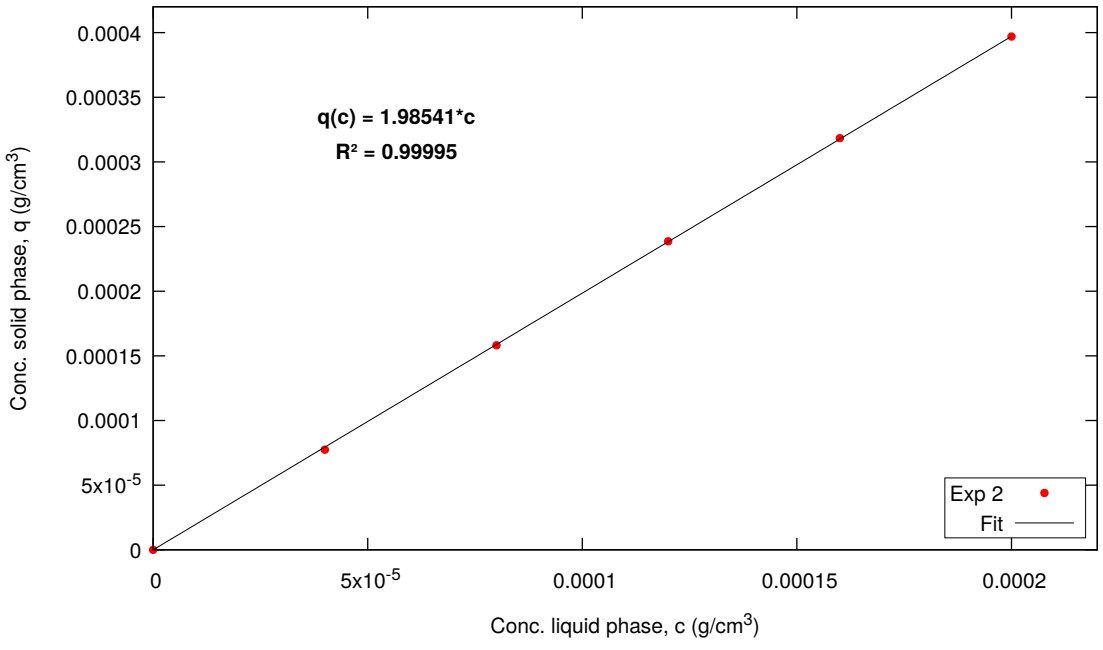

(b) Guanosine.

Figure 4.18: Adsorption Isotherm for each component i (uridine and guanosine). The graphs proved the linear behaviour of isotherms for dilute solutions of each component.

Table 4.4: Henry's constant calculated by the slope of adsorption isotherm curve. The values obtained are very close to the obtained with the pulse experiments, previously presented in this chapter. Exp1 and Exp2 are the duplicate experiments, μ is the arithmetic mean of H values for each component, and $\sigma_{realive}$ is the relative standard deviation.

	Henry's constant (H)	
	Uridine	**Guanosine**
Exp 1	1.375	1.974
Exp 2	1.297	1.985
μ	1.336	1.979
$\sigma_{realive}$ (%)	0.116	0.002

Knowing the adsorbed solute mass (m_{ads}) and the stationary phase volume ($V_{matrix} = (1-\epsilon)V_c = 21.726$ cm^3), the equilibrium concentration in the adsorbed phase (q^*) is calculated by the formula:

$$q^*_{i,j} = \frac{m_{ads_{i,j}}}{V_{matrix}}. \tag{4.18}$$

Hence, the adsorption isotherm plot was finally generated, shown in Figure 4.18.

The experimentally determined isotherm showed linear behaviour ($q^* = Hc$) for both nucleosides at concentrations up to, at least, 0.2 g/L. This indicates that $c_i = 0.05$ g/L, the concentration used for prototype validation, is in a safe region of linearity. As a positive consequence, the prototype validation experiments can be performed with the isolated solutes, in order to equate the separation of a mixing solution from the two solutes by analysing their respective graphs.

In addition, Henry's values obtained through the linear isotherm, where H_i is the slope of the linear relation between q^*_i and c_i, are showed in Table 4.4. Since the values differed very little from those previously calculated, earlier Henry constants were considered for subsequent work.

4.3.2.4 Péclet Number (Pe)

The gPROMS software has advanced parameter estimation capabilities and can even estimate multiple parameters from multiple steady-state and dynamic experiments [211].

The following equilibrium dispersed plug-flow model (already discussed in previous chapter) was implemented in gPROMS:

$$x = 0: \qquad c_i - \frac{1}{\mathrm{Pe}_i}\frac{\partial c_i}{\partial x} = c_i^{\mathrm{in}}, \tag{4.19}$$

$$0 < x < 1 \qquad \frac{\partial c_i}{\partial t} = \frac{Q}{\epsilon V_i}\left(\frac{1}{\mathrm{Pe}_i}\frac{\partial^2 c_i}{\partial x^2} - \frac{\partial c_i}{\partial x}\right), \tag{4.20}$$

$$x = 1: \qquad \frac{\partial c_i}{\partial x} = 0, \tag{4.21}$$

Table 4.5: Estimated column Peclet number (Pe) for the nucleosides on five different flow rates. Pe_1, uridine; Pe_2, guanosine. The values assumed for the following tasks are those found for $Q = 4$ mL/min.

Q (mL/min)	Pe_1	Pe_2
1	994	941
2	1040	910
3	1153	771
4	1151	765
5	1185	584

where $V_i = [\epsilon + (1-\epsilon)H_i]V_c$, x is a dimensional axial coordinate along the column length, V_c the column volume, ϵ the interparticle porosity, H_i the Henry constant, Q the flow rate, and c_i^{in} the inlet conditions for the solute concentration, which for a rectangular pulse injection are

$$c_i^{in} = \begin{cases} c_i^F & \text{for} \quad t \leq t_{inj} \\ 0 & \text{for} \quad t > t_{inj} \end{cases} . \tag{4.22}$$

Here, c_i^F is the solute concentration in the injected fluid and t_{inj} the injection duration; these conditions assume that the flow rate of the injection is the same as that of the elution (Q is constant throughout the experiment). If instead of time t as independent variable we opt for eluted volume, $\theta = Qt$, the dispersed plug-flow model becomes

$$x = 0: \qquad c_i - \frac{1}{\mathrm{Pe}_i}\frac{\partial c_i}{\partial x} = c_i^{in}, \tag{4.23}$$

$$0 < x < 1 \qquad \frac{\partial c_i}{\partial \theta} = \frac{1}{\epsilon V_i}\left(\frac{1}{\mathrm{Pe}_i}\frac{\partial^2 c_i}{\partial x^2} - \frac{\partial c_i}{\partial x}\right), \tag{4.24}$$

$$x = 1: \qquad \frac{\partial c_i}{\partial x} = 0, \tag{4.25}$$

$$c_i^{in} = \begin{cases} c_i^F & \text{for} \quad \theta \leq V_{inj} \\ 0 & \text{for} \quad \theta < V_{inj} \end{cases} , \tag{4.26}$$

where V_{inj} is the volume of the injection. where c_i is the solute concentration at mobile phase, Q is the volumetric flow rate, H_i is the Henry's constant, ϵ is the interparticle porosity and V_c the column volume.

This model was implemented in gPROMS and fitted to the experimental data of dilute solute pulses showed in section 4.3.2.2 for the five different flow rates using the Péclet number as a fitting parameter to characterize the hydrodynamic behaviour at the column. The estimated Péclet numbers (Pe) are given in Table 4.5.

The relationship between $1/Pe$ and the flow rate (Q) is shown in Figure 4.19. The dependence of $1/Pe$ on the flow rate was expected to be given by a straight line with a negative slope, ie, decreasing $1/Pe$ as the flow rate increases. Experimental points for uridine followed this behaviour; however, experimental data for guanosine did not

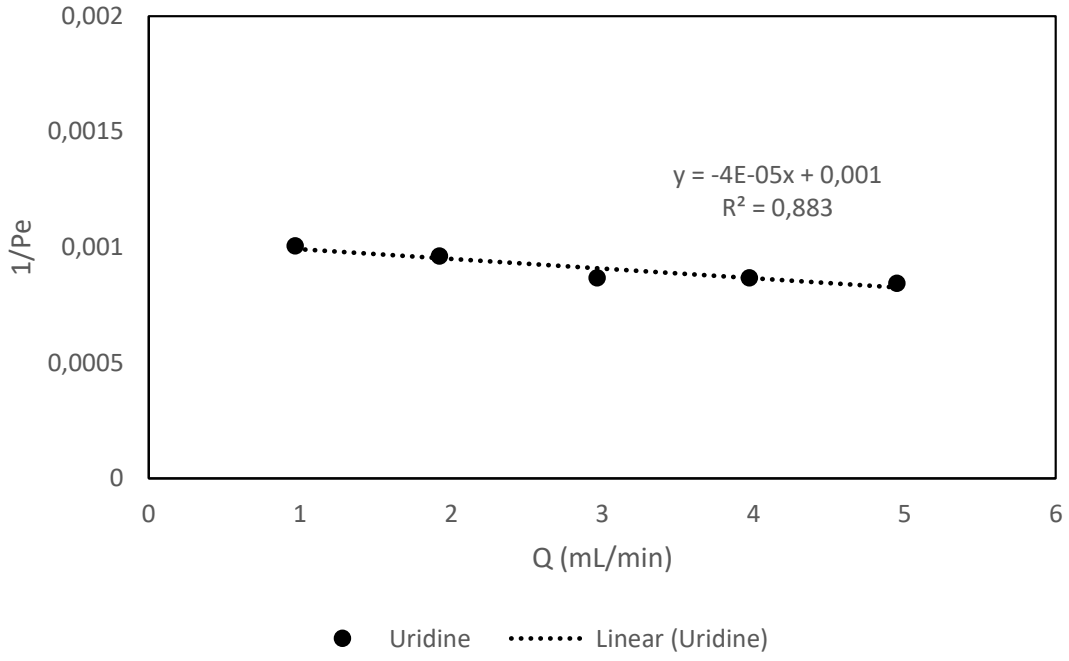

(a) Uridine.

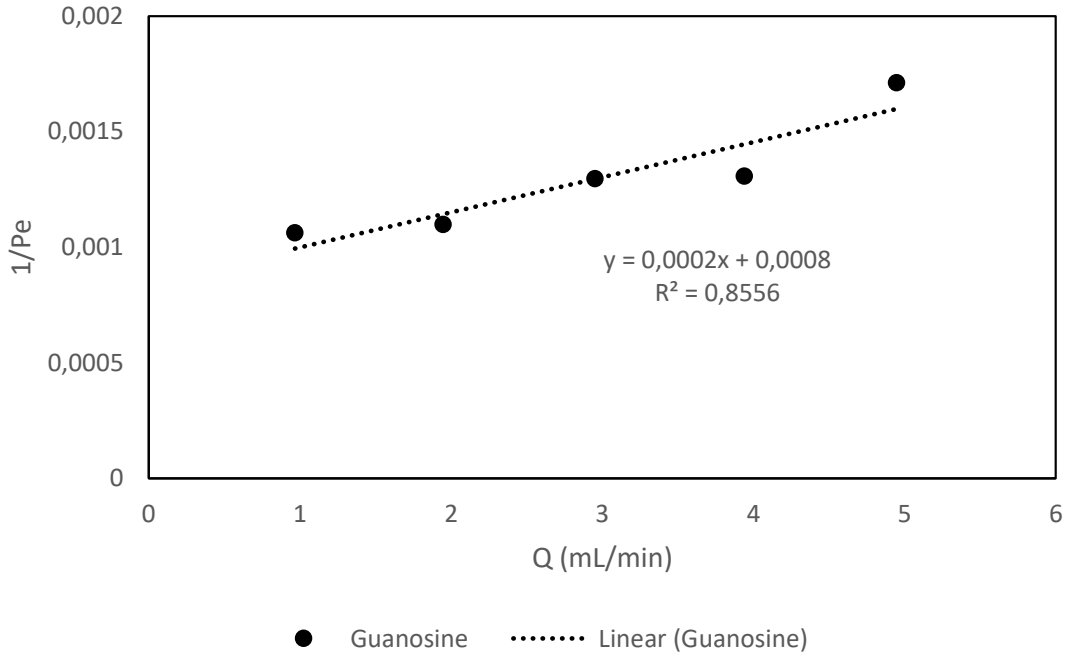

(b) Guanosine.

Figure 4.19: Relationship between $1/Pe$ and corresponding real flow rate for each component i (uridine and guanosine). The values assumed for the following tasks are those found for $Q = 4$ mL/min.

Table 4.6: Column and piston characterization for the linear separation of uridine and guanosine on Source 30 RPC (reversed phase) and 5% (v/v) ethanol in water at 30ºC, with the setup of the Single-column Analog with Recycle Lag. ϵ is the packing interparticle porosity, H is the Henry constant, Pe is the Péclet number, V_0 is the inlet piston dead volume, V_L is the outlet piston dead volume, D_L^{RP} is the axial dispersion coefficient of piston, and D_L^{Frit} is the axial dispersion coefficient of each frit. D_L^{RP} and D_L^{Frit} were determined through parameter estimation in gPROMS, using the experiment of different heights in the static piston, presented in the section 4.3.1.

$\epsilon = 0.318$ $V_0 = V_L = 0.273$ cm^3	H	Pe	D_L^{RP}	D_L^{Frit}
Uridine ($i = 1$)	1.264	1151	1/25.0	1/80.0
Guanosine ($i = 2$)	1.896	765	1/25.0	1/80.0

demonstrate this relationship. Although there is no clear explanation for this behavior, the triplicate curves showed the reproducibility of the experiment, as well as the success of Henry's calculation. Therefore, as the nucleosides separation were performed at the constant flow rate $Q = 4$ mL/min, the Pe values the next tasks were fixed at the values obtained for this flow rate: $Pe_1 = 1151$ (uridine) and $Pe_2 = 765$ (guanosine).

4.3.2.5 Recycle Piston Dead Volumes (V_0 and V_L)

The reflux container has two fluid distributors (frits) inside, both with 20 μm porosity, one located on the upper fixed part of the device and the other on the upper part of the mobile plunger. The fluid distributors are intended to radially disperse the fluid that is injected by the capillary into the piston, the latter being located in the radial center of the device (in the case of the upper frit) and ensure that the fluid received by the capillary outlet, in a very short time interval (Δt), is homogeneous to be re-injected into the chromatographic column (in the case of the lower frit). Distributors are essential to ensure that there is equal radial distribution of the fluid concentration and to avoid possible preferred paths, since radial dispersion is disregarded in the mathematical model.

The frits, as it is expected, print dead volumes for the piston, the V_0 for the distributor from the top and V_L to the distributor at the bottom (can be seen in the Figure 3.19). For the dead volume to be minimal, the base of the mobile plunger and the top of the equipment that receive the frits are flat, i.e. there is no cone shape.

Experimental results for calculating piston dead volumes are presented in Figure 4.20. The estimated values of the dead volumes were $V_0 = V_L = 0.273$ cm^3, which are very small when compared to the chromatographic column volume, representing only 0.86 % of the chromatographic column volume. In any case, these volumes were taken into account in the process simulation.

Table 4.6 lists the experimentally calculated values of the set-up parameters.

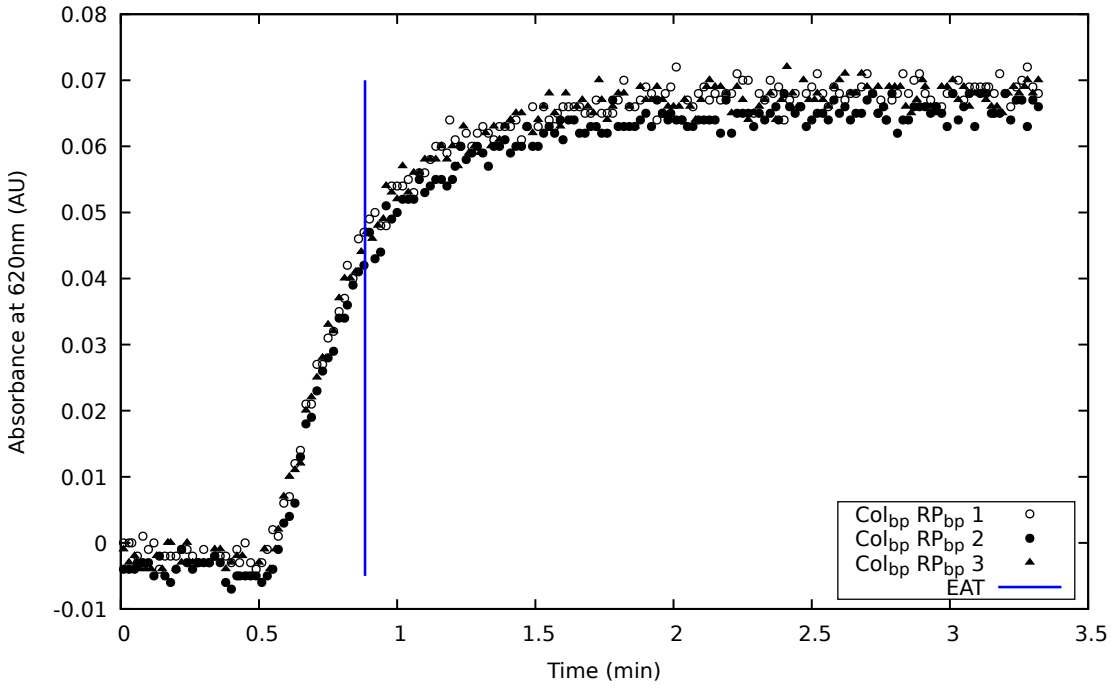

(a) Step injection (200 s) of blue dextran bypassing the recycle piston. The retention volume was $\theta_R^{RP_{bp}} = 0.884$ cm^3.

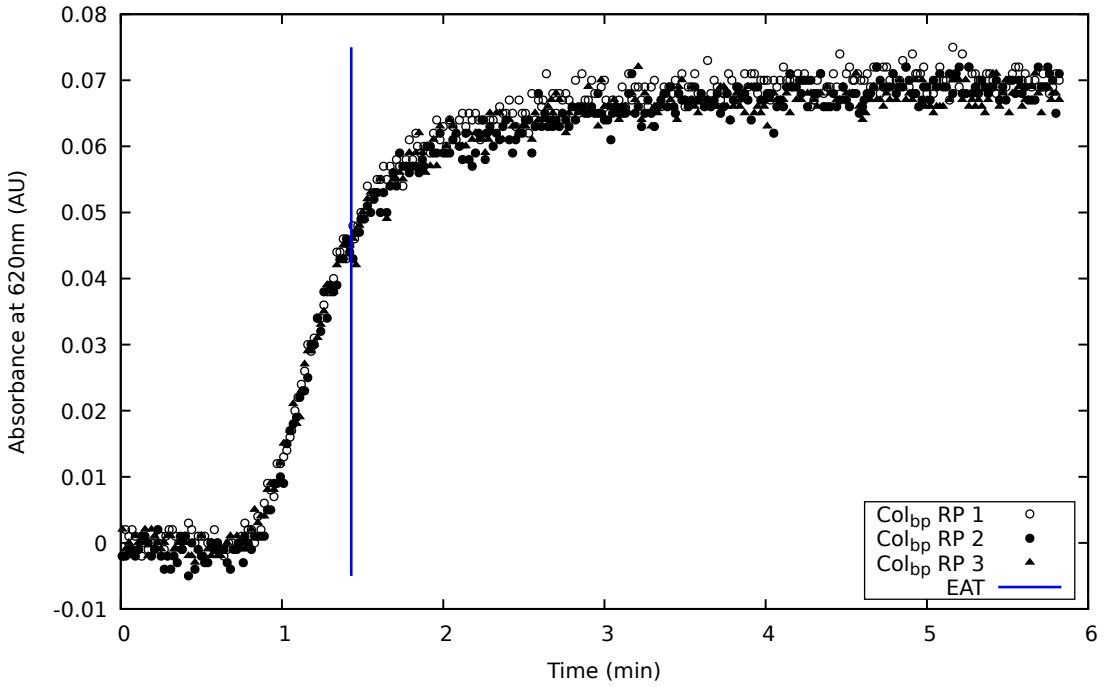

(b) Step injection (350 s) of blue dextran passing through the recycle device. The retention volume was $\theta_R^{RP} = 1.430$ cm^3.

Figure 4.20: Blue dextran step injection curves for dead volumes calculation of the recycle device. The differences between the retention volumes of the Blue Dextran solution, bypassing ($\theta_R^{RP_{bp}}$) and passing through the reflux container (θ_R^{RP}), allow to calculate the frits void volume. Since the experiments were performed at a flow rate of 1 mL/min, the time (min) shown in the graph also represents θ (cm^3). The experiments were performed in triplicate for each experiment.

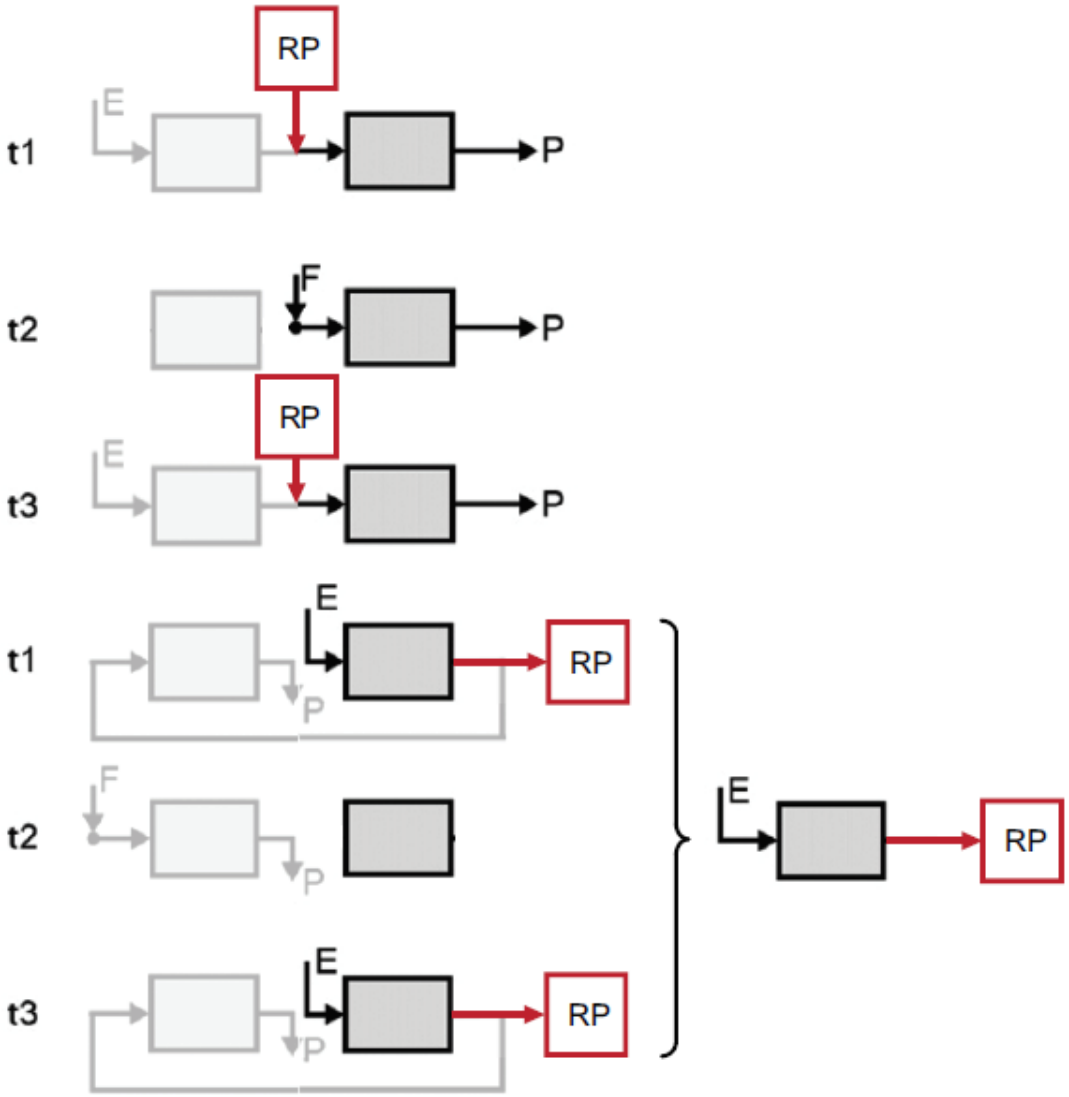

Figure 4.21: Schematic of converting the process depicted in Figure 4.2 into its one-column analog. Each step in which the flow goes to the next column must be replaced by the flow being redirected, in the new single column process, to the reflux piston.

4.3.3 Nucleosides Separation by RPC

4.3.3.1 Cycle Determination: From two-column to one-column process

After isolating only the downstream column from the two-column chromatographic process for nucleosides separation [228], and following its operation for a complete cycle in order to replace each step at which the fluid stream went to the upstream column by redirecting that fluid to the recycling device, the schematic shown in Fig. 4.21 was obtained.

Note that in the penultimate step the column stays idle, that is, there is no flow through it. Hence, this step can be eliminated. If this is done, the last two steps of the cycle are identical (`E ⇒ COL ⇒ R`) and can be merged into a single one. So the original

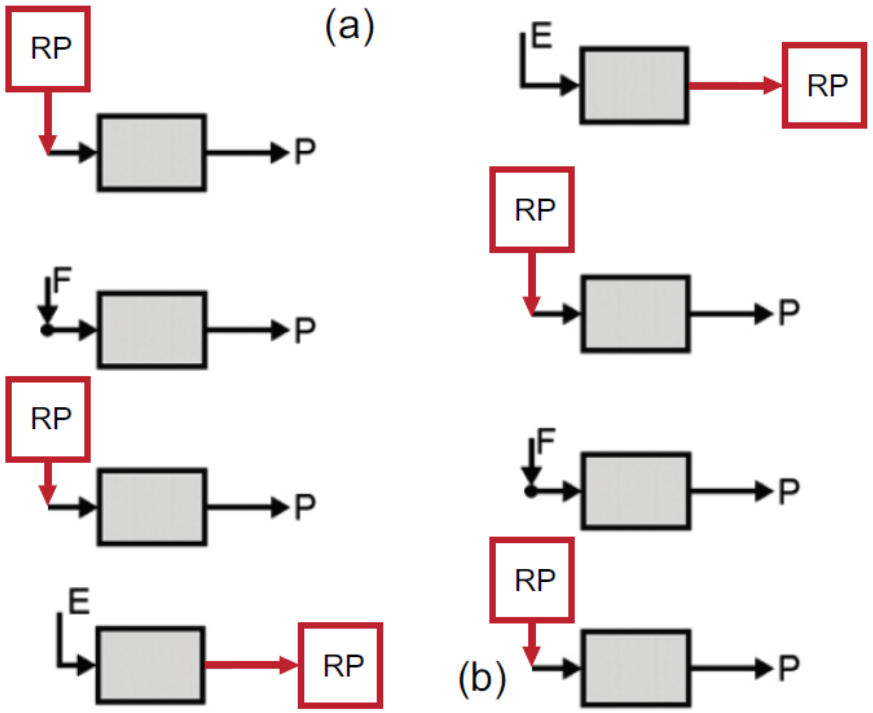

Figure 4.22: Schematic of the one-column analog's cycle. At (a) is the final cycle after executing the recipe for converting the two-column process for nucleosides separation into the equivalent single-column system. Since the column at the beginning of the process is completely clear, the process can start at any of the steps since the sequence is not changed, so in (b) is the cycle that it was decided to work in this chapter.

cycle that had six steps, now, with the new process, boils down to just four steps. This already adds an advantage since step changes can lead to experimental errors or pressure drop changes.

The resulting cycle for the one-column analog is depicted in Fig. 4.22a. The cycle can start with any of the steps as long as the sequence is not changed. For example, it was decided to start the cycle with step `E ⇒ COL ⇒ R`; this is depicted in Fig. 4.22b.

The full sequence for this cycle is:

1. `E ⇒ COL ⇒ R` : τ_1
2. `R ⇒ COL ⇒ P` or `W` : τ_2
3. `F ⇒ COL ⇒ P` or `W` : τ_3
4. `R ⇒ COL ⇒ P` or `W` : τ_4

Here, P stands for the fractions where the purified guanosine is collected and W for the fractions where the purified uridine is collected; τ_k is the duration of the k^{th} step. Then, necessarily, $\tau_1 = \tau_2 + \tau_4$, because the piston must return to it's original position after each cycle.

At process startup the column is initially clean. Thus, if step 1 is executed, (`E ⇒ COL ⇒ R`), it is essentially filling the recycle piston with pure eluent. The next step is `R ⇒ COL ⇒ P`. However, since the column is still clean and the recycle piston filled with eluent, this step does basically nothing. In the last step of the first cycle, the column is basically being eluted, because the remaining liquid in the recycle piston is pure eluent. Thus, to speed up the inicial cycle, it is possible to start it with step 3, `F ⇒ COL ⇒ P`, and replace step 4 by `E ⇒ COL ⇒ P`.

Then, the full sequence is:
(*Initial cycle*)

3. `F ⇒ COL ⇒ P` : τ_3
4. `E ⇒ COL ⇒ P` or `W` : τ_4

(*Cycles 1 to 17*)

1. `E ⇒ COL ⇒ R` : τ_1
2. `R ⇒ COL ⇒ P` or `W` : τ_2
3. `F ⇒ COL ⇒ P` or `W` : τ_3
4. `R ⇒ COL ⇒ P` or `W` : τ_4

Where:

- `E ⇒ COL ⇒ P`: fresh solvent is pumped from the solvent container, passes inside of the chromatographic column and pushes the outlet of the column into the product recipient, present on top of the weight scale;
- `F ⇒ COL ⇒ P`: fresh feed is pumped from the feed container, passing inside of the chromatographic column, pushing the outlet of the column into the product recipient, without the usage of the recycle piston;
- `E ⇒ COL ⇒ R`: fresh solvent is pumped, passing inside of the chromatographic column, pushing the outlet of the column into section A of the recycle device, lowering the piston and transferring the solvent from section B to the solvent recipient;
- `R ⇒ COL ⇒ P`: fresh solvent is pumped into section B of the recycle device, rising the piston and transferring the mixture inside section A into the chromatographic column, pushing the outlet of the chromatographic column into the product recipient.

The obtained cycle features a semi-continuous process with pulsed feed injection and product collection at selected cycle intervals.

4.3.3.2 Cycle Steps Injection Time

As shown in the previous section, for the Single-column analog process that mimics the two-column SMB process for nucleosides separation, each cycle is composed by four steps. The cycle length is determined by the sum of the time durations of the four steps, then:

$$\textit{Cycle duration } (\tau) = \sum_{k=1}^{4} \tau_k. \tag{4.27}$$

At each cycle, the process is fed during step 3. As Q_F is the flow rate of the feed pump, the feed volume injected per cycle (V_F^{cycle}) is:

$$V_F^{cycle} = Q_F \tau_3. \tag{4.28}$$

Therefore, the average feed flow rate per cycle ($\overline{Q_F}$) is:

$$\overline{Q_F} = \frac{V_F^{cycle}}{\tau} = \frac{Q_F \tau_3}{\tau} = \frac{Q_F \tau_3}{\tau_1 + \tau_2 + \tau_3 + \tau_4}, \tag{4.29}$$

and in order to calculate the specific productivity (min^{-1}):

$$\textit{Specific productivity } (\text{min}^{-1}) = \frac{\overline{Q_F}}{V_c}. \tag{4.30}$$

Taking this into account, the process optimization in the case of nucleosides separation consisted of maximizing the specific productivity, or more specifically, $\overline{Q}_F$, subject to the following restrictions for products purity, feed flow rate, and eluent flow rate:

$$\begin{aligned} Pur_X &\geq 0.95, \\ Pur_R &\geq 0.95, \\ Q_F &= 4\ \text{mL/min} \\ Q_E &= 4\ \text{mL/min} \end{aligned} \tag{4.31}$$

where Pur_X is the extract purity and Pur_R the raffinate purity. After applying these restrictions together with the already mimicked process cycle (Figure 4.22b) and the previously determined column and piston parameters (Table 4.6), the duration of each step was obtained.

Here, we briefly outline how the step durations were determined. Let $t_0 = 0$ and $t_k = t_{k-1} + \tau_k$, $k = 1 \ldots, 4$, where τ_k is the duration of the kth step and t_k the instant at which it finishes. The duration of a full cycle is simply $\tau = \sum_k \tau_k$. Let $\theta_k = (t - t_{k-1})/\tau_k \in (0, 1)$ be the dimensionless time for step k. Moreover, let $c_i(x, \theta_k)$ denote the axial concentration profile of solute i in the liquid phase in the chromatography column at dimensionless time θ_k where $x = z/L_c$ is the dimensionless axial position along the length L_c of the column.

The workings of the recycle piston have been detailed in the previous chapter; here, we recover its governing equations without further details. For this purpose, let $\tilde{c}_i(x, \theta_k)$

denote the axial concentration profile of solute i in the liquid in the recycle piston at dimensionless time θ_k, where $x = z/L_{\mathrm{P}}(\theta_k)$ is the dimensionless axial position along the (time-variable) length L_{P} of the moving piston, V_{P} its (time-variable) volume, Q_0 its inlet flow rate and Q_{L} its outlet flow rate.

Given this notation the mathematical model governing the time-periodic dynamics of the one-column analog process is given by the following set of equations.

(*Column breakthrough model*, $0 < \theta_k \leq 1$)

$$x = 0: \qquad c_i - \frac{1}{\mathrm{Pe}_i}\frac{\partial c_i}{\partial x} = c_i^{\mathrm{in}}, \tag{4.32}$$

$$0 < x < 1 \qquad \frac{\partial c_i}{\partial \theta_k} = \frac{\tau_k Q}{\epsilon V_i}\left(\frac{1}{\mathrm{Pe}_i}\frac{\partial^2 c_i}{\partial x^2} - \frac{\partial c_i}{\partial x}\right), \tag{4.33}$$

$$x = 1: \qquad \frac{\partial c_i}{\partial x} = 0. \tag{4.34}$$

(*Recycle piston*, $0 < \theta_k \leq 1$)

$$\frac{dV_{\mathrm{P}}}{d\theta_k} = \tau_k(Q_0 - Q_{\mathrm{L}}), \tag{4.35}$$

$$V_{\mathrm{P}}^2\frac{\partial \tilde{c}_i}{\partial \theta_k} = \tau_k(\gamma_{\mathrm{m}} + \gamma_{\mathrm{h}}Q_0)\left(\frac{\partial^2 \tilde{c}_i}{\partial x^2}\right) - \tau_k V_{\mathrm{P}}\left[Q_0 - (Q_0 - Q_{\mathrm{L}})x\right]\left(\frac{\partial \tilde{c}_i}{\partial x}\right) \text{ for } 0 < x < 1, \tag{4.36}$$

$$\begin{aligned} V_{\mathrm{P}}Q_0\tilde{c}_i - (\gamma_{\mathrm{m}} + \gamma_{\mathrm{h}}Q_0)\frac{\partial \tilde{c}_i}{\partial x} &= V_{\mathrm{P}}Q_0\tilde{c}_i^{in} \quad \text{for } x = 0, \\ \frac{\partial \tilde{c}_i}{\partial x} &= 0 \qquad\qquad \text{for } x = 1. \end{aligned} \tag{4.37}$$

(*Cyclic operating conditions*, $0 < \theta_k \leq 1$)

$$k = 1: \quad Q_0 = Q = Q_E,\ Q_{\mathrm{L}} = 0, \quad c_i^{\mathrm{in}} = c_i^{\mathrm{E}}, \quad \tilde{c}_i^{\mathrm{in}} = c_i^{\mathrm{out}}, \tag{4.38}$$

$$k = 2: \quad Q_L = Q = Q_R,\ Q_0 = 0, \quad c_i^{\mathrm{in}} = \tilde{c}_i^{\mathrm{out}}, \quad (\partial \tilde{c}_i/\partial x)_{x=0} = 0, \tag{4.39}$$

$$k = 3: \quad Q_0 = Q_L = 0, \quad Q = Q_F, \quad c_i^{\mathrm{in}} = c_i^{\mathrm{F}}, \quad (\partial \tilde{c}_i/\partial x)_{x=0} = 0, \tag{4.40}$$

$$k = 4: \quad Q_L = Q = Q_R,\ Q_0 = 0, \quad c_i^{\mathrm{in}} = \tilde{c}_i^{\mathrm{out}}, \quad (\partial \tilde{c}_i/\partial x)_{x=0} = 0, \tag{4.41}$$

where Q_E, Q_F and Q_R are the eluent, feed, and recycle flow rates, respectively, $c_i^{\mathrm{E}} = 0$ is the solute concentration in the fresh eluent, c_i^{F} the concentration in the feed, and $\tilde{c}_i^{\mathrm{out}}$ the outlet concentration of the recycle piston at dimensionless instant θ_k.

(*Time-periodic boundary conditions*)

$$c_i(x, t = 0) = c_i(x, t = \tau) \quad \text{for} \quad 0 < x < 1, \tag{4.42}$$

$$V_{\mathrm{P}}(t = 0) = 0, \tag{4.43}$$

$$\tilde{c}_i(x, t = 0) = \tilde{c}_i(x, t = \tau) \quad \text{for} \quad 0 < x < 1. \tag{4.44}$$

As stated above, in the present work we fixed $Q_E = Q_F = Q_R = 4$ mL/min and solved the following optimization problem that aims at maximizing the average feed flow rate

Table 4.7: Parameters values of the cycle, determined by model-based optimization, for the separation of nucleosides using the one-column analog. Each step has a specific time of operation expressed in minutes.

Step, k	τ_k (min)
1	10.15
2	6.15
3	3.94
4	4.01

per cycle (which is directly proportional to the productivity):

$$\max_{\tau_k} \quad \overline{Q}_F \tag{4.45}$$

$$\text{s.t.} \quad \tau_k \geq 0, \tag{4.46}$$

$$\tau_2 + \tau_4 = \tau_1, \tag{4.47}$$

$$\text{Pur}_R \geq 0.95, \tag{4.48}$$

$$\text{Pur}_X \geq 0.95. \tag{4.49}$$

This nonlinear mathematical programming problem has been implemented in AMPL by J. P. Mota via a full discretization approach and solved using the nonlinear interior point solver Ipopt v. 3.11 coupled to the parallel linear solver WSMP v. 16.0. These optimal step durations are given in Table 4.7.

4.3.3.3 Experimental Results

A clever implementation of single-column chromatography with recycle to mimic the operation and performance of a two-column, semi-continuous, open-loop configuration, for a efficient binary separation was proceeded experimentally.

For this, the separation of two nucleosides, uridine and guanosine, was employed. This mixture was chosen because of the ease of separation at low concentrations, as these low concentration compounds have linear isotherm, and no experiments with the mixture need to be performed, i.e. experiments can be performed with the compounds alone to reproduce the separation behaviour proceeded with mixed bulk. This facilitates the handling of the experiment.

Guanosine has important neuroprotective and neuromodulator functions in the central nervous system [114]. This molecule is associated with diseases such as colorectal cancer [169], Crohn's disease, ulceratite colitis [37], and purine nucleoside phosphorylase deficiency [50]. As well as guanosine, uridine is also one of the five standard nucleosides which make up nucleic acids, and is located in most biofluids, including urine, breast milk, cerebrospinal fluid (CSF), and blood. In humans, uridine is involved in several

metabolic disorders, as MNGIE (mitochondrial neurogastrointestinal encephalopathy), beta-ureidopropionase deficiency, and dhydropyrimidinase deficiency [115].

At this operation, the eluent pump and the feed pump were operated with constant flow rates, so that when one of these solutions was not being injected into the column, it was being recirculated to its own containers, avoiding the need for constant change in the flow of the pumps of the system.

The cycles were reproduced experimentally in the prototype apparatus, having been carried out from an initial cycle until thirteen complete cycles. The system takes some time to reach steady state operation.

For data processing, the time data was scaled to a dimensionless coordinate (α), each unit of α representing a cycle, i.e. with dimensionless time one to two corresponding to the first cycle, two to three corresponding to the second cycle, successively until the fourteen cycles (initial + 13 complete cycles) are represented in the graphs. The calculation for α is following:

$$\alpha = n + \frac{t - t_{i,n}}{\tau}, \tag{4.50}$$

being n the cycle number and $t_{i,n}$ the initial time of each cycle The curves are also normalized to the chromatogram's y-axis, showing values for c/c_{max}.

The dimensionless concentration profiles for all fourteen cycles (initial + 13 complete cycles), experimentally obtained at outlet of the column, are expressed in Figure 4.23. The extract (guanosine) and raffinate (uridine) were recovered at the downstream end of the column. The first component to be collected, in this experiment, is the more retained, that is guanosine, because the less retained one goes directed to the piston device at initial cycle. The cyclic steady state was achieved, at nucleosides separation, after approximately six cycles. From cycle 1, each colored region of the graph represents one step of the operating cycle, so that the white region represents step 1, the gray block covers step 2, and the light red region indicates steps 3 + 4. This makes it easy to identify the steps in which products are recovered.

For a better understanding of the results, a graph was generated with fewer cycles, comprising the operating region already under cyclic steady state. Therefore, cycles ten through thirteen are shown in Figure 4.24. Each step operation period is indicated, clearly showing the collection intervals of guanosine at step 2 and uridine at steps 3 and 4, proving that the two components were successfully collected separately in each cycle and that the process developed in this chapter has the potential to separate nucleosides and strongly mimic this kind of two-column process.

The calculations performed for each component of the mixture showed that the products, guanosine and uridine, reached medium purity values of 99.57 % and 97.03 %, respectively. The purity values per cycle, for each component, are shown in Figure 4.25. In addition, Figure 4.26 exhibit calculated values for recovery in each cycle. The system achieved mean recovery values, after cyclic steady state was reached, of 97.8% for guanosine and nearly 100.0% for uridine. Note that the recoveries increase from cycle to cycle

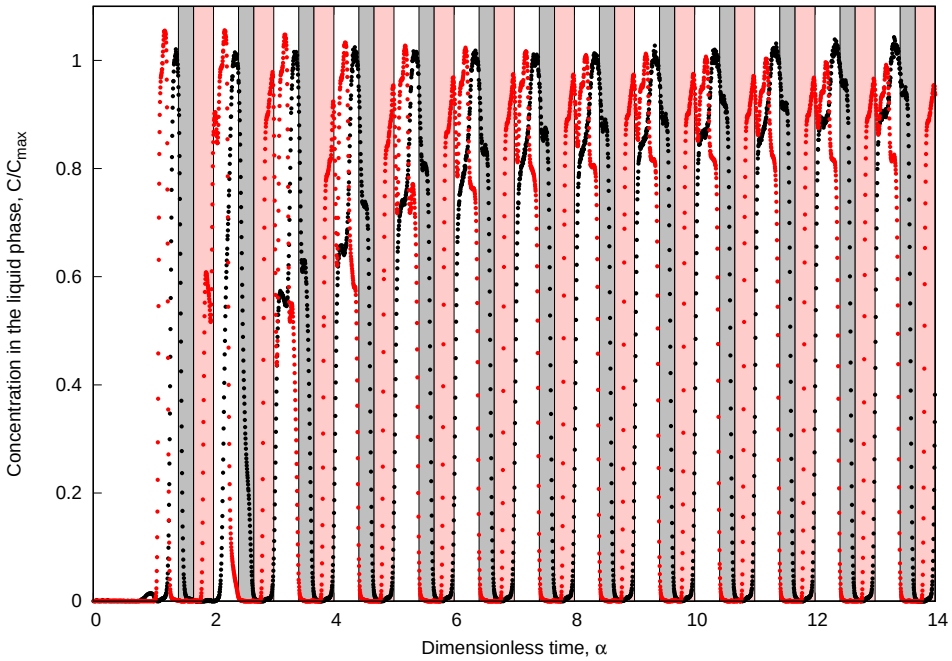

Figure 4.23: Experimental concentration profiles for nucleosides separation. The points represent: black, guanosine; red, uridine. From cycle 1, the injection intervals of each step (t_K) are represented in different area colors: step 1, white area of the graph; step 2, gray area; step 3 and 4, light red area. Guanosine is clearly recovered in step 2, while uridine is recovered in steps 3 and 4.

because the fluids containing the pure compounds are stored in the piston and reinjected into the system with a lag in time. These high purity and recovery results highlight the separation capacity of the Single-column Analog with Recycle Lag process, validating the chromatographic process through the case study chosen.

Besides purities and recoveries, since the injected feed volume per cycle (V_F^{cycle}) was 15.8 mL and the average feed flow rate ($\overline{Q_F}$) was 0.65 mL/min, the separation process achieved productivity of 0.66 mL/min, specific productivity ($\overline{Q_F}/V_c$) of 0.020 min^{-1} and eluent consumption ($\overline{Q_E}/\overline{Q_F}$) of 2.54. These productivity and specific productivity values are just for informational purposes, as they are not considerably important in this chapter, since the main focus is on the effectiveness of the separation process in terms of purity and recovery.

In order to promote further analysis, Figure 4.27 shows the axial concentration profiles of the steady periodic solution in liquid phase and placement of the outlet lines for a unique full cycle, the 12nd cycle. In a more detailed approach to a complete cycle of operation, it is noted that much of the output fluid in step 3 is pure eluent, represented in the graph by the gray area. The blue block expresses the collection interval needed for

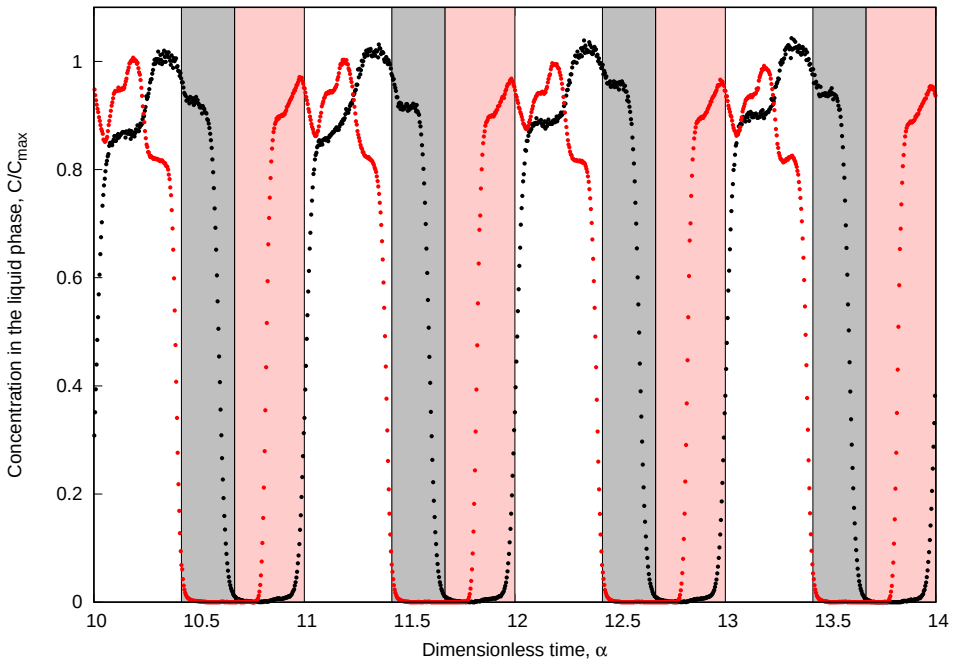

Figure 4.24: Experimental chromatogram for steady state cycles at nucleosides separation. The points represent: black, guanosine; red, uridine. The injection intervals of each step (t_K) are represented in different area colors: step 1, white area of the graph; step 2, gray area; step 3 and 4, light red area. Guanosine withdrawal occurs at 2nd step of the cycle. Meanwhile, withdrawal of uridine happens at 3rd and 4th steps.

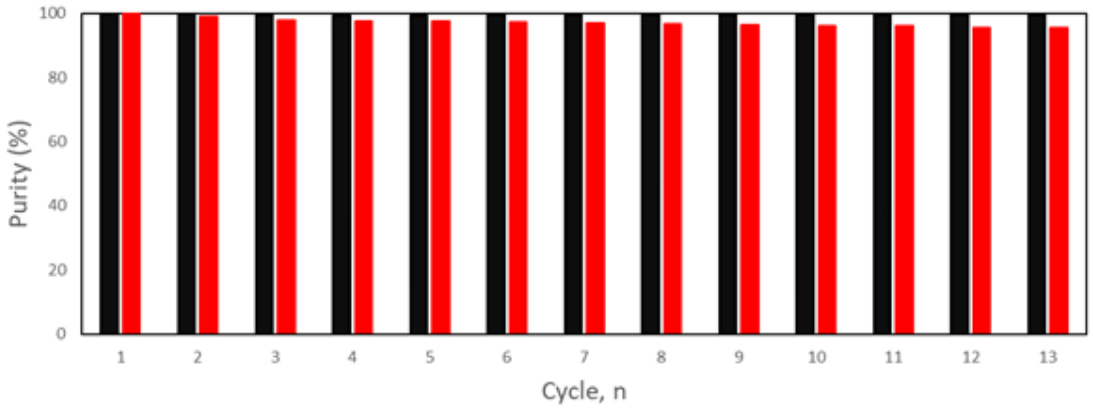

Figure 4.25: Guanosine (black) and uridine (red) purities per cycle for the separation of nucleosides using One-column Analog to SMB. Guanosine: $\overline{Pur}_{gua} = 99.57\%$; Uridine: $\overline{Pur}_{uri} = 97.03\%$.

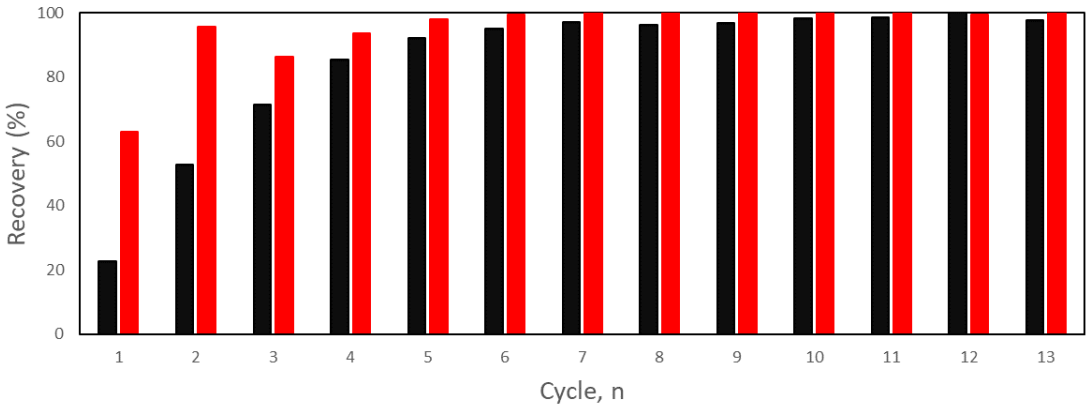

Figure 4.26: Guanosine (black) and uridine (red) recoveries per cycle for the separation of nucleosides using One-column Analog to SMB. Guanosine: $\overline{Rec}_{gua}$ = 97.76%; Uridine: $\overline{Rec}_{uri}$ = 100.00%.

the guanosine, and green area is the uridine picking interval. After calculations using the experimental data, it was concluded that at least 10.5 mL of solvent can be saved per cycle, which would result in a 25.87% decrease in solvent consumption at each cycle. The most effective solution is to redirect the fluid within that time interval of pure eluent through an internal recycle for the solvent tank and reuse it. An advantage when compared to the two-column is the number of pumps that the installation needs to operate with solvent recirculation, since the operation of the one-column with recycle lag occurs with only two pumps, confronting with the three pumps necessary for the two-column, semi-continuous configuration, if solvent recirculation is needed (closed-loop operation case) [228].

In view of the good results, an important aspect to be evaluated is how much the single-column system allows to reduce the cost in contrast to the benchmark process. In this exercise several other factors should be accounted for in this budget, for example, the reduction in the length of capillaries required for installation, or number of valves (ten ON/OFF valves in the two-column system versus seven ON/OFF valves and one 2-pos-6-port valve in the single-column system). Although the number of pumps is equal in both systems when considering open-loop configuration, i.e. two pumps, if internal recirculation is required, two-column (closed-loop configuration in this case) needs one pump for each outlet and more two recirculating pumps, totaling four pumps, while single-column setup only requires still two pumps. It is clear, therefore, that the equipment employed in single-column is much simpler than two-column.

In addition to the added simplicity, there are other adjacent benefits, the setup is smaller, less complex, and then less expensive than the technology covered by the two column system. It is worth noting that complexity usually increases costs. In terms of efficiency, the new process presented in this chapter seems competitive with the previously developed 2-column technology.

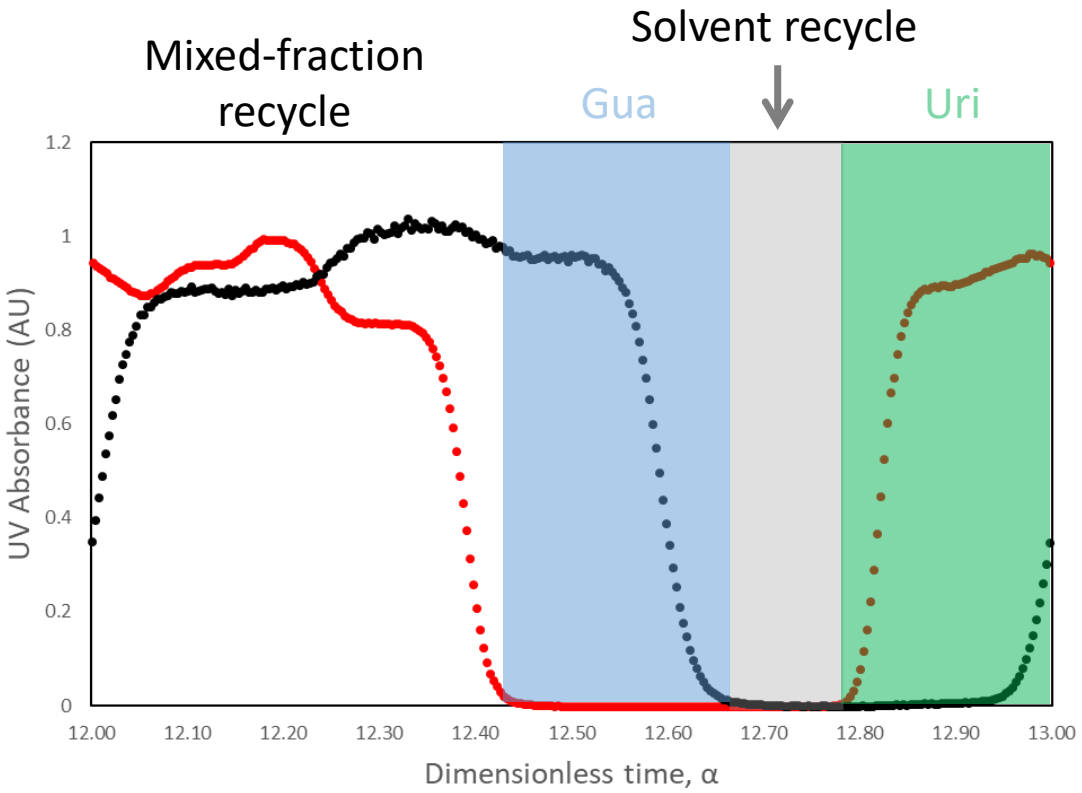

Figure 4.27: Guanosine (black) and uridine (red) concentration profiles for cycle 12 of the One-column Analog to SMB. The gray region of the graph represents the range at which the pure solvent can be recovered, representing a decrease of 25.87 % in solvent consumption. Blue area, guanosine recovery; green area, uridine collection.

4.3.3.4 Comparison with Simulated Data

gPROMS simulation for contrast with experimental data is an essential tool in the analysis of hydrodynamic behaviour within the recycle piston. Because of its ability to generate predictive information with high accuracy, it serves as decision support for product and process innovations, design and operation [211].

Taking into account the dynamic simulation variations for the recycling device: dispersive plug-flow and perfectly agitated tank, were built as demonstrated in Appendix B.7.

A parametric adjustment was performed to characterize the process in the simulation, adjusting the simulated curves to the experimental curves. Thus, the parameters used in the simulation are presented in Table 4.8.

The simulated solute composition profiles were compared, for each component, to the experimental ones, as can be seen in the Figure 4.28. The top graph shows the chromatograms for uridine, while the bottom graph shows the results for guanosine. The experimental points are expressed in red, while the results of the simulations are shown by blue lines for piston considered as dispersed plug-flow, and black lines for the data regarding the piston condition as perfectly stirred tank.

Table 4.8: Parametric adjustment to characterize the entire process. Parametric adjustment is required to fit simulated curves to experimental curves. ϵ is the packing interparticle porosity, H is the Henry constant, Pe is the Péclet number, V_0 is the inlet piston dead volume, V_L is the outlet piston dead volume.

$\epsilon = 0.295$ $V_0 = V_L = 0.35$ cm^3	H	Pe
Uridine ($i = 1$)	1.34	1100
Guanosine ($i = 2$)	2.20	1100

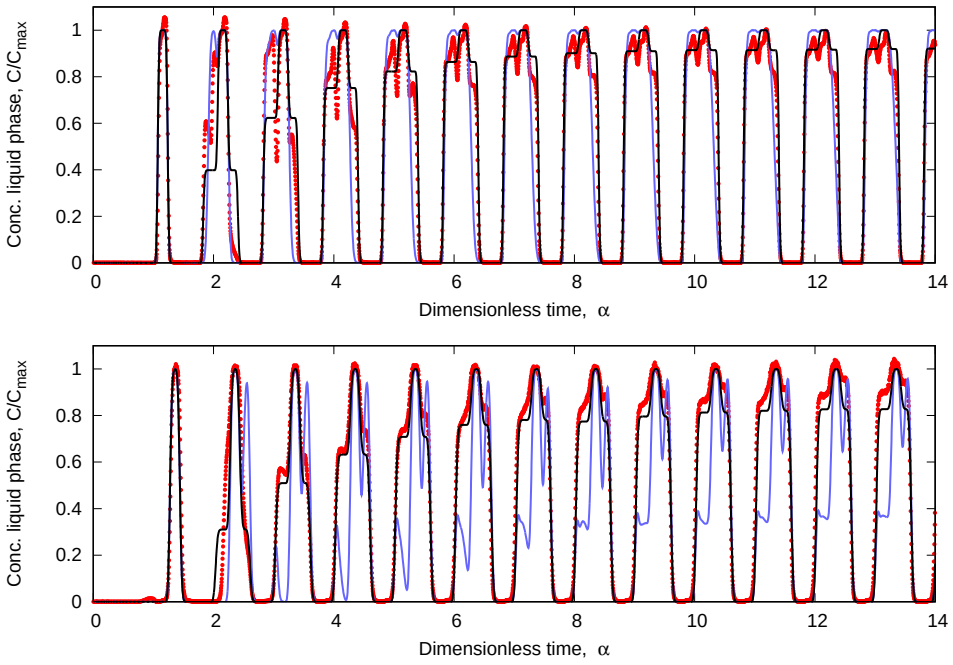

Figure 4.28: Comparison between experimental and simulated data for solute concentration profiles at the column outlet of the One-column analog to SMB defined in Figure 4.22(b). The top graphic shows the result for uridine, while the bottom one for guanosine. Points denotes experimental data, whereas lines represent the solutions of the dynamic process models (blue, piston as dispersed plug-flow; black, piston as perfect mixed tank.)

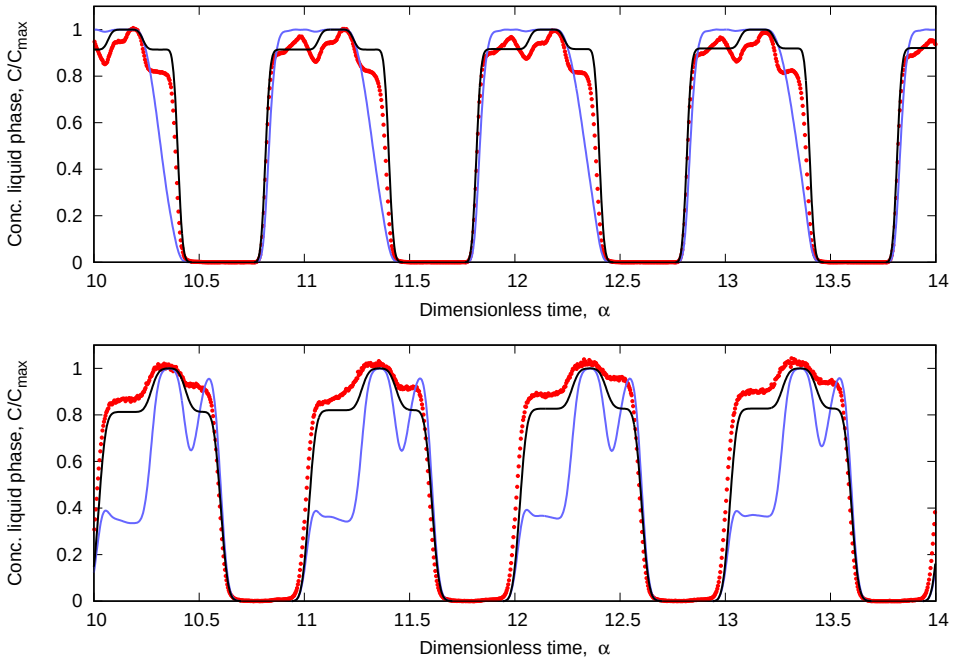

Figure 4.29: Comparison between experimental and simulated data, considering only steady state cycles at nucleosides separation, for solute concentration profiles at the column outlet of the One-column analog to SMB defined in Figure 4.22(b). The top graphic shows the result for uridine, while the bottom one for guanosine. Points denotes experimental data, whereas lines represent the solutions of the dynamic process models (blue, piston as dispersed plug-flow; black, piston as perfect mixed tank.)

Due to the number of cycles performed, a simpler graph was again generated, considering only steady state cycles (cycles 10 to 13), in order to facilitate the analysis, which is shown in Figure 4.29. When analysing the graphs, it was noticed that, for uridine (top graph), the concentration front rises were better captured by the simulation of piston as dispersed plug-flow, while the concentration front descents were better represented by the simulation in which the piston has behaviour of perfectly mixed tank, while for guanosine (bottom graph), the opposite happens, where the concentration front rises approached better to the simulation of piston as perfectly stirred tank, while the concentration front descents were better constituted by the simulation in which the piston is as a dispersed plug-flow.

Nevertheless, although the results are not exactly alike, a certain qualitative and quantitative agreement between the experimental and simulated results is easily noticeable, so it was concluded that the behaviour of the piston is somewhat intermediate between dispersed plug-flow and perfectly mixed tank. However, as shown in the previous section (4.3.3.3) through results of purities, recoveries and solvent consumption, this undefined

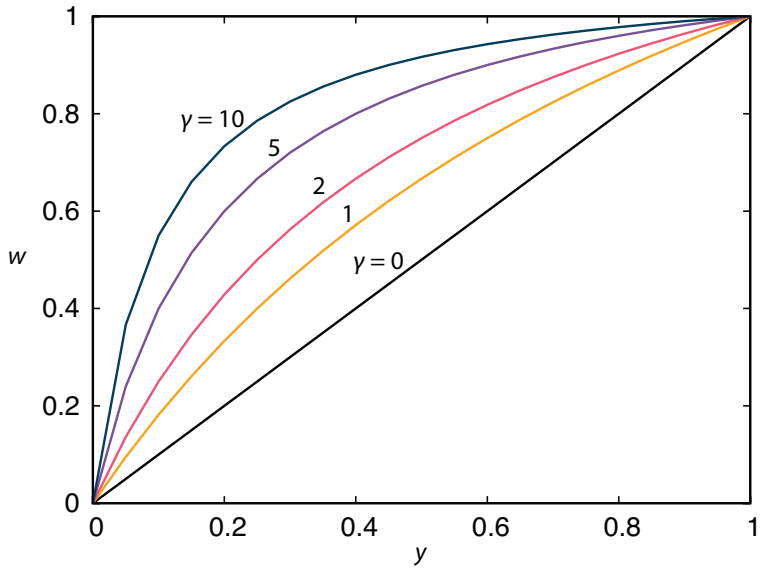

Figure 4.30: Shape of the dimensionless Langmuir adsorption isotherm as a function of γ.

hydrodynamic piston behaviour does not affect the good response of the chromatographic process when performing the separation of uridine and guanosine molecules, which does not invalidate the prototype's effectiveness.

Before concluding it is important to note that the prototype system was tested with a linear separation which, although counter-intuitively, can be considered more challenging than many nonlinear separations. This is because a linear isotherm is the boundary between favorable and unfavorable isotherms: the moving concentration front for a linear adsorption isotherm is not compressed during adsorption nor broadened during desorption. The resins for most overloaded (bio)separations are chosen to yield favorable adsorption isotherms under overloaded conditions so that the concentration fronts get compressed during the adsorption or capture steps. And in many cases the mobile phase is changed for the elution or washing steps to produce faster desorption, so the problem of band broadening is not even an issue there. Hence, the effect of fluid mixing in the recycle device has less adverse effects with a favorable adsorption isotherm than with a linear one.

To further elaborate on this point consider the problem of comparing breakthrough curves obtained under linear and nonlinear conditions when the chromatographic column is connected to an unmixed recycle device and to a perfectly mixed one. The reference isotherm is the linear one:

$$q = Hc, \tag{4.51}$$

where H is the Henry constant. The aim here is to compare the breakthrough curve for this isotherm and those for a family of Langmuir isotherms:

$$q = \frac{q^{\infty}\alpha c}{1+\alpha c}, \tag{4.52}$$

where $q^{\infty} = \lim_{c\to\infty} q$ is the saturation capacity and $q^{\infty}\alpha = \lim_{c\to 0} q/c$ the Henry constant.

In order to obtain a meaningful comparison between the two types of isotherms, the Langmuir one should yield the same adsorption capacity as the linear one at the feed concentration c^{F}, that is,

$$\frac{q^{\infty}\alpha c^{\mathrm{F}}}{1+\alpha c^{\mathrm{F}}} = Hc^{\mathrm{F}}. \tag{4.53}$$

This allows us to express the Langmuir isotherm as

$$q = \frac{H(1+\alpha c^{\mathrm{F}})c}{1+\alpha c^{\mathrm{F}}c}. \tag{4.54}$$

Moreover, by introducing the changes of variable $y = c/c^{\mathrm{F}}$ and $w = q/(Hc^{\mathrm{F}})$ the Langmuir isotherm can be rewritten as

$$w = \frac{(1+\gamma)y}{1+\gamma y}, \quad \gamma \equiv \alpha c^{\mathrm{F}}. \tag{4.55}$$

Notice that the linear adsorption isotherm, $w = y$, is recovered by setting $\gamma = 0$, whereas increasing its value makes the shape of the adsorption isotherm progressively more concave. This is illustrated in Fig. 4.30.

The equilibrium, dispersed plug-flow model governing the dynamics of the adsorption column can be written as

$$x = 0: \qquad y - \frac{1}{\mathrm{Pe}}\frac{\partial y}{\partial x} = y^{\mathrm{in}}, \tag{4.56}$$

$$0 < x < 1: \qquad \frac{\partial y}{\partial \theta} = \frac{\tau Q/(\epsilon V)}{1+\beta(dq/dc)}\left(\frac{1}{\mathrm{Pe}}\frac{\partial^2 y}{\partial x^2} - \frac{\partial y}{\partial x}\right) \tag{4.57}$$

$$x = 1: \qquad \frac{\partial y}{\partial x} = 0, \tag{4.58}$$

where ϵ is the bed porosity, $\beta \equiv (1-\epsilon)/\epsilon$ the phase ratio, $x = z/L$ the dimensionless axial coordinate along the column of length L and volume V, Q the volumetric flowrate, and Pe the Péclet number.

Expanding dq/dc gives

$$\frac{dq}{dc} = H\frac{1+\gamma}{(1+\gamma y)^2} \tag{4.59}$$

and if the chosen time scale is $\tau = (1+\beta H)\epsilon V/Q$, the governing equation for the interior of the domain simplifies to[1]

$$0 < x < 1: \quad \frac{\partial y}{\partial \theta} = \frac{(1+\beta H)(1+\gamma y)^2}{\beta H(1+\gamma)+(1+\gamma y)^2}\left(\frac{1}{\mathrm{Pe}}\frac{\partial^2 y}{\partial x^2} - \frac{\partial y}{\partial x}\right). \tag{4.60}$$

Let us now consider the two limiting cases of operation of the recycle device. Suppose that when the column is connected to the unmixed recycle device the former is subject to an inlet concentration profile consisting of a linear gradient from 0 to c^{F} followed by saturation of the column at c^{F}. This is an idealization of, say, moving the mass-transfer zone stored in the recycle device into the column. In the second case, when the column is connected to a perfectly mixed tank, the mass transfer zone is completely mixed in the

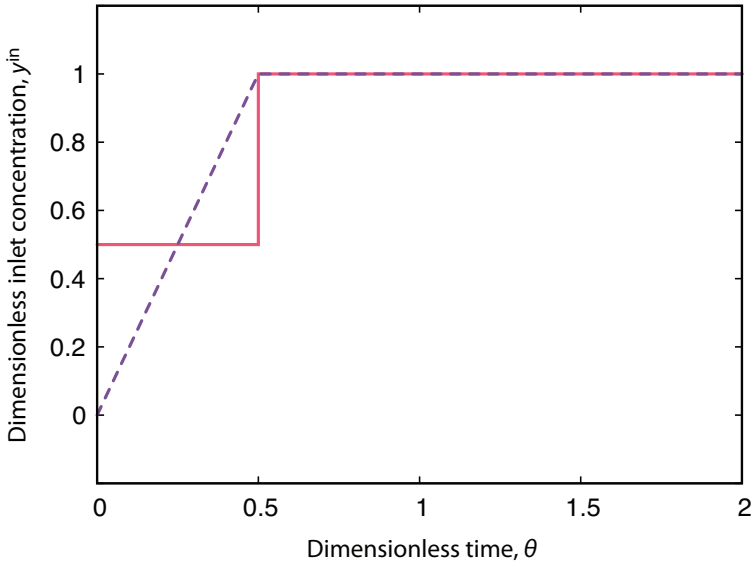

Figure 4.31: Inlet concentration profile of the column when it is connected to an unmixed device (dashed, purple line) and a mixed tank (solid, red line).

recycle piston, so the column is initially fed with a step concentration at $c^F/2$ followed by saturation of the column at c^F. Fig. 4.31 illustrates these two inlet concentration profiles.

Fig. 4.32 shows that for $\gamma = 0$ (linear adsorption isotherm) the outlet concentration profile when the column is fed from the mixed tank is clearly different from when the column is fed from the unmixed device. However, as the value of γ is increased the outlet concentration profile for the column connected to the mixed tank gets progressively closer to that when the column is fed from an unmixed recycle device. Hence, for very favorable adsorption systems the degree of mixing in the recycle device is not very important as long as the mixed fractions are reinjected into the column ahead of the fresh feed fraction (for a favorable isotherm lower concentrations travel slower than higher ones).

4.4 Conclusions

Seeking to validate the experimental prototype created in the laboratory and show its effectiveness, the first experimental validation was proceeded. For this, a linear binary separation of nucleosides, considered a simple and easy separation, was performed for open-loop operating configuration. Before executing the experiment for this configuration, preliminary experiments were performed to test the recycle device operation.

The recycle device has been validated for the successful operation of its movable piston. The hydrodynamic behaviour of the piston is somehow aligned with the plan of the previous chapter, in which, at first analysis, the fluid concentration profile is maintained, i.e. the "first in, first out" method is being obeyed by the recycling device. The maximum pressure reached with the piston in operation, 6 bar, is much lower than the maximum

[1] When $\gamma = 0$ this time scale yields $\partial y/\partial\theta = (\partial^2 y/\partial x^2)/\mathrm{Pe} - (\partial y/\partial x)$, which explains our choice.

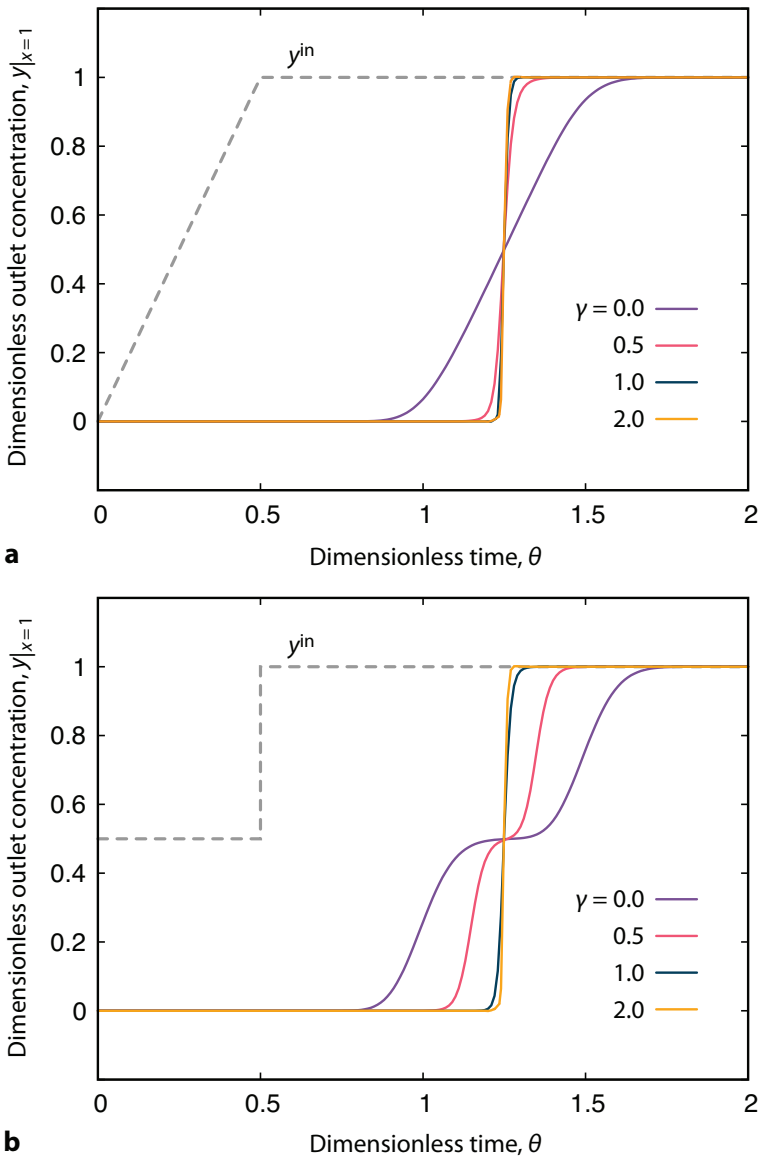

Figure 4.32: Outlet concentration profile of the column when it is connected to (a) an unmixed device and (b) a mixed tank, as a function of parameter γ; $\beta H = 3.0$, Pe = 300.0.

pressure supported by the equipment, which is very positive since operation with the complete setup would give to the system a higher pressure drop, and is crucial for the installation to operate at safe pressure margins.

As the first analysis was done only with the naked eye, further detailed study of the fluid behaviour within the piston was performed, this time with UV reading and for different piston heights, resulting in graphs with behaviour very close to the dispersed piston flow.

Furthermore, characterization regarding the chromatographic column and recycle device was proceeded.

The experimentally calculated interparticle porosity of the bed, $\epsilon = 0.318$, is identical to the porosity presented in the literature [228] for the same chromatographic column.

The same occurred with the constants of Henry experimentally calculated from pulse injections of each component. Therefore, the most recent results, calculated in this chapter, were used for the following chapter works. Peclet number of each compound were calculated for five flowrates, although only Pe_i values at $Q = 4$ mL/min were considered for the following steps.

The calculated piston dead volumes, $V_0 = V_L = 0.273$ cm^3, are very low volumes, which was intended for the system. Despite being very small values, they were not neglected in the mathematical model applied in the process simulation in gPROMS.

Overall, the general cycle depicted in this chapter for the Single-column Analog to SMB can be viewed as a streamlined version of a previously optimized two-column, open-loop SMB [228] with pulsed feed and selective product withdrawal, which characterizes as a quasi-continuous chromatographic operation. As another important point, the cycle determination has been able to reduce the number of cycle steps when comparing with the mimicked multicolumn process, from six to four steps, which is an advantage since step changes can come along with experimental errors and pressure changes.

Optimization in AMPL, maximizing the average feed flow rate, coupled with the purities and feed flow rate constraints, has provided optimum cycle times for each step of the cycle.

The experimental data was approached, for comparison purposes, with simulated data in gPROMS. The simulation against the experimental data serves to aid in process validation to evaluate the hydrodynamic behaviour of the fluid within the piston. The piston used in One-column SMB Analog system has been designed and engineered to maintain a dispersed plug-flow operation inside. However, the experimental curves of the 13 complete cycles compared to the simulated ones showed that the piston has an intermediate behaviour between dispersed plug-flow and perfect mixed tank, however, this does not cast doubt on the prototype effectiveness once the challenges of purity, recovery and solvent consumption have been met. The very high values of purities (99.57 % for guanosine and 97.03 % for uridine) and recoveries (97.76 % for guanosine and 100 % for uridine), and the reduced desorbent consumption showed that, despite the still undefined behaviour of the fluid inside the piston, the prototype presented excellent results in the nucleosides, uridine and guanosine, separation process, proving the efficacy of the new system.

In addition, the single column is very easy to perform, thanks to its simplicity of equipments, consequently bringing a process with reduced dimensions, smaller components number, reduced complexity, reduced costs, greater ease of maintenance, and even reduced time needed to perform one cycle in comparison to the conventional technology, the two-column mimicked system, while maintaining the efficiency.

Through the results, it was examined whether it would be necessary to improve the plug-flow operation inside the recycle container. Therefore, this topic will be covered in the following chapter.

Chapter 5

Improvements of Plug-flow Operation in the Recycle Device

5.1 Introduction and Objective

Three-dimensional (3D) printing, also called Additive Manufacturing (AM), Rapid Prototyping (RP), or Solid-FreeForm Technology (SFF), designates parts fabrication with the principle of material layer by layer exposure [91]. This technology emerged in the early 1980s, developed by Charles Hull [97], after which countless patents have emerged in these thirty years. 3D printing allows focusing on innovative product development, realizing creative ideas for the industrial market [82].

A large number of printer models already allow the user to focus on 3D model design, putting the printing software responsible for the difficult tasks, offering options to automatically orient, support, and present the 3D model.

There is a large diversity of 3D printing methods. The most common technologies are presented in Table 5.1.

Accompanying the variety of technologies, various materials for high-resolution rapid prototyping are already explored, destined for a wide range of purposes. With different materials, it is possible to produce pieces of plastic, metal, ceramics, among others.

The 3D printing market has grown quickly, with the emergence of an increasing number in high-precision machines, as well as a wide variety of modelling materials to cater to various industries' needs. The latest 3D production systems are capable, not only of producing 3D models for mechanical testing, but also of successfully manufacturing functional prototypes as an industrial production unit [56]. The 3D printing technology has achieved applications in the automotive and aerospace industries, through the production of car and airplane parts, in architecture, building structural models, in the consumer

Table 5.1: Overview of the most common 3D printing processes. Source: [9, 58, 97, 264]

3D Printing Technology	**Methods**	**Principle**	**Materials**
Vat Polymerization	Stereolithography (SLA), Direct Light Processing (DLP).	Curing of photoresin layers by the incidence of UV light.	Photopolymer resin (Standard, Castable, Transparent, High Temperature). Epoxy or acrylate based resins with photoinitiators.
Material Extrusion	Fused Deposition Modeling (FDM).	Extrusion of molten thermoplastics.	Filament of PLA, ABS, PET, TPU, PEEK, nylon.
Binder Jetting	Binder Jetting (BJ)	Powder-liquid binding.	Sand or metal powder: stainless / bronze.
Material Jetting	Material Jetting (MJ), Drop on Demand (DOD).	Hybrid between SLA and BJ. Photopolymers are cured when exposed to light.	Photopolymer resin (Standard, Castable, Transparent, High Temperature).
Power Bed Fusion	Selective Laser Sintering (SLS).	Powder particle heating provided by laser incidence.	Thermoplastic powder (ABS, PVC, nylon, resin), ceramic powders.
Power Bed Fusion (Metals)	Direct Metal Laser Sintering (DMLS); Selective Laser Melting (SLM); Electron Beam Melting (EBM).	A thermal source induces fusion between metal powder particles.	Metal powder: aluminum, stainless Steel, titanium.
Sheet Lamination	Laminated object manufacturing (LOM).	Cutting (with laser or razor) of heated coated sheet material.	Adhesive-coated polymer, cellulose, paper, metal sheets.

goods industry [245], in the food industry [93], in fashion, with the production of textiles [202], in the medical sector, with dental prostheses production and implants [163], and even in the field of government defence through weaponry production for the military.

In addition, 3D printing technology is set to revolutionize not only manufacturing but also research and teaching laboratories, with a potential impact on biotechnology and chemical sciences, addressing a comparison between new 3D printed methods and other traditional ones used in these areas. In biomedical engineering, for instance, 3D printing has been an increasingly addressed tool for producing biocompatible and resorbable materials, specifically tissue scaffolding, from bone and teeth, and still vascular and organ scaffolding. Scaffolds usually consist of the individual's own tissue (autogenous tissue), because bio-resorption and biocompatibility (where it can be rejected or not by the body) are the main constraints of a foreign scaffold. Therefore, the ability to produce scaffolds through 3D printing for tissue regeneration avoids the use of the patient's own tissue. This is very valuable when large amounts of autogenous tissue are needed, to the point of being infeasible by the patient [148, 221].

Moreover, in the biotechnology field, 3D printing has been an attractive pathway in surgical preparation, through the printing of the patient's anatomy, allowing a patient-specific treatment plan and better preparation for surgery due to early study of body anatomy [221]. Moreover, drug delivery devices have been widely manufactured, because 3D-printed drug implants make it easier for control drug release by providing a barrier between drug and tissue through the binder printing, a solution capable of solubilizing a specific powder onto a matrix powder bed [282]. This ensures that the infection will be treated locally and will not affect other tissues, as traditionally occurs with drug treatments. As chemical applications, macro/microfluidic devices have been extensively produced through 3D printing, with the potential for producing a complex microvascular network with channels capable of diffusion-based mixing under laminar flow profiles, as well as mixing from turbulent flow [259].

A highlight application of 3D printing in recent years is the customization of laboratory material, producing customized parts to complement laboratory equipment of different functionalities, through rapid prototyping, easily acquiring the necessary material [66, 130, 145, 255]. It is about this application that this chapter focuses.

Recent approaches to 3D printing has been applied to chromatographic columns production [76, 185, 186, 201, 231], mainly for liquid chromatographic separations. Porous beds with perfectly ordered micro-structures, novel flow-distributors, collector, column (walls) designs and standard liquid chromatography fittings were manufactured in a single printed artefact, to achieve more efficient separations. Despite the adoption of 3D-printing as a column production method, it is currently limited by several key challenges such as: resolution, material choice and print times. This study can serve as a basis for improving the piston operation, a subject that will be addressed in this chapter.

The popularization of 3D printers for different features comes together with the prices

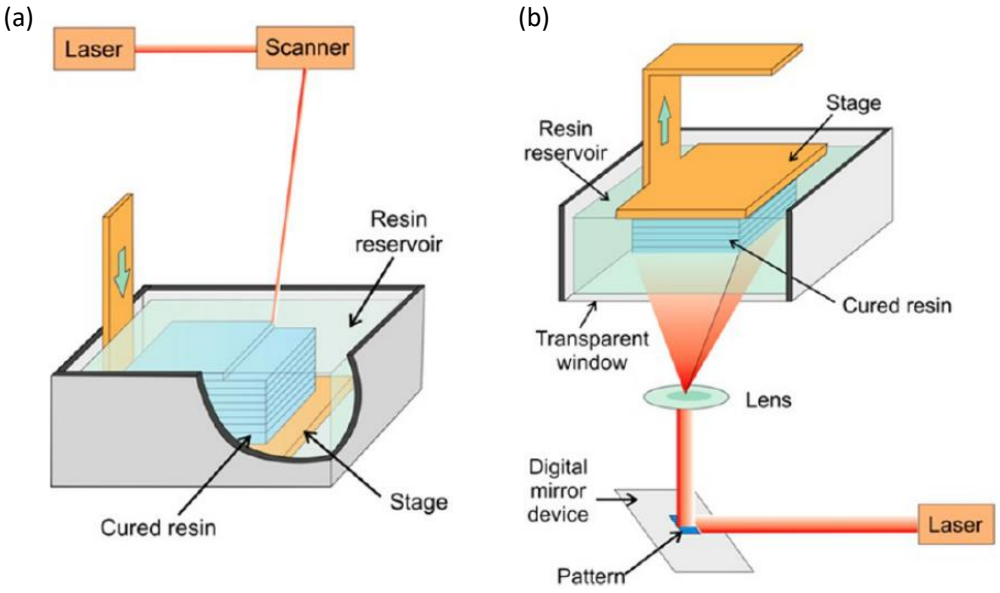

Figure 5.1: Schematic of an SLA 3D printers. **(a)** Bath configuration SLA printer with a direct curing method. **(b)** Layer configuration SLA printer with a projection based curing process. Source: [97].

associated with the equipment, which has been decreasing sharply over the last four years. Machines that once cost $20,000 can now be purchased for less than $1,000. This is largely due to Chinese companies, which are investing their efforts in the manufacturing of this technology [35]. The attractive pricing, and also the key advantages of 3D printing, namely, simplicity in the manufacturing process, short production time, model and manufacturing reproducibility, make this technology potentially envisioned in the most diverse areas [269].

5.1.1 Stereolithography (SLA) Technology

Stereolithography (SLA) was the first patented 3D printing method, which occurred in 1986 by Charles Hull at 3D Systems [119].

SLA print technology is a light-polymerized type process, which uses a laser incident on a liquid photopolymer resin, causing the monomer (liquid) to link together to form a polymer (solid) [120], then the polymer composes the three-dimensional solid body.

There are two approaches to SLA, as shown in Figure 5.1, one based on direct/laser writing (a), and mask-based writing (b) [97]. Both forms contain a movable base, a tank of liquid resin, a UV light beam and a computer interface. The mask-based writing also contains a digital mirror device (DMD) "mask"that allows curing a single layer at a time.

In the bath method, the oldest method for SLA, the platform is positioned just below the surface of photoactive liquid resin and is thus submerged. The UV beam traces a 2D section over the submerged base, causing the resin to polymerize when subjected to such illumination. In this configuration, the laser moves line by line along the surface until

the desired layer is completely cured. The stage is lowered slightly to a set height to start a new layer so that a thin height of liquid resin is left over the previously cured material, and then the curing process is repeated.

It is worth noticing that the thickness of the cured layer is dependent on the UV light energy, more precisely the exposure duration, scan speed, and intensity of power source [97]. In addition, between one layer and another, the resin surface is flushed with a resin-loaded blade to ensure a uniform liquid layer.

In terms of limitations, this configuration is constrained by the tank size, which restricts the height of the prototype to be printed, resin waste, and massive cleaning procedures. These drawbacks are overcome by layer configuration, so they are a better alternative to SLA technology [48, 59, 159].

The layer configuration, unlike the previously explained configuration, has the stage suspended above the resin tank, while the light source is below the reservoir. The reservoir has a transparent bottom that allows light to pass from UV to the resin. This change of position allows the volume of resin needed to be reduced in the vat, where only a thin layer of liquid is between the reservoir base and the submerged platform at the set height. Therefore, the liquid is in contact with the platform when UV light is shone. Because the reservoir base is transparent, the cure is done on the entire layer at once, giving a much faster healing process than the bath configuration. When the curing process of a layer is completed, the platform lifts along with the cured material adhered to it, and then the process is repeated until the final object is achieved, with minimal cleaning stages [118]. The UV light source varies with the type of resin used [33].

A post-cure process is required for both configurations after part fabrication to strengthen bonding in the final 3D prototype [274].

In SLA technology, the vertical resolution is determined by the thickness of the cured layer. Reducing the layer thickness increases the curing efficiency, instead, the horizontal resolution is defined by the diameter of the UV beam [106].

The drawbacks of SLA primarily involve resins, not only for the associated cost but also because only one resin can be used at a time in a printing process, which limits prototype design. In addition, most of the final material is brittle and may shrink after polymerization as the resins are epoxy or acrylic based [106, 173].

Although SLA 3D printers are highly expensive, they feature high resolution (25μm layers). In addition, efficient models (1.5 cm/h building speed) are already becoming more accessible to labs, such as Formlabs printers [81].

5.1.2 Fused Deposition Modeling (FDM) Technology

Fused Deposition Modeling (FDM) was developed by S.Scott Crump, co-founder of Stratasys, in 1988 and the patent was awarded in 1992 [56]. The FDM print technology, the most popular 3D process by the number of machines, is a process that uses a thermoplastic material as continuous filament [105], extruded from a moving, heated printer

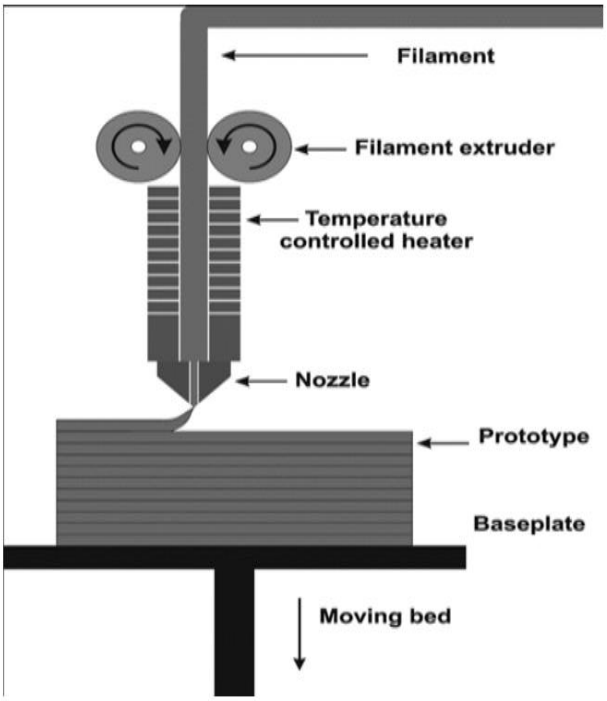

Figure 5.2: Schematic of an FDM 3D printer. Source: [197].

extruder head and deposited on the growing work, which is placed on a heated bed. The head movement that defines the desired shape is performed by computational control. Figure 5.2 shows the printer layout FDM.

In this printer type, the extruder has two ends, a hot and a cold one. The cold end consists of the roller, which is responsible for pulling the material filament towards the hot end and controlling the feed flow through a stepper motor. This represents the drive mechanism in the material delivery system. The hot end is composed of a liquifier, an essential component in this printer type, hosted in the heating chamber and a nozzle, which are responsible for transforming the filament into a thin liquid that adheres to the bed and the previously deposited material. For each material, a specific nozzle is used, with different tip diameter, manufactured from different raw material, and working at a different temperature.

Firstly, the head moves in two dimensions to deposit the extruded material in a horizontal plane, thus forming a layer. Then the head is moved vertically to start working on a new layer [32]. And so, the work begins again under the two dimensions of the plane. This process continues until the final object is totally completed. The vertical height of the layer defines the layer resolution, in this manner, as much lower height, better resolution is obtained.

The speed of the extruder head must be controlled to stop and begin material deposition to achieve an interrupted plane, in other words, without any binding between the

Table 5.2: Materials used in the execution of the activities of Chapter 5.

Material	Molecular formula	Manufacturer
Clear Formlabs Resin	-	Formlabs
Pure Isopropyl Alcohol	C_3H_8O	LabChem
PEEK filament	-	Henan Suwei Eletronic Technology
Ethanol absolute	CH_3CH_2OH	Panreac
Sodium hydroxide	NaOH	Anko Nobel, EKA Chemicals
Hydrochloric acid	HCl	Carlo Erba Reagents
Fluorescent Tracer	-	-

sections of raw material. In addition, for the vertical layers of the process to bond successfully, the ambient temperature must be controlled. Therefore, the system is kept in a chamber, at a temperature slightly below to the material melting point being deposited. In this printer type, the thermoplastic is rapidly cooled due to the low-temperature maintenance in the platform, where the material is deposited, and also the environment of the system chamber. Since this kind of technology is the most commonly used in the field of 3D printing, a wide variety of filament materials are also already being used for extrusion, for example polylactic acid (PLA) [70, 107, 111],aliphatic polyamides (nylon) [158, 175, 243, 286], polyether ether ketone (PEEK) [64, 89, 117, 273], acrylonitrile butadiene styrene (ABS) [36], and so on.

FDM, when it is compared to other 3D printing technologies, presents itself as an inexpensive alternative [125], and is mostly used for prototyping and rapid manufacturing, facilitating iterative tests and very short runs. They may also be used in the field of human health in scaffolding prototypes for medical tissue engineering applications [172], or for processing post-consumer plastic waste into filament, and other uses.

While it has the advantage of offering a low-cost solution over other technologies, the FDM method's drawback is the requirement for supports to deposit the liquid material, in other words, it is impossible to create shapes with unsupported regions, which limits the part shape to be printed.

5.1.3 Objective

In order to improve the fluid distribution in the recycle piston, the purpose of this chapter is to develop flow distributors using 3D printing technology, addressing two distinct printing methods: SLA and FDM. The numerous configurations produced will then be analysed in an attempt to explore improvements.

5.2 Materials

The reagents and raw materials used in Chapter 5 are shown in Table 5.2.

5.3 Methods

The 3D printing methods employed in this chapter were used at different times of the thesis development. Therefore, although the following sections address the two different methods, it should be borne in mind that the SLA method was worked on in advance, and only after the results obtained with this method, the FDM method was further explored.

5.3.1 Production of New 3D Distributors

(*SLA Technology*)

The SLA printer used to produce 3D distributors was the Form 2 (Formlabs, Germany)(Figure 5.3) with Clear Formlabs Resin (Standard Resin from Formlabs, Germany). The Clear Resin is composed by methacrylated oligomers, methacrylated monomer and photoinitiators [86].

The operating temperature is automatically controlled at 35°C, the supports are automatically generated and easily removed, with auto-orientation for the optimal print position. However, in the present work the supports were mostly generated manually to improve their placement and minimize their number. The layer resolution is 0.025 mm, the highest attainable with the current machine, the laser spot size is 0.14 mm and is emitted with wavelength of 405nm [84].

The Open Source Blender software v. 2.79 (https://www.blender.org) was used to generate the drawings, and the Preform program was used to send different shapes to the printer. Blender is a free and open source 3D creation suite. It supports the entirety of the 3D pipeline—modeling, rigging, animation, simulation, rendering, compositing and motion tracking, video editing and 2D animation pipeline. The 3D drawings produced in this thesis were always generated using the Blender scripting language programmed in the Python scripting language and never produced by hand. Python is an interpreted, interactive, object-oriented programming language. It incorporates modules, exceptions, dynamic typing, very high-level dynamic data types, and classes. Python combines remarkable power with very clear syntax.

Python scripts are a versatile way to extend Blender functionality. Most areas of Blender can be scripted, including animation, rendering, import and export, object creation and automating repetitive tasks. To interact with Blender, scripts can make use of the tightly integrated Application Programming Interface (https://docs.blender.org/manual/en/latest/advanced/scripting/introduction.html).

To ensure that there is no monomer residue on the printed body and subsequent danger of polymerization in contact with the light, the solid printed material should immediately undergo two washing procedures, each bath with 10 minutes immersion in pure isopropyl alcohol (LabChem, Zelienople-PA, USA). After the first 5 minutes of each bath, the material is lightly subjected to shaking for 30 seconds. And then the piece is put to dry. After being completely dry, it is subjected to post-cure, a process to improve

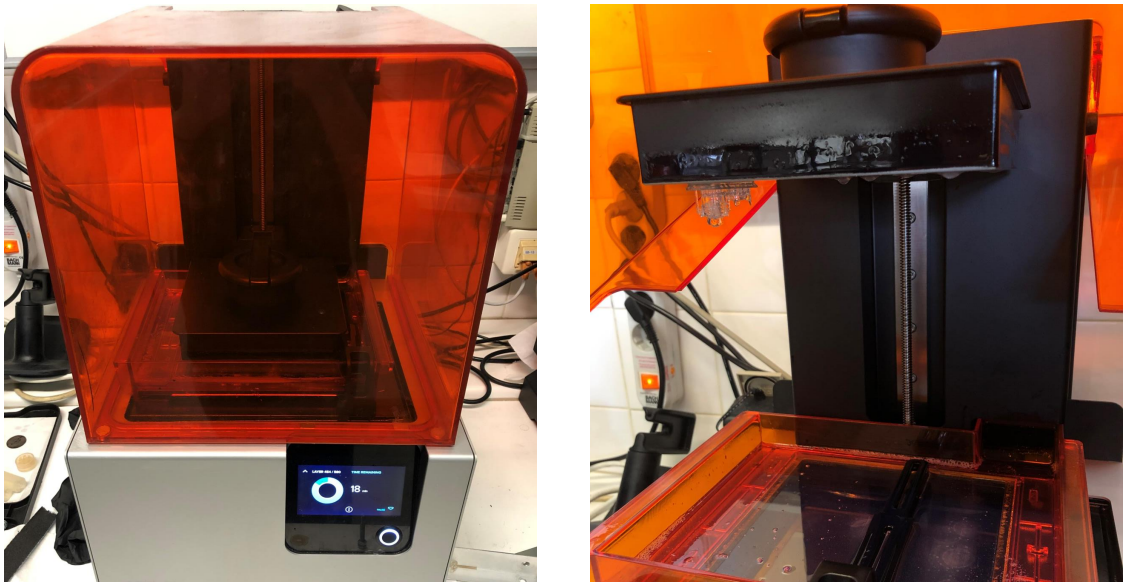

Figure 5.3: Form 2 printer (from Formlabs) used to produce complementary piston parts. This 3D printer uses stereolithography (SLA) as printing method.

the mechanical properties of the part, enabling to achieve their highest possible strength (tensile strength) and stiffness (Young's modulus). For post-cure of structures produced with Formlabs Clear Resin, the supplier recommends subjecting the material to a 405 nm light for a fast and effective post-cure, at a temperature of 60 ºC, for 30 minutes [83, 85, 285]. In the laboratory, post-cure was performed using a 395nm LED flashlight (LE brand), a VMS-C7 magnetic heating plate (VWR, Portugal) at 60ºC, for 30 minutes. The post-cure process should be performed under the shelter of external light, i.e. the only light affecting the material was the post-cure light, and should be ensured that the light falls equally on all faces of the prototype.

(*FDM Technology*)

The FDM printer utilized was the CreatBot F160 Model (Henan Suwei Eletronic Technology, Zhengzhou-Erqi, China) (Figure 5.4) with PEEK as load filament. The operating temperature is set for each print, the supports are automatically generated, the printer has self-adjusting fan speed, the maximum layer resolution is 0.01 mm, and a single martensite steel nozzle with 0.4 mm of extruder end diameter is used to generate the structure of printing. The filament diameter is 1.75 mm. Paper glue must be applied to adhere to the base of the print piece to the printer bed. The Blender software was also used to generate the drawings, and the CreatWare V6.4.6 software program was used to send different shapes to the printer.

Figure 5.4: Form 2 printer (from Formlabs) used to produce piston distributors. This 3D printer uses fused deposition modeling (FDM) as printing method.

5.3.2 Characterization of the 3D Printed Material

Some experiments were carried out to characterize the materials produced from each resin/filament used.

i) Thermal Gravimetric Analysis (TGA): This test comprises the thermal stability study of the 3D material. An analysis of degradation, or mass loss, of the sample under different temperature was proceeded, using LABSYS evo platform (Setaram Instrumentation, Hong Kong) The atmosphere used for the experiment is argon, an inert gas, which constantly passes through the sample during the experiment, to ensure that there is no interaction of the sample with any gas. The temperature range used in this experiment was 34.43 - 900 ºC for polymer from Clear resin, and 34.43 - 500 ºC for PEEK. Heating speed was set at 3 ºC/min.

ii) Solvent Compatibility Test: This test comprises the chemical stability study of the 3D material. The technical specifications provided by the manufacturer of each resin do not inform its compatibility with the solvents that are used in biomolecules separation/purification [80]. This experiment represents a test of absorption (interaction) of the 3D form with a certain solvent. Therefore, it was performed compatibility tests, through the analysis of percentage weight gain of one piece printed on the 3D printers, after three days of immersion in three different solvents. The solvents chosen are solvents with very high pH (0.1 M NaOH - pH 13.0), very low pH (0.001 HCl - pH 3.0) and the solvent used for elution of nucleosides (ethanol 5% v/v in H_2O).

To work with the FDM method, it was needed additional characterization experiments:

i) Printing Parameters for FDM printer: At FDM method, the printed material comes out completely dry and no additional procedure is required. However, to start up using the CreatBot printer, it is first necessary to calibrate the printer for each raw material, in this case, the PEEK filament. Even with indication of the print parameters in the literature and the manufacturer, optimum print conditions may change depending on the desired part geometry as well as the print orientation. There are three parameters to take into account for calibration:

   a) Bed temperature;

   b) Extrusion temperature;

   c) Extrusion speed.

   These parameters may differ from one feedstock to another, and analysis of the optimum printing condition is performed with the naked eye, observing whether the printed material follows the minimum resolution required, such as the absence of filaments between parts of the impression in different positions of the printing bed, or overhangs, for example.

   Conventionally, for calibration experiments, boat thumbnails (see Figure 5.5a) are printed, as they contain a wide variety of shapes in their design [1, 260]: horizontal, vertical and at different angles surfaces, at different heights (z), vertices, arcs, smooth and rough surfaces, embossed printing (different printing plans), regions requiring supports, among other variations. Therefore, the standard boat, also known as 3D Benchy, was printed to calibrate the variables. Calibration by printing the part is also important to understand machine limitations, whether in translation, extrusion, fan cooling, and so on.

   However, in addition to this part, calibration was also done using parts with the design shown in Figure 5.5b.

   After adjusted, the variables were kept constant for the distributors printing.

ii) Optimizing Part Dimensions: Metric specifications of the 3D printing part have been optimized by varying the following dimensions: internal diameter (Di), external diameter (OD), branches (or filament) thickness (e), crown thickness (E_c), workpiece height (Ew).

iii) Deformation of PEEK part: The deformation of a specific piece (the shape will be presented in the following sections), produced with PEEK filament, was developed at furnace, controller B170 model (Nabertherm, Germany). The parameters Δt_1 (heating ramp time, min), Δt_2 (isothermal time, min) and T_{iso} (temperature to keep

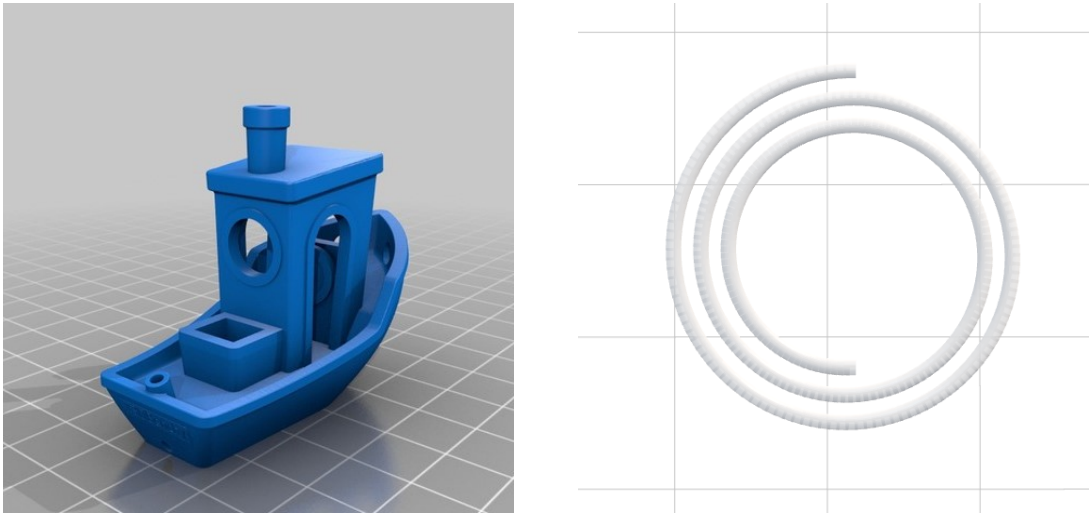

(a) 3D Boat thumbnail.

(b) 3D circular part.

Figure 5.5: Designs used for FDM printer calibration. (a) 3D Benchy. Traditionally used due to the diversity of shapes inside the design. Image source: [260]. (b) Spiral, printed only in the XY plane. This design is similar to the 3D element required to insert into the piston.

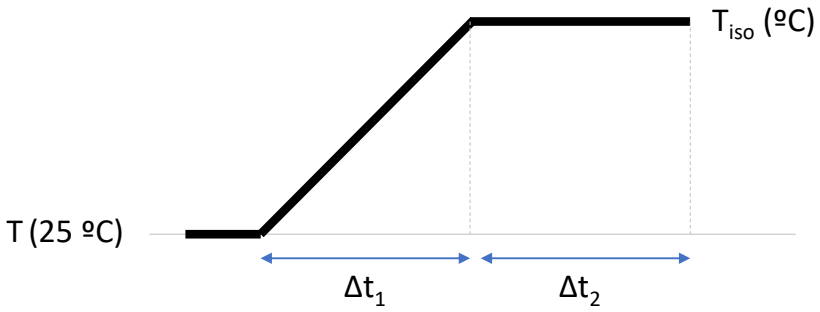

Figure 5.6: Spiral Deformation Method. The original piece is subjected to the furnace with a heating ramp of Δt_1 min from room temperature up to T_{iso} ºC and further Δt_2 min in isothermal environment.

the material in isothermal conditions, ºC) were initially varied until the optimal conditions of prototype deformation were found. See Figure 5.6. The variations tested for each parameter were: Δt_1 = 15 and 30 min; Δt_2 = 15 and 30 min; T_{iso} = 155, 160, 165, 170 and 180 ºC.

5.3.3 Performance of the 3D Distributors

The distributor performance experiments presented below were developed by the stereolithography 3D printing method.

5.3.3.1 Tracer Test

Each frit shape, among the various printed distributor models, was individually tested by fluorescent and intense colour tracer injection for analysis of fluid behaviour within the piston. A 395 nm LED Ultra-Violet Lamp (LE, Las Vegas, NV, USA) was used for this purpose. The experiment is done by introducing the new 3D printed frit on the piston; then, eluent injection (5 % v/v ethanol in H_2O) is proceeded up to 20 mm and then 20 mm of tracer diluted solution, causing the piston to go down. Then the piston is placed to rise completely. The extent of fluorescent dye concentration profile, when introduced into section area A of the device, was quantified by measuring yellow intensity across the reflux piston.

5.3.3.2 Nucleosides Separation

The best performing dispenser was separated and used to replicate the prototype validation experiment described in the previous chapter, and compare to the results of the original recycle container (with polyethylene frit). The solutes concentration profile was also compared with gPROMS simulation already presented in the previous chapter, which considered piston as dispersed plug-flow.

5.3.3.3 Pulse and Gradient Injection Test

The purpose of this experiment is to determine the concentration profile inside the recycle piston for the final piston configurations, due to the different 3D printed frits plus supports inserted between the inlet and outlet of section A (the section where the feed and eluent passes, not just eluent) of the piston.

The experiment consists of pulse feed injection, full piston cleaning with eluent injection during the time needed to return the absorbance signal to the reference, and subsequent gradient injection increasing the concentration from pure eluent to pure feed solution. The gradient concentration control was done by changing the flow rates of the feed and solvent pumps every 0.5 s, with the sum of the two flow rates always remaining constant. This was done automatically through Julia's software. Thus, at the gradient beginning, the eluent pump is at its maximum flow rate and the feed pump is at flow rate equal to zero, opposite to what happens at the end of the gradient, where the feed pump is at a maximum flow rate and the eluent pump is pumping nothing.

For each experiment, the feed and gradient volumes to be injected were proportional to the volume of the piston (V_P), where each injection is inserted up to twice the internal volume of the piston. At the end of the gradient, more feed solution is injected during ten seconds to ensure it has reached the maximum absorbance level.

These experiments were performed using solutions of 0.05 g/L uridine in ethanol 5% v/v in H_2O, at an absorbance of 260 nm, with Deuterium light only. The reference solution for the UV detectors is ethanol 5% v/v in H_2O. Two UV detectors were used:

one at piston inlet and another at the outlet of the recycle device. Constant flow rates of 4 mL/min were used, with differences in the flow rates of both pumps (feed and eluent) only in the gradient step.

5.4 Results and Discussions

5.4.1 Characterization of the 3D Printed Material

5.4.1.1 Thermal Gravimetric Analysis

The sample of Clear resin and PEEK polymers were analysed by TGA, done by recording the weight loss as a function of temperature increase. The operating temperature of the Single-column analog to SMB is 25 ± 5 ºC, therefore, the objective is not to ensure that the 3d printed material is stable at the system operating temperature, once the ambient temperature is a safe margin of stability for solid material produced from both Clear resin and PEEK filament. It is highlighted the importance to know the behaviour of the material when subject to high temperature variation.

Figure 5.7 presents the graphical results of the performed TGA test for both samples. Results are expressed graphically as a percentage of weight loss as a temperature function.

It was observed that for the printed part using SLA technology, the structure is stable up to approximately 250ºC, undergoing degradation process from slightly higher temperatures. At 155ºC, for example, less than 2% of the initial mass was lost. Thus, at this temperature, the material can be considered stable at the decomposition level as it is still far from the steep slope of the curve (which characterizes the decomposition of the solid). The slight loss of mass can be explained by possible moisture loss or evaporation of remaining solvent used in the cleaning process or even remaining material (monomer) adhered to the polymer walls.

Through the analysis, it was also observed that the heat deflection temperature (HDT) indicated by the manufacturer (73.1ºC, at 4.5 bar, for post-cured material) [80] is substantially lower than that found in the analysis (318ºC). This is a positive factor once the material has proven to have a higher temperature resistance than indicated.

The TGA decomposition profile for PEEK showed that there was no degradation of the compound until 500 ºC, maximum temperature analyzed.

5.4.1.2 Solvent Compatibility

Most polymeric materials can absorb small organic molecules, and also can absorb organic or aqueous solvents, resulting in swelling of the bulk material [97]. Therefore, the relevance of the solvent compatibility experiment.

The results for solvent compatibility test are depicted in the Table 5.3. The result for Clear resin presents that the polymeric material achieves a <1 % mass gain for the 3 solvents after 3 days of immersion. In addition, it was noted that the polymer remained

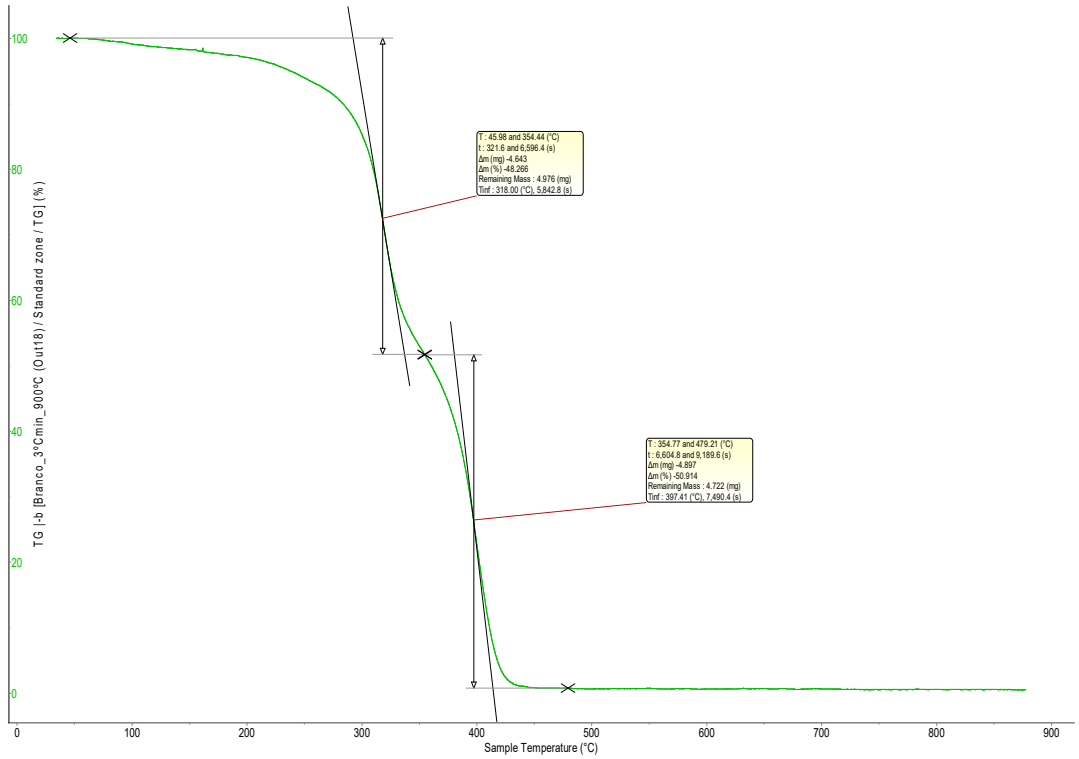

(a) Polymer formed from Clear resin.

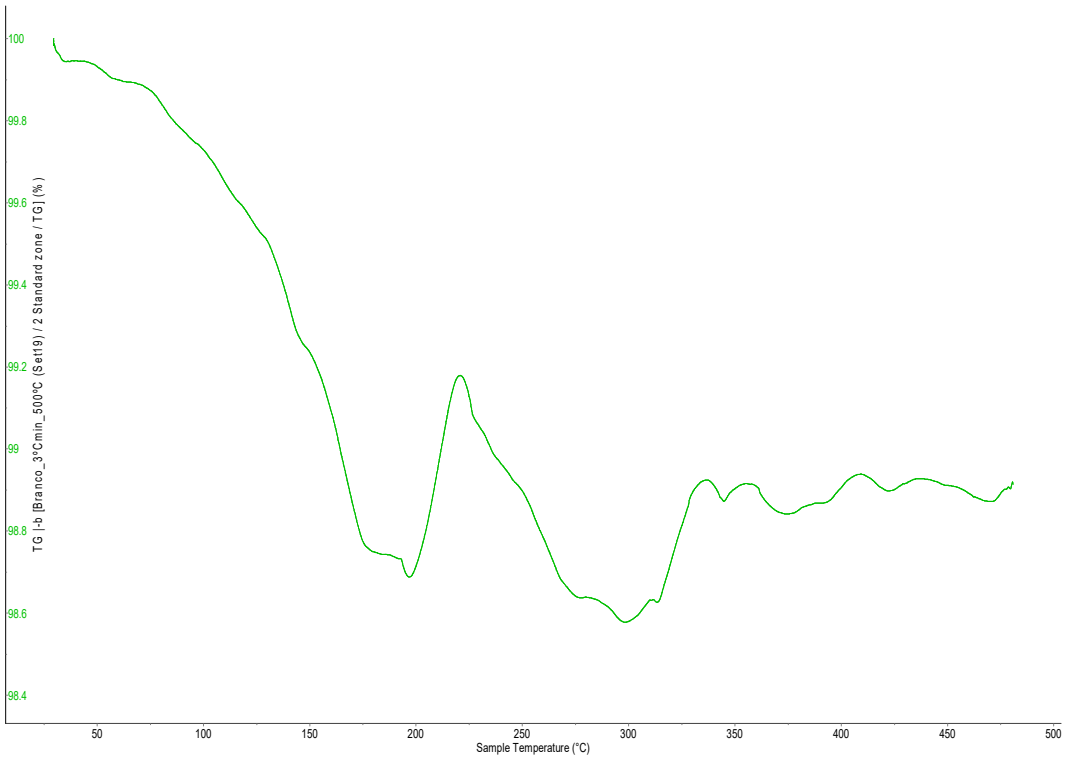

(b) PEEK Polymer.

Figure 5.7: Thermal Gravimetric Analysis. (a) Polymer produced by SLA method, with Clear Formlabs resin. (b) Polymer produced by FDM method, with PEEK filament. Analysis made by the Analysis Laboratory (REQUIMTE - FCT/UNL).

Table 5.3: Solvent compatibility test. After three days of material immersion in solvents with different properties. The 3D printed polymers had less than 1% mass gain/loss, showing to be compatible with the three solvents chosen.

3D Material	Solvent	Initial Weight (g)	Weight After 3 Days (g)	Weight Gain (%)
Clear Resin	0.1 M NaOH (pH 13.0)	0.1309	0.1319	0.76
	0.001 M HCl (pH 3.0)	0.0949	0.0958	0.95
	5% v/v Ethanol in H2O	0.1314	0.1326	0.91
PEEK	0.1 M NaOH (pH 13.0)	0.1700	0.1697	-0.18
	0.001 M HCl (pH 3.0)	0.1657	0.1650	-0.42
	5% v/v Ethanol in H2O	0.1238	0.1238	0.00

rigid, did not gain flexibility. However, in order to have more effective stiffness variation results, a more accurate test would be required as this analysis was done only visually when applying hand movements.

Therefore, this analysis showed that Clear resin polymer and PEEK polymer are compatible with the nucleoside separation solvent (5% v / v ethanol in H_2) as well as solvents similar to those used for purification of protein A resin monoclonal antibodies [30]. The concern was to test solvents with very high or very low pH, it was used 0.1 M of sodium hydroxide (NaOH, pH 13.0) and 0.001 M hydrochloric acid (HCl, pH 3.0). The NaOH solution can be used in the cleaning-in-place (CIP) step for mAbs purification, while the HCl solution suggests the low pH solutions used as elution buffer (20mM citrate, for example).

5.4.1.3 Printing Parameters for CreatBot Printer

While the Form 2 printer (used for the SLA method) has well-defined print parameters, the CreatBot printer required parameter adjustment to print well-defined parts, since the information provided by both the manufacturer [112] and found in the literature [11], for printing PEEK material, have ranges for operating parameters. Therefore, the optimum printing conditions had to be well determined before starting to manufacture the desired parts.

In this calibration test, the points evaluated in the 3D Benchy were: definition of angles, vertices, surfaces definition (so that you can not notice the transition from one layer to another) and dragging between different sections of the same plane. The points evaluated in the circular piece were: formation of bubbles or grains in the 3D piece and cohesion between layers (the piece must be solid and unique, without "unraveling"the piece).

After printing samples with layout similar to the part desired for subsequent tasks in this chapter (XY plane spiral part), manufactured under varying parameters, the optimum printing conditions found were: layer height = 0.1 mm (defines the quality, or

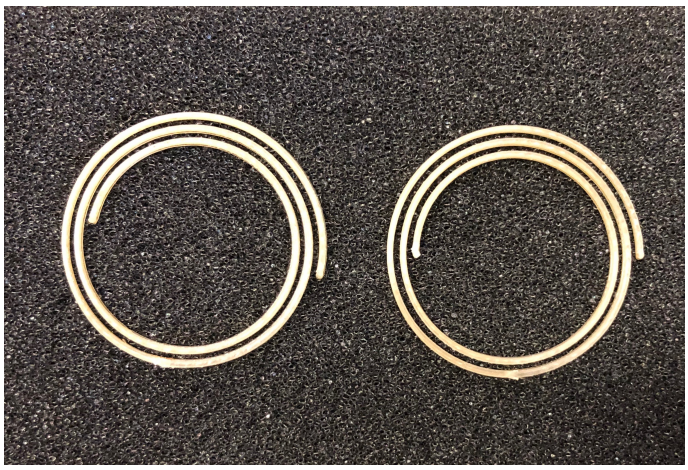

Figure 5.8: Parts printed under optimal printing parameters of the CreatBot 3D printer. This design is similar to one needed in a section of this chapter, which is explored later.

layer resolution), bed temperature = 120ºC, printing temperature (nozzle) = 420ºC, ambient temperature inside the printer = 150ºC, with print speed = 5 mm/s. The high air temperature inside the printer has been set to prevent PEEK from cooling too quickly. In addition, this temperature is adjusted by the printer through fan speed. Since the printer inside never gets to 70ºC, because it is a too high temperature, the fact is that the fan does not turn on, and that is the goal: keep the temperature too hot so that the fan speed is 0 %, to promote the correct material crystallization. For nozzle retraction, the nozzle travel speed is 30 mm/s, with a Z distance (height) of 1.2 mm. The Figure 5.8 shows the spiral printed under the best printing parameters.

The result for the latest PEEK 3D part characterization experiment, "Deformation of PEEK part", is presented below, along with the production results of the FDM part, to facilitate understanding of the results.

5.4.2 SLA Method: Production and Performance of New 3D Distributors

The following tasks are separated by phases of work development, once the production of new frits conformations was performed as needed as performance tests were continuously carried out.

5.4.2.1 Phase 1: Massive 3D Confection and Tracer Experiment

At the end of the previous chapter, the idea of distributor adaptation was raised, to improve as much as possible the radial and axial fluid distribution, in an attempt to maintain the concentration profile not only in the ascension but also in the descent of movable piston, implementing the "first in, first out method". The improvement of the flow distributor was done by 3D printing.

Very few approaches present in the literature explore 3D printing applied to chromatographic columns. The author S.H. Nawada et al. [76, 185, 186] has developed a

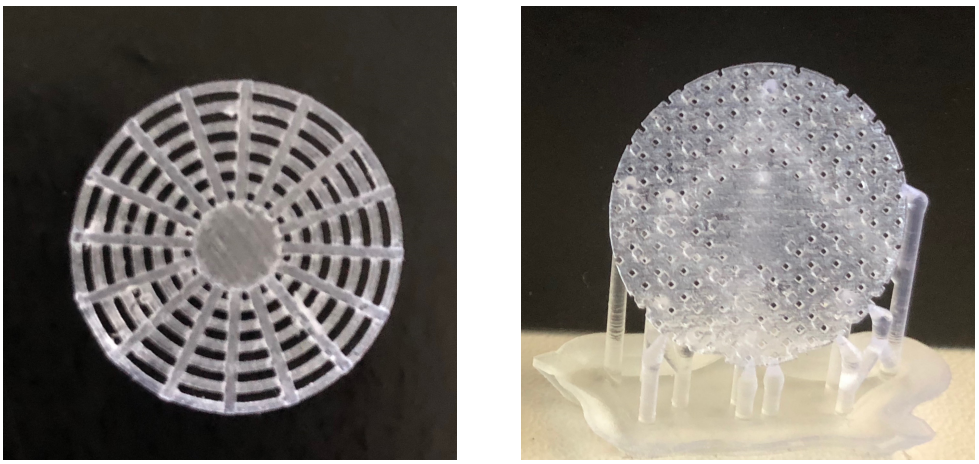

(a) Web 3D frit. (b) Grid 3D frit.

Figure 5.9: Base design for 3D frits. These were the original (first) conformations. Throughout the work, design complexity was introduced, changing several parameters. (a) Web design; (b) Grid design.

study for complete chromatographic column design through 3D print, forming a single monolithic entity, taking in consideration a porous bed, ancillary features such as column walls, flow distributors and external fittings, establishing different combinations of specifications and geometries.

Thus, according to the literature and the previous studies cited, the interest here is focused in gathering the 3D printer applicability in easily developing single pieces of recycling device, specifically to produce and test different flow distributor arrangements in an attempt to optimize flow dispersion performance as much as possible in our developed work, starting from a radial standard distributor geometry as considered by S.H. Nawada [186] and a grid 3D frit, with similar structure of 3D printed monoliths (for catalyst fabrication) found in the literature [201].

The SLA printer was chosen as the first 3D printing option because of its high resolution (XY/Z) [97], compared to other 3D technologies. The Form 2 delivers high-resolution parts with footprint of industrial 3D printers, producing parts with precision and reliability [82]. After post-curing, that helps 3D printed parts to achieve optimal material properties, the resulting 3D parts consisted of strong and detailed models, with impressive surface finish.

The first forms of 3D printed distributors produced were described in the literature, with web (radial) and network (or grid) format. Figure 5.9 shows the basic constructed layouts. However, countless parts conformations have been produced. First, simple parts were produced, only in the XY plane. Secondly, the pieces complexity was increased by introducing new frit layers with the channels ("pores") shifted from one layer to another in the Z plane (height), in other words, one is never exactly overlapping the top layer and/or lower, as shown in Figure 5.10.

The number of layouts was exorbitant (>30) (Appendix C.1). In addition, for each

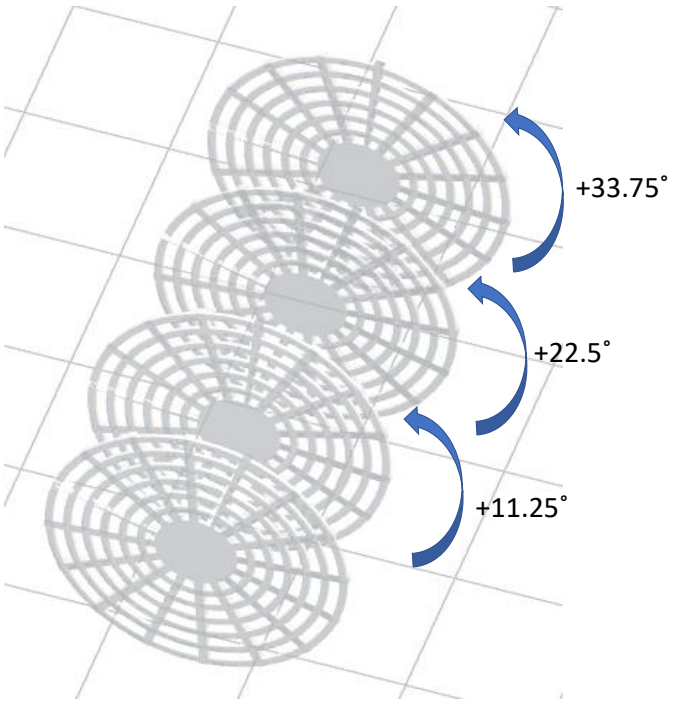

Figure 5.10: Example of frit with multiple layers. The layers are always offset from each other, i.e. there is no overlap of equal layers.

layout, the pore diameters were varied (for grid format, for example), or the spacing between radial lines (at channels radial model), the number of layers (in the most complex frits), the type of layer interleaving (varying between webs and grids for the same part), the spacing between the layers, the lock diameter in the center of the radius, and still other changes.

Due to the massive number of prototype fabrications, the first analysis of each distributor shape produced was performed by placing this part on the piston and performing tracer injection tests, which has a strong yellow colouration. The visual analysis allowed to rule out those inconsistent conformations, while the most acceptable prototypes, with a better radial and axial fluid distribution were submitted to the following analyzes.

Among the 3D printed parts produced in this phase, the frit with the best configuration was a distributor consisting of 4 layers in a radial format. (Figure 5.11 demonstrates some 3D printed parts in phase 1, as well as the best performing distributor). The layers have been arranged so that the web of a layer is uneven with respect to the web of the lower layer.

Since the piston has neither perfectly stirred tank behaviour nor dispersed plug-flow, several experiments have been carried out to study the hydrodynamic behaviour of the fluid inside the piston. This is a video that shows an experiment of injecting eluent up to 20 millimetres and then 20 millimetres of solution with tracer, causing the piston to go down. Then the piston is placed to rise completely. What we see is the fluid travels a preferred path to the movable plunger as it descends, while on the rise, the concentration

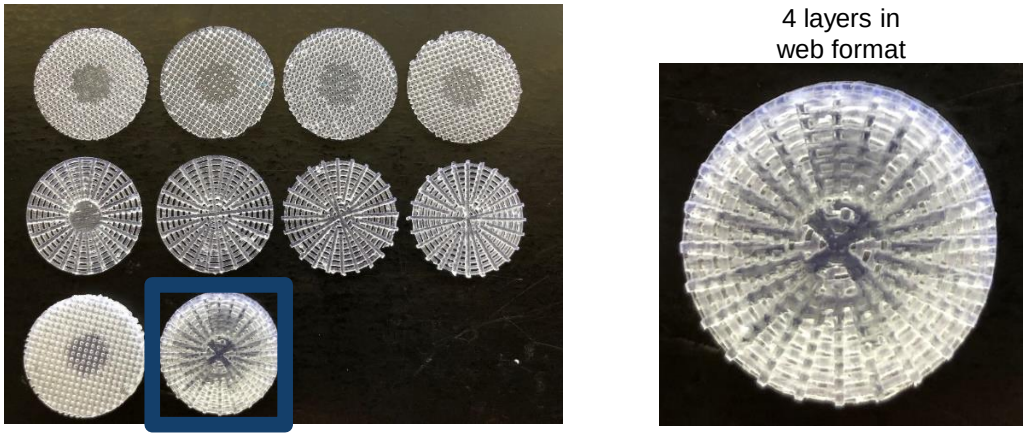

Figure 5.11: The best 3D Frit design obtained in Production Phase 1. This result was obtained by analyzing piston tracer injections with the various 3D distributors produced, one at a time.

profile is maintained in the outlet of the device. This happened because the frit was not homogeneous.

Figure 5.12 shows the result of tracer experiment, which presents a visual comparison for fluid distribution within the piston between the presence of polyethylene frit and 3D printed frit (the best design) at the top of recycling device. It is observed for the piston with polyethylene frit that the fluid travels a preferred path to the movable plunger as it descends, while on the rise, the concentration profile is maintained in the outlet of the device. Meanwhile, performing the experiment with web format 3D printed frit, it is noted that, although the tracer solution did not maintain the axial concentration profile, fluid was distributed over the radial axis much more evenly than the original piston configuration, as the fluorescent solution was injected and forced the piston down. Therefore, a considerable improvement in piston performance has been achieved.

The 3D printed part conformation success in relation to the original frit can be explained by the radial centre blocking, where the tracer solution followed a preferred path, and also by the difference in pore sizes in the 3D part itself. The pores enlarge as they move away from the radial centre, giving a kind of blockage to the fluid, forcing it to disperse more and more towards the ends of the piston as it travels between the innermost layer of the frit to the outermost layer.

5.4.2.2 Phase 2: Nucleosides Experiment with 3D printed frit

The nucleosides separation experiment was reproduced under the same conditions as in the previous chapter, by modifying only the frit to the 4-layer 3D printed frit. The result for the concentration profile can be seen in Figure 5.13.The top graphic shows the results for uridine, while the bottom one for guanosine. The blue line represents the result for the dynamic process model simulated in gPROMS (presented at previous chapter)

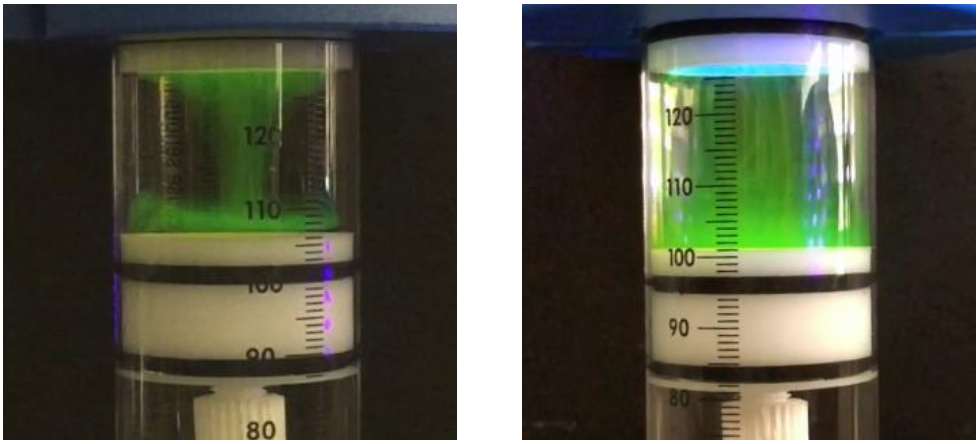

(a) Polyethylene Frit. (b) Radial 3D Frit, with four layers.

Figure 5.12: Comparison between the efficiency of (a) polyethylene frit and (b) the radial distributor, the best designed 3D printed frit. The polyethylene frit is the original configuration used in the recycle piston. The analysis was performed visually due to the number of pieces printed. Therefore, the feed solution was an intensely coloured tracer.

considering piston as dispersed plug-flow. The experimental curves are presented by points: red, polyethylene frit piston; black, recycling device with 3D dispenser.

These graphs prove that the black curve, which uses frit 3D, approached more of a plug-flow behaviour than the red curve, which uses polyethylene frit, for both compounds. For both guanosine and uridine, the improvement could be seen mainly from the rise in the concentration profile. Despite a slight approximation of the experimental curve to the simulated model, it can be seen that the goal of this chapter has not yet been completely achieved, so a new approach has been taken.

5.4.2.3 Phase 3: New Distributor Conformations and Pulse & Gradient Injection Test

The 3D radial distributor chosen in the previous phase of the work, it was coupled to the top of the piston throughout phase 3 of the experiments. In this last phase, the flow distributors were no longer composed only of 3D printed frits, but also by a 3D printed holder with different heights. Then the frits were interspersed with the equally spaced brackets. The number of supports is always (N + 1) the number of frits, where N is the number of frits. Figure 5.14 shows the 3D print configurations produced in this step. The 3D printed distributors used have a network format with a pore diameter of 0.1 cm.

Experimentally testing the residence time distribution profiles, the following experiments were performed, with piston heights (z) ranging from:

1. z = 25 mm: without holders, and with four small holders;
2. z = 34 mm: without holders, with six small holders, and with three medium holders;
3. z = 45 mm: without holders, with four medium holders, and with two big holders;

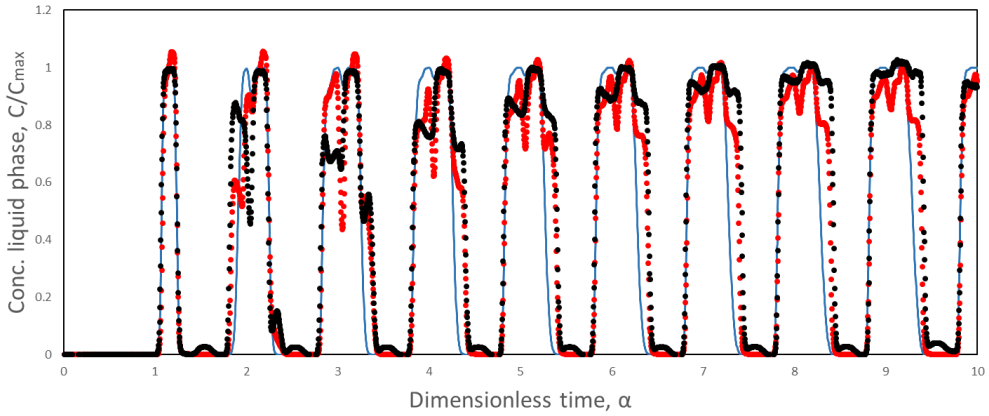

(a) Uridine.

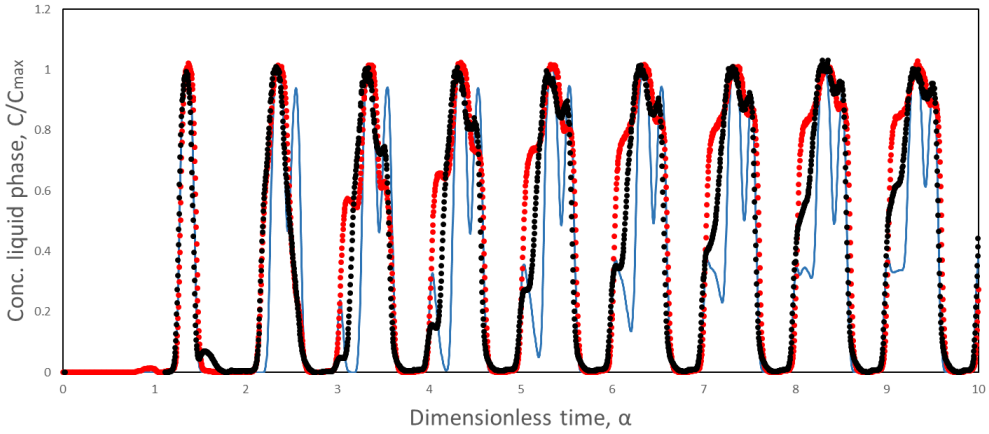

(b) Guanosine.

Figure 5.13: Solute concentration profiles at the outlet of column for nucleosides separation at one-column analog to SMB, using 3D printed frit. The top graphic shows the results for uridine, while the bottom one for guanosine. Red points denote the experiment with polyethylene frit, whereas black points represent the experiment with 3D printed frit. The blue line represents the simulation of the dynamic process model considering piston as dispersed plug-flow. Replacing the frit with a 3D part resulted in a slight approximation of the experimental profile to the simulated curve.

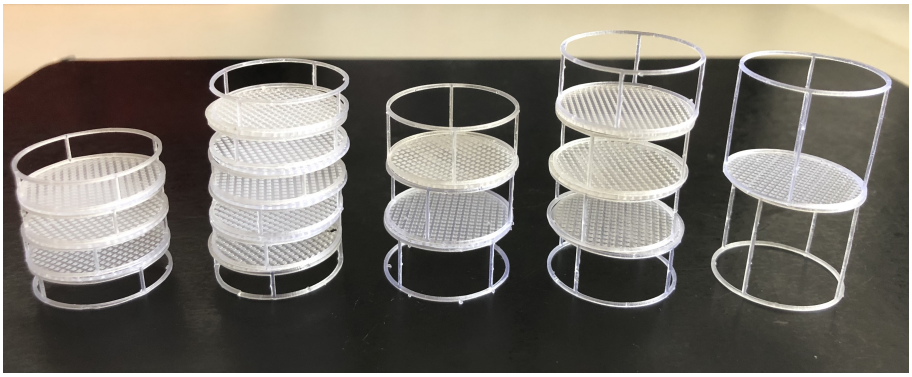

Figure 5.14: Different types of piston supports, that is, different heights and amounts of grids. From left to right: z (height) ≅ 25 mm, z ≅ 34 mm, z ≅ 34 mm, z ≅ 45 mm, z ≅ 45 mm.

The results of pulse and gradient injections are shown in Figure 5.15. UVA B is the UV reader at the piston inlet, while UVA A is the UV cell at the outlet of the recycle device. The results showed that related to the holder presence or absence, the presence of holders with frits along the reflux piston caused a significant difference in the results. On the unsupported piston, the feed solution is collected earlier, while solutes take longer to exit the piston when holders have been inserted into the device. This indicates that there was a larger radial scatter in the experiment with the holder, once the same feed volume was injected. Moreover, in the gradient part of the curve, the concentration profile of the product is much more stable (uniform), this was noted mainly for the two highest piston heights. It was further noted that at high piston heights, when the piston is without holder, product residues remained on the piston and came out with difficulty over time, when in fact the piston should already be completely filled with eluent only, however, in piston with holder the elution of uridine solution was successfully achieved.

Another interesting analysis was produced by comparing only the curves results that considered holders, it was found that the greater the number of holders inside the reflux piston at a fixed height, the better the UV signal stability, which shows a better approximation of the concentration profile of an empty column with axial dispersion.

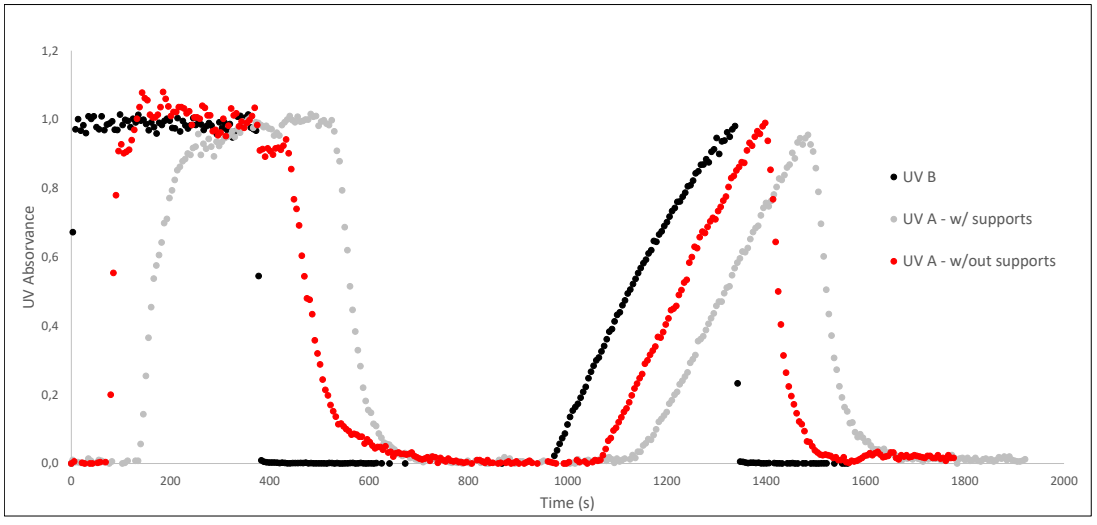

a Pulse Injection + Gradient, z = 25 mm.

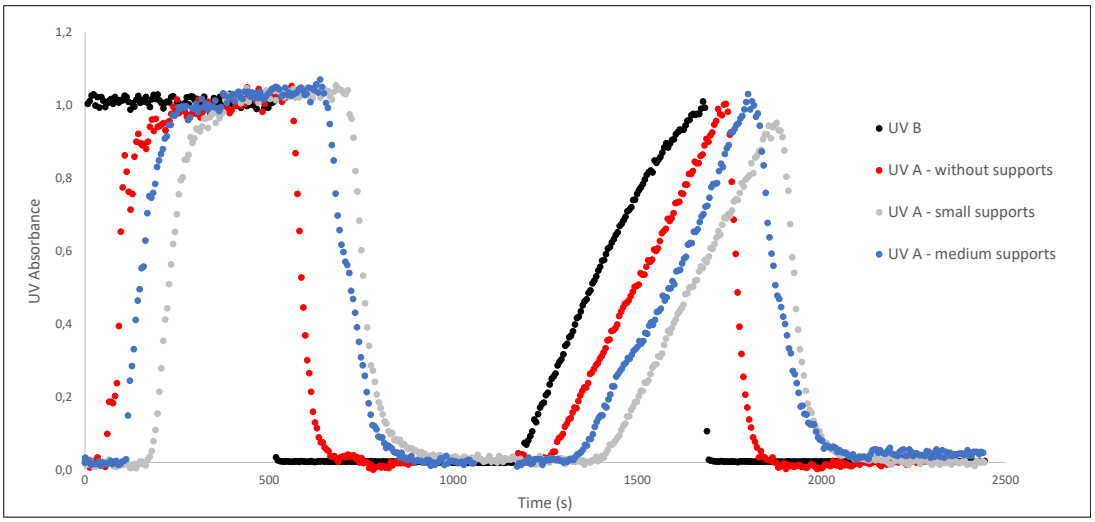

b Pulse Injection + Gradient, z = 34 mm.

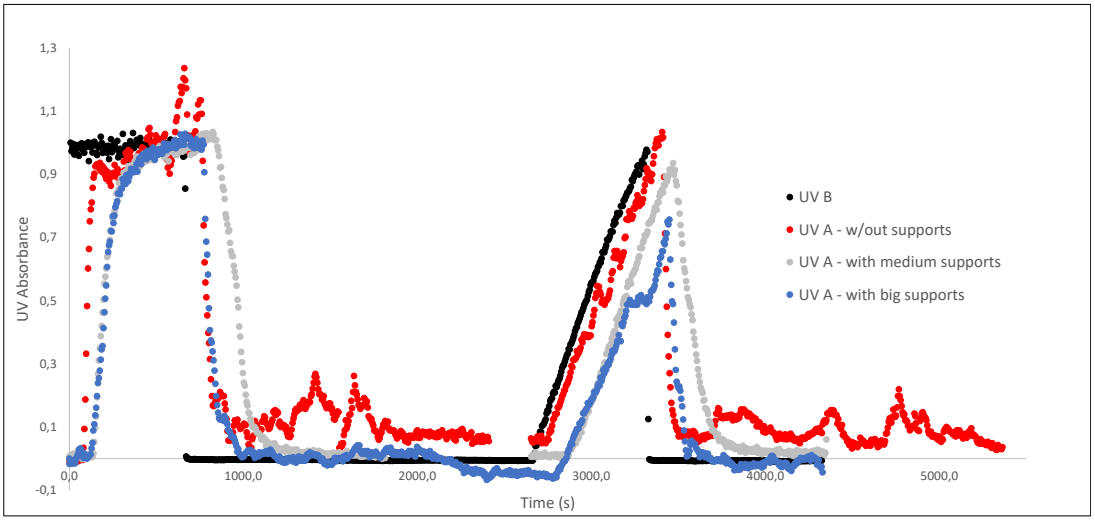

c Pulse Injection + Gradient, z = 45 mm.

Figure 5.15: Pulse & Gradient injection at piston with different heights (25, 34 and 45 mm), and distinct 3D dispensers configurations. In this phase, the 3D dispersers are composed by 3D printed frits + 3D printed holders. For each chart, the gradient starts at the same time for the different curves. UVC B: UV cell at piston inlet; UVC A: UV cell at piston outlet. As a result, the shorter distance between the Frits, and therefore a higher amount of frits, improves the dispersion of the fluid inside reflux device. The difference between the tested configurations is more significant as the piston volume increases.

5.4.3 FDM Method: Modeling and Production of 3D Spirals

From the previous experiment, it was seen that introducing grids along the piston improved the fluid distribution within the piston. However, holders produced in SLA were not flexible. Because of that, it was started the work with FDM 3D printing technology,

in which spirals were produced.

Although the SLA printer has the ability to print material with smooth surface finish and fine feature details, the material is brittle, not suitable for mechanical parts [9].

Therefore, the FDM printer was mainly chosen to work with a flexible material, in this case, the PEEK. Along with this quality, the printer cost compared to other technologies is attractive [97], as there are already a variety of Chinese brands investing efforts in this technology where it is possible to buy printers around 100.00 dollars and may reach values of 500,000.00 dollars for other technologies.

The new CreatBot F160 printer has been used to produce spiral holders made of durable, and especially more flexible material than the aforementioned technology, in a way to interleave frits along the length of section A of the piston. This clever spiral configuration allows the piston to be completely closed by fully compressing the spirals. For this, PEEK material appeared to be a good choice, since it supports high temperatures to infer part deformation (as seen in the TGA test), while being quite flexible for continuous movements in the part, serving as a kind of spring, but differing from the latter by the advantage that when closed it occupies only the XY plane. This last quality, the flexibility, is indispensable for the success of the 3D spiral, as the recycling device is constantly varying its internal volume.

Therefore, the idea here is not to use the FDM method purely to improve piston fluid distribution, but to combine the two 3D printing technologies to achieve the optimum configuration. Thus, the 3D printed frits remained the same as the latest SLA design, but now Clear resin rigid holders are replaced by highly flexible PEEK holders.

A disadvantage of FDM 3D printing is that the material must contain holders, that is, it is impossible to deposit material without a holder to keep it in the desired position. Therefore, the spirals produced with the CreatBot printer necessarily had to be produced in a horizontal plane.

The production for the metric specifications optimization of the 3D spiral are presented in Figure 5.16. Optimal sizes for the new 3D holders conformation were: internal diameter (D_i) = 10 mm, external diameter (D_e) = 30 mm, spiral filament thickness (e) = 0.6 mm, crown thickness (E_w) = 0.5 mm, spiral height (E_c) = 1.2 mm.

Therefore, 3D printing production did not result in the final piece. Only after 3D printing did the material undergo structural deformation to spiral out. For this, the deformation conditions had to be tested, since slight changes could change not only the Z-axis conformation but also the filament conformation by itself.

It is worth highlight that the temperatures tested should be above the glass transition temperature (T_g), i.e. reversible transition range where the polymer substrate changes from a hard, rigid state and a soft, "rubbery"(not melted) state [31]. The temperatures analyzed should also be below the PEEK decomposition temperature (obtained by the TGA test). For PEEK polymer, T_g = 143 ºC [117], so the temperatures that made up the test were slightly above 143 ºC.

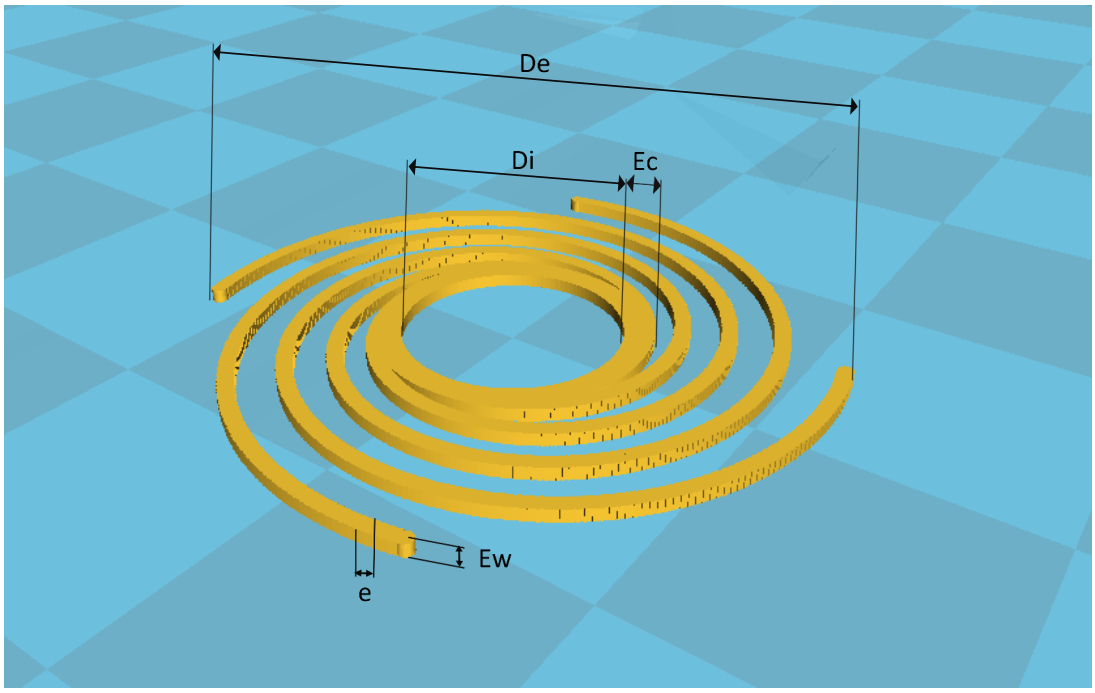

(a) Optimized parameters for 3D spiral.

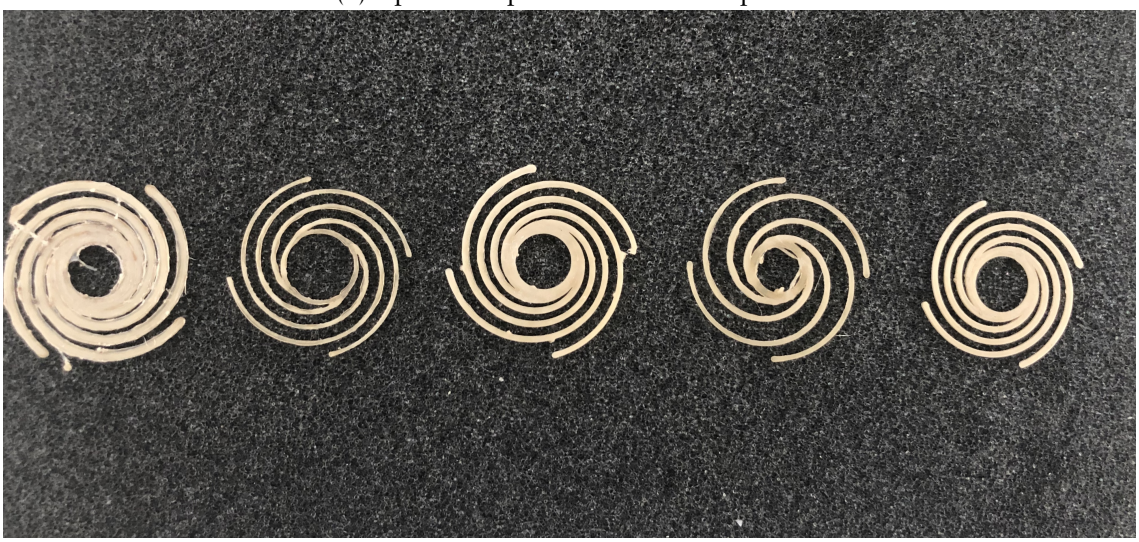

(b) 3D printed spirals for metric specifications optimization..

Figure 5.16: 3D production for metric specifications optimization of the 3D spiral. The final version of the 3D part, already optimized, is displayed at the right end of the image. Optimized parameters: D_i = 10 mm, external diameter D_e = 30 mm, spiral filament thickness e = 0.6 mm, crown thickness E_w = 0.5 mm, spiral height E_c = 1.2 mm.

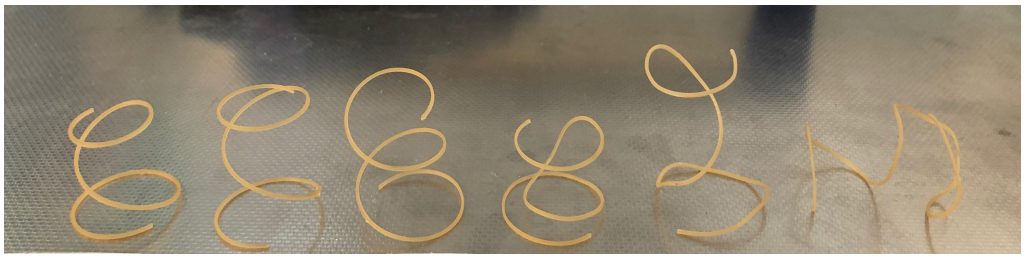

Figure 5.17: Printed PEEK deformation tests, from XY plane for the 3D spiral. Optimum furnace operating conditions were tested with the following parameters evaluated: heating ramp time (gradual heating, Δt_1), time interval with stabilized temperature (Δt_2) and isothermal temperature (T_{iso}). In the picture above, $\Delta t_1 = 15$ min for all pieces. The resulting optimal parameters are: $\Delta t_1 = 15$ min, $\Delta t_2 = 15$ min, $T_{iso} = 155$ ºC.

As a result of the optimal deformation conditions obtained for the spiral base piece using the furnace equipment, temperatures of 155º and 160ºC have shown to be most suitable for shaping the spirals. Therefore, the lowest temperature, 155ºC, was established as the ideal deformation temperature. It is worth remembering that when subjected to temperature 155ºC, the mass loss can be neglected for materials produced from Clear resin and PEEK filament, as could be analyzed from the TGA test discussed in the previous section.

In addition, a 15 min heating ramp and a further 15 min submitted to 155ºC isothermal environment were the ideal times obtained. Thus, the spiral is perfectly shaped, and the PEEK part comes into existence on the Z axis, not just on the XY plane. The consequence of the spiral shape from the change of these parameters (ramp time, isothermal time, and heating temperature) can be seen in Figure 5.17. Furthermore, it has been found that the final 3D printed spiral is flexible enough to be compressed and extended several times, always returning to the height Z defined in the furnace step, which defines a long service life for the part. This further ensures that when inserted into the piston, the spring effect extends over countless repetitions of separation/purification experiments.

After calibration of the FDM printer and determination of the furnace parameters for spiral shaping, the standardization of fabricated spiral parts could be performed. For this, a smart prototype was created to serve as the structure for the spiral in the deformation process, which will be referred to as the Distortion Standard Equipments (DSE). The prototype was also produced through 3D printing, but using SLA technology, since the material must be hard and withstand high temperatures. Figure 5.18 shows the constituent equipments of the DSE. It consists of a screw fitting that engages to the flat spiral (XY axis) and is inserted into the glass container to proceed the first deformation phase, a structural base (b), where the previously extended spiral is inserted to begin the second deformation phase, responsible for height and diameter adjustment, and a

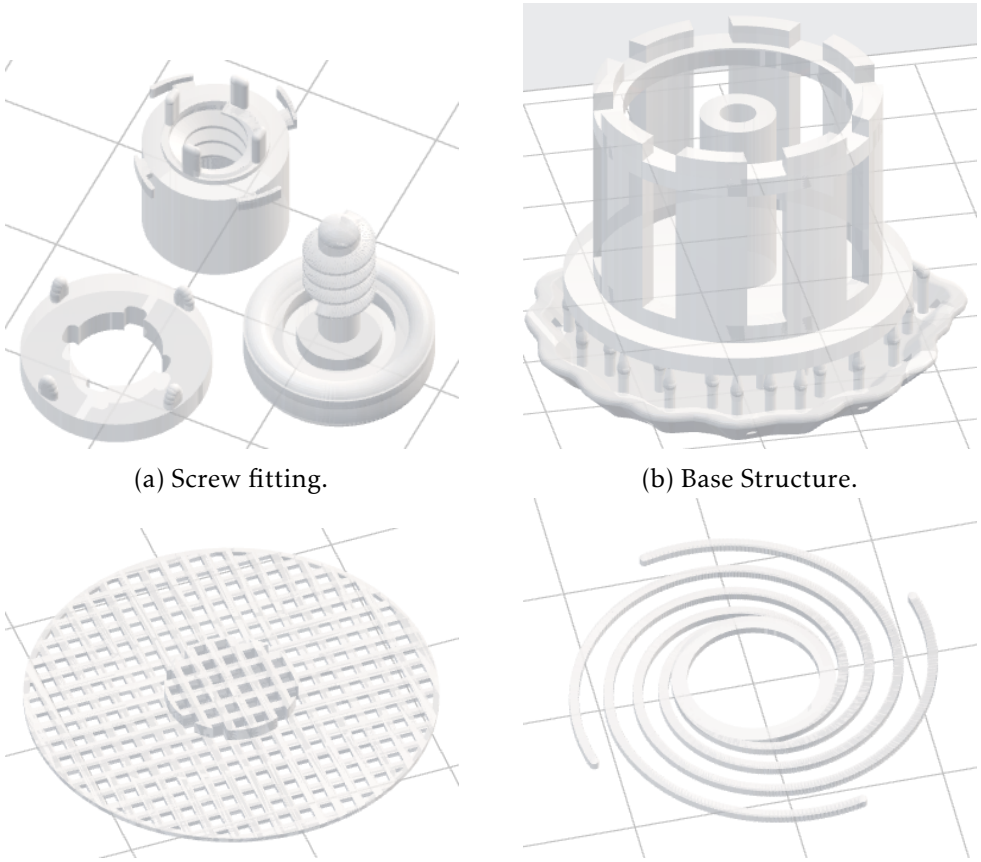

(a) Screw fitting.

(b) Base Structure.

(c) Net for spiral.

(d) Spiral.

Figure 5.18: Distortion Standard Equipments (DSE) and spiral final version. The DSE, built with SLA technology, consists of a screw fitting (a) to extend the flat spiral (XY axis) in a first distortion phase, a structural base (b), where the spiral is inserted to adjust its height (Z plane) and external diameter (OD), and a net-adapted to the spiral (c) that serves as cover for the structural base and as frit for piston.

net with support to the centre of the spiral (c), which, while serving as a cover for the structural base, is also the frit that will be inserted into the piston. The height of each spiral has been set to 2.5 cm, so this is also the internal height of the fabricated SDR, while the inside diameter (ID) of the equipment is 2.5 cm to perfectly fit the recycle device.

The steps for spiral deformation is shown in Figure 5.19. The first step for modifying the single-layer spiral is to fasten the flat spiral to the screw fitting, insert it at a height of 5.0 cm and ID = 1.5 cm, and proceed to the primary modification of the part using the furnace under conditions already mentioned. After cooling the new structure, the second phase consists in the spiral distortion, where it is placed inside the structural base made of Clear resin, which acts as a kind of "dome", its radial centre is attached to the network that will serve as a cover to the dome. The material then goes back to the oven under the same operating parameters. The part is cooled to remove from the frame and the finished frame is ready.

The production and use of the SDR resulted in consistent, satisfyingly flexible and

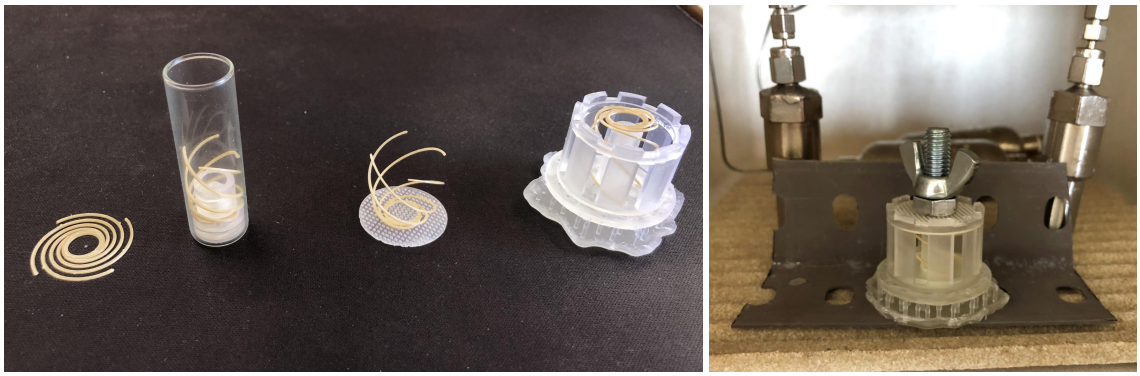

Figure 5.19: Deformation steps for the 3D printed spiral. The single layer spiral is attached to the screw fitting, inserted into a small vial and placed in the oven to undergo the first part modification step. Once cooled, the spiral already in three dimensions is connected to the frit and inserted into the 3D "dome", where it will go back to the furnace. Once cooled, the frit-spiral structure is ready.

easily reproducible spirals. Advantageously, the part has a very short production time and is easily reproducible due to the manufacturing technology used. Thus, a clever fluid distribution system composed of 3D printed frits (by SLA) together with spiral holder (by FDM) was successfully manufactured.

5.5 Conclusions

The need to improve the axial and radial distribution of the fluid therein was analyzed. Since the original piston had neither perfectly stirred tank nor dispersed plug-flow behaviour, several experiments had been carried out to study the hydrodynamic behaviour of the fluid inside the piston. 3D printing technology was used to solve this task. 3D printing has shown potential results in a variety of disciplines [97]. Therefore, this 3D technology was used to solve this task.

Two 3D printing methods were used to print new piston frits: first, SLA print technology was used; the second printing method was based on FDM print technology.

It's to note that, replacing the frit of the upper side of the recycle device with customizable frits that can change the inlet profile, improves the hydrodynamic behaviour inside the recycle device.

The samples characterization produced with the two 3D printing technologies was performed. Thermal and chemical stability of the two raw material (Clear resin and PEEK) were evaluated. TGA analysis has shown that the polymer resulting from Clear resin has much higher thermal stability than the manufacturer had indicated, so the heat distortion temperature (318ºC) is far above the temperature used in the last task of this chapter (SLA mold for spiral production), 155ºC. For the PEEK filament, the TGA showed that this material did not suffer degradation up to 500ºC. Therefore, the furnace operating temperature is stable for both 3D materials. In addition, both polymer

types are obviously stable at the operating temperature of the recycle piston (ambient temperature).

Additionally, the two substrates used for the production of fluid dispersers have been shown to be compatible with the solvent used for nucleoside separation, as well as very acidic and basic solvents, a feature necessary for use in the purification process of other biomolecules, such as in the process of capturing monoclonal antibodies in Protein A, for example.

In the first phase of 3D distributors production, SLA technology was used and the frits were produced in the most diverse configurations and doing the respective tracer tests. From there, it was selected the frit that provided the best distribution of the fluid so far and the experiment of nucleosides separation was repeated. The frit with the best configuration was a frit consisting of 4 layers, each one offset from the next, in web format. Through this 3D part, the fluid distributed substantially more evenly in the radial plane of the piston. In addition, using this 3D distributor for reproduction of nucleoside separation in the Single-column with Recycle Lag, a slight approximation of the experimental concentration profile to the simulated one, which considers the dispersed plug-flow model piston. In a new phase (phase 3) of 3D part productions, where both radial 3D print frit and a new 3D print conformation (holders + grid frits) along the piston length were used, it was concluded that the greater amount of frits inside the piston, with a smaller spacing between them, it results in a better distribution of the fluid inside the piston.

The CreatBot printer, which uses FDM printing technology, is now being used to follow the production of structural holders, but using a substantially more flexible material, PEEK. The optimal printing parameters of PEEK material with the FDM 3D printer were determined. Also, both the spiral parameters (dimensions) and the furnace parameters for 3D part deformation were also analyzed. As a spiral distortion promoter, an ingenious set of parts was produced in 3D, called DSE, which allowed the spirals to be sized to exact needs (Z-extension, OD OD), as well as to standardize the parts produced.

This chapter is an ongoing work in which new 3D configurations are constantly being produced and tested. In any case, the potential of 3D printing to complement piston equipment is remarkable.

If improved piston parts, i.e. frits/distributors, are successfully developed to a greater extend, the One-column Analog may win the same market share. This also enables Single-column Analog to Recycle Lag to become the next generation of continuous chromatography, allowing not only to reduce the solvent consumption and increasing the simplicity of the process, while, at the same time, maintaining extremely high levels of purity and recovery of simple/easy biomolecules separation, but also mimics any type of continuous multicolumn process. This can be achieved due to the introduction of cleverly designed 3D distributors into the process.

Chapter 6

2nd Case Study: mAb Capture by Protein A Affinity Chromatography

6.1 Introduction and Objective

In recent years, therapeutic drugs formed by monoclonal antibodies (mAbs) are the most produced class of biopharmaceuticals [187], being applied in prevention and treatment of cancers, autoimmune and infectious diseases, among several other diseases [189]. Due to its high specificity and production capacity in large quantities, this biomolecule has revolutionized the research and medicine areas.

Because of the high market demand, the optimization of production processes has been increasingly required, seeking to reduce the time and cost of production for the industries, but also aiming to facilitate access to these products not only in developed countries, but also in countries with more difficult access to health.

Therefore, continuous manufacturing has gained space over batch processes. The advantages include small equipment size, steady-state operation, low cycle times, high volumetric productivity, streamlined process flow, and reduced capital cost [275].

The traditional method of mAb purification is composed of a stage of capture with Protein A affinity chromatography using pH step elution, where the mAb is initially retained and impurities flow-though the column (bind/elute mode), and two polishing steps constituted by cation exchange chromatography (bind/elute mode) and still a anion exchange chromatography (flowthrough mode) [123, 267].

In cases of biomolecule separation where it is possible to employ an affinity resin, such as protein A for mAb purification, single-column batch processes can achieve high purity [166]. However, this type of resin (protein A) usually exhibits strong mass transfer limitations, facing shallow breakthrough curves, and therefore low resin utilization [104].

To overcome this limitation, a great number of mAb capture methods based on the

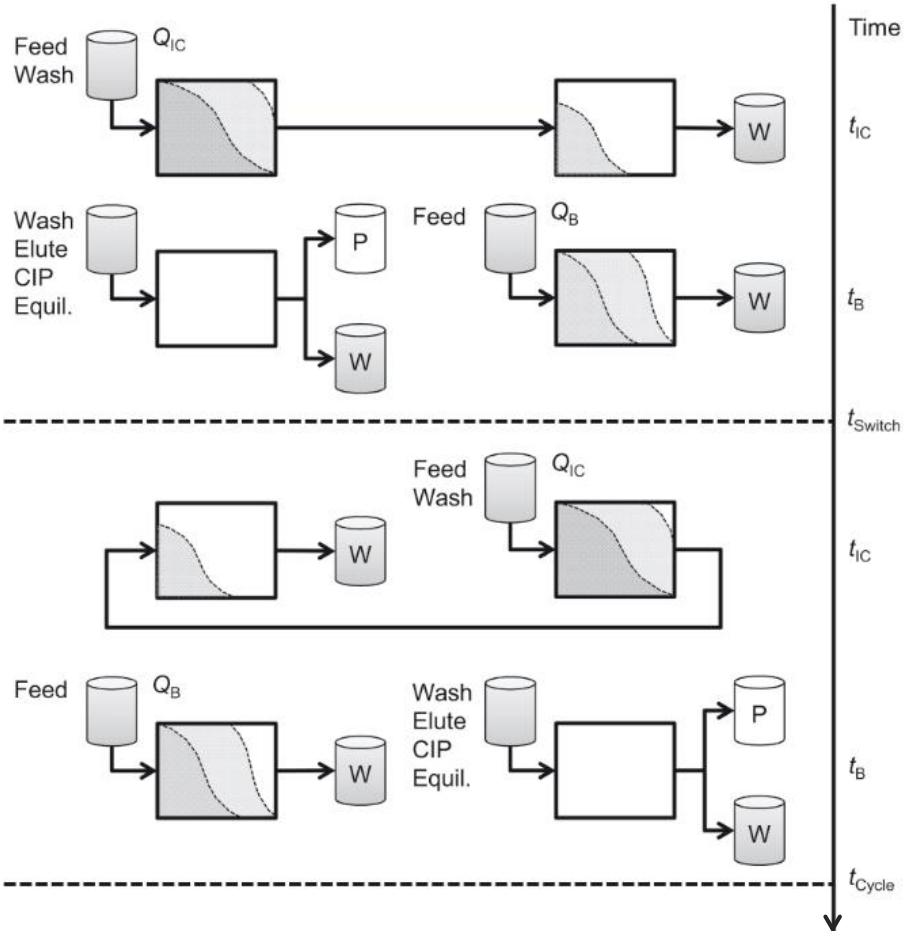

Figure 6.1: Schematic diagram of one cycle of the twin-column CaptureSMB process. Two identical columns are used, working in interconnected (IC) and batch (B) phases. The feed stream is injected semi-continuously while the product is collected periodically. Source: [30].

concept of sequential loading for affinity chromatography were developed. Among them, in 2015, a novel twin-column counter current chromatography process was proposed by Angarita et al. [14]. The twin-column CaptureSMB is used for the Protein A affinity capture of mAbs.

Figure 6.1 shows the schematic diagram of one cycle of the twin-column CaptureSMB process. Two identical columns are used, working in interconnected (IC) and batch (B) phases. The feed stream is injected semi-continuously while the product is collected periodically.

When the columns are connected in series, a longer feed is allowed comparatively to a batch process, because the eventual breakthrough is caught by the downstream column instead of being lost. Therefore, the key feature of this process is that it works by overloading a first column far beyond its $DBC_{1\%}$ when a second column is interconnected, improving the utilization of the stationary phase and allowing the first column to be loaded much closer to its static binding capacity. The $DBC_{1\%}$ is the typically used

dynamic binding capacity (DBC) value (at a specific residence time), which indicates the feed volume that can be loaded onto the column so that the percentage of 1% feed concentration is reached at the column outlet [14].

Describing the process depicted in Figure 6.1, during the interconnecting phase, the first part of the switch interval, the upstream column is being loaded with feed, with flow rate Q_{IC} during the time t_{IC}. Before the columns are disconnected, the washing step begins for the fully loaded column, in order to catch any product that could elute during this initial wash step. In this phase, the impurities traverse the columns and are discarded in the waste (W) [30].

In the batch phase (proceeded during t_B), the fully loaded column is further washed, while more impurities are discarded. Then, the elution of pure product (P) is proceeded, where it is collected. After, CIP and equilibration are done to prepare the column for the next switch. In the meantime, in the other column is loaded more feed, at flow rate Q_B. Thus, the first switch terminates before any product starts exiting the second column.

Then the columns swap function and a new switch interval begins, $t_{Switch} = t_{IC} + t_B$, exactly equal to the previous one. When this second switch interval terminates, a cycle has been completed, $t_{Cycle} = 2(t_{IC} + t_B)$. Cycles can be reproduced as many time as needed.

Because of the already proved enhanced performance of the Twin-column CaptureSMB, when compared with batch chromatography [30]—in terms of productivity and capacity utilization—this method was suited chosen to be mimicked by the Single-column with Recycle Device in order to compare process results.

6.1.1 Objective

The main objective of the present Chapter is the application of the Single-column Analog to SMB in a second case study, the purification of monoclonal antibodies in protein A resin, by mimicking the optimized Twin-column CaptureSMB process. The purpose is to perform the comparison of the performance and efficiency of the new One-column system with other chromatographic processes, different from that already covered in Chapter 4.

6.2 Chromatographic Column Model for mAb capture by protein-A affinity chromatography

The model developed in this section is adapted from [30]. The modeled process is the capture step by protein-A affinity chromatography of a protein or monoclonal antibody (mAb) from a cell culture supernatant containing a group of impurities. It is assumed that the impurities are not retained by the protein-A resin and for modeling purposes they are lumped into a single pseudo-component.

The following notation is employed here: $c(z,t)$ and $c'(z,t)$ are the concentrations of the mAb product and of the impurities in the liquid phase flowing through the column

at axial position z and time t (i.e., the instantaneous axial concentration profiles in the column), and $\mathrm{pH}(z,t)$ is the instantaneous axial pH profile.

By modeling the dynamic breakthrough behavior of the impurities in a chromatographic column packed with protein-A resin, the differential material balance can be written as

$$\frac{\partial c'}{\partial \theta} + \frac{\tau Q}{\epsilon_\mathrm{t} V_\mathrm{c}} \left(\frac{\partial c'}{\partial x} - \frac{1}{\mathrm{Pe}} \frac{\partial^2 c'}{\partial x^2} \right) = 0 \quad (0 < x < 1), \tag{6.1}$$

where $c'(x,\theta)$ is the instantaneous axial concentration profile of the impurities in the interparticle liquid along the column, $x = z/L$ the dimensionless axial coordinate along the column of length L and volume V_c, $\theta = t/\tau$ is a reduced time coordinate scaled by a reference time τ, Q the volumetric flow rate, Pe the axial Péclet number, and $\epsilon_\mathrm{t} = \epsilon + (1-\epsilon)\epsilon_\mathrm{p}$ the total porosity of the packed bed (ϵ and ϵ_p are the inter- and the intraparticle porosities). The Péclet number, $\mathrm{Pe} = h/2 = vL/D_\mathrm{L}$ (v is the interstitial fluid velocity, D_L the axial dispersion coefficient, and h the dimensionless plate height), lumps the contributions of molecular diffusion, hydrodynamic dispersion, and film resistance to mass transfer.

Various values of the reference time τ can be selected for different purposes. For example, setting $\tau = 1$ makes $\theta = t$, that is, the θ-coordinate is the same as the true time coordinate t. On the other hand, if $\tau = 1/Q$ then the scaled time θ gives the volume of eluted fluid through the column up to the present time instant t. Finally, given that the time taken to fill an empty chromatographic column is V_c/Q, setting $\tau = V_\mathrm{c}/Q$ gives the time scale θ in terms of the number of eluted column volumes of fluid.

If desired, c' can also be rendered dimensionless, that is, instead of working with c' one works with $w = c'/c'_\mathrm{ref}$, where c'_ref is a reference concentration, for example, equal to the feed concentration, c'_F. Note, however, that this change of variable does not alter the material balance because all terms are linear operators of c':

$$\frac{\partial w}{\partial \theta} + \frac{\tau Q}{\epsilon_\mathrm{t} V_\mathrm{c}} \left(\frac{\partial w}{\partial x} - \frac{1}{\mathrm{Pe}} \frac{\partial^2 w}{\partial x^2} \right) = 0, \quad (0 < x < 1). \tag{6.2}$$

The typical boundary conditions for eq. (6.1) are

$$\begin{cases} c' - \dfrac{1}{\mathrm{Pe}} \dfrac{\partial c'}{\partial x} &= c'_{in} \quad \text{for } x = 0, \\ \dfrac{\partial c'}{\partial x} &= 0 \quad \text{for } x = 1. \end{cases} \tag{6.3}$$

where c'_{in} is the concentration of the impurities in the inlet fluid. The boundary condition at $x = 0$ is valid as long as there is liquid flowing through the column ($Q > 0$); if the flow through the column is temporary halted ($Q = 0$), the correct boundary condition at the column inlet is $(\partial c'/\partial x)_{x=0} = 0$. The above boundary conditions can be converted into their dimensionless analogs by simply replacing c' with w (and c'_{in} by w^in).

The adsorption of the mAb product is assumed to be described by a Langmuir isotherm model with the pH value as modifier [252]. In this case, the concentration of adsorbed

mAb, q^*, in equilibrium with mAb concentration c in the liquid at a given pH can be expressed as

$$q^*(c, \mathrm{pH}) = \frac{Hc}{1 + (Hc/q^\infty)}, \qquad H(\mathrm{pH}) = H_{\mathrm{ref}}\left(\frac{\mathrm{pH}}{\mathrm{pH}_{\mathrm{ref}}}\right)^\nu, \tag{6.4}$$

where H_{ref} is the Henry constant at the reference pH value $\mathrm{pH}_{\mathrm{ref}}$, ν is a coefficient that relates the change of Henry's constant according to the pH value, and q^∞ is the adsorption capacity of the resin for the mAb.

It is convenient to scale the concentrations c and q, as well as the pH. Thus, c is replaced by $y = c/c_{\mathrm{ref}}$, q by $Y = q/q_{\mathrm{ref}}$, and pH by $s = \mathrm{pH}/\mathrm{pH}_{\mathrm{ref}}$. The choice of q_{ref} is straightforward: $q_{\mathrm{ref}} = q^\infty$, because this simplifies the expression of the adsorption isotherm:

$$Y^* = \frac{q^*}{q^\infty} = \frac{b\, s^\nu y}{1 + b\, s^\nu y}, \qquad b = H_{\mathrm{ref}} c_{\mathrm{ref}}/q^\infty. \tag{6.5}$$

It is worth noting that if the choice for c_{ref} is $c_{\mathrm{ref}} = q^\infty/H_{\mathrm{ref}}$ then $b = 1$ and

$$Y^* = \frac{s^\nu y}{1 + s^\nu y} \qquad (c_{\mathrm{ref}} = q^\infty/H_{\mathrm{ref}}). \tag{6.6}$$

The intraparticle diffusion, which is assumed to be strongly dependent upon the mAb loading, severely limits the adsorption kinetics. A linear diving force approximation is adopted to model the adsorption kinetics [99]. The expression reads

$$\frac{\partial q}{\partial t} = k_{\mathrm{m}}(q^* - q), \qquad k_{\mathrm{m}} = k_{\mathrm{m}}^\infty\left[S_1 + (1 - S_1)\left(1 - \frac{q}{q^\infty}\right)^{S_2}\right], \tag{6.7}$$

where k_{m}^∞ is the maximum value of mass transfer coefficient, k_{m}. The empirical correlation used for k_{m} is done to approximate the effect of hindered mass transfer due to pore blockage and other effects [30, 194]. S_1 is a coefficient describing the maximum obstacle to mass transfer, for which $0 < S_1 \leqslant 1$, the coefficient $S_2 > 0$ models the non-linearity of the hindrance increase. S_1, S_2 are constant parameters. Introducing the above changes of variable gives

$$\frac{\partial Y}{\partial \theta} = \tau k_{\mathrm{m}}(Y^* - Y), \quad k_{\mathrm{m}}/k_{\mathrm{m}}^\infty = S_1 + (1 - S_1)(1 - Y)^{S_2}. \tag{6.8}$$

The differential material balance for the mAb can be written as

$$\frac{\partial c}{\partial \theta} + \left(\frac{1 - \epsilon}{\epsilon_{\mathrm{t}}}\right)\frac{\partial q}{\partial \theta} + \frac{\tau Q}{\epsilon_{\mathrm{t}} V_{\mathrm{c}}}\left(\frac{\partial c}{\partial x} - \frac{1}{\mathrm{Pe}}\frac{\partial^2 c}{\partial x^2}\right) = 0 \quad (0 < x < 1). \tag{6.9}$$

If the concentrations are scaled as above, the following expression is obtained:

$$\frac{\partial y}{\partial \theta} + \frac{q^\infty}{c_{\mathrm{ref}}}\left(\frac{1 - \epsilon}{\epsilon_{\mathrm{t}}}\right)\frac{\partial Y}{\partial \theta} + \frac{\tau Q}{\epsilon_{\mathrm{t}} V_{\mathrm{c}}}\left(\frac{\partial y}{\partial x} - \frac{1}{\mathrm{Pe}}\frac{\partial^2 y}{\partial x^2}\right) = 0 \quad (0 < x < 1). \tag{6.10}$$

The appropriate boundary conditions for eq. 6.10 are

$$\begin{cases} y - \dfrac{1}{\mathrm{Pe}}\dfrac{\partial y}{\partial x} &= y^{\mathrm{in}} \quad \text{for } x = 0, \\ \dfrac{\partial y}{\partial x} &= 0 \quad \text{for } x = 1. \end{cases} \tag{6.11}$$

where $y^{\text{in}} = c^{\text{in}}/c_{\text{ref}}$ is the dimensionless concentration of mAb product in the inlet fluid.

It is worth noting that the pH is also transported along the column; it behaves very much like the impurities, that is, the pH is equivalent to a pseudo-solute that does not interact with the resin. The transport equation for the solute is thus identical to that for the impurities.

To summarize, the model is as follows.

- **Impurity** transport along the column:

$$\frac{\partial w}{\partial \theta} = \frac{\tau Q}{\epsilon_{\text{t}} V_{\text{c}}}\left(\frac{1}{\text{Pe}}\frac{\partial^2 w}{\partial x^2} - \frac{\partial w}{\partial x}\right) \quad (0 < x < 1), \tag{6.12}$$

$$\left(w - \frac{1}{\text{Pe}}\frac{\partial w}{\partial x}\right)_{x=0} = w^{\text{in}} \quad \left(\frac{\partial w}{\partial x}\right)_{x=1} = 1. \tag{6.13}$$

- **pH** transport along the column:

$$\frac{\partial s}{\partial \theta} = \frac{\tau Q}{\epsilon_{\text{t}} V_{\text{c}}}\left(\frac{1}{\text{Pe}}\frac{\partial^2 s}{\partial x^2} - \frac{\partial s}{\partial x}\right) \quad (0 < x < 1), \tag{6.14}$$

$$\left(s - \frac{1}{\text{Pe}}\frac{\partial s}{\partial x}\right)_{x=0} = s^{\text{in}}, \quad \left(\frac{\partial s}{\partial x}\right)_{x=1} = 1. \tag{6.15}$$

- **mAb**-product transport along the column:

$$\frac{\partial y}{\partial \theta} + \frac{q^{\infty}}{c_{\text{ref}}}\left(\frac{1-\epsilon}{\epsilon_{\text{t}}}\right)\frac{\partial Y}{\partial \theta} = \frac{\tau Q}{\epsilon_{\text{t}} V_{\text{c}}}\left(\frac{1}{\text{Pe}}\frac{\partial^2 y}{\partial x^2} - \frac{\partial y}{\partial x}\right) \quad (0 < x < 1), \tag{6.16}$$

$$\left(y - \frac{1}{\text{Pe}}\frac{\partial y}{\partial x}\right)_{x=0} = y^{\text{in}}, \quad \left(\frac{\partial y}{\partial x}\right)_{x=1} = 1. \tag{6.17}$$

- **Adsorption kinetics** of the mAb on the protein-A resin:

$$\frac{\partial Y}{\partial \theta} = \tau k_{\text{m}}(Y^* - Y), \quad (0 \le x \le 1), \tag{6.18}$$

- **Adsorption equilibrium** of the mAb on the protein-A resin:

$$Y^* = \frac{b s^{\nu} y}{1 + b s^{\nu} y}, \qquad \frac{k_{\text{m}}}{k_{\text{m}}^{\infty}} = S_1 + (1 - S_1)(1 - Y)^{S_2}. \quad (0 \le x \le 1). \tag{6.19}$$

6.3 Twin-column CaptureSMB Process

The process flow chart for the Twin-Column CaptureSMB process is shown more detailed in Fig. 6.2. The process uses two identical columns, which we denote as column 1 and column 2. A subscript is added to the concentration variables to indicate the column they refer to; for example, y_1 denotes the dimensionless mAb concentration profile in column 1. To render the notation more compact the following shorthands for the outlet concentrations are introduced: $w^{\text{out}}(\theta) \equiv w(\theta, x = 1)$, $y^{\text{out}}(\theta) \equiv y(\theta, x = 1)$, etc.

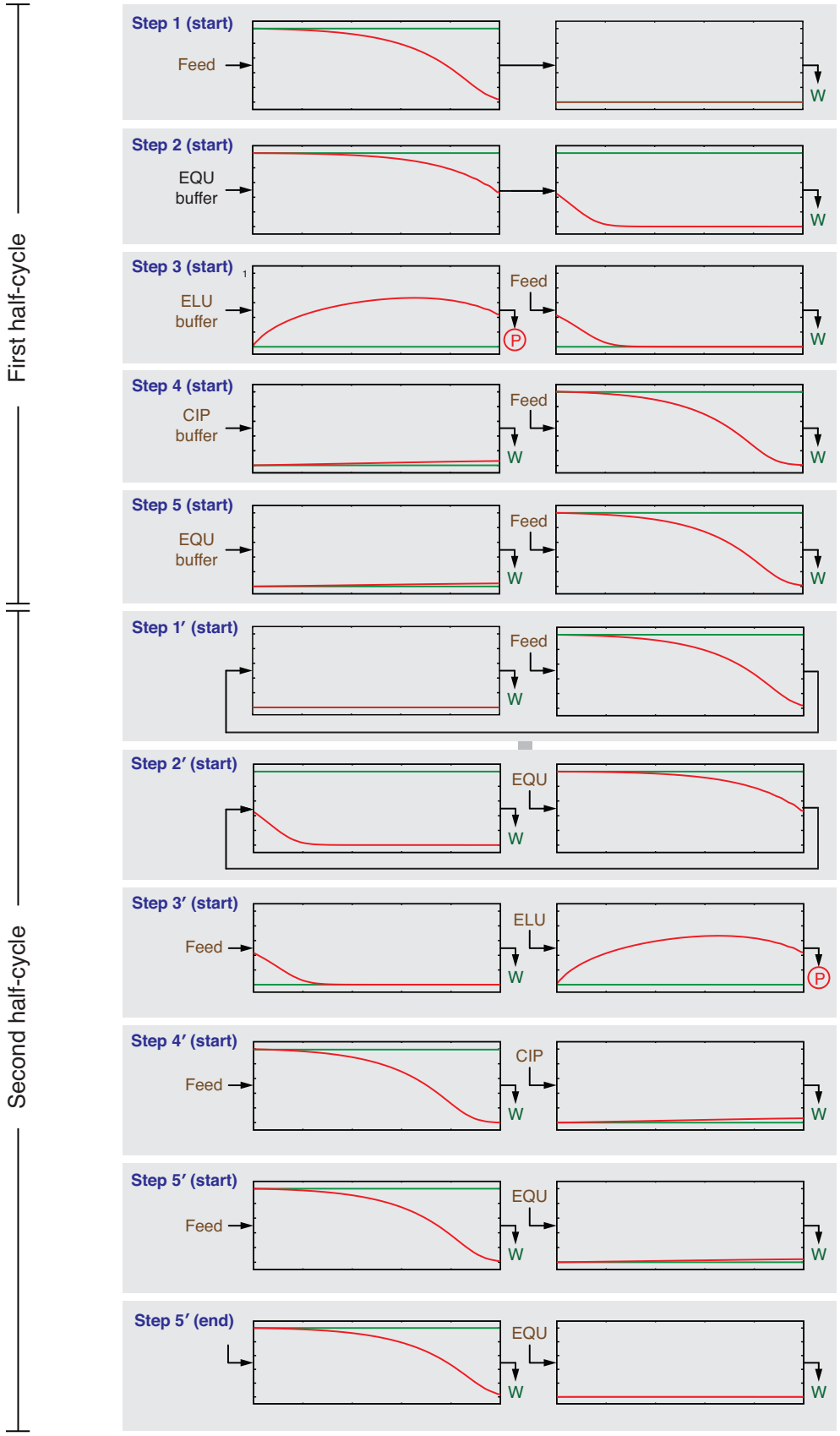

Figure 6.2: Schematic of the Twin-column CaptureSMB process. The axial concentration profiles in the liquid phase: red lines, mAb; green lines, impurity.

Each half-cycle or switching interval is divided into two phases: an interconnected phase (IC), where the columns are interconnected by connecting the outlet of the first column to the inlet of the second column, and a batch phase (B) in which the second column is disconnected from the first. The duration of the former phase is τ_{IC} and that of the latter is τ_B.

Four different buffers were used in the experiments reported in [30].

Buffer A: 20 mM phosphate, 150 mM NaCl, pH 7.5, used for equilibration, washing, and binding;

Buffer B: 20 mM phosphate, 1.5 M NaCl, pH 7.5, used as second washing buffer;

Buffer C: 20 mM citrate, pH 3.2, used as elution buffer;

Buffer CIP: 0.1 M NaOH, pH 13.0, used as cleaning-in-place (CIP) solution.

The important point about each buffer is its pH because it is the only parameter that influences the mAb's adsorption behavior: the lower the pH, the weaker the binding of the mAb to the protein-A resin. Thus, from a modeling perspective, buffers A and B behave identically because they have the same pH; so for all practical purposes we take buffer A = buffer B = $(\text{pH})^{\text{EQU}} = 7.5$, where $(\text{pH})^{\text{EQU}}$ is the pH at which the equilibration, washing, secondary washing, and binding take place. Buffer C = $(\text{pH})^{\text{ELU}} = 3.2$ is the pH at which the elution takes place. Finally, the real pH of the CIP solution is 13.0 ($14 - \text{pOH} = 14 + \log_{10}[\text{OH}^-]$); however, this value is not meaningful for our model as the CIP buffer is just a strong basic solution for cleaning the resin. The pH of the CIP buffer should be set at a value smaller than $(\text{pH})^{\text{ELU}}$ to mimic the cleaning effect of the CIP solution; we arbitrarily set it to $(\text{pH})^{\text{CIP}} = 2.5$.

During step 1 and step 2 the two columns are interconnected (interconnected phase). During step 1 feed is injected into the upstream column to move the mass-transfer zone into the downstream column; this increases the loading of mAb in the upstream column thus increasing the usage of the stationary phase. Note that no mAb is lost because the mAb that breaks through from the upstream column is directed and trapped in the downstream column. During step 1 the eluent of the downstream column is diverted to the waste line.

The purpose of step 2 is to displace the impurities in the upstream column, which are mostly present in the interparticle fluid, to the downstream column before starting the collection of the purified mAb fraction. Thus, during this step the upstream column is washed with a mild buffer able to wash out the impurities but desorb the mAb as little as possible. But even if some mAb is desorbed, it is captured by the downstream column. During this step the effluent of the downstream column is diverted to the waste line.

Steps 3 to 5 are the batch phase wherein the two columns operate disconnected. Feed is continuously injected into the downstream column until near breakthrough of the mAb

Table 6.1: Boundary conditions for the first half-cycle of the CaptureSMB process.

		Column 1				Column 2			
Step	IC/B	Q_1	y_1^{in}	w_1^{in}	s_1^{in}	Q_2	y_2^{in}	w_2^{in}	s_2^{in}
Feed	IC	Q_{IC}	y^F	w^F	s^F	Q_{IC}	y_1^{out}	w_1^{out}	s_1^{out}
Wash	IC	Q_{IC}	0	0	s^W	Q_{IC}	y_1^{out}	w_1^{out}	s_1^{out}
Elution	B	Q_B	0	0	s^E	Q_B	y^F	w^F	s^F
CIP	B	Q_B	0	0	s^{CIP}	Q_B	y^F	w^F	s^F
Equilibration	B	Q_B	0	0	s^{EQ}	Q_B	y^F	w^F	s^F

concentration profile, while the upstream column is first eluted to recover the purified mAb, thoroughly cleaned, and then equilibrated to be ready for the next half cycle.

Table 6.1 lists the boundary conditions that apply to the first half-cycle of the CaptureSMB process.

During the first half-cycle, column 2 is either connected to column 1 or connected to the feed line; in the former case, the outlet effluent of column 1 is directed to the inlet of column 2. Thus,

$$\{s^{in}, w^{in}, y^{in}\}_2 = \{s^{out}, w^{out}, y^{out}\}_1 \qquad \text{for the IC steps,} \tag{6.20}$$

$$\{s^{in}, w^{in}, y^{in}\}_2 = \{s^F, w^F, y^F\} \qquad \text{for the B steps.} \tag{6.21}$$

This can be written as

$$\{s^{in}, w^{in}, y^{in}\}_2 = v_{IC} \times \{s^{out}, w^{out}, y^{out}\}_1 + (1 - v_{IC}) \times \{s^F, w^F, y^F\}, \tag{6.22}$$

$$v_{IC} = \begin{cases} 1 & \text{for the IC steps} \\ 0 & \text{for the B steps} \end{cases}. \tag{6.23}$$

Appendix D.1.1 shows how to implement the above equations in gPROMS software.

At the end of the first half-cycle, the two columns switch roles and go through another half-cycle. At the start of the half-cycle (step 1') the upstream column is fully loaded with mAb (and impurity) from the previous half-cycle; the mAb's axial concentration profile in the liquid phase is about to break through, that is, the leading tail of its concentration profile starts to appear the downstream end of the column. The second column is initially clean and equilibrated with equilibration buffer.

There are two ways to model the columns switch. In one case, the steps above are repeated but with column 1 in the place of column 2 and vice versa. The other alternative, the one which was used, is to exchange the internal state (i.e., the axial concentration profiles in the liquid and adsorbed phase) of the two columns at the end of each half-cycle and redo the steps above.

In the first half cycle the purified mAb fraction is collected during step 3 (elution step). The amount of component i (mAb or impurity), a_i^P collected in the product fraction

during this step is

$$a_i^{\mathrm{P}} = Q_{\mathrm{B}} \int_{\tau_3} c_i^{\mathrm{out}}(t)\, dt. \tag{6.24}$$

The implementation of the above equation in gPROMS software is explained in Appendix D.1.2.

Thus, the mAb purity in the collected product fraction, P_{mAb}, is

$$P_{\mathrm{mAb}} = \frac{a_{\mathrm{mAb}}^{\mathrm{P}}}{a_{\mathrm{mAb}}^{\mathrm{P}} + a_{\mathrm{w}}^{\mathrm{P}}}. \tag{6.25}$$

On the other hand, the amount of mAb injected into the system during the first half cycle is

$$a_i^{\mathrm{F}} = [\, Q_{\mathrm{IC}}\tau_1 + Q_{\mathrm{B}}(\tau_3 + \tau_4 + \tau 5)\,]\, c_{\mathrm{mAb}}^{\mathrm{F}}, \tag{6.26}$$

where $c_{\mathrm{mAb}}^{\mathrm{F}}$ is the mAb concentration in the feed mixture. Thus, the product recovery, R_{mAb}, is

$$R_{\mathrm{mAb}} = \frac{a_{\mathrm{mAb}}^{\mathrm{P}}}{a_{\mathrm{mAb}}^{\mathrm{F}}}/. \tag{6.27}$$

6.4 Replacing the Twin-column CaptureSMB System: Cycle Design of the Single-column Process

The second case study that was applied to the new monocolumn chromatographic process employed the isolation of a monoclonal antibody, a separation considerably more difficult than that of nucleosides due to the similarity between the target product and its impurities.

The method was applied to mAb capture with protein A affinity resin, a type of highly specific resin to the target biomolecule. For this, an already validated multicolumn counter-current process, the twin-column CaptureSMB, was used as reference and its cycle was mimetized. The recipe for determining the Single-column process cycle based on the multicolumn processes cycle has already been addressed in chapter 3.

Therefore, for the comparison, the cycle design of the single-column system was first determined. The equivalence between the standard two-column CaptureSMB process and the new one-column process is shown in Figure 6.3.

During the cycle's first two steps, the outlet of the column is sent to section A of the recycle device, which is the top section, forcing the movable piston to go down and thus storing the fluid collected from the chromatographic column. During the other steps of the half-cycle the chromatographic column is generating pure product or waste fractions and the recycle device sits idle waiting for the start of the next half-cycle. During steps 1'-2' of the cycle, the recycle device re-injects the fluid stored in section A back to the inlet of the column by moving the piston up. The fluid is reinjected into the column in the order into which it was collected from the column during the previous half-cycle.

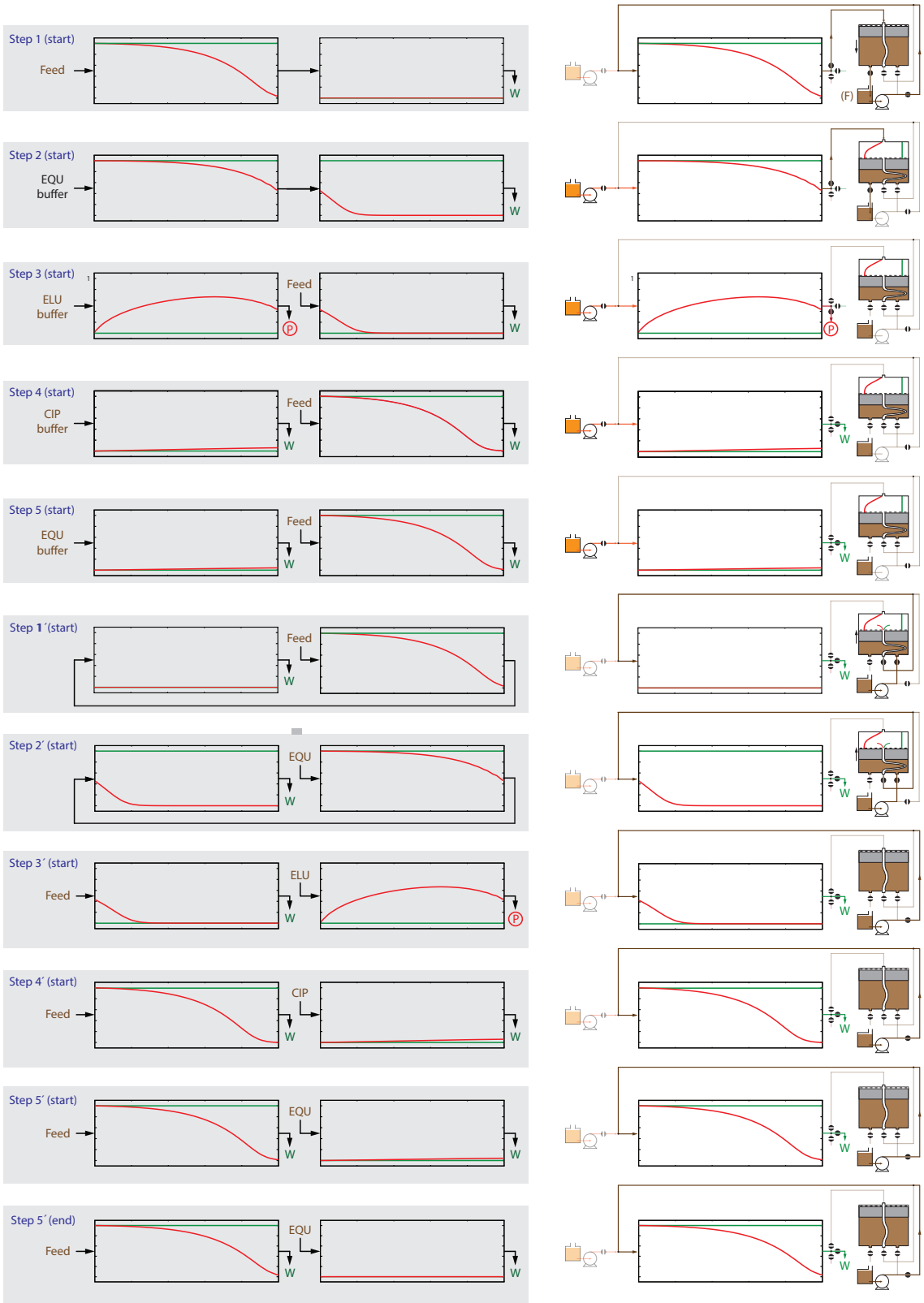

Figure 6.3: Schematic of the cycle of the One-column CaptureSMB process for mAb purification. Axial concentration profiles in the liquid phase: red lines, mAb; green lines, impurity.

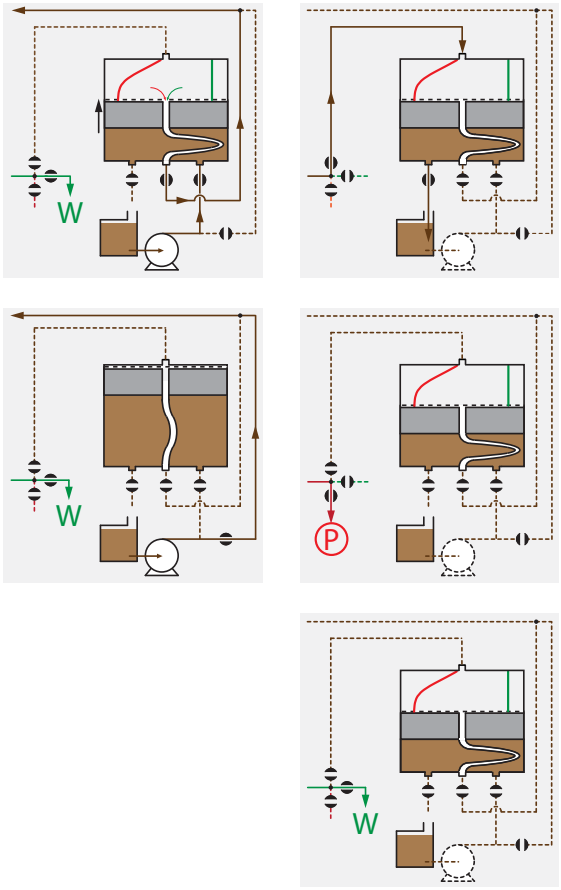

Figure 6.4: Schematic of the set of operating configurations of the plug-flow device.

An approximate "1st in, 1st out" method is thus being implemented for organizing & manipulating the fractions of fluid from the chromatographic column.

Since the cycle for two-column processes comprises two switching intervals, mixed fractions are reinjected into the one-column analog with a lag in time of one switching interval based on the principle of recycle fractions with a lag in time of $(N-1)\tau$ (or one switching interval).

Figure 6.4 shows the different configurations of the plug-flow device during the standard operating cycle of the one-column CaptureSMB analog. In the schematics of Figure 6.4 the operation of the piston is manipulated via several one-way (i.e., on/off) valves: the symbol ⊸ means that the on-off valve is open, whereas ⊣⊢ means that the on-off valve is closed.

Although the flow path configurations based on one-way valves are very flexible, their assembly tends to be bulky because an one-way (or on-off) valve has only two positions: open, which allows the fluid to flow through; and closed, which blocks the fluid flow. For this reason, come two way-valves were replaced by a combination of injection valves. Although these electrically-actuated, two-position 6-port/3-channel-injection valves also switch between only two positions, each position is more flexible than those of the simpler

one-way valve.

Note that Figure 6.3 shows that the eluent pump is not operated continuously over the cycle—there are sub-steps during which the feed pump is turned off. However, it might be of interest to operate continuously the feed pump. The simplest way to do this is to direct the pumping fluid back to the eluent tank during the sub-steps during which the eluent pump is supposed to be turned off. Actually, as shown in Figure 6.5 this leads to a smaller set of operating configurations of the plug-flow device.

The cycle steps of a full cycle of the two-column CaptureSMB process and those of its one-column analog are shown, in a simplified way, at Figure 6.6. Note that the one-column CaptureSMB analog's cycle can be simplified by merging identical, consecutive steps. The resulting process is shown in Figure 6.7.

6.5 Data for Simulation: Operational Conditions and Parameters

Using the dynamic process simulator gPROMS, ver. 4.0.0, the twin-column CaptureSMB process was simulated for the present case study. gPROMS is a fast and effective tool for performing simulation and optimization in steady and dynamic state, allowing the user to make quick decisions about the process operation. In addition, process modelling and simulation has been a key tool to gain understanding of processes that require broad time and resource consumption, as is the case of protein A chromatography for monoclonal antibodies, where both the feed and the column resin are usually extremely expensive [146].

Therefore, after the operation cycles were well defined, the simulations were carried out. The parameters used in the simulation were exactly the same as those provided by the author of this purification process [29, 30]. The operational conditions and parameters used can be seen in Tables 6.2 and 6.3.

The simulation of the single-column process described at previous section, that mimics the twin-column system, was also created, and two different piston operational models were considered: a simulation approached the recycle tube as a perfectly agitated tank, while another considered the reflux device as axially dispersed plug-flow model. The mathematical models used for the piston were the same as those presented in Chapter 3. The two reproductions were also submitted to the same conditions of the experiment done with the twin-column chromatographic system.

The operating conditions and parameters used in the simulation were based on the purification of the monoclonal IgG_1-type antibody, at concentration c_F = 1.2 mg/mL, contained in a supernatant cell culture, using Protein A resin in columns of dimensions 0.5 (OD) x 10 (L) cm, system equivalent to that addressed by Baur et al. [29, 30]. The parameters used at the three simulations are expressed in Table 6.2 and Table 6.3.

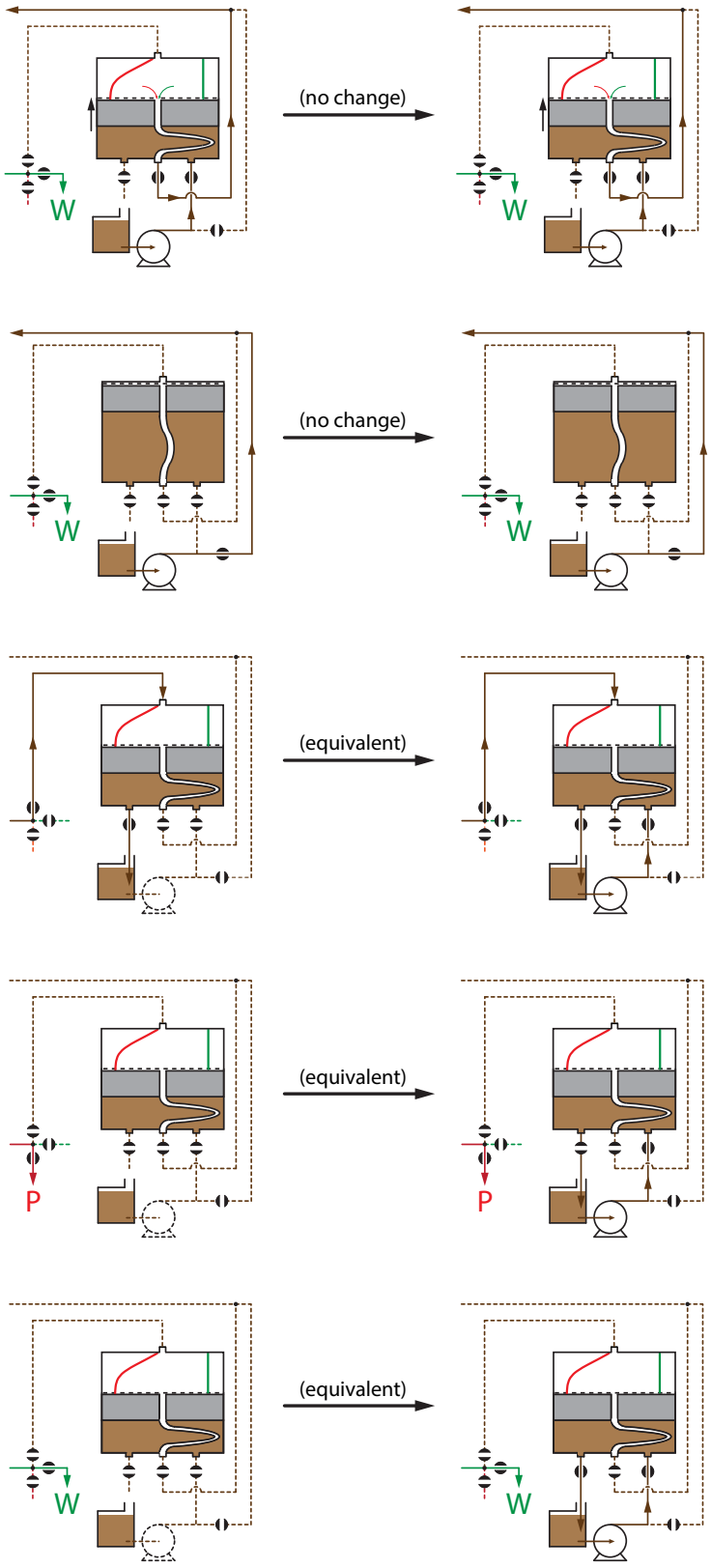

Figure 6.5: Schematic of the reduced set of operating configurations of the plug-flow device for the case when the eluent pump is operated continuously.

Two-column Process		One-column analog
Step	Flow-path	Flow-path
(1st half-cycle)		
S1	F ----> COL1 ------------> COL2 -> W	F -------> COL --> Piston
S2	EQU --> COL1 ------------> COL2 -> W	EQU -----> COL --> Piston
S3	ELU --> COL1 --> P F --> COL2 -> W	ELU -----> COL --> P
S4	CIP --> COL1 --> W F --> COL2 -> W	CIP -----> COL --> W
S5	EQU --> COL1 --> W F --> COL2 -> W	EQU -----> COL --> W
(2nd half-cycle)		
S1′	F ----> COL2 ------------> COL1 -> W	Piston --> COL --> W
S2′	EQU --> COL2 ------------> COL1 -> W	Piston --> COL --> W
S3′	ELU --> COL2 --> P F --> COL1 -> W	F -------> COL --> W
S4′	CIP --> COL2 --> W F --> COL1 -> W	F -------> COL --> W
S5′	EQU --> COL2 --> W F --> COL1 -> W	F -------> COL --> W

Figure 6.6: Steps of a full cycle of the twin-column Capture SMB process and its one-column analog.

Step	Flow path
S1	F -------> COL --> Piston
S2	EQU -----> COL --> Piston
S3	ELU -----> COL --> P
S4	CIP -----> COL --> W
S5	EQU -----> COL --> W
S1′+S2′	Piston --> COL --> W
S3′+S4′+S5′	F -------> COL --> W

Figure 6.7: Steps of a full cycle of the one-column Capture SMB process after merging identical, consecutive steps.

The three simulations, one for twin-column process and the two others for single-column process, allows comparing the performance of purification processes when subjected to the same parameters of operation. The analysis was done in terms of solute concentration profile evaluation, purity and recovery values at steady state cycles, and specific productivity.

6.6 Results and Comparison with the Twin-column CaptureSMB

With the simulation results of the multicolumn system and single-column systems, the efficiency of the processes can be compared. In a first analysis, the concentration profile at the chromatographic column outlet was analyzed for the Twin-column process and the

Table 6.2: Parameters of Protein A Column used at simulations, based at Baur et al [29, 30] case study.

Parameter	Symbol	Units	Value
Interparticle porosity	ϵ	-	0.368
Intraparticle porosity	ϵ_p	-	0.0
Peclet number for axial dispersion	Pe	-	400
Maximum mass transfer coefficient	k_{m}^{∞}	min^{-1}	0.180
Pore blockage coefficient	S_1	-	0.6245
Pore blockage coefficient	S_2	-	2.071
Power exponent of Henry coefficient	v	-	16.6
Saturation capacity per resin volume	q_{sat} or q^{∞}	mg/mL	94.72
Henry's constant at reference pH	H_{ref}	-	246.8
Reference pH	pH_{ref}	-	7.5
Reference mAb concentration	c_{ref}	mg/mL	1.2
Reference impurity concentration	w_{ref}	mg/mL	0.12
Reference impurity concentration	w_{ref}	mg/mL	0.12

Table 6.3: Operating conditions for the different simulated CaptureSMB processes. The parameters Q_{IC}, Q_B, and t_{step_i}, were optimized by J.P.B.Mota using AMPL software.

Parameter	Symbol	Units	Value
Flow rate of interconnected step	Q_{IC}	mL/min	1.4
Flow rate of batch step	Q_B	mL/min	1.4
Equilibration, loading and washing pH	pH^{EQU}	-	7.5
Elution pH	pH^{ELU}	-	3.2
CIP pH	pH^{CIP}	-	2.5
Sub-step 1 duration (IC, Feed)	t_{step_1}	min	10.1617
Sub-step 2 duration (IC, wash)	t_{step_2}	min	2.0
Sub-step 3 duration (B, elute)	t_{step_3}	min	30.7583
Sub-step 4 duration (B, CIP)	t_{step_4}	min	2.0
Sub-step 5 duration (B, EQU)	t_{step_5}	min	2.0

One-column Analog with piston as axially dispersed plug-flow. It is worth noting that, for the two-column process, the output concentration of column 1 is the only one analyzed, since in terms of simulation the columns are not exchanged at each switch interval, but the concentration profiles are exchanged. Consequently, this indicates that the product is always being withdrawn in the output stream of the same column (i.e. column 1 in the gPROMS implementation).

Figure 6.8 shows the graphic result, where the black curve represents the multicolumn system and the blue dots represent the data for the single-column process with axially dispersed flow model for the piston. In addition, each time unit represents a sub-step, therefore, as one cycle has ten sub-steps, ten time units indicate a complete cycle. With the graphic result, it is seen that the profiles of monoclonal antibody concentration in

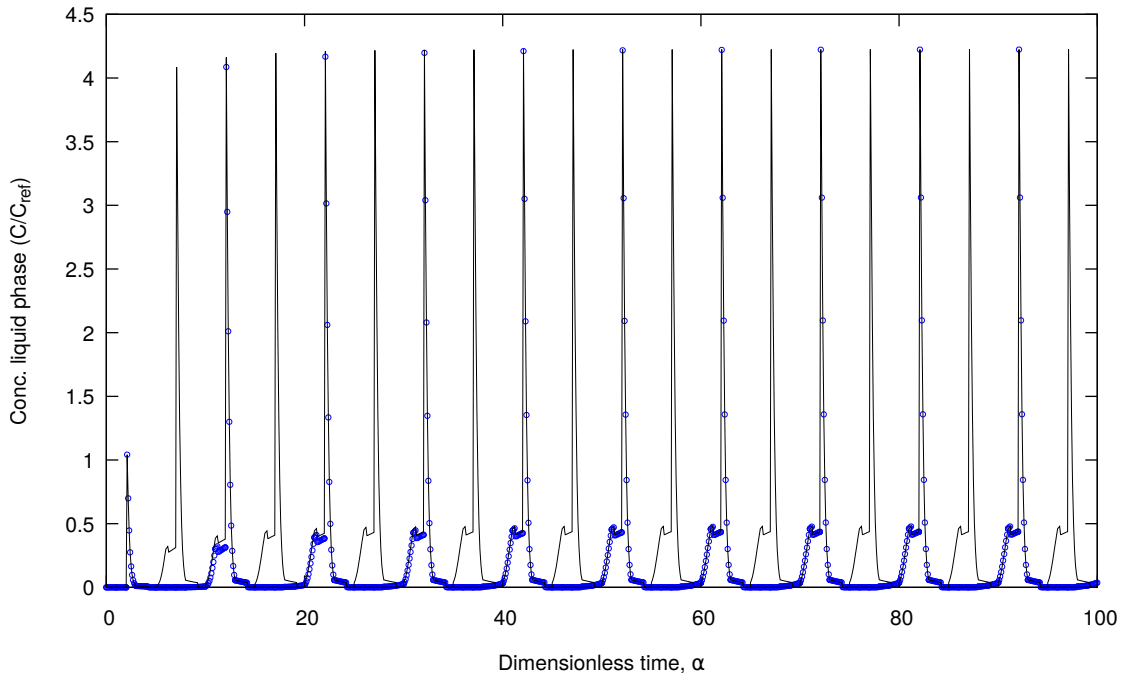

Figure 6.8: Concentration profiles of column outlet stream, for two mAb CaptureSMB processes: Twin-column and One-column Analog with axially dispersed plug-flow model for the recycle device. Black curve, twin-column process; blue dots, one-column analog with piston as dispersed plug-flow model. The curve was plotted with dimensionless time (α, or θ at mathematical model), where each ten units of time represents one full cycle. The two processes had similar concentration profiles at steady-state operation, and presented the same specific productivity, proving the effectiveness of the monocolumn system in mimicked the twin-column process

the liquid phase have very similar behaviour comparing the two processes, being slightly different only in the transient state (i.e. approximately the first three cycles), which does not infer significant impact on the desired analysis. In addition, the two processes show the same specific productivity, i.e. feed processed per time unit per resin volume. These two analyses have proven the ability of the single-column system to effectively mimic the process of monoclonal antibody capture that uses to two identical columns.

Secondly, the concentration profiles of the two simulated one-column processes (piston as dispersed plug-flow or perfectly stirred tank) were compared, as shown in Figure 6.9, where it is shown that, for this case study, the fluid behaviour within the piston does not condition the smooth functioning of the chromatographic process developed in this thesis.

We have already addressed this issue in Chapter 4. When the adsorption isotherm is strongly favorable, as is the case of protein A, the concentration front of the adsorbed product is compressed as it travels along the column. Hence, under these conditions, the effect of fluid mixing in the recycle piston has less influence on the shape of the breakthrough curve than when the adsorption isotherm is less concave and closer to a

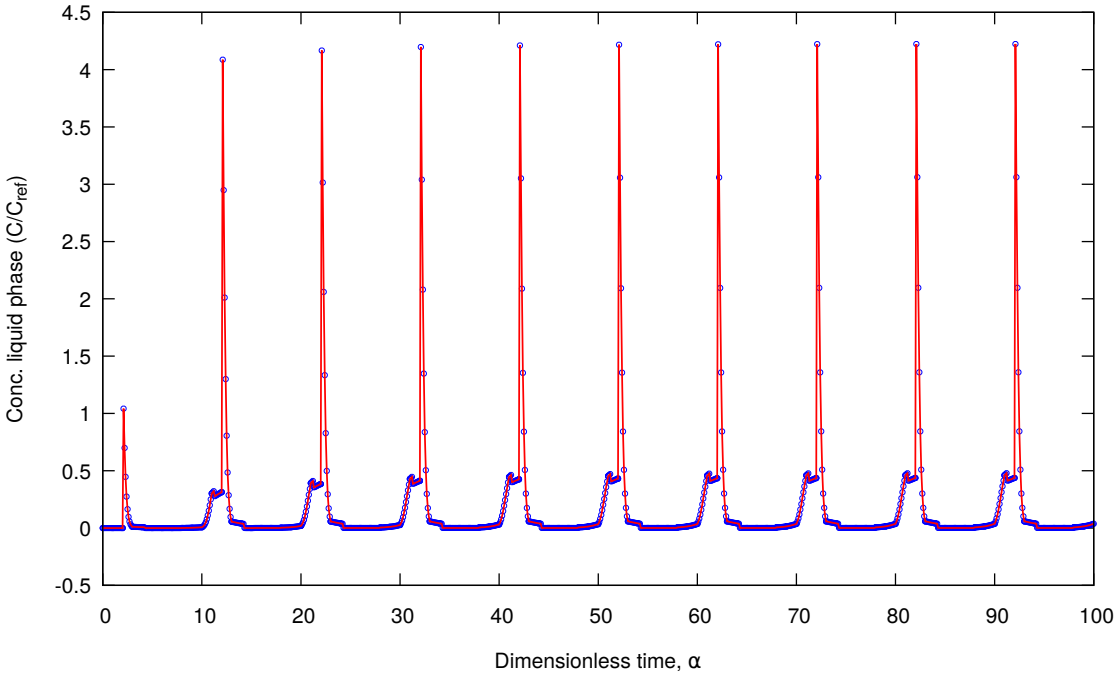

Figure 6.9: Concentration profiles of column outlet stream, for the two simulated mAb CaptureSMB processes: Piston as dispersed plug-flow or perfectly stirred tank. Blue dots, one-column analog with piston as dispersed plug-flow model; Red curve, one-column analog with piston as perfectly mixed tank. The two processes identical concentration profiles, proving that the effectiveness of the monocolumn process is not put into question by the type of hydrodynamic behaviour of the fluid within the piston.

linear shape.

With the purpose of analyzing only steady periodic cycles for the Single-column, the graph for cycles 9 and 10 (Figure 6.10) were plotted, a safe region to be in the cyclic steady-state regime. The concentration profiles for the product (red line) and for impurities (black line) are presented. The colored regions indicate the sub-steps of the cycle, so that the yellow block represents the sub-steps that the column outlet stream is being redirected to the piston (S1 + S2), the gray area indicates the elution sub-step, or product collection (S3), and the blank region expresses the remaining sub-steps of the cycle (S4 + S5 + S(1:5)'). This graph shows that part of the product coming out of the column is mixed with impurities. This mixed fraction is redirected to the piston, avoiding the loss of mAb. Moreover, the recirculation of impure product allows a better use of the column resin, since more product can be loaded without risk of being discarded at the column exit. It is also seen that very little product is discarded in the waste stream, resulting in a high recovery of mAb. Finally, it was verified that the moment when the impurities are eluted does not interfere in the purity of the collected product.

It is important to note that the two impurity fractions that come out in the white region of the graph are similar, in the twin-column system, to the impurity concentration profile of the downstream column (represented by the first impurity step curve) plus upstream

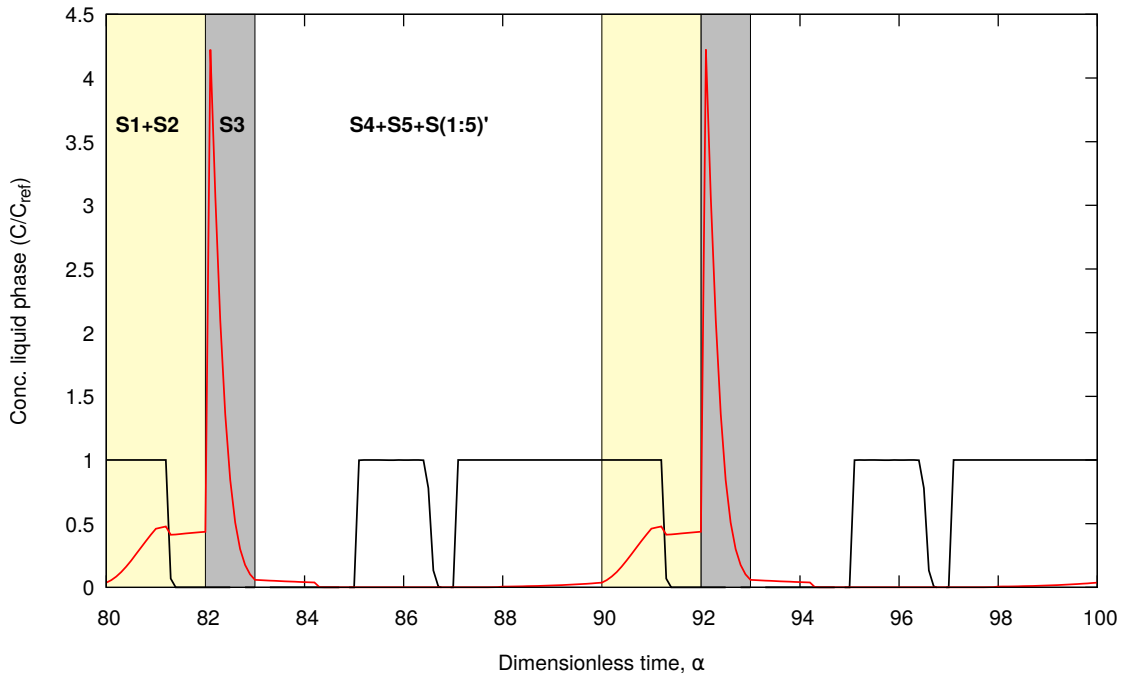

Figure 6.10: Cycle 9 and 10 of the One-column Capture SMB with dispersed plug-flow piston behaviour. The red line indicates the mAb concentration profile at the outlet of the chromatographic column. The colored regions of the chart, indicates different sub-steps. The yellow area indicates the S1+S2 sub-steps, showing the concentration profile of the mAb that is directed to the piston. The gray area shows the elution step, S3, with product collection. In the blank space, it shows the remaining sub-steps of the cycle. In this last region, impurities are discarded at the outlet of the column.

column (represented by the second impurity step curve), since in this process the rejection of impurities occurs at both downstream and upstream column waste streams, depending on the cycle sub-steps.

Finally, the purities and recoveries were then calculated for the simulated processes. Figure 6.11 and Figure 6.12 show, respectively, the purity and recovery graphs. The Table 6.4 reveals the calculated values for the cycles in steady-state condition. The values of 100% indicate that the impurities came out completely in the waste stream, not showing remnants in the elution stream (S3) or the stream passing to the next column, or piston, (S1 + S2), i.e. when the devices are interconnected. In the analysis of monoclonal antibody recovery, very similar values were obtained for the three simulated processes, close to 99.5%, differing only in the second decimal place.

In addition, the three systems take just a few cycles to achieve cyclic steady state: three cycles for the multicolumn process and six cycles for the analogous single-column process. However, through the analysis of the recovery graph for the One-column process, it is seen that, before reaching the steady state, high recovery values were already being obtained from the second cycle, showing that this difference of three cycles between the two processes is not a determinant factor that disqualifies the process.

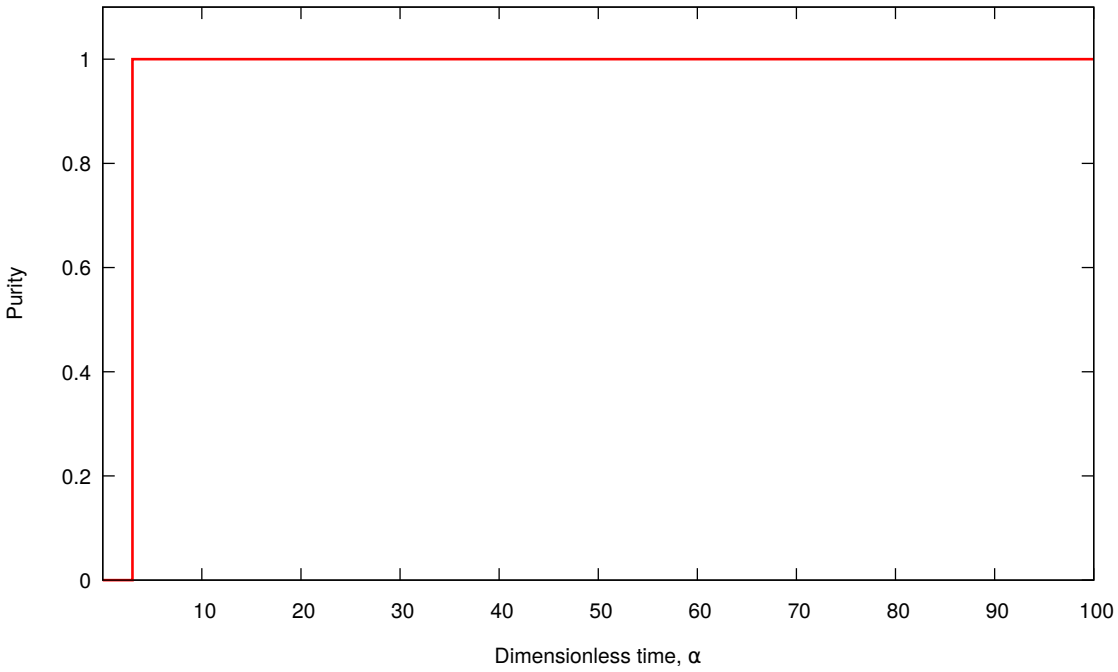

(a) mAb purity for Twin-column CaptureSMB.

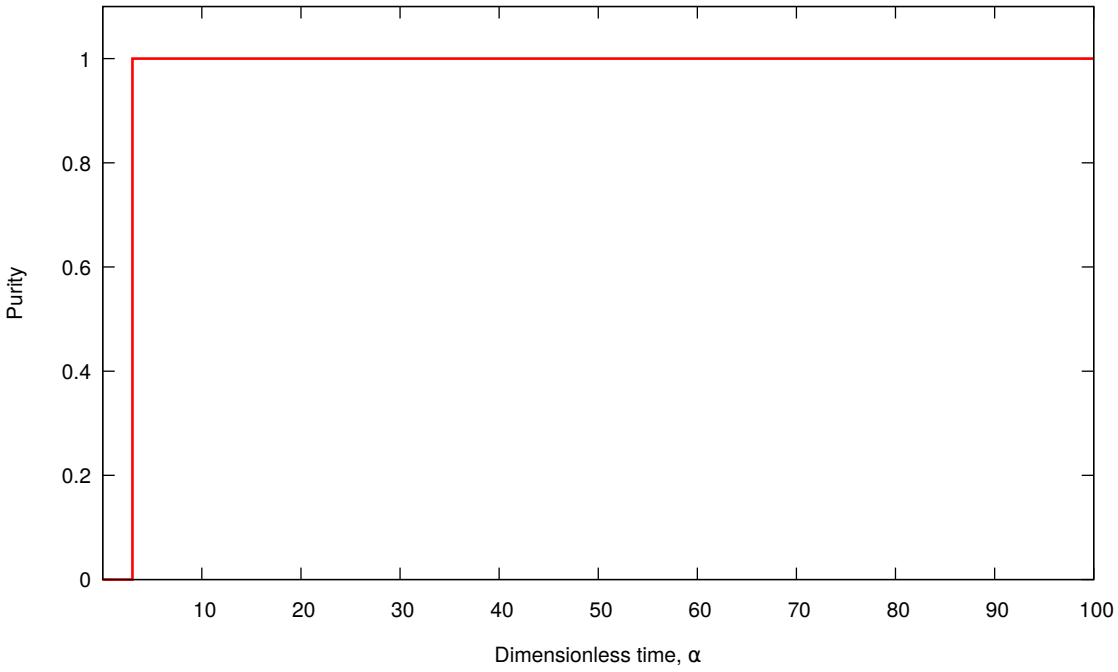

(b) mAb purity for One-column CaptureSMB.

Figure 6.11: mAb purity per dimensionless time unit, at (a) Twin-column process and (b) One-column process, considering the case of piston with axially dispersed plug-flow behaviour. Purity of 100 % was achieved for both processes with steady-state operation, indicating that there are no traces of impurities leaving in elution step S3+S3', for twin-column, or S3, for one-column, of the cycle.

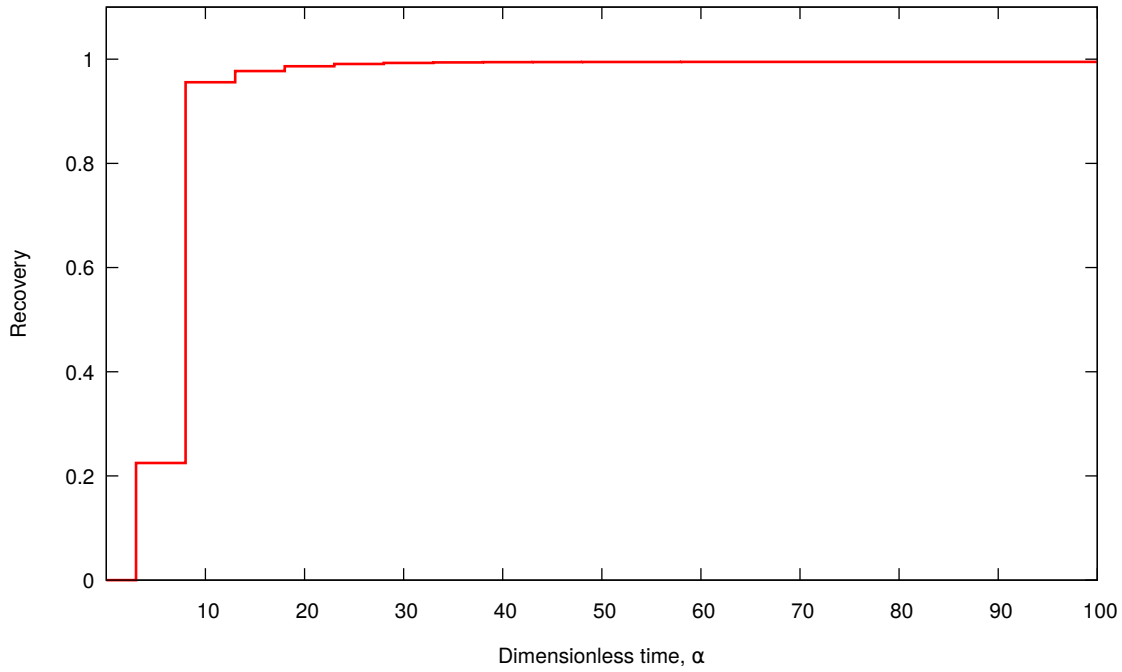

(a) mAb recovery for Twin-column CaptureSMB.

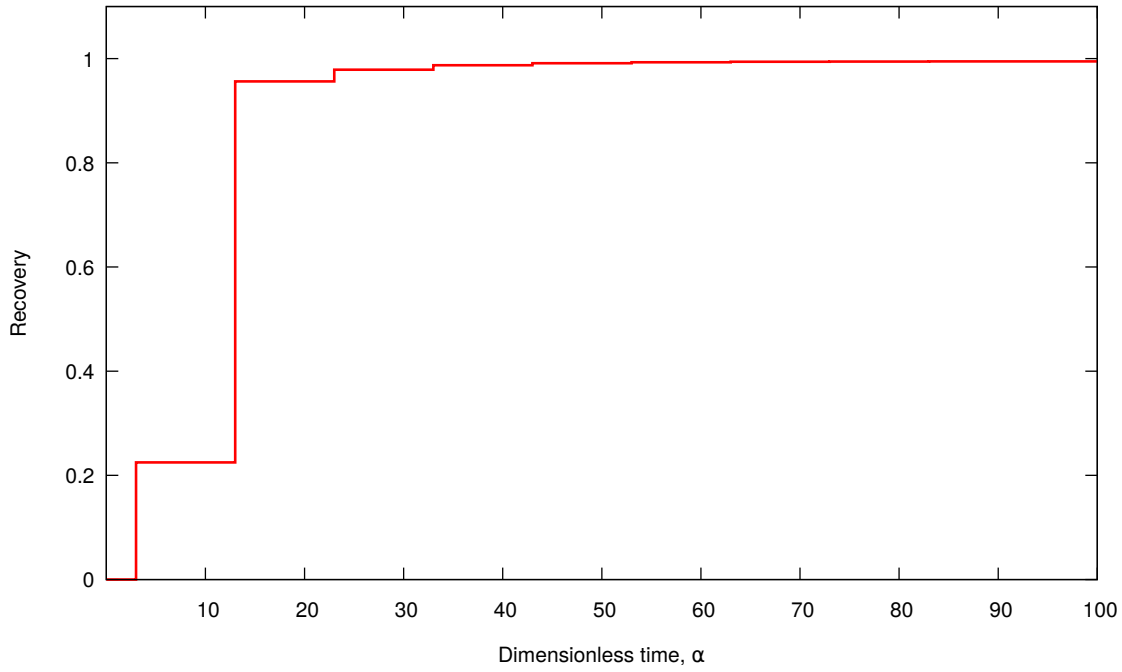

(b) mAb recovery for One-column CaptureSMB.

Figure 6.12: mAb recovery per dimensionless time unit, at (a) Twin-column process and (b) One-column process, considering the case of piston with axially dispersed plug-flow behaviour. In (a) the steady-state was reached from the fourth cycle, with recovery of 99.48 %, while in (b) the stationary state was reached in the seventh cycle, with recovery of 99.47 %. This shows that the two systems are very competitive in terms of efficiency.

Table 6.4: Comparison of Purity and Recovery in different operating systems.

	Twin-column	**One-column with Recycle Lag**	
		Dispersed plug-flow	**Perfectly mixed tank**
Purity (%)	~ 100	~ 100	~ 100
Recovery (%)	99.5	99.5	99.5

The high purity and recovery results obtained showed that the Single-column CaptureSMB system is a potential candidate for the purification of monoclonal antibodies, since it presents advantages over the existing multicolumn process, present in the literature [30]. Since the resin is a major component of the overall production cost of biopharmaceuticals, especially in cases where the resin is expensive (as the case of protein A resin) [116], working with the limit case of only one chromatographic column is a broad step towards the introduction of this process in the manufacture of these bioproducts, as well as an opportunity of great visibility to the market, taking into consideration the substantial reduction of production costs. Furthermore, the smallest number of equipment implies a simpler, more flexible system and with lower pressure drop, decreasing the chances of setup damage.

6.7 Conclusions

After the system has shown its efficiency for simple separations, the second case study was performed, this time a more complex separation. The purpose of this chapter was to replace the standard Twin-Column CaptureSMB process, which employs two identical chromatographic columns, by a Single-Column chromatographic analog that employs a special type of plug-flow device for recycling mixed fractions to the chromatography column with a lag in time.

The comparison was proceeded, using gPROMS simulation tool, evaluating the performance and efficiency of the single-column with recycle lag, for the purification of a isoform of monoclonal antibody, and comparing with the multicolumn countercurrent SMB process already studied and validated in the literature, the Twin-column CaptureSMB [14, 29, 30]. The Twin-column Capture SMB process showed (in studies presented by the respective author) to have a better performance than the batch system applied to the same mAb capture, obtaining capacity utilization and specific productivity superior to the batch system, with constant values of purity and yield. A higher productivity of the twin-column CaptureSMB, against the Batch system, means that fewer cycles are needed to obtain the same amount of product, implying a slower deterioration of the resin and, consequently, a decrease in the resin costs. Therefore, this process was considered a good case of study to be mimicked.

Hence, the process model was implemented to the capture of monoclonal antibody in

protein A, considering piston as a perfectly mixed tank and piston with axially dispersed plug flow behaviour. When dealing with a new process, gaining understanding of the process is crucial in designing an efficient and robust process, and determining the optimum conditions of the process [30]. Thus, the cycle design was first planned and, then, the validation for this application was done by gPROMS simulation.

The Single-column with recycle lag analog to SMB was evaluated in this case study through purity, yield, specific productivity and concentration profile evaluation.When comparing the concentration profiles in the product outlet stream, for the three processes simulated CaptureSMB: Twin-column, One-column with perfectly mixed tank model for the piston and other considering the device as axially dispersed plug-flow; the results showed that the curves, after the transient state, had very similar performance, concluding that the fluid behaviour within the piston does not restrict the mimetization capacity of the new process. In addition, the specific productivity obtained for the three processes were exactly the same.

Still, for the twin-column, the monoclonal antibody was recovered in 99.48 %, while the single-column recovered 99.47 % of the desired product. The purity was 100 % for all processes. This proves the efficiency of the One-column CaptureSMB process, either with or without perfect mixture inside recycle device, to isolate monoclonal antibody with protein A resin in affinity chromatography.

Despite achieving comparable purity and recovery levels with the twin-column CaptureSMB, the Single-column with Recycle Lag analog features valuable advantages. The price of protein A resin is almost one order of magnitude higher than stationary phases of non-affinity [90]. This indicates that, reducing from two to one column in monoclonal antibody isolation process, it drastically reduces the purification costs of this biomolecule and consequently the total costs of production. In addition, the reduction of columns number brings flexibility to the system, simplicity, and reduction of operating pressure. No less important, the change from one mixture to another, i.e. the preparation to start a new purification, is faster, since only one column needs to be cleaned. Especially for monoclonal antibodies, the latter quality really makes sense, since the process of monoclonal antibodies purification usually takes a long time. Therefore, with all these qualities, the Single-column CaptureSMB chromatographic process is a visioned alternative process to be established in the industry.

CHAPTER 7

Final Considerations

The increasing acceptance of biopharmaceuticals, their ability to treat previously untreatable diseases, and their huge market demand, are the major factors driving the exponential growth of the biopharmaceutical market. However, increasing demand for affordable biopharmaceuticals, high-end manufacturing requirements, and complicated and cumbersome regulatory requirements are hindering the market growth.

The pressure to increase process performance and reduce costs spreads over the whole development and manufacturing chain, encompassing research, analytics, clinical trials, and production. The production of a biopharmaceutical can, in turn, be divided into upstream and downstream processing, which are both under slow but continuous improvement. The focus of this thesis is on the contribution of chromatography to downstream processing. In order to increase the performance of a chromatographic separation unit beyond traditional batch technology, several continuous countercurrent processes for distinct applications have been developed and many of them patented [207, 248].

The overall objective of the present work was to develop a new chromatographic unit as effective as the existing multicolumn systems for the capture and polishing steps in downstream processing of biomolecules, but simpler, cheaper and with a smaller footprint, using just a single chromatographic column and a new developed recycle device. Three specific objectives guided the research direction:

- Establish the design, mathematical model, and assembly of the prototype;
- Experimentally validate the set-up, through the mimetization of a multicolumn separation process;
- Improve the operation of the set-up, using 3D printing as a tool for the process optimization;

- Apply the newly developed biomolecule purification process in another case study, seeking to certify the effectiveness of the set-up.

7.1 Main conclusions

Chapter 3 described a new single-column set-up capable of mimicking multicolumn SMB processes and other existing countercurrent continuous processes to perform downstream biopurification. The recipe of how to mimic multicolumn continuous chromatography with just a single-column apparatus, the conceptual set-up design, its mathematical model, and the assembly of its prototype, as well as their operational capabilities, were presented. As result, it was shown that with a clever implementation of single-column chromatography with recycle it is possible to mimic the operation of the continuous multicolumn process, obtaining a system as compact and simple-to-operate as the standard single-column batch process. The new apparatus can be used both in the capture step as polishing stage of a purification train and the valuable advantages of the process were explored, such as reduction of the total amount of equipment used and consequent total size of the installation, reduction of required resin quantity and decrease of the total pressure drop. In addition, because only one chromatographic column needs to be repacked when switching from one mixture to another, changing separations is easier and takes less time than with a multicolumn SMB system. Furthermore, system automation helps avoiding operational errors and expenses with additional human operators, since the process requires skilled labor. As consequence, a considerably simpler, more flexible and stable system is obtained, in addition to being more economical.

Chapter 4 focused on the experimental proof-of-concept of the developed set-up, using the linear separation of nucleosides, uridine and guanosine, by reversed phase as case study to demonstrate the effective use of the proposed chromatography apparatus. Before the biomolecules separation experiment, preliminary experiments were performed to test the recycle device operation, as well as the functionality of the different possible configurations operated by the set-up. The recycle piston, operates with small-to-moderate mixing of fluid between the sections and with the mobile plunger in perfect operation, giving a pressure drop of only 6 bar when traveling the length of the device, implying the process of opening and closing the piston. In the initial tests, the piston seemed to comply with the plug-flow dispersed model. The characterization of the prototype, for this separative process, was performed through experiments, prior to the execution of the separation. For the chromatographic column, the interparticular porosity, the Henry's constants and the Péclet numbers were determined. The values obtained were very similar to those found by the authors of the mimetized system, a two-column, open-loop, SMB system [228]. For the piston, the dead volumes, which gave very low values ($V_0 = V_L = 0.273$) cm^3, and the axial dispersion coefficients were calculated. For the nucleosides separation process, the concentration profiles of each biomolecule demonstrated that the hydrodynamic fluid behaviour inside the recycle device was between

the dispersed plug-flow model and a perfectly agitated tank. But, although the exact hydrodynamic behaviour within the piston has not been exactly determined, this is not a determinant limitation, because the One-column Analog to SMB system overcome the separation challenges and separated the nucleosides very efficiently, obtaining very high values of purity (99.57 % for guanosine and 97.03 % for uridine) and recovery (97.76 % for guanosine and 100 % for uridine), in addition to low solvent consumption.

Based on previous chapter results, in order to improve the operation of piston device, in Chapter 5 it was developed new piston distributors and collectors configurations through 3D printing, which was explored a broad range of frit layouts for the dispenser. Two 3D methods were used: SLA and FDM. Chemical and thermal stability tests were made with 3D printed material made by each method, which proved to be stable both for the solvent used in the nucleosides separation, as solvents with similar pH to the solvents used in the purification of monoclonal antibodies. Through experiments with the 3D Frits produced from the Clear resin (experiments with tracer, separation of nucleosides and evaluation of the residence time distribution profiles), it was obtained a improvement of the fluid distribution within the piston when compared to original polyethylene frits. The presence of brackets inside the reflux piston, preferably higher number of distributors and consequently smaller height of each bracket, proved to be substantially better than the use of the original polyethylene frits, which had shown concentration profiles at the piston outlet with minor disturbances and even closer to a dispersed plug-flow model. Due to this result, the FDM method has been used to overcome the limitation of the Clear resin holders, the high rigidity of the 3D material, becoming brittle. Therefore, with the PEEK material was achieved substantially more flexible 3D brackets, enabling the movement of the mobile plunger inside the recycle tube. It is important to note that considerable improvement has been achieved, however, additional geometric designs are being constantly produced using 3D technology, in the perspective of further optimization of the prototype by achieving the really desired plug-flow operation inside the recycle container, since the only thing that can compromise the product purity and productivity of this process comparing to the analogous SMB is the efficiency of the plug-flow device.

The results obtained with the case study approached in Chapter 6, the purification of a monoclonal antibody through protein A resin, showed that, although it is a desire to maintain a dispersive tubular behaviour within the piston, it is not a restricted condition for the proper functioning of the facility. The Single-column chromatographic system mimicked the Twin-column CaptureSMB process operation with the same specific productivity (feed processed per unit time per resin volume), or absolute productivity (feed processed per unit time) divided by the number of columns. The monocolumn process reached mAb purity of 100% and recovery of 99.47%, values exactly the same as those obtained with the simulation for the twin-columns process mimetized. With this, it was concluded that the newly developed platform is capable to imitate more complex separation processes (than approached in Chapter 4), and mainly, this platform shares the

benefits of SMB chromatography in that it not only gives significantly higher yields of purer product, but also enables processing more feed and thereby increasing the overall throughput when compared with batch chromatography. However, the process developed by this thesis uses just a single chromatographic column.

It is expected that the work presented in this thesis has scientific repercussions and is an important step for the optimization of chromatographic processes applied to the biopharmaceutical industry, where product quality and operating costs are constantly in question to meet the health needs worldwide.

7.2 Suggestions for Future Work

Single-column Chromatography with Recycle Lag, as already exposed throughout this document, has the potential to mimic continuous multicolumn chromatographic process for separation and/or purification of biomolecules, reducing equipment costs and increasing simplicity of operation, while maintaining the same specific productivity, as well as high values for product purity and recovery. In addition, the proposal of this thesis enables the use of 3D printing in a field still very little explored by this technology, 3D parts for chromatographic processes. Some important steps were given in the technical feasibility and validation of the system, but there is still a path to be travelled.

It is suggested to analyze the hydrodynamic behaviour of the fluid at piston equipped with the new spiral configuration in PEEK plus grids in Clear resin equally spaced inside the piston. The analysis can be through:

1. Pulse and gradient solute injection tests, proceeded at piston device, experimentally testing the residence time distribution profiles;

2. Proceed with the separation of nucleosides and compare with the results obtained in this thesis.

It is also suggested the continuity of the use of 3D technology to address more models of distributors and piston collectors, to approximate as much as possible the dispersion of the fluid to the dispersed plug-flow model.

In addition to these suggestions, it is plausible the experimental validation of the simulated process presented in Chapter 6, experimentally mimicking the Twin-column CaptureSMB.

Finally, it is still suggested the application of the prototype to mimic other purification processes approached in the literature, recently developed and already validated, such as the twin-column MCSGP process, developed by Steinebach et al. [250], for purification of monoclonal antibodies, or the Gradient with Steady State Recycle (GSSR) three-column process, developed by Silva et al. [242] and apply for purification of peptides (another case of reversed-phase purification), showing the effectiveness of the process developed in this thesis when applied solvent-gradient and when mimicking processes more complex than

two columns. The validation of the new monocolumn process can still be accomplished through adenovirus purification using size-exclusion chromatography, based on the two-column process developed by Nestola et al. [193]. This would show the effectiveness of the process when applied to different types of chromatography, and not only to reversed phase chromatography with protein A, and to different types of biomolecules.

Bibliography

[1] 3DBenchy. *#3DBenchy – The jolly 3D printing torture-test*. 2019. URL: http://www.3dbenchy.com/ (visited on 09/11/2019).

[2] S. Abel, M. Mazzotti, and M. Morbidelli. "Solvent gradient operation of simulated moving beds: I. Linear isotherms." In: *Journal of Chromatography A* 944.1-2 (2002), pp. 23–39. ISSN: 0021-9673. DOI: 10.1016/S0021-9673(01)01087-1.

[3] S. Abel, G. Erdem, M. Amanullah, M. Morari, M. Mazzotti, and M. Morbidelli. "Optimizing control of simulated moving beds - experimental implementation." In: *Journal of Chromatography A* 1092 (2005), pp. 2–16. DOI: 10.1016/j.chroma.2005.04.101.

[4] N. Abunasser and P. C. Wankat. "Improving the performance of one column analogs to SMBs." In: *AIChE Journal* 52.7 (2006), pp. 2461–2472. ISSN: 0001-1541. DOI: 10.1002/aic.10867.

[5] N. Abunasser and P. Wankat. "Ternary separations with one-column analogs to SMB." In: *Separation Science and Technology* 40.16 (2005), pp. 3239–3259. ISSN: 01496395. DOI: 10.1080/01496390500423615.

[6] N. Abunasser and P. C. Wankat. "One-Column Chromatograph with Recycle Analogous to Simulated Moving Bed Adsorbers: Analysis and Applications." In: *Industrial & Engineering Chemistry Research* 43.17 (2004), pp. 5291–5299. ISSN: 0888-5885. DOI: 10.1021/ie0400346.

[7] N. Abunasser, P. C. Wankat, Y. S. Kim, and Y. M. Koo. "One-column chromatograph with recycle analogous to a four-zone simulated moving bed." In: *Industrial and Engineering Chemistry Research* 42.21 (2003), pp. 5268–5279. ISSN: 08885885. DOI: 10.1021/ie030283e.

[8] P. Adam, R. M. Nicoud, M. Bailly, and O. Ludemann-Hombourger. *Process and device for separation with variable-length chromatographic zones*. 2000. URL: https://patents.google.com/patent/US20020174769.

[9] All3DP. *2019 3D Printing Technology Guide – 10 Types of 3D Printers | All3DP*. 2019. URL: https://all3dp.com/1/types-of-3d-printers-3d-printing-technology/ (visited on 09/10/2019).

[10] Amersham Biosciences. *Reversed Phase Chromatography: Principles and Methods*. AA. Uppsala Sweden: Amersham Biosciences, 1999, p. 85. ISBN: 18-1134-16. URL: http://wolfson.huji.ac.il/purification/PDF/ReversePhase/AmershamRPCManual.pdf.

[11] AMFG. *ULTEM and PEEK: the Ultimate Guide to High-Performance 3D Printing Materials*. Tech. rep. AMFG (Autonomous Manufacturing), 2018. URL: https://amfg.ai/2018/07/09/ultem-peek-high-performance-3d-printing-materials-guide/.

[12] Amgen. *Biologics and Biosimilars: An Overview*. Tech. rep. Amgen Inc., 2017, p. 55. URL: https://www.amgenbiosimilars.com/pdfs/pages-from-amgen-biosimiliars-booklet{_}e-version-final.pdf.

[13] M. Ando, M. Tanimura, and M. Tamura. *Method of chromatographic separation*. 1990. URL: https://patents.google.com/patent/US4970002A/en.

[14] M. Angarita, T. Muller-Spath, D. Baur, R. Lievrouw, G. Lissens, and M. Morbidelli. "Twin-column CaptureSMB: A novel cyclic process for protein A affinity chromatography." In: *Journal of Chromatography A* 1389 (2015), pp. 85–95. ISSN: 18733778. DOI: 10.1016/j.chroma.2015.02.046.

[15] D. Antos and A. Seidel-Morgenstern. "Two-step solvent gradients in simulated moving bed chromatography Numerical study for linear equilibria." In: *Journal of Chromatography A* 944.1-2 (2002), pp. 77–91. DOI: https://doi.org/10.1016/S0021-9673(01)01365-6Get.

[16] J. C. Antunes. "Programming and Control of a Single-Column Analog Moving Bed Process." Master Thesis. Faculdade de Ciências e Tecnologia - Universidade NOVA de Lisboa, 2018, p. 63.

[17] J. Araújo, R. Rodrigues, R. Silva, and J. Mota. "Single-column Simulated Moving-bed Process with Recycle Lag: Analysis and Applications." In: *Adsorption Science & Technology* 25.9 (2007), pp. 647–659. ISSN: 0263-6174. DOI: 10.1260/026361707785082369.

[18] J. M. M. Araújo, R. C. R. Rodrigues, and J. P. B. Mota. "Optimal design and operation of a certain class of asynchronous simulated moving bed processes." In: *Journal of Chromatography A* 1132 (2006), pp. 76–89. DOI: 10.1016/j.chroma.2006.07.016.

[19] J. M. M. Araújo. "Optimal Design and Operation of Compact Simulated Moving Bed Processes For Enantioseparations." PhD Thesis. FCT - Universidade NOVA de Lisboa, 2009, p. 266.

[20] J. M. Araújo, R. Rodrigues, and J. P. Mota. "Optimal design and operation of a certain class of asynchronous simulated moving bed processes." In: *Journal of Chromatography A* 1132.1-2 (2006), pp. 76–89. ISSN: 00219673. DOI: 10.1016/j.chroma.2006.07.016.

[21] J. M. Araújo, R. C. Rodrigues, M. F. Eusébio, and J. P. Mota. "Chiral separation by two-column, semi-continuous, open-loop simulated moving-bed chromatography." In: *Journal of Chromatography A* 1217.33 (2010), pp. 5407–5419. ISSN: 00219673. DOI: 10.1016/j.chroma.2010.06.040.

[22] J. M. M. Araújo, R. C. R. Rodrigues, and J. P. B. Mota. "Use of Single-Column Models for Efficient Computation of the Periodic State of a Simulated Moving-Bed Process." In: *Industrial and Engineering Chemistry Research* 45.15 (2006), pp. 5314–5325. ISSN: 08885885. DOI: 10.1021/ie051108w.

[23] R. Aris. "A. On the dispersion of a solute in a fluid flowing through a tube." In: *Process Systems Engineering* 1.C (1999), pp. 109–120. ISSN: 18745970. DOI: 10.1016/S1874-5970(99)80009-5.

[24] L. Aumann and M. Morbidelli. "A continuous multicolumn countercurrent solvent gradient purification (MCSGP) process." In: *Biotechnology and Bioengineering* 98.5 (2007), pp. 1043–1055. ISSN: 00063592. DOI: 10.1002/bit.21527.

[25] L. Aumann and M. Morbidelli. "A semicontinuous 3-column countercurrent solvent gradient purification (MCSGP) process." In: *Biotechnology and Bioengineering* 99.3 (2008), pp. 728–733. ISSN: 00063592. DOI: 10.1002/bit.21585.

[26] L. Aumann, G. Stroehlein, and M. Morbidelli. "Parametric study of a 6-column countercurrent solvent gradient purification (MCSGP) unit." In: *Biotechnology and Bioengineering* 98.5 (2007), pp. 1029–1042. ISSN: 00063592. DOI: 10.1002/bit.21529.

[27] M. Bailly and R.-M. Nicoud. "The simulated moving bed: a powerful process for purification." In: *Colloques-Instiut National de La Sante et de la Recherche Medicale Colloques eu Seminaires* 5 (1992), pp. 43–47.

[28] A. Basso, G. Prado, P. Pelegrini, and M. Grossi-de Sa. "Biopharmaceuticals and Biosimilars." In: *Current Developments in Biotechnology and Bioengineering: Human and Animal Health Applications*. Ed. by V. Thomaz-Soccol, A. Pandey, and R. R. Resende. 1st ed. Elsevier, 2016. Chap. 2nd, pp. 23–50. ISBN: 9780444636607. DOI: 10.1016/C2014-0-04871-X.

[29] D. Baur, M. Angarita, T. Müller-Späth, and M. Morbidelli. "Optimal model-based design of the twin-column CaptureSMB process improves capacity utilization and productivity in protein A affinity capture (additional information)." In: *Biotechnology Journal* (2015). ISSN: 18607314. DOI: 10.1002/biot.201500223.

[30] D. Baur, M. Angarita, T. Müller-Späth, and M. Morbidelli. "Optimal model-based design of the twin-column CaptureSMB process improves capacity utilization and productivity in protein A affinity capture." In: *Biotechnology Journal* (2016), pp. 135–145. ISSN: 18607314. DOI: 10.1002/biot.201500223.

[31] H. Becker and L. E. Locascio. "Polymer microfluidic devices." In: *Talanta* 56.2 (2002), pp. 267–287. DOI: 10.1016/S0039-9140(01)00594-X.

[32] A. Bellini, S. Gu¨c¸eri, and M. Bertoldi. "Liquefier Dynamics in Fused Deposition." In: *Journal of Manufacturing Science and Engineering* 126.2 (2004), pp. 237–246. DOI: 10.1115/1.1688377.

[33] A. Bertsch and P. Renaud. "Microstereolithography." In: *Stereolithography: Materials, Processes and Applications*. Ed. by P. J. Bártolo. New York: Springer US, 2011, pp. 81–112. ISBN: 978-0-387-92903-3. DOI: 10.1007/978-0-387-92904-0.

[34] J. Bezanson, A. Edelman, S. Karpinski, and V. B. Shah. "Julia: A Fresh Approach to Numerical Computing." In: *SIAM Review* 59.1 (2017), pp. 65–98. DOI: 10.1137/141000671.

[35] N. Bilton. *Disruptions: 3-D Printing Is on the Fast Track*. 2017. URL: https://bits.blogs.nytimes.com/2013/02/17/disruptions-3-d-printing-is-on-the-fast-track/?nl=todaysheadlines{\&}emc=edit{_}th{_}20130218 (visited on 09/09/2019).

[36] H. H. Bin Hamzah, O. Keattch, D. Covill, and B. A. Patel. "The effects of printing orientation on the electrochemical behaviour of 3D printed acrylonitrile butadiene styrene (ABS)/carbon black electrodes." In: *Scientific reports* 8.1 (2018), p. 9135. DOI: 10.1038/s41598-018-27188-5.

[37] J. T. Bjerrum, Y. Wang, F. Hao, M. Coskun, C. Ludwig, U. Günther, and O. H. Nielsen. "Metabonomics of human fecal extracts characterize ulcerative colitis, Crohn's disease and healthy individuals." In: *Metabolomics* 11.1 (2015), pp. 122–133. DOI: 10.1007/s11306-014-0677-3.

[38] E. A. Blackstone and J. P. Fuhr. "The economics of biosimilars." In: *American Health and Drug Benefits* 6.8 (2013), pp. 469–477. ISSN: 19422962. DOI: 10.1016/S1574-0676(06)01021-0. arXiv: arXiv:1011.1669v3.

[39] M. W. Bolt and P. A. Mahoney. "High-Efficiency Blotting of Proteins of Diverse Sizes Following Sodium Dodecyl Sulfate–Polyacrylamide Gel Electrophoresis." In: *Analytical Biochemistry* 247.2 (1997), pp. 185–192. ISSN: 0003-2697. DOI: 10.1006/ABIO.1997.2061.

[40] J. Bonham-Carter and J. Shevitz. *A Brief History of Perfusion Biomanufacturing*. 2011. URL: https://bioprocessintl.com/upstream-processing/bioreactors/a-brief-history-of-perfusion-biomanufacturing-322322/ (visited on 03/11/2019).

[41] D. D. B. Broughton and C. C. G. Gerhold. *Continuous sorption process employing fixed bed of sorbent and moving inlets and outlets*. 1961. URL: https://patents.google.com/patent/US2985589A/enhttp://www.freepatentsonline.com/2985589.html.

[42] C-Studio. *Transformação Digital - Automação de processos. O que tem a sua empresa a ganhar?* 2017. URL: https://www.jornaldenegocios.pt/transformacao-digital/detalhe/automacao-de-processos-o-que-tem-a-sua-empresa-a-ganhar (visited on 08/01/2019).

[43] P. Campíns-Falcó, R. Herráez-Hernández, and P. Serra-Mora. "Liquid Chromatography." In: *Encyclopedia of Analytical Science*. Ed. by P. Worsfold, C. Poole, and M. Miró. 3rd. Academic Press, 2019, pp. 108–116. ISBN: 9780081019849. DOI: 10.1016/B978-0-12-409547-2.14218-0.

[44] G. Carta and A. Jungbauer. *Protein Chromatography: Process Development and Scale-Up*. Wiley-VCH, 2010, p. 346. ISBN: 978-3-527-31819-3. URL: https://www.wiley.com/en-pt/Protein+Chromatography:+Process+Development+and+Scale+Up-p-9783527318193.

[45] CDER - FDA. *Reviewer Guidance: Validation of Chromatographic Methods*. Tech. rep. Rockville, MD, US: Center for Drug Evaluation and Research (CDER - FDA), 1994, p. 33. URL: https://www.fda.gov/media/75643/download.

[46] CDER - FDA. *Analytical Procedures and Methods Validation for Drugs and Biologics - Guidance for Industry*. Tech. rep. Silver Spring, MD, US: US FDA, 2015, p. 18. URL: http://www.fda.gov/Drugs/GuidanceComplianceRegulatoryInformation/Guidances/default.htmand/orhttp://www.fda.gov/BiologicsBloodVaccines/GuidanceComplianceRegulatoryInformation/Guidances/default.htm.

[47] C. A. Challener. "Making the Move to Continuous Chromatography." In: *BioPharm International* 31.4 (2018), pp. 14–18.

[48] V. Chan, P. Zorlutuna, J. H. Jeong, H. Kong, and R. Bashir. "Three-dimensional photopatterning of hydrogels using stereolithography for long-term cell encapsulation." In: *Lab on a Chip* 10.16 (2010), p. 2062. DOI: 10.1039/c004285d.

[49] W. Chan and P. White. *Fmoc Solid Phase Peptide Synthesis*. Ed. by W. Chan and P. White. 1st ed. New York , US: Oxford University Press, 2000, p. 371. ISBN: 0199637253.

[50] C Chantin, B Bonin, R Boulieu, and C Bory. "Liquid-chromatographic study of purine metabolism abnormalities in purine nucleoside phosphorylase deficiency." In: *Clinical Chemistry* 42.2 (1996), pp. 326–8. ISSN: 1530-8561.

[51] S. Chatterjee. *FDA Perspective on Continuous Manufacturing*. Tech. rep. Baltimore: IFPAC Annual Meeting, 2012, pp. 34–42. URL: https://www.fda.gov/downloads/AboutFDA/CentersOffices/OfficeofMedicalProductsandTobacco/CDER/UCM341197.pdf.

[52] Chemical Book. *Guanosine CAS#: 118-00-3*. 2019. URL: https://www.chemicalbook.com/ProductChemicalPropertiesCB2701721{_}EN.htm (visited on 09/04/2019).

[53] Chemical Entities of Biological Interest (ChEBI). *Guanosine*. 2019. URL: https://www.ebi.ac.uk/chebi/searchId.do?chebiId=CHEBI:16750 (visited on 09/02/2019).

[54] Chemical Entities of Biological Interest (ChEBI). *Uridine*. 2019. URL: http://www.ebi.ac.uk/chebi/searchId.do?chebiId=CHEBI:16704 (visited on 09/02/2019).

[55] R. Chess and J. Makinen. *Note On The Biopharmaceutical Industry | Stanford Graduate School of Business*. 2018. URL: https://www.gsb.stanford.edu/faculty-research/case-studies/note-biopharmaceutical-industry.

[56] C. K. Chua, K. F. Leong, and C. S. Lim. *Rapid Prototyping: Principles and Applications*. 3rd. World Scientific, 2010, p. 540. ISBN: 978-981-277-897-0. DOI: 10.1142/6665.

[57] M.-F. Clincke, C. Mölleryd, Y. Zhang, E. Lindskog, K. Walsh, and V. Chotteau. "Very high density of CHO cells in perfusion by ATF or TFF in WAVE bioreactor™. Part I. Effect of the cell density on the process." In: *Biotechnology Progress* 29.3 (2013), pp. 754–767. ISSN: 87567938. DOI: 10.1002/btpr.1704.

[58] B. P. Conner, G. P. Manogharan, A. N. Martof, L. M. Rodomsky, C. M. Rodomsky, D. C. Jordan, and J. W. Limperos. "Making sense of 3-D printing: Creating a map of additive manufacturing products and services." In: *Additive Manufacturing* 1-4 (2014), pp. 64–76. DOI: 10.1016/J.ADDMA.2014.08.005.

[59] M. N. Cooke, J. P. Fisher, D. Dean, C. Rimnac, and A. G. Mikos. "Use of stereolithography to manufacture critical-sized 3D biodegradable scaffolds for bone ingrowth." In: *Journal of Biomedical Materials Research* 64B.2 (2003), pp. 65–69. ISSN: 0021-9304. DOI: 10.1002/jbm.b.10485. URL: http://www.ncbi.nlm.nih.gov/pubmed/12516080http://doi.wiley.com/10.1002/jbm.b.10485.

[60] O. Coskun. "Separation techniques: Chromatography." In: *Northern clinics of Istanbul* 3.2 (2016), pp. 156–160. ISSN: 2536-4553. DOI: 10.14744/nci.2016.32757.

[61] D. M. Ruthven. *Principles of adsorption and adsorption processes*. John Wiley & Sons, Inc., 1984, p. 453. ISBN: 0-471-86606-7.

[62] H. Determann. *Gel Chromatography: Gel Filtration · Gel Permeation · Molecular Sieves |A Laboratory Handbook*. 2nd ed. Springer-Verlag Berlin Heidelberg, 1969, p. 202. ISBN: 978-3-642-49886-2. DOI: 10.1007/978-3-642-49886-2.

[63] J. A. DiMasi, L Feldman, A Seckler, and A Wilson. "Trends in Risks Associated With New Drug Development: Success Rates for Investigational Drugs." In: *Clinical Pharmacology & Therapeutics* 87.3 (2010), pp. 272–277. DOI: 10.1038/clpt.2009.295.

[64] S. Ding, B. Zou, P. Wang, and H. Ding. "Effects of nozzle temperature and building orientation on mechanical properties and microstructure of PEEK and PEI printed by 3D-FDM." In: *Polymer Testing* 78 (2019), p. 105948. DOI: 10.1016/J.POLYMERTESTING.2019.105948.

[65] M. Diogo, J. Queiroz, and D. Prazeres. "Assessment of purity and quantification of plasmid DNA in process solutions using high-performance hydrophobic interaction chromatography." In: *Journal of Chromatography A* 998.1-2 (2003), pp. 109–117. ISSN: 0021-9673. DOI: 10.1016/S0021-9673(03)00618-6.

[66] V. Dragone, V. Sans, M. H. Rosnes, P. J. Kitson, and L. Cronin. "3D-printed devices for continuous-flow organic chemistry." In: *Beilstein Journal of Organic Chemistry* 9.1 (2013), pp. 951–959. DOI: 10.3762/bjoc.9.109.

[67] Drugbank. *Guanosine*. 2019. URL: https://www.drugbank.ca/drugs/DB02857 (visited on 09/02/2019).

[68] G. Dünnebier and K.-U. Klatt. "Optimal operation of simulated moving bed chromatographic processes." In: *Computers & Chemical Engineering* 23 (1999), S195–S198. ISSN: 00981354. DOI: 10.1016/S0098-1354(99)80048-9.

[69] G. Dünnebier, J. Fricke, and K. U. Klatt. "Optimal design and operation of simulated moving bed chromatographic reactors." In: *Industrial and Engineering Chemistry Research* 39.7 (2000), pp. 2290–2304. ISSN: 08885885. DOI: 10.1021/ie990820o.

[70] V. Durga Prasada Rao, P. Rajiv, and V. Navya Geethika. "Effect of fused deposition modelling (FDM) process parameters on tensile strength of carbon fibre PLA." In: *Materials Today: Proceedings* (2019). DOI: 10.1016/J.MATPR.2019.06.009.

[71] D. M. Ecker, S. Dana Jones, and H. L. Levine. "The therapeutic monoclonal antibody market." In: 7.1 (2015), pp. 9–14. DOI: 10.4161/19420862.2015.989042.

[72] K.-O. Eriksson and M. Belew. "Hydrophobic Interaction Chromatography." In: *Protein Purification: Principles, High Resolution Methods, and Applications*. Ed. by J.-C. Janson. 3rd. Wiley, 2011. Chap. 6, pp. 165–179. ISBN: 978-0-471-74661-4.

[73] S. Fanali, P. Haddad, C. Poole, P. Schoenmakers, and D. Lloyd. *Liquid Chromatography: Fundamentals and Instrumentation*. Ed. by S. Fanali, P. Haddad, C. Poole, P. Schoenmakers, and D. Lloyd. 1st. Elsevier, 2013, p. 520. ISBN: 978-0-12-415807-8.

[74] FDA. "FDA'S policy statement for the development of new stereoisomeric drugs." In: *Chirality* 4.5 (1992), pp. 338–340. ISSN: 0899-0042. DOI: 10.1002/chir.530040513.

[75] FDA Consumer. *Is It Really 'FDA Approved?'* 2018. URL: https://www.fda.gov/ForConsumers/ConsumerUpdates/ucm047470.htm.

[76] C. Fee, S. Nawada, and S. Dimartino. "3D printed porous media columns with fine control of column packing morphology." In: *Journal of Chromatography A* 1333 (2014), pp. 18–24. ISSN: 00219673. DOI: 10.1016/j.chroma.2014.01.043.

[77] M. A. Firer. "Efficient elution of functional proteins in affinity chromatography." In: *Journal of biochemical and biophysical methods* 49.1-3 (2001), pp. 433–42. ISSN: 0165-022X. DOI: https://doi.org/10.1016/S0165-022X(01)00211-1.

[78] H. S. Fogler. *Elements of Chemical Reaction Engineering*. 5 th. Prentice Hall, 2016, p. 993. ISBN: 9780133887518.

[79] P. Fontoura. "Monoclonal antibody therapy in multiple sclerosis: Paradigm shifts and emerging challenges." In: *mAbs* 2.6 (2010), pp. 670–681. ISSN: 19420862. DOI: 10.4161/mabs.2.6.13270.

[80] Formalabs Enterprise. *Material Data Sheet: Standard*. Tech. rep. 2017, pp. 4–6.

[81] Formlabs. *High Resolution SLA and SLS 3D Printers for Professionals | Formlabs*. URL: https://formlabs.com/ (visited on 09/09/2019).

[82] Formlabs Enterprise. *Form 2: Affordable Desktop SLA 3D Printer*. 2019. URL: https://formlabs.com/3d-printers/form-2/ (visited on 09/08/2019).

[83] Formlabs Enterprise. *Form Cure time and temperature settings*. Tech. rep. 2019. URL: https://support.formlabs.com/s/article/Form-Cure-Time-and-Temperature-Settings?language=en{_}US.

[84] Formlabs Enterprise. *Formlabs SLA 3D Printer: Technical Specification*. 2019. URL: https://formlabs.com/3d-printers/form-3/tech-specs/ (visited on 09/08/2019).

[85] Formlabs Enterprise. *Post-Curing with Form Cure*. Tech. rep. 2019, p. 2.

[86] Formlabs Inc. *Clear Photoreactive Resin for Form 1, Form 1+, Form 2: SAFETY DATA SHEET*. Tech. rep. 2016, pp. 1–8. URL: https://formlabs.com/media/upload/Clear-SDS{_}u324bsC.pdf.

[87] C. L. Gaughan. "The present state of the art in expression, production and characterization of monoclonal antibodies." In: *Molecular Diversity* 20.1 (2016), pp. 255–270. ISSN: 1381-1991. DOI: 10.1007/s11030-015-9625-z.

[88] GE Healthcare. *Hydrophobic Interaction and Reversed Phase Chromatography*. Ed. by G. Healthcare. Uppsala, Sweden: General Electric Company, 2006, p. 165. ISBN: 11-0012-69.

[89] P. Geng, J. Zhao, W. Wu, W. Ye, Y. Wang, S. Wang, and S. Zhang. "Effects of extrusion speed and printing speed on the 3D printing stability of extruded PEEK filament." In: *Journal of Manufacturing Processes* 37 (2019), pp. 266–273. DOI: 10.1016/J.JMAPRO.2018.11.023.

[90] S. Ghose, B. Hubbard, and S. M. Cramer. "Binding capacity differences for antibodies and Fc-fusion proteins on protein A chromatographic materials." In: *Biotechnology and Bioengineering* 96.4 (2007), pp. 768–779. DOI: 10.1002/bit.21044.

[91] I. Gibson, D. W. Rosen, and B. Stucker. *Additive Manufacturing Technologies: Rapid Prototyping to Direct Digital Manufacturing*. Boston, MA: Springer US, 2010, p. 459. ISBN: 978-1-4419-1119-3. DOI: 10.1007/978-1-4419-1120-9.

[92] X. Gjoka, R. Gantier, and M. Schofield. "Transfer of a three step mAb chromatography process from batch to continuous: Optimizing productivity to minimize consumable requirements." In: *Journal of Biotechnology* 242 (2017), pp. 11–18. ISSN: 18734863. DOI: 10.1016/j.jbiotec.2016.12.005.

[93] F. C. Godoi. *Fundamentals of 3D food printing and applications*. Ed. by F. C. Godoi, B. R. Bhandari, S. Prakash, and M. Zhang. Academic Press, 2010. ISBN: 9780128145 647.

[94] J. P. Griffiths and S. J. Pirt. "The uptake of amino acids by mouse cells (strain LS) during growth in batch culture and chemostat culture: the influence of cell growth rate." In: *Proceedings of the Royal Society of London. Series B. Biological Sciences* 168.1013 (1967), pp. 421–438. ISSN: 2053-9193. DOI: 10.1098/rspb.1967.0073.

[95] C. M. Grill, L. Miller, and T. Q. Yan. "Resolution of a racemic pharmaceutical intermediate: A comparison of preparative HPLC, steady state recycling, and simulated moving bed." In: *Journal of Chromatography A* 1026.1-2 (2004), pp. 101–108. ISSN: 00219673. DOI: 10.1016/j.chroma.2003.11.049.

[96] M. Grom, M. Kozorog, S. Caserman, A. Pohar, and B. Likozar. "Protein A affinity chromatography of Chinese hamster ovary (CHO) cell culture broths containing biopharmaceutical monoclonal antibody (mAb): Experiments and mechanistic transport, binding and equilibrium modeling." In: *Journal of Chromatography B: Analytical Technologies in the Biomedical and Life Sciences* 1083.January (2018), pp. 44–56. ISSN: 1873376X. DOI: 10.1016/j.jchromb.2018.02.032.

[97] B. C. Gross, J. L. Erkal, S. Y. Lockwood, C. Chen, and D. M. Spence. "Evaluation of 3D printing and its potential impact on biotechnology and the chemical sciences." In: *Analytical Chemistry* 86.7 (2014), pp. 3240–3253. ISSN: 15206882. DOI: 10.1021/ac403397r.

[98] T. Gu. *Mathematical Modeling and Scale-Up of Liquid Chromatography: With Application Examples*. 2nd ed. Switzerland: Springer International Publishing, 2015, pp. XV, 207. DOI: 10.1007/978-3-319-16145-7.

[99] G. Guiochon. "Preparative liquid chromatography." In: *Journal of chromatography. A* 965.1-2 (2002), pp. 129–61. DOI: 10.1016/s0021-9673(01)01471-6.

[100] G. Guiochon, D. G. Shirazi, A. Felinger, and A. M. Katti. *Fundamentals of preparative and nonlinear chromatography*. 2nd. Academic Press, 2006, p. 975. ISBN: 9780080457222.

[101] G. Guiochon, A. Felinger, D. G. Shirazi, and A. M. Katti. *Fundamentals of Preparative Chomatography*. 2006, p. 990. ISBN: 9780123705372.

[102] B. Hafez and E. Hafez. *Reproduction in Farm Animals*. Ed. by D. Balado. 7th. Lippincott Williams & Wilkins, 2013, p. 509. ISBN: 9781118710289.

[103] D. S. Hage. "Chromatography." In: *Principles and Applications of Clinical Mass Spectrometry*. Ed. by N. Rifai, C. T. Wittwer, and A. R. Horvath. Elsevier, 2018. Chap. 1, pp. 1–32. ISBN: 9780128160633. DOI: 10.1016/B978-0-12-816063-3.00001-3.

[104] R. Hahn, P. Bauerhansl, K. Shimahara, C. Wizniewski, A. Tscheliessnig, and A. Jungbauer. "Comparison of protein A affinity sorbents II. Mass transfer properties." In: *Journal of Chromatography A* 1093.1-2 (2005), pp. 98–110. DOI: 10.1016/j.chroma.2005.07.050.

[105] H. H. Hamzah, S. A. Shafiee, A. Abdalla, and B. A. Patel. "3D printable conductive materials for the fabrication of electrochemical sensors: A mini review." In: *Electrochemistry Communications* 96 (2018), pp. 27–31. ISSN: 1388-2481. DOI: 10.1016/J.ELECOM.2018.09.006.

[106] R. Harris, R. Hague, and P. Dickens. "The structure of parts produced by stereolithgrapghy injection mould tools and the effect on part shrinkage." In: *International Journal of Machine Tools and Manufacture* 44.1 (2004), pp. 59–64.

[107] V. Harshitha and S. Srinivasa Rao. "Design and analysis of ISO standard bolt and nut in FDM 3D printer using PLA and ABS materials." In: *Materials Today: Proceedings* (2019). DOI: 10.1016/J.MATPR.2019.07.737.

[108] G. E. Healthcare. *Ion Exchange Chromatography: Principles and Methods*. Uppsala, Sweden: General Electric Company, 2016, p. 167. ISBN: 11-0004-21.

[109] G. E. Healthcare. *Size Exclusion Chromatography: Principles and Methods*. Ed. by G. E. Company. 2018, pp. 1–122. DOI: 10.1016/j.enggeo.2006.07.007.

[110] G. Healthcare. *Affinity Chromatography, Vol.3: Specific Groups of Biomolecules*. Vol. 3. Uppsala, Sweden: General Electric Company, 2016, p. 153. DOI: 10.1001/archinte.1962.03620200001001.

[111] M. Heidari-Rarani, M. Rafiee-Afarani, and A. Zahedi. "Mechanical characterization of FDM 3D printing of continuous carbon fiber reinforced PLA composites." In: *Composites Part B: Engineering* 175 (2019), p. 107147. ISSN: 1359-8368. DOI: 10.1016/J.COMPOSITESB.2019.107147.

[112] Henan Suwei Electronics Technology co. *CreatBot 3D Printer User manual*. Tech. rep. 2017, p. 40.

[113] O. Henry, E. Kwok, and J. M. Piret. "Simpler noninstrumented batch and semicontinuous cultures provide mammalian cell kinetic data comparable to continuous and perfusion cultures." In: *Biotechnology Progress* 24.4 (2008), pp. 921–931. ISSN: 87567938. DOI: 10.1002/btpr.17.

[114] HMDB. *Guanosine*. 2019. URL: http://www.hmdb.ca/metabolites/HMDB0000133 (visited on 09/02/2019).

[115] HMDB. *Uridine*. 2019. URL: http://www.hmdb.ca/metabolites/HMDB0000296 (visited on 09/02/2019).

[116] S. Hober, K. Nord, and M. Linhult. "Protein A chromatography for antibody purification." In: *Journal of Chromatography B* 848.1 (2007), pp. 40–47. DOI: 10.1016/J.JCHROMB.2006.09.030.

[117] B. Hu, X. Duan, Z. Xing, Z. Xu, C. Du, H. Zhou, R. Chen, and B. Shan. "Improved design of fused deposition modeling equipment for 3D printing of high-performance PEEK parts." In: *Mechanics of Materials* 137 (2019), p. 103139. DOI: 10.1016/J.MECHMAT.2019.103139.

[118] Y. Huang, S. Kuriyama, and C.-P. Jiang. "Fundamental study and theoretical analysis in a constrained-surface stereolithography system." In: *The International Journal of Advanced Manufacturing Technology* 24.5-6 (2004), pp. 361–369. DOI: 10.1007/s00170-003-1627-9.

[119] C. Hull. *Apparatus for production of three-dimensional objects by stereolithography*. 1986. URL: https://patents.google.com/patent/US4575330A/en.

[120] C. W. Hull. *Apparatus for production of three-dimensional objects by stereolithography*. 1984. URL: https://patents.google.com/patent/US4575330A/en.

[121] J. S. Hur and P. C. Wankat. "New Design of Simulated Moving Bed (SMB) for Ternary Separations." In: *Industrial & Engeneering Chemistry Research* 44.6 (2005), pp. 1906–1913. DOI: 10.1021/IE040164E.

[122] J. S. Hur and P. C. Wankat. "Two-Zone SMB/Chromatography for Center-Cut Separation from Ternary Mixtures: Linear Isotherm Systems." In: *Industrial & Engeneering Chemistry Research* 45.4 (2006), pp. 1426–2100. DOI: 10.1021/IE058046U.

[123] T. Ishihara, M. Miyahara, and K. Yamamoto. "Monoclonal antibody purification using activated carbon as a replacement for Protein A affinity chromatography." In: *Journal of Chromatography B: Analytical Technologies in the Biomedical and Life Sciences* 1102-1103.June (2018), pp. 1–7. ISSN: 1873376X. DOI: 10.1016/j.jchromb.2018.10.004.

[124] S Iuliano, J. R. Fisher, M Chen, and W. J. Kelly. "Rapid analysis of a plasmid by hydrophobic-interaction chromatography with a non-porous resin." In: *Journal of chromatography. A* 972.1 (2002), pp. 77–86. ISSN: 0021-9673. DOI: https://doi.org/10.1016/S0021-9673(02)00901-9.

[125] D. M. Jacobson, A. E. W. Rennie, and C. E. Bocking. *Fifth National Conference on Rapid Design, Prototyping, and Manufacture*. Professional Engineering Publ, 2004, p. 101. ISBN: 1860584659.

[126] G. Jagschies and K. M. Łącki. "Process Capability Requirements." In: *Biopharmaceutical Processing*. Ed. by G. Jagschies, E. Lindskog, K. Łącki, and P. Galliher. Elsevier, 2018. Chap. 4, pp. 73–94. ISBN: 9780081006238. DOI: https://doi.org/10.1016/B978-0-08-100623-8.00004-9.

[127] T. B. Jensen, T. G. P. Reijns, H. A. H. Billiet, and L. A. M. Van Der Wielen. "Novel simulated moving-bed method for reduced solvent consumption." In: *Journal of Chromatography A* 873.2 (2000), pp. 149–162. DOI: https://doi.org/10.1016/S0021-9673(99)01352-7.

[128] W. Jin and P. C. Wankat. "Two-zone SMB process for binary separation." In: *Industrial and Engineering Chemistry Research* 44.5 (2005), pp. 1565–1575. ISSN: 08885885. DOI: 10.1021/ie040132r.

[129] W. Jin and P. C. Wankat. "Scaling rules and increasing feed rates in two-zone and four-zone simulated moving bed systems." In: *Industrial and Engineering Chemistry Research* 45.8 (2006), pp. 2793–2807. ISSN: 08885885. DOI: 10.1021/ie0580102.

[130] R. D. Johnson. "Chemical creativity with 3D printing." In: *Nature Chemistry* 4.5 (2012), pp. 338–339. DOI: 10.1038/nchem.1333.

[131] A. Jungbauer and R. Hahn. "Ion-Exchange Chromatography." In: *Methods in Enzymology: Guide to Protein Purification*. Ed. by R. R. Burgess and M. P. Deutscher. 2nd. Academic Press, 2009. Chap. 22, pp. 349–372. ISBN: 978-0-12-374978-9.

[132] A. Jupke, A. Epping, and H. Schmidt-Traub. "Optimal design of batch and simulated moving bed chromatographic separation processes." In: *Journal of Chromatography A* 944.1-2 (2002), pp. 93–117. ISSN: 00219673. DOI: 10.1016/S0021-9673(01)01311-5.

[133] M. Juza, M. Mazzotti, and M. Morbidelli. "Simulated moving-bed chromatography and its application to chirotechnology." In: *Trends in Biotechnology* 18.3 (2000), pp. 108–118. ISSN: 0167-7799. DOI: 10.1016/S0167-7799(99)01419-5.

[134] E. Karlsson and I. Hirsh. "Ion Exchange Chromatography." In: *Protein Purification: Principles, High Resolution Methods, and Applications*. Ed. by J.-C. Janson. 3rd. Wiley, 2011. Chap. 4, pp. 93–134. ISBN: 978-0-471-74661-4.

[135] D. J. Karst, E. Serra, T. K. Villiger, M. Soos, and M. Morbidelli. "Characterization and comparison of ATF and TFF in stirred bioreactors for continuous mammalian cell culture processes." In: *Biochemical Engineering Journal* 110 (2016), pp. 17–26. ISSN: 1369-703X. DOI: 10.1016/J.BEJ.2016.02.003.

[136] P. R. Kasten and N. R. Amundson. "Analytical Solution for Simple Systems in Moving Bed Adsorbers." In: *Industrial & Engineering Chemistry* 44.7 (1952), pp. 1704–1711. ISSN: 0019-7866. DOI: 10.1021/ie50511a059.

[137] Y. Kawajiri and L. T. Biegler. "Nonlinear Programming Superstructure for Optimal Dynamic Operations of Simulated Moving Bed Processes." In: *Industrial & Engineering Chemistry Research* 45.25 (2006), pp. 8503–8513. DOI: 10.1021/ie0601192.

[138] Y. Kawajiri and L. T. Biegler. "Optimization strategies for simulated moving bed and PowerFeed processes." In: *AIChE Journal* 52.4 (2006), pp. 1343–1350. ISSN: 0001-1541. DOI: 10.1002/aic.10736.

[139] M. M. Kearney and K. L. Hieb. *Time variable simulated moving bed process*. 1991. URL: https://patents.google.com/patent/US5102553A/en.

[140] B. Kelley. "Very large scale monoclonal antibody purification: The case for conventional unit operations." In: *Biotechnology Progress* 23.5 (2007), pp. 995–1008. ISSN: 87567938. DOI: 10.1021/bp070117s.

[141] Khan Academy. *Principles of chromatography*. URL: https://www.khanacademy.org/test-prep/mcat/chemical-processes/separations-purifications/a/principles-of-chromatography (visited on 03/19/2019).

[142] J. K. Kim and P. C. Wankat. "Scaling and intensification procedures for simulated moving-bed systems." In: *AIChE Journal* 49.11 (2003), pp. 2810–2821. ISSN: 00011541. DOI: 10.1002/aic.690491114.

[143] J. K. Kim, N. Abunasser, and P. C. Wankat. "Use of two feeds in simulated moving beds for binary separations." In: *Korean Journal of Chemical Engineering* 22.4 (2005), pp. 619–627. ISSN: 0256-1115. DOI: 10.1007/BF02706654.

[144] Y. S. Kim, C. H. Lee, Y. M. Koo, and P. Wankat. "Studies on the One-Column Analogue of a Four-zone SMB." In: *Adsorption Science & Technology, Proceedings of the Third Pacific Basin Conference*. Kyongju, Republic of Korea, 2003, pp. 468–473. ISBN: 9789812383495. DOI: 10.1142/9789812704320_0084.

[145] P. J. Kitson, M. D. Symes, V. Dragone, and L. Cronin. "Combining 3D printing and liquid handling to produce user-friendly reactionware for chemical synthesis and purification." In: *Chemical Science* 4 (2013), pp. 3099–3103.

[146] K.-U. Klatt, F. Hanisch, G. Dünnebier, and S. Engell. "Model-based optimization and control of chromatographic processes." In: *Computers & Chemical Engineering* 24.2-7 (2000), pp. 1119–1126. ISSN: 00981354. DOI: 10.1016/S0098-1354(00)00492-0.

[147] K.-U. Klatt, F. Hanisch, and G. Dünnebier. "Model-based control of a simulated moving bed chromatographic process for the separation of fructose and glucose." In: *Journal of Process Control* 12.2 (2002), pp. 203–219. ISSN: 0959-1524. DOI: 10.1016/S0959-1524(01)00005-1.

[148] G. T. Klein, Y. Lu, and M. Y. Wang. "3D printing and neurosurgery–ready for prime time?" In: *World neurosurgery* 80.3-4 (2013), pp. 233–5. DOI: 10.1016/j.wneu.2013.07.009.

[149] E. Kloppenburg and E. D. Gilles. "A New Concept for Operating Simulated Moving-Bed Processes." In: *Chemical Engineering & Technology* 22.10 (1999), pp. 813–817. ISSN: 0930-7516. DOI: 10.1002/(SICI)1521-4125(199910)22:10<813::AID-CEAT813>3.0.CO;2-G.

[150] E. Kloppenburg and E. Gilles. "Automatic control of the simulated moving bed process for C8 aromatics separation using asymptotically exact input/output-lineariza- tion." In: *Journal of Process Control* 9.1 (1999), pp. 41–50. ISSN: 09591524. DOI: 10.1016/S0959-1524(98)00026-2.

[151] K. Konstantinov, Y.-s. Tsai, D. Moles, and R. Matanguihan. "Control of Long-Term Perfusion Chinese Hamster Ovary Cell Culture by Glucose Auxostat." In: *Biotechnology Progress* 12.1 (1996), pp. 100–109. ISSN: 8756-7938. DOI: 10.1021/bp950044p.

[152] K. B. Konstantinov and C. L. Cooney. "White Paper on Continuous Bioprocessing, May 20-21 2014, Continuous Manufacturing Symposium." In: *Journal of pharmaceutical sciences* 104.3 (2015), pp. 813–820. ISSN: 1520-6017. DOI: 10.1002/jps.24268.

[153] I. Kostareva, F. Hung, and C. Campbell. "Purification of antibody heteropolymers using hydrophobic interaction chromatography." In: *Journal of Chromatography A* 1177.2 (2008), pp. 254–264. ISSN: 00219673. DOI: 10.1016/j.chroma.2007.09.088.

[154] M. Krättli, F. Steinebach, and M. Morbidelli. "Online control of the twin-column countercurrent solvent gradient process for biochromatography." In: *Journal of Chromatography A* 1293 (2013), pp. 51–59. ISSN: 0021-9673. DOI: 10.1016/J.CHROMA.2013.03.069.

[155] M. Krättli, T. Müller-Späth, and M. Morbidelli. "Multifraction separation in countercurrent chromatography (MCSGP)." In: *Biotechnology and Bioengineering* 110.9 (2013), pp. 2436–2444. DOI: 10.1002/bit.24901.

[156] E. Küsters, G. Gerber, and F. D. Antia. "Enantioseparation of a chiral epoxide by simulated moving bed chromatography using Chiralcel-OD." In: *Chromatographia* 40.7-8 (1995), pp. 387–393. ISSN: 0009-5893. DOI: 10.1007/BF02269900.

[157] E. S. Langer. *2017 Biopharmaceutical Trends — Opportunities For The New Year*. Tech. rep. Bioprocess Online, 2016. URL: https://www.bioprocessonline.com/doc/biopharmaceutical-trends-opportunities-for-the-new-year-0001.

[158] M. Lay, N. L. N. Thajudin, Z. A. A. Hamid, A. Rusli, M. K. Abdullah, and R. K. Shuib. "Comparison of physical and mechanical properties of PLA, ABS and nylon 6 fabricated using fused deposition modeling and injection molding." In: *Composites Part B: Engineering* 176 (2019), p. 107341. DOI: 10.1016/J.COMPOSITESB.2019.107341.

[159] J. W. Lee, P. X. Lan, B. Kim, G. Lim, and D.-W. Cho. "3D scaffold fabrication with PPF/DEF using micro-stereolithography." In: *Microelectronic Engineering* 84.5-8 (2007), pp. 1702–1705. DOI: 10.1016/J.MEE.2007.01.267.

[160] K. Lee. "Two-Section Simulated Moving-Bed Process." In: *Separation Science and Technology* 35.4 (2000), pp. 519–534. ISSN: 1520-5754. DOI: 10.1081/SS-100100173.

[161] K. Lee. "Two-Section Simulated Moving-Bed Process." In: *Separation Science and Technology* 35.4 (2000), pp. 519–534. DOI: 10.1081/SS-100100173.

[162] S. L. Lee, T. F. O'Connor, X. Yang, C. N. Cruz, S. Chatterjee, R. D. Madurawe, C. M. V. Moore, L. X. Yu, and J. Woodcock. "Modernizing Pharmaceutical Manufacturing: from Batch to Continuous Production." In: *Journal of Pharmaceutical Innovation* 10.3 (2015), pp. 191–199. ISSN: 1872-5120. DOI: 10.1007/s12247-015-9215-8.

[163] B. Leukers, H. Gülkan, S. H. Irsen, S. Milz, C. Tille, M. Schieker, and H. Seitz. "Hydroxyapatite scaffolds for bone tissue engineering made by 3D printing." In: *Journal of Materials Science: Materials in Medicine* 16.12 (2005), pp. 1121–1124. DOI: 10.1007/s10856-005-4716-5.

[164] G. W. Litman, J. P. Rast, and S. D. Fugmann. "The origins of vertebrate adaptive immunity." In: *Nature Reviews Immunology* 10.8 (2010), pp. 543–553. ISSN: 1474-1733. DOI: 10.1038/nri2807.

[165] O. Ludemann-Hombourger, R. M. Nicoud, and M. Bailly. "The "VARICOL" Process: A New Multicolumn Continuous Chromatographic Process." In: *Separation Science and Technology* 35.12 (2000), pp. 1829–1862. ISSN: 0149-6395. DOI: 10.1081/SS-100100622.

[166] E. Mahajan, A. George, and B. Wolk. "Improving affinity chromatography resin efficiency using semi-continuous chromatography." In: *Journal of Chromatography A* 1227 (2012), pp. 154–162. ISSN: 0021-9673. DOI: 10.1016/J.CHROMA.2011.12.106.

[167] N. Mahmud, D. Klipa, and N. Ahsan. "Antibody immunosuppressive therapy in solid-organ transplant." In: *mAbs* 2.2 (2010), pp. 148–156. DOI: 10.4161/mabs.2.2.11159.

[168] K. Malik. *Human Development Report 2013: The Rise of the South: Human Progress in a Diverse World*. Tech. rep. NY (NY): United Nations Development Programme, 2013, p. 216. URL: http://hdr.undp.org/sites/default/files/reports/14/hdr2013{_}en{_}complete.pdf.

[169] S. Matysik, C. I. Le Roy, G. Liebisch, and S. P. Claus. "Metabolomics of fecal samples: A practical consideration." In: *Trends in Food Science & Technology* 57 (2016), pp. 244–255. DOI: 10.1016/J.TIFS.2016.05.011.

[170] J. T. McCue. "Theory and Use of Hydrophobic Interaction Chromatography in Protein Purification Applications." In: *Methods in Enzymology: Guide to Protein Purification*. Ed. by R. R. Burgess and M. P. Deutscher. 2nd. Academic Press, 2009. Chap. 25, pp. 405–414. ISBN: 978-0-12-374978-9.

[171] J. P. Meissner and G. Carta*. "Continuous Regioselective Enzymatic Esterification in a Simulated Moving Bed Reactor." In: *Industrial & Engeneering Chemistry Research* 41.19 (2002), pp. 4722–4732. DOI: 10.1021/IE0202625.

[172] F. Melchels, P. S. Wiggenhauser, D. Warne, M. Barry, F. R. Ong, W. S. Chong, D. W. Hutmacher, and J.-T. Schantz. "CAD/CAM-assisted breast reconstruction." In: *Biofabrication* 3.3 (2011), p. 034114. DOI: 10.1088/1758-5082/3/3/034114.

[173] F. P. Melchels, J. Feijen, and D. W. Grijpma. "A review on stereolithography and its applications in biomedical engineering." In: *Biomaterials* 31.24 (2010), pp. 6121–6130. ISSN: 01429612. DOI: 10.1016/j.biomaterials.2010.04.050. URL: http://dx.doi.org/10.1016/j.biomaterials.2010.04.050.

[174] L. Miller, C. Grill, T. Yan, O. Dapremont, and E. Huthmann. "Batch and simulated moving bed chromatographic resolution of a pharmaceutical racemate." In: *Journal of Chromatography A* 1006 (2003), pp. 267–280.

[175] K. G. Mostafa, C. Montemagno, and A. J. Qureshi. "Strength to cost ratio analysis of FDM Nylon 12 3D Printed Parts." In: *Procedia Manufacturing* 26 (2018), pp. 753–762. DOI: 10.1016/J.PROMFG.2018.07.086.

[176] J. P. Mota and J. M. Araújo. "Single-column simulated-moving-bed process with recycle lag." In: *AIChE Journal* 51.6 (2005), pp. 1641–1653. ISSN: 00011541. DOI: 10.1002/aic.10426.

[177] J. P. F.-U. Mota. *Cromatografia em Leito Móvel Simulado: Avanços recentes*. Tech. rep. Caparica: Faculdade de Ciências e Tecnologia - Universidade Nova de Lisboa, 2007, p. 47.

[178] T. Müller-Späth, L. Aumann, G. Ströhlein, and M. Morbidelli. "Improvement of specific monoclonal antibody (mAb) activity by reduction of the mAb heterogeneity using continuous chromatography (MCSGP)." In: *New Biotechnology* 25 (2009), S187. ISSN: 1871-6784. DOI: 10.1016/J.NBT.2009.06.740.

[179] T. Müller-Späth, M. Krättli, L. Aumann, G. Ströhlein, and M. Morbidelli. "Increasing the activity of monoclonal antibody therapeutics by continuous chromatography (MCSGP)." In: *Biotechnology and Bioengineering* 107.4 (2010), pp. 652–662. ISSN: 00063592. DOI: 10.1002/bit.22843.

[180] T. Müller-Späth, L. Aumann, G. Ströhlein, H. Kornmann, P. Valax, L. Delegrange, E. Charbaut, G. Baer, A. Lamproye, M. Jöhnck, M. Schulte, and M. Morbidelli. "Two step capture and purification of IgG2 using multicolumn countercurrent solvent gradient purification (MCSGP)." In: *Biotechnology and Bioengineering* 107.6 (2010), pp. 974–984. ISSN: 00063592. DOI: 10.1002/bit.22887.

[181] T. Müller-Späth and M. Morbidelli. "Multicolumn Countercurrent Gradient Chromatography for the Purification of Biopharmaceuticals." In: *Continuous Processing in Pharmaceutical Manufacturing*. Weinheim, Germany: Wiley-VCH Verlag GmbH & Co. KGaA, 2014. Chap. 10, pp. 227–254. DOI: 10.1002/9783527673681.ch10.

[182] T. Müller-Späth, L. Aumann, L. Melter, G. Ströhlein, and M. Morbidelli. "Chromatographic separation of three monoclonal antibody variants using multicolumn countercurrent solvent gradient purification (MCSGP)." In: *Biotechnology and Bioengineering* 100.6 (2008), pp. 1166–1177. ISSN: 00063592. DOI: 10.1002/bit.21843.

[183] T. Müller-Späth, L. Aumann, and M. Morbidelli. "Role of Cleaning-in-Place in the Purification of mAb Supernatants Using Continuous Cation Exchange Chromatography." In: *Separation Science and Technology* 44.1 (2009), pp. 1–26. ISSN: 1520-5754. DOI: 10.1080/01496390802581243.

[184] S. Mun, Y. Xie, and N.-H. L. Wang. "Residence time distribution in a size-exclusion SMB for insulin purification." In: *AIChE Journal* 49.8 (2003), pp. 2039–2058. ISSN: 00011541. DOI: 10.1002/aic.690490814.

[185] S. Nawada, S. Dimartino, and C. Fee. "Dispersion behavior of 3D-printed columns with homogeneous microstructures comprising differing element shapes." In: *Chemical Engineering Science* 164 (2017), pp. 90–98. ISSN: 00092509. DOI: 10.1016/j.ces.2017.02.012.

[186] S. H. Nawada. "The Use of 3D-Printing in the Study of Chromatographic Packed Bed." PhD Thesis. University of Canterbury, Christchurch, New Zealand, 2018, p. 167.

[187] NBC2. "Downstream Processing." In: *Introduction to Biomanufacturing*. Ed. by Northeast Biomanufacturing Center & Collaborative. 1st. Northeast Biomanufacturing Center & Collaborative, 2012. Chap. 11, pp. 423–458. ISBN: 9781939070012.

[188] NBC2. "Upstream Processing." In: *Introduction to Biomanufacturing*. Ed. by N. B. C. &. Collaborative. 1st. Northeast Biomanufacturing Center & Collaborative, 2012. Chap. 10, pp. 379–422. ISBN: 9781939070012.

[189] S. Ndoja and H. Lima. "Monoclonal Antibodies." In: *Current Developments in Biotechnology and Bioengineering: Human and Animal Health Applications*. Ed. by V. Thomaz-Soccol, A. Pandey, and R. R. Resende. 1st ed. Elsevier, 2016. Chap. 4th, pp. 71–96. ISBN: 9780444636607. DOI: 10.1016/C2014-0-04871-X.

[190] M. Negawa and F. Shoji. "Optical resolution by simulated moving-bed adsorption technology." In: *Journal of Chromatography A* 590.1 (1992), pp. 113–117. ISSN: 00219673. DOI: 10.1016/0021-9673(92)87011-V.

[191] A. L. Nelson, E. Dhimolea, and J. M. Reichert. "Development trends for human monoclonal antibody therapeutics." In: *Nature Reviews Drug Discovery* 9.10 (2010), pp. 767–774. ISSN: 1474-1776. DOI: 10.1038/nrd3229.

[192] P. Nestola, R. J. Silva, C. Peixoto, P. M. Alves, M. J. Carrondo, and J. P. Mota. "Adenovirus purification by two-column, size-exclusion, simulated countercurrent chromatography." In: *Journal of Chromatography A* 1347 (2014), pp. 111–121. ISSN: 18733778. DOI: 10.1016/j.chroma.2014.04.079. URL: http://dx.doi.org/10.1016/j.chroma.2014.04.079.

[193] P. Nestola, R. J. S. Silva, C. Peixoto, P. M. Alves, M. J. T. Carrondo, and J. P. B. Mota. "Robust design of adenovirus purification by two-column, simulated moving-bed, size-exclusion chromatography." In: *Journal of Biotechnology* 213 (2015), pp. 109–119. ISSN: 18734863. DOI: 10.1016/j.jbiotec.2015.01.030.

[194] C. K. Ng, H. Osuna-Sanchez, E. Valéry, E. Sørensen, and D. G. Bracewell. "Design of high productivity antibody capture by protein A chromatography using an integrated experimental and modeling approach." In: *Journal of Chromatography B* 899 (2012), pp. 116–126. DOI: 10.1016/j.jchromb.2012.05.010.

[195] R.-M. Nicoud, G. Fuchs, P. Adam, M. Bailly, E. Küsters, F. D. Antia, R. Reuille, and E. Schmid. "Preparative scale enantioseparation of a chiral epoxide: Comparison of liquid chromatography and simulated moving bed adsorption technology." In: *Chirality* 5.4 (1993), pp. 267–271. ISSN: 08990042. DOI: 10.1002/chir.530050415.

[196] C. Ó'Fágáin, P. M. Cummins, and B. F. O'Connor. "Gel-Filtration Chromatography." In: *Protein Chromatography: Methods and Protocols*. Ed. by D. Walls and S. Loughran. Vol. 681. Humana Press, 2011. Chap. 2nd, pp. 25–33. ISBN: 978-1-60761-912-3. DOI: 10.1007/978-1-60761-913-0.

[197] S. Olivera, H. B. Muralidhara, K. Venkatesh, and K. Gopalakrishna. "Evaluation of Surface Integrity and Strength Characteristics of Electroplated ABS Plastics Developmed Using FDM Process." In: *The 17th Asian Pacific Corrosion Control Conference* January 27-30 (2016), pp. 1–6. DOI: 10.2459/JCM.0b013e328011c256.

[198] R. Otto, A. Santagostino, and U. Schrader. "Rapid growth in biopharma : Challenges and opportunities." In: *From Science to Operations: Questions, Choices and Strategies for Success in Biopharma*. Ed. by R. Otto, A. Santagostino, and U. Schrader. McKinsey & Company, 2014, pp. 1–21.

[199] K. P. Clapp, A. Castan, and E. K. Lindskog. "Upstream Processing Equipment." In: *Biopharmaceutical Processing*. Ed. by G. Jagschies, E. Lindskog, K. Łącki, and P. Galliher. Elsevier, 2018. Chap. 24, pp. 457–476. ISBN: 9780081006238. DOI: https://doi.org/10.1016/B978-0-08-100623-8.00024-4.

[200] M. M. Papathanasiou, F. Steinebach, G. Stroehlein, T. Müller-Späth, I. Nascu, R. Oberdieck, M. Morbidelli, A. Mantalaris, and E. N. Pistikopoulos. "A control strategy for periodic systems – application to the twin-column MCSGP." In: *Computer Aided Chemical Engineering* 37 (2015), pp. 1505–1510. ISSN: 1570-7946. DOI: 10.1016/B978-0-444-63577-8.50096-6.

[201] C. Parra-Cabrera, C. Achille, S. Kuhn, and R. Ameloot. "3D printing in chemical engineering and catalytic technology: Structured catalysts, mixers and reactors." In: *Chemical Society Reviews* 47.1 (2018), pp. 209–230. ISSN: 14604744. DOI: 10.1039/c7cs00631d.

[202] J. L. Parsons and J. R. Campbell. "Digital Apparel Design Process: Placing a New Technology Into a Framework for the Creative Design Process." In: *Clothing and Textiles Research Journal* 22.1-2 (2004), pp. 88–98. DOI: 10/fp3dgg.

[203] W. E. Paul. "Bridging innate and adaptive immunity." In: *Cell* 147.6 (2011), pp. 1212–5. ISSN: 1097-4172. DOI: 10.1016/j.cell.2011.11.036.

[204] D. L. Pavia and G. M. Lampman. *Introduction to organic laboratory techniques : a microscale approach*. 4th. Thomson Brooks/Cole, 2006, p. 1008. ISBN: 9780495016304.

[205] A. K. Pavlou and J. M. Reichert. "Recombinant protein therapeutics - success rates, market trends and values to 2010." In: *Nature Biotechnology* 22.12 (2004), pp. 1513–1519. ISSN: 1087-0156. DOI: 10.1038/nbt1204-1513.

[206] S. W. Pettersson. "High-Resolution Reversed-phase Chromatography of Proteins." In: *Protein Purification: Principles, High Resolution Methods, and Applications*. Ed. by J.-C. Janson. 3rd. Wiley, 2011. Chap. 5, pp. 136–163. ISBN: 978-0-471-74661-4.

[207] D. Pfister, L. Nicoud, and M. Morbidelli. *Continuous Biopharmaceutical Processes*. Cambridge University Press, 2018. ISBN: 9781108332897. DOI: 10/dc4r.

[208] Pharmaceutical Research and Manufacturers of America. *Medicines in development: Biologics 2013 Report*. Tech. rep. Washington, DC: Pharmaceutical Research and Manufacturers of America, 2013. URL: http://phrma-docs.phrma.org/sites/default/files/pdf/biologics2013.pdf.

[209] G. Policarpo. "Nucleosides Separation by Reversed-Phase, Single-column Chromatography with Recycle Lag." Master Thesis. Faculdade de Ciências e Tecnologia - Universidade NOVA de Lisboa, 2018, p. 51.

[210] J. Pollock, J. Coffman, S. V. Ho, and S. S. Farid. "Integrated continuous bioprocessing: Economic, operational, and environmental feasibility for clinical and commercial antibody manufacture." In: *Biotechnology Progress* 33.4 (2017), pp. 854–866. ISSN: 87567938. DOI: 10.1002/btpr.2492.

[211] Process Systems Enterprise. *PSE: gPROMS ModelBuilder*. 2019. URL: https://www.psenterprise.com/products/gproms/modelbuilder (visited on 08/31/2019).

[212] J. Queiroz, C. Tomaz, and J. Cabral. "Hydrophobic interaction chromatography of proteins." In: *Journal of Biotechnology* 87.2 (2001), pp. 143–159. ISSN: 0168-1656. DOI: 10.1016/S0168-1656(01)00237-1.

[213] S. Rabindran and V. Yusibov. "Novel Expression Systems for Vaccine Production." In: *Vaccine Development and Manufacturing*. Ed. by E. P. Wen, R. Ellis, and N. Pujar. Hoboken, NJ, USA: John Wiley & Sons, Inc., 2014, pp. 81–95. DOI: 10.1002/9781118870914.ch4.

[214] R. Rader and E. Langer. *TOP 1000 Global Biopharmaceutical Facilities Index*. 2018. URL: http://top1000bio.com/ (visited on 12/06/2018).

[215] R. A. Rader. *BIOPHARMA: Biopharmaceutical Products in the U.S. and European Markets*. URL: http://biopharma.com/ (visited on 12/04/2018).

[216] R. A. Rader and Biotechnology Information Institute. *BIOPHARMA : Biopharmaceutical Products in the U.S. Market*. 2nd. Biotechnology Information Institute, 2003, p. 654. ISBN: 0963957325.

[217] R. A. Rader and E. Langer. "Fifteen years of progress: Biopharmaceutical industry survey results." In: *Pharmaceutical Technology* 42.7 (2018), pp. 56–59. ISSN: 19391862.

[218] A. Ramos. *CCS System Modelling Toolkit (SMTK) Project*. Tech. rep. Energy Technologies Institute, 2017, p. 34. URL: https://d2umxnkyjne36n.cloudfront.net/documents/10YoI_CCS_AlfredoRamos_PSE.pdf?mtime=20171124095223.

[219] J. M. Reichert. "Antibodies to watch in 2016." In: *mAbs* 8.2 (2016), pp. 197–204. DOI: 10.1080/19420862.2015.1125583.

[220] C. Reis, A. Landim, and J. P. Pieroni. "Lições da experiência internacional e propostas para incorporação da rota biotecnológica na indústria farmacêutica brasileira." In: *BNDES Setorial* 34 (2011), pp. 5–44.

[221] F. Rengier, A. Mehndiratta, H. von Tengg-Kobligk, C. M. Zechmann, R. Unterhinninghofen, H.-U. Kauczor, and F. L. Giesel. "3D printing based on imaging data: review of medical applications." In: *International Journal of Computer Assisted Radiology and Surgery* 5.4 (2010), pp. 335–341. DOI: 10.1007/s11548-010-0476-x.

[222] A. E. Rodrigues, C. Pereira, M. Minceva, A. M. Pais, A. Ribeiro, M. Silva, N. Graça, and J. C. Santos. *Simulated Moving Bed Technology: Principles, Design and Process Applications*. Butterworth-Heinemann, 2015, p. 304. ISBN: 978-0-12-802024-1. DOI: https://doi.org/10.1016/C2013-0-19564-5.

[223] R. C. R. Rodrigues, J. Araújo, and P. B. Mota. "Optimization and Experimental Validation of SMB Cascade Schemes and JO Process for Ternary Separation." In: *9th International Conference on Fundamentals of Adsorption (FOA)*. Giardini Naxos, Sicily - Italy, 2007.

[224] R. C. d. R. Rodrigues. "Compact SMB Chromatography for Binary Separation." phD Thesis. Faculdade de Ciências e Tecnologia - Universidade Nova de Lisboa, 2009, p. 176.

[225] R. C. Rodrigues, J. M. Araújo, M. F. Eusébio, and J. P. Mota. "Experimental assessment of simulated moving bed and varicol processes using a single-column setup." In: *Journal of Chromatography A* 1142.1 (2007), pp. 69–80. ISSN: 0021-9673. DOI: 10.1016/J.CHROMA.2006.10.044.

[226] R. C. Rodrigues, J. M. Araújo, and J. P. Mota. "Optimal design and experimental validation of synchronous, asynchronous and flow-modulated, simulated moving-bed processes using a single-column setup." In: *Journal of Chromatography A* 1162.1 SPEC. ISS. (2007), pp. 14–23. ISSN: 00219673. DOI: 10.1016/j.chroma.2007.01.103.

[227] R. C. Rodrigues, T. J. Canhoto, J. M. Araújo, and J. P. Mota. "Two-column simulated moving-bed process for binary separation." In: *Journal of Chromatography A* 1180.1-2 (2008), pp. 42–52. ISSN: 00219673. DOI: 10.1016/j.chroma.2007.11.106.

[228] R. C. Rodrigues, R. J. Silva, and J. P. Mota. "Streamlined, two-column, simulated countercurrent chromatography for binary separation." In: *Journal of Chromatography A* 1217.20 (2010), pp. 3382–3391. ISSN: 00219673. DOI: 10.1016/j.chroma.2010.03.009.

[229] A. C. A. Roque, C. R. Lowe, and M. Â. Taipa. "Antibodies and genetically engineered related molecules: Production and purification." In: *Biotechnology Progress* 20.3 (2004), pp. 639–654. ISSN: 87567938. DOI: 10.1021/bp030070k.

[230] D. M. Ruthven and C. Ching. "Counter-current and simulated counter-current adsorption separation processes." In: *Chemical Engineering Science* 44.5 (1989), pp. 1011–1038. ISSN: 0009-2509. DOI: 10.1016/0009-2509(89)87002-2.

[231] C. Salmean and S. Dimartino. "3D-Printed Stationary Phases with Ordered Morphology: State of the Art and Future Development in Liquid Chromatography." In: *Chromatographia* 82.1 (2019), pp. 443–463. DOI: 10.1007/s10337-018-3671-5.

[232] T. Sandle. "FDA issues revised guidance for analytical method validation." In: *GMP Review* 14.3 (2015), pp. 8–10.

[233] D. Sawyer, K. Sanderson, R. Lu, T. Daszkowski, E. Clark, P. Mcduff, J. Astrom, C. Heffernan, L. Duffy, S. Poole, T. Ryll, P. Sheehy, D. Strachan, J. Souquet, D. Beattie, D. Pollard, O. Stauch, P. Bezy, T. Sauer, L. Boettcher, C. Simpson, J. Dakin, S. Pitt, and A. Boyle. *Biomanufacturing Technology Roadmap - Overview*. Tech. rep. BioPhorum Operations Group, 2017, pp. 1–48. URL: https://www.biophorum.com/wp-content/uploads/2017/07/SupplyPartMgmnt.pdf.

[234] S.C. Stinson. "Chiral drugs: Sistema de descoberta para FCCN." In: *Chemical and Engineering News* 73(41) (1995), p. 44.

[235] H. Schellekens. "Follow-on biologics: challenges of the 'next generation'." In: *Nephrology Dialysis Transplantation* 20.suppl_4 (2005), pp. iv31–iv36. ISSN: 1460-2385. DOI: 10.1093/ndt/gfh1085.

[236] H. Schramm, M. Kaspereit, A. Kienle, and A. Seidel-Morgenstern. "Improving Simulated Moving Bed Processes by Cyclic Modulation of the Feed Concentration." In: *Chemical Engineering & Technology* 25.12 (2002), pp. 1151–1155. ISSN: 09307516. DOI: 10.1002/1521-4125(20021210)25:12<1151::AID-CEAT1151>3.0.CO;2-Y.

[237] H Schramm, A Kienle, M Kaspereit, and A Seidel-Morgenstern. "Improved operation of simulated moving bed processes through cyclic modulation of feed dow and feed concentration." In: *Chemical Engineering Science* 58 (2003), pp. 5217–5227. DOI: 10.1016/j.ces.2003.08.015.

[238] H. Schramm, S. Grüner, and A. Kienle. "Optimal operation of simulated moving bed chromatographic processes by means of simple feedback control." In: *Journal of Chromatography A* 1006.1-2 (2003), pp. 3–13. ISSN: 0021-9673. DOI: 10.1016/S0021-9673(03)00946-4.

[239] H. Schramm, M. Kaspereit, A. Kienle, and A. Seidel-Morgenstern. "Simulated moving bed process with cyclic modulation of the feed concentration." In: *Journal of chromatography. A* 1006.1-2 (2003), pp. 77–86. ISSN: 0021-9673. DOI: https://doi.org/10.1016/S0021-9673(03)00327-3.

[240] A. M. Scott, J. P. Allison, and J. D. Wolchok. *Monoclonal antibodies in cancer therapy*. Tech. rep. 2012, p. 14. URL: www.cancerimmunity.org.

[241] Sigma Aldrich. *Uridine: Product Information Sheet*. Tech. rep. Missourini, USA: Sigma Aldrich, 2019, p. 2. URL: https://www.sigmaaldrich.com/content/dam/sigma-aldrich/docs/Sigma/Product{_}Information{_}Sheet/1/u3750pis.pdf.

[242] R. J. S. Silva, R. C. R. Rodrigues, H. Osuna-Sanchez, M. Bailly, E. Valery, and J. P. B. Mota. "A new multicolumn, open-loop process for center-cut separation by solvent-gradient chromatography." In: *Journal of Chromatography A* 1217.52 (2010), pp. 8257–8269. ISSN: 00219673. DOI: 10.1016/j.chroma.2010.11.005.

[243] R. Singh, J. Singh, and S. Singh. "Investigation for dimensional accuracy of AMC prepared by FDM assisted investment casting using nylon-6 waste based reinforced filament." In: *Measurement* 78 (2016), pp. 253–259. DOI: 10.1016/J.MEASUREMENT.2015.10.016.

[244] S. Skogestad. *Chemical and Energy Process Engineering*. 1. 2014, pp. 1–5. ISBN: 9780874216561. DOI: 10.1007/s13398-014-0173-7.2. arXiv: arXiv:1011.1669v3.

[245] Solutions. *3D Systems: Solutions by Applications*. URL: https://www.3dsystems.com/solutions (visited on 09/09/2019).

[246] J. G. Speight. "Sources and Types of Inorganic Pollutants." In: *Environmental Inorganic Chemistry for Engineers*. Laramie, Wyoming, United States: Butterworth-Heinemann, 2017. Chap. 5, pp. 231–282. ISBN: 978-0-12-849891-0. DOI: 10.1016/B978-0-12-849891-0.00005-9.

[247] R. Srinivasan and E. Ruckenstein. "Role of Physical Forces in Hydrophobic Interaction Chromatography." In: *Separation and Purification Methods* 9.2 (1980), pp. 267–370. ISSN: 0360-2540. DOI: 10.1080/03602548008066002.

[248] F. Steinebach, T. Müller-Späth, and M. Morbidelli. "Continuous counter-current chromatography for capture and polishing steps in biopharmaceutical production." In: *Biotechnology Journal* 11.9 (2016), pp. 1126–1141. ISSN: 18606768. DOI: 10.1002/biot.201500354.

[249] F. Steinebach, N. Ulmer, M. Wolf, L. Decker, V. Schneider, R. Wälchli, D. Karst, J. Souquet, and M. Morbidelli. "Design and operation of a continuous integrated monoclonal antibody production process." In: *Biotechnology Progress* 33.5 (2017), pp. 1303–1313. ISSN: 87567938. DOI: 10.1002/btpr.2522.

[250] F. Steinebach, N. Ulmer, L. Decker, L. Aumann, and M. Morbidelli. "Experimental design of a twin-column countercurrent gradient purification process." In: *Journal of Chromatography A* 1492 (2017), pp. 19–26. ISSN: 0021-9673. DOI: 10.1016/J.CHROMA.2017.02.049.

[251] G. Storti, M. Mazzotti, M. Morbidelli, and S. Carrà. "Robust design of binary countercurrent adsorption separation processes." In: *AIChE Journal* 39.3 (1993), pp. 471–492. ISSN: 0001-1541. DOI: 10.1002/aic.690390310.

[252] G. Ströhlein, L. Aumann, M. Mazzotti, and M. Morbidelli. "A continuous, countercurrent multi-column chromatographic process incorporating modifier gradients for ternary separations." In: *Journal of Chromatography A* 1126.1-2 (2006), pp. 338–346. ISSN: 0021-9673. DOI: 10.1016/J.CHROMA.2006.05.011.

[253] G. Ströhlein, T. Müller-Späth, and L. Aumann. "Continuous Chromatography (Multicolumn Countercurrent Solvent Gradient Purification) for Protein Purification." In: *Biopharmaceutical Production Technology*. Ed. by G. Subramanian. Weinheim, Germany: Wiley-VCH Verlag GmbH & Co. KGaA, 2012. Chap. 4, pp. 107–137. ISBN: 9783527653096. DOI: 10.1002/9783527653096.ch4.

[254] J. Strube, S. Haumreisser, H. Schmidt-Traub, M. Schulte, and R. Ditz. "Comparison of batch elution and continuous simulated moving bed chromatography." In: *Organic Process Research and Development* 2.5 (1998), pp. 305–319. ISSN: 10836160. DOI: 10.1021/op980019a.

[255] M. D. Symes, P. J. Kitson, J. Yan, C. J. Richmond, G. J. T. Cooper, R. W. Bowman, T. Vilbrandt, and L. Cronin. "Integrated 3D-printed reactionware for chemical synthesis and analysis." In: *Nature Chemistry* 4.5 (2012), pp. 349–354. DOI: 10.1038/nchem.1313.

[256] T. Tahara, K. Usuki, H. Sato, H. Ohashi, H. Morita, H. Tsumura, A. Matsumoto, H. Miyazaki, A. Urabe, and T. Kato. "A sensitive sandwich ELISA for measuring thrombopoietin in human serum: serum thrombopoietin levels in healthy volunteers and in patients with haemopoietic disorders." In: *British Journal of Haematology* 93.4 (1996), pp. 783–788. ISSN: 0007-1048. DOI: 10.1046/j.1365-2141.1996.d01-1741.x.

[257] G. Taylor. "Dispersion of Soluble Matter in Solvent Flowing Slowly through a Tube." In: *Proceedings of the Royal Society A: Mathematical, Physical and Engineering Sciences* 219.1137 (1953), pp. 186–203. ISSN: 1364-5021. DOI: 10.1098/rspa.1953.0139. arXiv: 1402.1118.

[258] G. Taylor. "Conditions under Which Dispersion of a Solute in a Stream of Solvent can be Used to Measure Molecular Diffusion." In: *Proceedings of the Royal Society of London. Series A, Mathematical and Physical Sciences* 225.1163 (1954), pp. 473–477. ISSN: 00804630. DOI: 10.2307/99517.

[259] D. Therriault, S. R. White, and J. A. Lewis. "Chaotic mixing in three-dimensional microvascular networks fabricated by direct-write assembly." In: *Nature Materials* 2.4 (2003), pp. 265–271. DOI: 10.1038/nmat863.

[260] Thingiverse. *#3DBenchy*. 2015. URL: https://www.thingiverse.com/thing:763622 (visited on 09/11/2019).

[261] A. Toumi, S. Engell, O. Ludemann-Hombourger, R. Nicoud, and M. Bailly. "Optimization of simulated moving bed and Varicol processes." In: *Journal of Chromatography A* 1006.1-2 (2003), pp. 15–31. ISSN: 00219673. DOI: 10.1016/S0021-9673(03)00430-8.

[262] A. Toumi, F. Hanisch, and S. Engell. "Optimal operation of continuous chromatographic processes: Mathematical optimization of the VARICOL process." In: *Industrial and Engineering Chemistry Research* 41.17 (2002), pp. 4328–4337. ISSN: 08885885. DOI: 10.1021/ie0103815.

[263] C Touzeau, P Moreau, and C Dumontet. "Monoclonal antibody therapy in multiple myeloma." In: *Leukemia* 31.5 (2017), pp. 1039–1047. ISSN: 0887-6924. DOI: 10.1038/leu.2017.60.

[264] R. Trombetta, J. A. Inzana, E. M. Schwarz, S. L. Kates, and H. A. Awad. "3D Printing of Calcium Phosphate Ceramics for Bone Tissue Engineering and Drug Delivery." In: *Annals of biomedical engineering* 45.1 (2017), pp. 23–44. DOI: 10.1007/s10439-016-1678-3.

[265] M. Urh, D. Simpson, and K. Zhao. "Affinity Chromatography: General Methods." In: *Methods in Enzymology: Guide to Protein Purification*. Ed. by R. R. Burgess and M. P. Deutscher. 2nd. Academic Press, 2009. Chap. 26, pp. 417–438. ISBN: 978-0-12-374978-9.

[266] T. Vermeulen. "Separation by Adsorption Methods." In: *Advances in Chemical Engineering* 2 (1958), pp. 147–208. ISSN: 0065-2377. DOI: 10.1016/S0065-2377(08)60228-8.

[267] S. Vogg, M. K. F. Wolf, and M. Morbidelli. "Continuous and Integrated Expression and Purification of Recombinant Antibodies." In: *Recombinant Protein Expression in Mammalian Cells - Methods and Protocols*. Ed. by D. L. Hacker. Springer Nature, 2018. Chap. 11, pp. 147–178. ISBN: 978-1-4939-8729-0. DOI: https://doi.org/10.1007/978-1-4939-8730-6.

[268] D. Voisard, F. Meuwly, P.-A. Ruffieux, G. Baer, and A. Kadouri. "Potential of cell retention techniques for large-scale high-density perfusion culture of suspended mammalian cells." In: *Biotechnology and Bioengineering* 82.7 (2003), pp. 751–765. ISSN: 00063592. DOI: 10.1002/bit.10629.

[269] A. Waldbaur, H. Rapp, K. Länge, and B. E. Rapp. "Let there be chip—towards rapid prototyping of microfluidic devices: one-step manufacturing processes." In: *Analytical Methods* 3.12 (2011), p. 2681. ISSN: 1759-9660. DOI: 10.1039/c1ay05253e.

[270] G. Walsh. "Biopharmaceuticals: recent approvals and likely directions." In: *Trends in Biotechnology* 23.11 (2005), pp. 553–558. ISSN: 0167-7799. DOI: 10.1016/J.TIBTECH.2005.07.005.

[271] G. Walsh. "Biopharmaceutical benchmarks 2010." In: *Nature Biotechnology* 28.9 (2010), pp. 917–924. ISSN: 1087-0156. DOI: 10.1038/nbt0910-917.

[272] J. Walther, R. Godawat, C. Hwang, Y. Abe, and A. Sinclair. "The business impact of an integrated continuous biomanufacturing platform for recombinant protein production." In: *Journal of Biotechnology* 213 (2015), pp. 3–12. ISSN: 0168-1656. DOI: 10.1016/J.JBIOTEC.2015.05.010.

[273] P. Wang, B. Zou, H. Xiao, S. Ding, and C. Huang. "Effects of printing parameters of fused deposition modeling on mechanical properties, surface quality, and microstructure of PEEK." In: *Journal of Materials Processing Technology* 271 (2019), pp. 62–74. DOI: 10.1016/J.JMATPROTEC.2019.03.016.

[274] Y. Wang, J. Balowski, C. Phillips, R. Phillips, C. E. Sims, and N. L. Allbritton. "Benchtop micromolding of polystyrene by soft lithography." In: *Lab on a Chip* 11.18 (2011), p. 3089. ISSN: 1473-0197. DOI: 10.1039/c1lc20281b. URL: http://xlink.rsc.org/?DOI=c1lc20281b.

[275] V. Warikoo, R. Godawat, K. Brower, S. Jain, D. Cummings, E. Simons, T. Johnson, J. Walther, M. Yu, B. Wright, J. McLarty, K. P. Karey, C. Hwang, W. Zhou, F. Riske, and K. Konstantinov. "Integrated continuous production of recombinant therapeutic proteins." In: *Biotechnology and Bioengineering* 109.12 (2012), pp. 3018–3029. DOI: 10.1002/bit.24584.

[276] R. G. Werner, F. Walz, W. Noé, and A. Konrad. "Safety and economic aspects of continuous mammalian cell culture." In: *Journal of Biotechnology* 22.1-2 (1992), pp. 51–68. ISSN: 0168-1656. DOI: 10.1016/0168-1656(92)90132-S.

[277] WHO - World Health Organization. "Hepatitis B Vaccines." In: *Weekly Epidemiological Record* 84.40 (2009), pp. 405–420. URL: http://www.who.int/wer.

[278] M. Wilchek and I. Chaiken. "An Overview of Affinity Chromatography." In: *Affinity Chromatography: Methods and Protocols*. Ed. by P. Bailon, G. Ehrlich, W. Fung, and W. Berthold. Humana Press, 2000. Chap. 1st, pp. 1–6. ISBN: 978-1-60327-261-2. DOI: 10.1007/978-1-60327-261-2_1.

[279] S.-L. Wu, W. S. Hancock, B. Pavlu, and P. Gellerfors. "Application of high-performance hydrophobic-interaction chromatography to the characterization of recombinant DNA-derived human growth hormone." In: *Journal of Chromatography A* 500 (1990), pp. 595–606. ISSN: 0021-9673. DOI: 10.1016/S0021-9673(00)96094-1.

[280] A. Xenopoulos. "A new, integrated, continuous purification process template for monoclonal antibodies: Process modeling and cost of goods studies." In: *Journal of Biotechnology* 213 (2015), pp. 42–53. ISSN: 0168-1656. DOI: 10.1016/J.JBIOTEC.2015.04.020.

[281] C. Yong Chin, N.-H. Linda Wang, C. Y. Chin, and N. H. L. Wang. "Simulated moving bed equipment designs." In: *Separation and Purification Reviews* 33.2 (2004), pp. 77–155. ISSN: 15422119. DOI: 10.1081/SPM-200042081.

[282] D.-G. Yu, C. Branford-White, Z.-H. Ma, L.-M. Zhu, X.-Y. Li, and X.-L. Yang. "Novel drug delivery devices for providing linear release profiles fabricated by 3DP." In: *International Journal of Pharmaceutics* 370.1-2 (2009), pp. 160–166. DOI: 10.1016/j.ijpharm.2008.12.008.

[283] Y. Zang and P. C. Wankat*. "SMB Operation Strategy - Partial Feed." In: *Industrial & Engeneering Chemistry Research* 41.10 (2002), pp. 2504–2511. DOI: 10.1021/IE010832L.

[284] Y. Zang and P. C. Wankat. "Three-zone simulated moving bed with partial feed and selective withdrawal." In: *Industrial and Engineering Chemistry Research* 41.21 (2002), pp. 5283–5289. ISSN: 08885885. DOI: 10.1021/ie020052s.

[285] Z. Zguris. "How Mechanical Properties of Stereolithography 3D Prints are Affected by UV Curing." In: *Formlabs White Paper* (2016), pp. 1–11. URL: https://formlabs.com/media/upload/How-Mechanical-Properties-of-SLA-3D-Prints-Are-Affected-by-UV-Curing.pdf.

[286] Y. Zhang, C. Purssell, K. Mao, and S. Leigh. "A physical investigation of wear and thermal characteristics of 3D printed nylon spur gears." In: *Tribology International* (2019), p. 105953. DOI: 10.1016/J.TRIBOINT.2019.105953.

[287] Z. Zhang, M. Mazzotti, and M. Morbidelli. "PowerFeed operation of simulated moving bed units: changing flow-rates during the switching interval." In: *Journal of chromatography. A* 1006.1-2 (2003), pp. 87–99. ISSN: 0021-9673. DOI: https://doi.org/10.1016/S0021-9673(03)00781-7.

[288] Z. Zhang, M. Morbidelli, and M. Mazzotti. "Experimental Assessment of PowerFeed Chromatography." In: *AIChE Journal* 50.3 (2004), pp. 625–632. DOI: 10.1002/aic.10056.

APPENDIX A

A.1 Publications Regarding Monocolumn Chromatographic Processes Similar to SMB

Evolution of the publications about the processes development for biomolecules separation and purification that use only one chromatographic column to mimic SMB operation, where it is observed that only two research groups have already approached systems of just one chromatographic column analogous to SMB, and the investigations occurred in a short period of time, from 2003 to 2007.

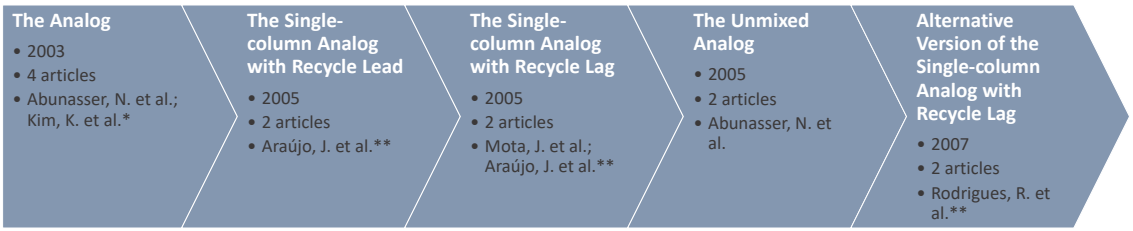

Figure A.1: Publications regarding monocolumn chromatographic processes similar to SMB for biomolecules separation/purification. They are separated by developed process, initial publication date, number of articles published about this method and respective responsible author. Data obtained from research done in b-on. *Author belongs to the research group of Professor Dr. Nadia Abunasser (School of Chemical Engineering, Purdue University, West Lafayette, IN, US). **Author belonging to the research group of Professor Dr. José Paulo Mota (Department of Chemical Engineering, Faculdade de Ciências e Tecnologia, Universidade Nova de Lisboa, Caparica, PT).

A.2 Piston Mounting Protocol

Recycle-device assembly steps assist the researcher in avoiding mounting errors, as well as facilitating the execution of this task. The steps are as follows:

1. Fit the frits: For this purpose, the acetal parts that receive the frits (top cover and movable piston) must be heated on the heating plate, in order to dilate these parts, and the frits should be placed in the freezer for about 20 minutes, in order to contract them;

2. Place the movable piston at the top of the device, with the glass column completely empty of any liquid. The movable piston hole must be closed with a fitting that prevents liquid from passing from section A to section B;

3. After being able to fit the movable plunger and unable to push it further by hand, due to the frictional resistance between the o-rings and the column glass, fill section A with a fluid (usually ethanol 5% v/v in deionized water) until the upper edges of the column and ensure that no bubbles remain in this section;

4. Close the device top and turn on the liquid pump in order to push down the movable plunger to a height that will allow to connect the capillary from the movable plunger to the bottom of the device;

5. Check that there is no leakage at both ends of the capillary;

6. Fill the bottom (section B) of the piston with the same 5% ethanol solution;

7. Close the bottom of the piston, ensuring that there is no bubble inside the section. To close the inner and outer parts, the outer fittings should be removed to reduce pressure and consequent force to be exerted by the person that is closing them;

8. If any bubbles are left in Section A, reopen the top, add 5% ethanol and ensure there are no internal bubbles.

A.3 Relationship between Relays and Pneumatic Valves

The two OptoRLY88 relay boards are addressed by matching each relay to a pneumatic valve. There are 16 on-off valves successfully installed to the boards. However, only 7 are currently required for the setup.

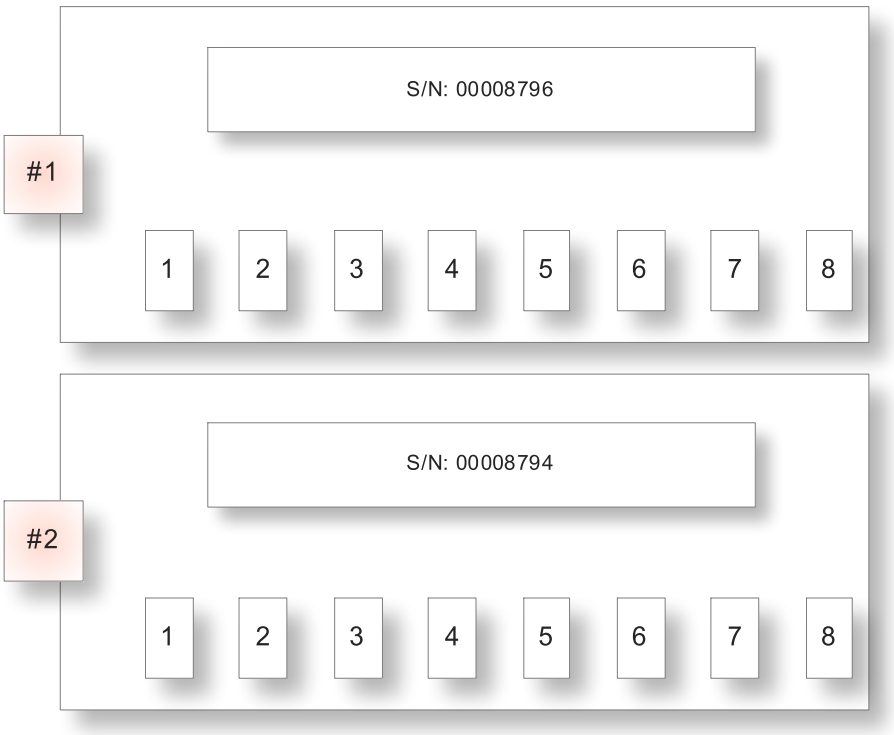

Supply Cable								
	Valve	8	7	6	5	4	3	2	1
	Board	#1	#1	#1	#1	#2	#2	#2	#2
	Relay	2	4	6	8	2	4	6	8
	Valve	16	15	14	13	12	11	10	9
	Board	#1	#1	#1	#1	#2	#2	#2	#2
	Relay	1	3	5	7	1	3	5	7

Figure A.2: Schematic of correspondence between Relays and Pneumatic Valves. The setup has two boards, even though only one is required. Each board has eight relays, and each relay corresponds to one on-off valve.

A.4 Specification of prototype components, proposals from suppliers and costs

Table A.1: Identification of components for the Single-column with Recycle Lag Prototype (see Figure 3.9), possible suppliers and costs. Items #16 and #17 are specific to the separation process discussed in the following chapter.

#	Component	Quant.	Supplier	Product designation	Technical information	Dimensions (mm)	Cost (€)	Drawing
1	Recycle Piston	1	Essential Life Solutions Ltd.	(Part No. A-25/125-CUSTOM-FCT-UNC)	Max Pressure: 24 bar; Temperature Range: 4-40 °C; Tubing Connections: 1/16"; Body: Borosilicate Glass; Pistons All: Acetal; O-Rings: EPDM; Frits: Polyethylene.	125x25 (L x ID)	4442.33	
2	Smartline Pump 100	1	Knauer	10 mL pump head (Part No. V5010A)	Temp. range: 4-40 °C; Flow rate range: 0.001–9.999 mL/min; Max. Pressure: 40 MPa up to 10 mL/min; Isocratic HPLC pump; RS-232.	220x110x130 (Length x Width x Height)	3806.00	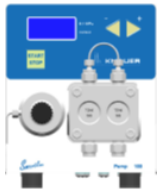
3	HPLC-Pump K-501	2	Knauer	10 mL pump head (Part No. V7543)	Same as #1.	345x105x185 (L x W x H)	4280.00 x 2	
4	Digital Scale	1	Sartorius	(Part No. TE3102S)	Weighing capacity: 3100 g; Allowable ambient operating temperature: 5-40 °C; Response time (average): 2.5 s; Readability: 0.01 g; Repatability: 0.01 g.	270x200x70 (L x W x H)	910.15	

(Table A.1 – continued)

#	Component	Quant.	Supplier	Product designation	Technical information	Dimensions (mm)	Cost (€)	Drawing
5	UV-VIS-NIR Lightsource	1	Ocean Optics	(Part No. DH-2000)	Sources: Deep-UV Deuterium & ; Tungsten Halogen; Wavelength range: 190-2500 nm; Output: Continuous.	285x150x135 (L x W x H)	3423.23	
6	Spectrometer	2	Ocean Optics	(Part No. USB4000-UV-VIS)	Wavelength range: 200-850 nm; Integration time: 3.8 ms-10 s.	89.1x63.3x34.4 (L x W x H)	3840.92 x 2	
7	Flow Cell UV	2	Icon Scientific	(Part No. A4044)	Capillary Connection: 1/16"; Path Length: 3mm; Flow Cell Volume: 2μL; Max Pressure: 300 bar; Max Flow Rate: 50 mL/min; Wetted Materials: Stainless Steel.	52x52x17 (L x W x H)	1144.00 x 2	
8	On-off Valve	7	VICI Valco	(Part No. ASFVO)	Air actuated; Fitting: 1/16"; Bore: 0.50 mm; Max. Pressure: 689.5 bar; Max. Temperature: 100 °C.	100x63 (L x OD)	134.66 x 7	

(Table A.1 – continued)

#	Component	Quant.	Supplier	Product designation	Technical information	Dimensions (mm)	Cost (€)	Drawing
9	2-pos-6-port Switching Valve	1	Rheodyne	(Part No. 7010)	2 Position, 6 Port Injector; Connection Dimension: 1/16"; Stainless Tubing; Max. Pressure: 480 bar; Max. Temperature: 150 °C.	75x34x27 (L x OD x Lever Length)	836.85	
10	2-pos-6-port HPLC valve	2	VICI Valco	Model EHMA (Part No. EPC6W)	2 Position Electric Actuator; 6 Port; Max. Pressure: 344.7 bar; Max. Temperatue: 75 °C; Rotor: Valcon H; Cappilary Connection: 1/16".	87x49x49 (L x W x H)	170.68 X 2	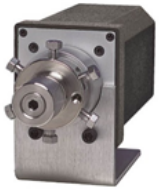
11	MicroVolume Connector	2	VICI Valco	(Part No. ZX1M)	300 series Stainless Steel; Cappilary Connection: 1/16"; 4-ports (Cross).	23 (OD)	33.19 x 2	
12	MicroVolume Connector	2	VICI Valco	(Part No. ZX1M)	300 series Stainless Steel; Cappilary Connection: 1/16"; 3-ports (Tee).	Same as #9	21.53 x 2	

(Table A.1 – continued)

#	Component	Quant.	Supplier	Product designation	Technical information	Dimensions (mm)	Cost (€)	Drawing
13	Cappilary Tubes	2	Upchurch Scientific	(Part No. UPCH1517)	ETFE HPLC Tubing; OD: 1/16"; Operating Temperature: <80ºC; Operating Pressure: 34-276 bar.	1500x1.O16x 1.5875 (L x ID x OD)	30.2 x 2	
14	Connectors	42	ACE	(Part No. ACE-CC10)	PEEK HPLC column connectors; Usable for 1/16"OD tubing; Operating Pressure: <350bar; Inert and Biocompatible.	20.8x9.3 (L x OD)	6.50 x 42	
15	Relay board	1	Robot Electronics	(Part No. USB-OPTO-RLY88)	Relays: 8; Control Interface: USB; Power: Powered from standard USB bus.	113.03x73.66 (L x W)	79.71	
16	8-port RS-232 PCI board	1	Moxa	(Part No. C168H/PC)	Operating Systems: Windows 95/98/ME/NT/2000/XP/200, Linux, . . . ; Bus: 32-bits.	123x100 (L x W)	175.34	

(Table A.1 – continued)

#	Component	Quant.	Supplier	Product designation	Technical information	Dimensions (mm)	Cost (€)	Drawing
17	Superformance Glass Column	1	E Merck	(Part No. G.20252)	Max. Pressure in Continuous Operation: 60 bar; Packing bed height: 60 mm.	300x26 (L x ID)	898.68	
18	Source 30RPC Resin	32 mL	GE Healthcare	(Part No. 17512002)	Rigid, spherical, porous, mono-sized polymeric matrix: polystyrene/divinyl benzene; Particle size: 30 μm; High Chemical Stability; Recommended pH: 1-14; Operating Temperature: 4-40 °C; Max. operating back pressure: 1.5 MPa.	Pack Size: 200 mL	145.00	

A.5 Pumps Calibration Protocol

Isocratic pumps connected to the One-column setup can be calibrated via the command interface in *Julia* software. The calibration protocol contain the following steps:

1. Start *Julia* software: (`julia1` ; `using ChromatographyStudio`);

2. Choose the setting that the stream will obey: (`@step`);

3. Calibrate to desired flow rates: (`cal=calibrate_pump...`);

4. Then do (`cal.fit[4].p)` : Provides the terms of the calibration equation. What's inside the bracket means the degree of polynomial you want to generate;

5. Get the inverse calibration data: (`cal.fit_inv[4].p`). Reverse calibration allows transformation of calibrated flow rates to original pump flow rates;

6. Write the equations coefficients into the *devices.jl* file and save it;

7. Finally, do the calibration once again with the same flows. The flow values to be obtained in this step should be closer to the desired values, so the pump will be calibrated and ready for use;

8. Four graphs will be generated by the system:

    - Calibration curve (desired flow rate vs. actual flow rate) prior to using the calibration equation (example in Figure A.3);
    - Calibration curve after using the calibration equation;
    - Weight vs. time graph for each chosen flow, before using the calibration equation (example in Figure A.4);
    - Weight vs. time graph for each chosen flow rate, after using the calibration equation;

9. Turn off *Julia* software: (`exit()`).

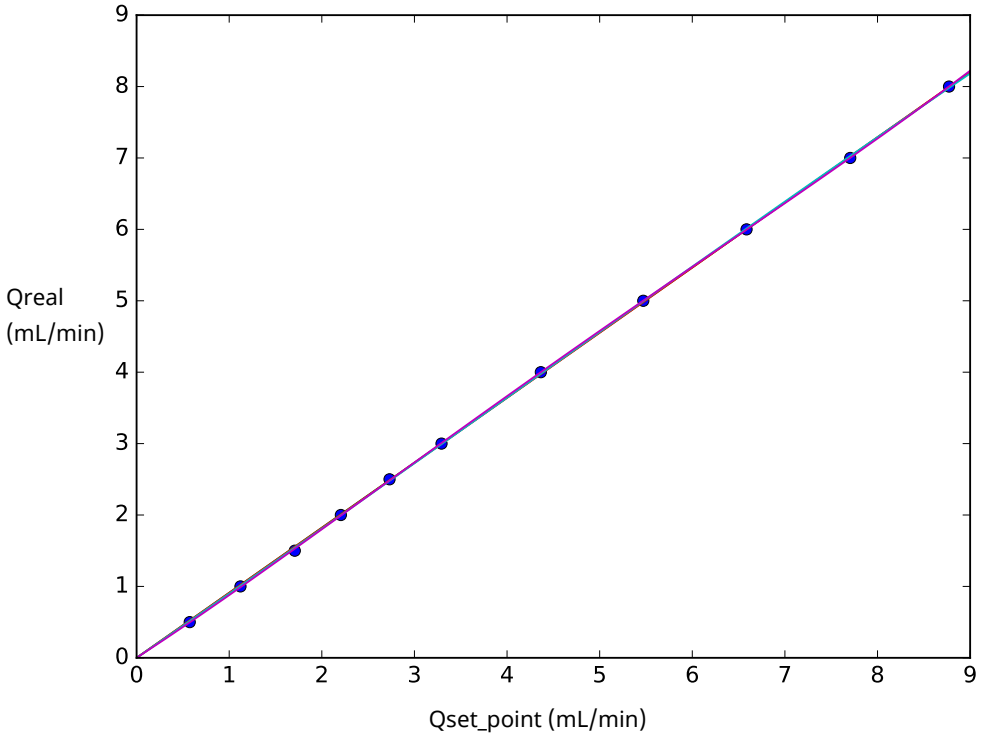

Figure A.3: Example of pump G calibration curve.

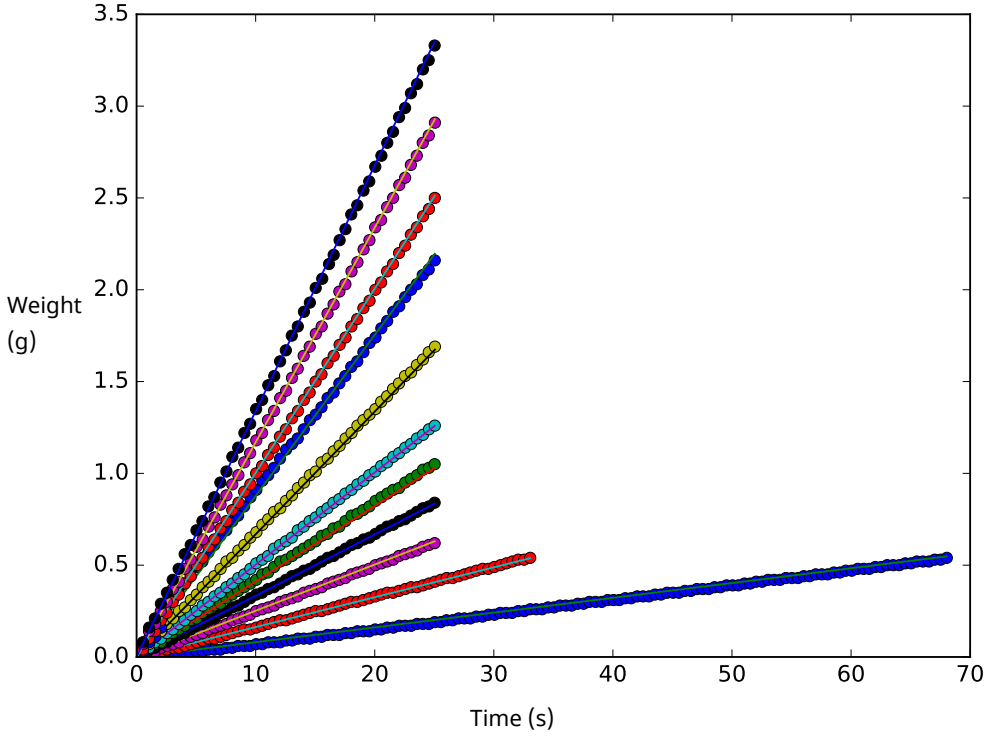

Figure A.4: Example of pump G weight curve.

A.6 Valves Position

Table A.2: On-Off and switching valves position. 1 = opened valve, 0 = closed valve.

Configuration	**On-Off Valves**							**Switching Valves**	
	V1	**V2**	**V3**	**V4**	**V5**	**V6**	**V7**	**COM2**	**COM8**
F+R=>COL=>R	1	0	0	1	1	1	0	A	A
R=>COL=>R	1	0	0	1	0	0	1	A	A
E=>COL=>R	1	0	0	1	1	0	1	B	A
E=>COL=>P/W	1	1	1	0	0	0	1	B	A
F=>COL=>P/W	0	1	1	0	1	1	0	B	B
F=>COL=>R	0	0	0	1	1	1	0	A	B
F+R=>COL=>P/W	1	1	1	0	0	1	0	B	B
R=>COL=>P/W	1	1	1	0	0	0	1	B	B

A.7 Implemented Steps in *ChromatographyStudio.jl*

Prototype operation steps, implemented at ChromatographyStudio.jl *Julia*'s package created to automate the setup. The following schemes were generated using Adobe Illustrator image editor. Each feed tank has a corresponding fluid color. The colors in the tubes indicate where each fluid is passing, while the gray paths indicate that there is no fluid passing through it in this step. F, E, P, W, R are the feed, eluent, product, waste, and recycle stream; COL, RP, UV_i, V_i refer, in this order, to the column, recycle piston, UV detector and on-off valve apparatus; the 2-pos-6-port valves are represented by the circles with their fluid passage position inside, which can be A, B, IN or BY; COM_i is the communication ports for each equipment.

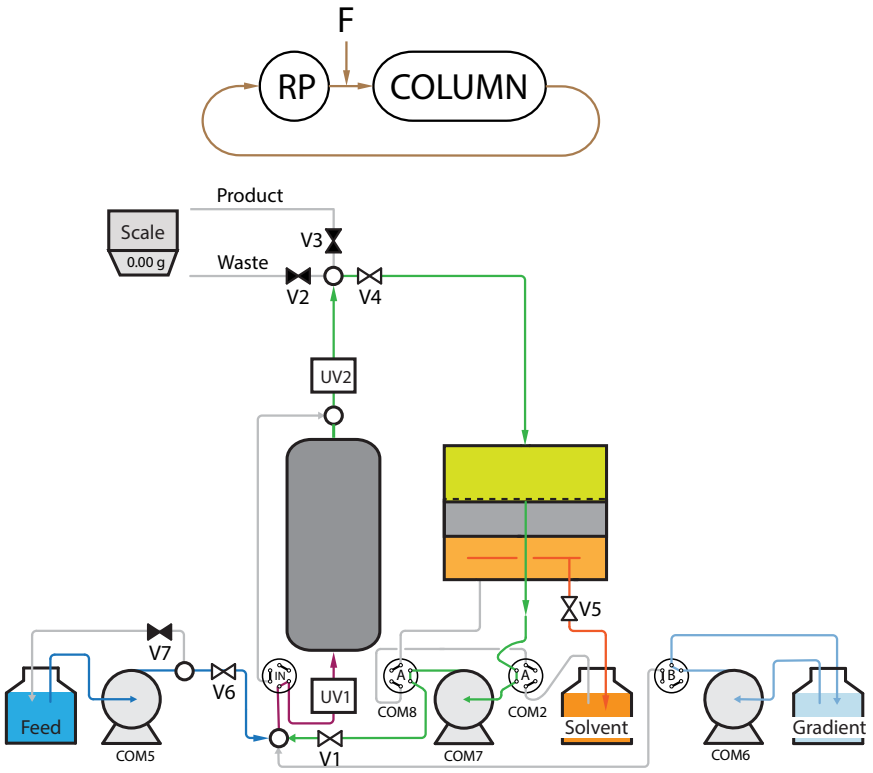

Figure A.5: Configuration F+R => COL => R.

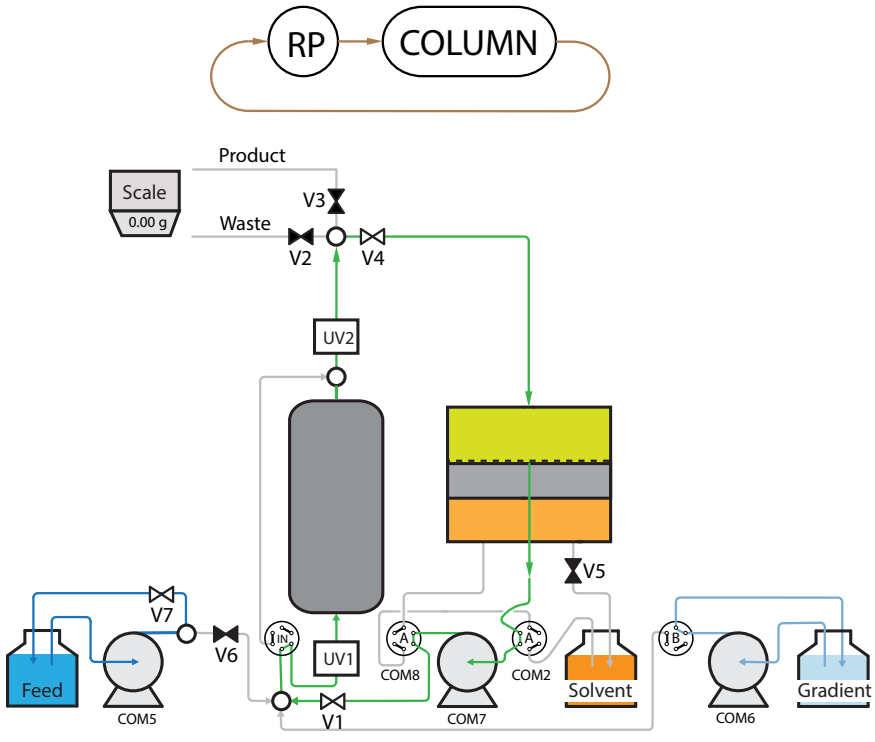

Figure A.6: Configuration R => COL => R.

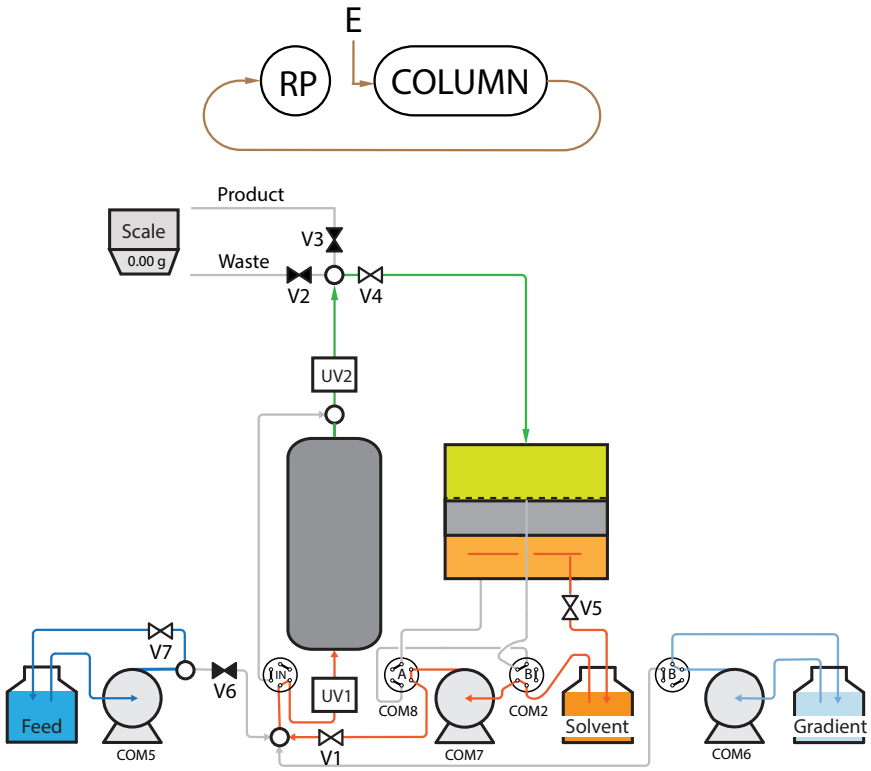

Figure A.7: Configuration E => COL => R.

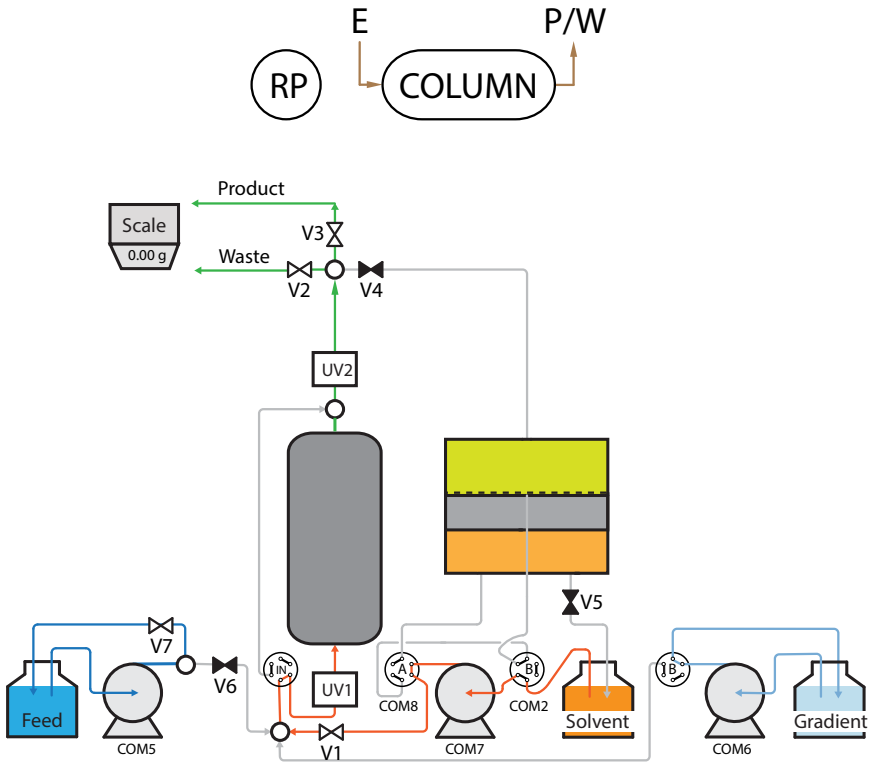

Figure A.8: Configuration E => COL => P/W.

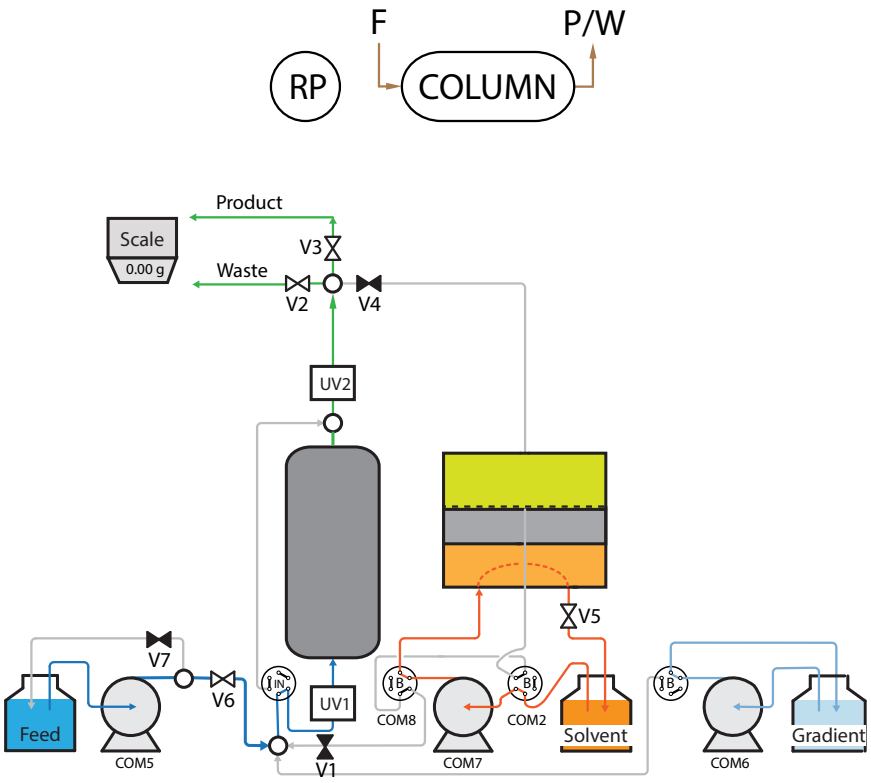

Figure A.9: Configuration F => COL => P/W.

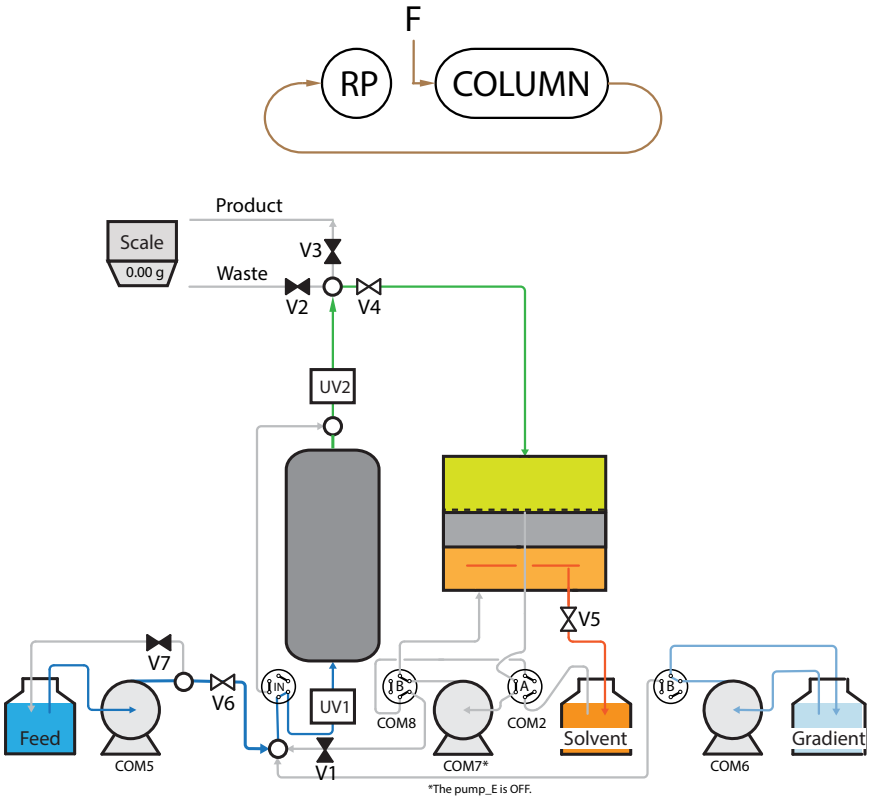

Figure A.10: Configuration F => COL => R.

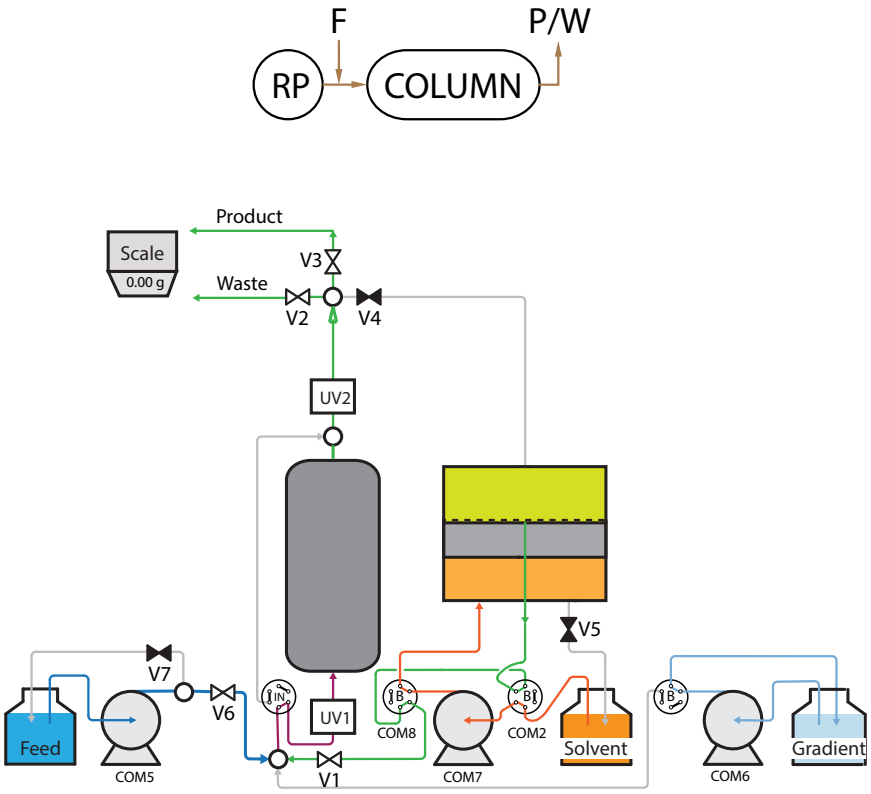

Figure A.11: Configuration F+R => COL => P/W.

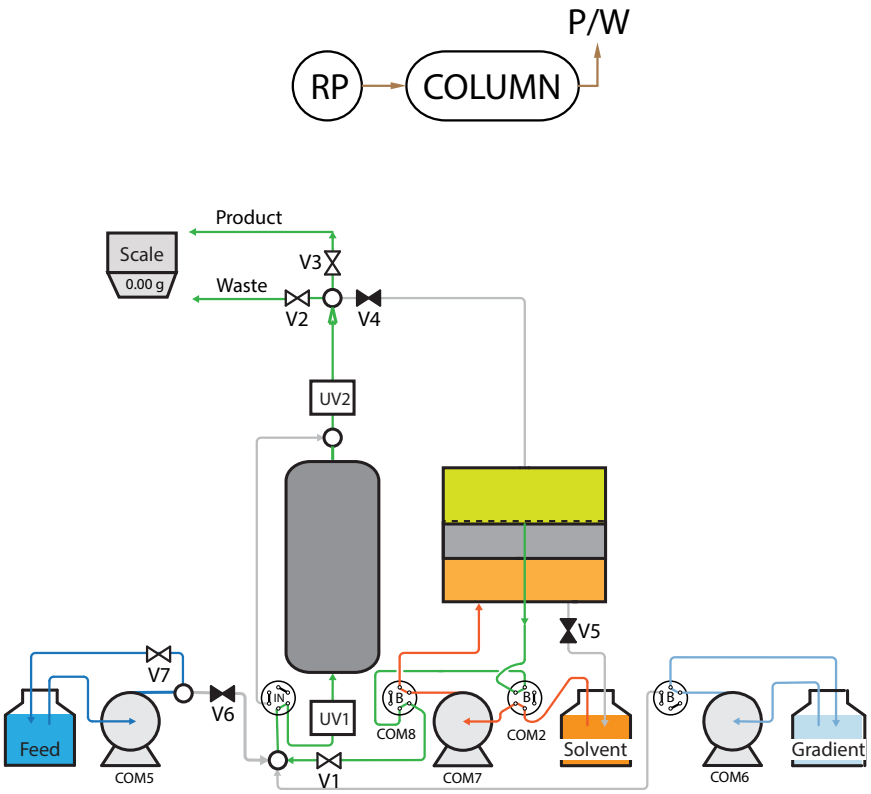

Figure A.12: Configuration R => COL => P/W.

APPENDIX B

Appendix B

B.1 Hydrodynamic Experiments *Julia* Commands

The experimental script submitted to *Julia* software for the preliminary hydrodynamic experiments, the "Exps.jl", is presented below:

Listing B.1: Exps.jl

```
@uvc A wavelengths=[260.0]
@uvc A set:dark
@uvc A set:ref
@uvc A plot:all
monitor_balance(bal, 1.0);
@pump F = 2.0; @pump E = 2.0
@monitor file = "uridineafter.mon"
@sequence begin
include("Exps.jl")
end
@monitor stop

% Exps.jl: (For UV after piston)

@step F => COL => W
@valve +V4
@valve -V2
@valve -V5
sleep(200.0)

@step E => COL => W
@valve +V4
@valve -V2
@pump E = 2.0
```

B.2 Ideal Wavelength for Blue Dextran Compound

Ideal wavelength (λ) for detection of Blue Dextran compound. For blue dextran solution at c = 0.24 g/L, the Absorbance Spectrum (Graph (a)) was read in the (approximate) range 260 < λ < 750 nm during a step injection. Therefore, 5 wavelengths were tested in this range: 285.0, 290.0, 305.0, 600.0, 620.0 and 630.0 nm. From the chromatogram obtained for each wavelength (Graph (b)), the λ = 620 nm wavelength was chosen to perform the experiments with blue dextran solution, due to the low disturbance of the UV signal. It is important to point out that the blue dextran experiments were performed using the USB4000 spectrometer, with only deuterium light turned on, and that for this spectrometer the ideal Integration Time (IT) is 65000 μs.

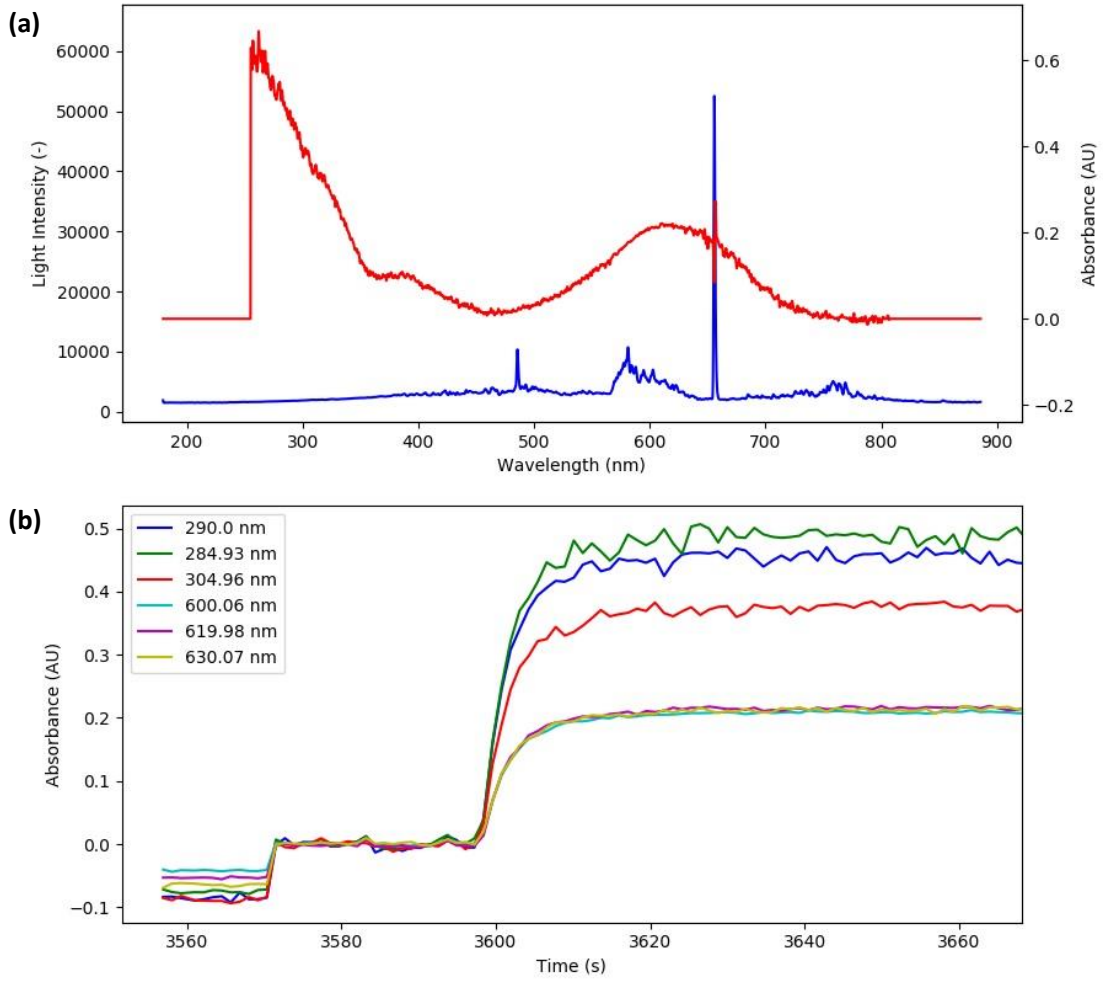

Figure B.1: UV detection for Blue Dextran solution (c = 0.24 g/L). **(a)** Absorbance Spectrum (–) and Intensity Spectrum (–); **(b)** Chromatogram for five wavelengths (285.0, 290.0, 305.0, 600.0, 620.0, 630.0 nm). The λ = 620 nm is within the detection range of the Absorbance Spectrum and showed a stable absorbance signal, therefore, this wavelength was chosen for the experiments to be performed with blue dextran.

B.3 Henry.jl

Script run at *Julia* software for Henry constant determination, the "Henry.jl":

Listing B.2: Henry.jl

```
@pump G = 0.0
@pump F = 0.0

println("\n Feeding during 40 s \n")
@step E+F => COL => P
@pump F = 3.0
sleep(40)

@pump F = 0.0
@pump G = 3.0
println("\n Eluent till end \n")
readline()
@pump G = 0.0

@monitor stop
sleep(1.0)
@valve -all
```

B.4 Components Absorbance Spectrum

Ideal wavelength (λ) for detection of Uridine and Guanosine compounds. For each component solution at c = 0.05 g/L, the Absorbance Spectrum (Graph (a)) was read in the approximate range of $210 < \lambda < 300$ nm during a step injection. Therefore, 3 wavelengths were tested in this range: 260.0, 280.0 and 285.0.0 nm. From the chromatogram obtained for each wavelength (Graph (b)), the $\lambda = 260$ nm wavelength was chosen to perform the experiments with uridine and guanosine solutions, due to the intensity of the UV signal. It is important to point out that the uridine and guanosine experiments were performed using the USB2000 spectrometer, with only deuterium light turned on, and that for this spectrometer the ideal Integration Time (IT) is 37000 μs.

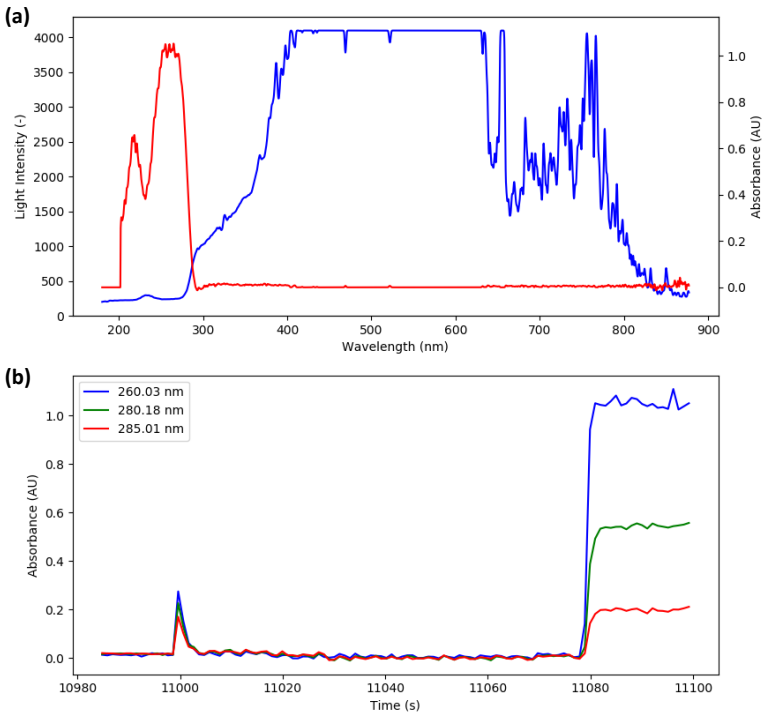

(i=1) Uridine.

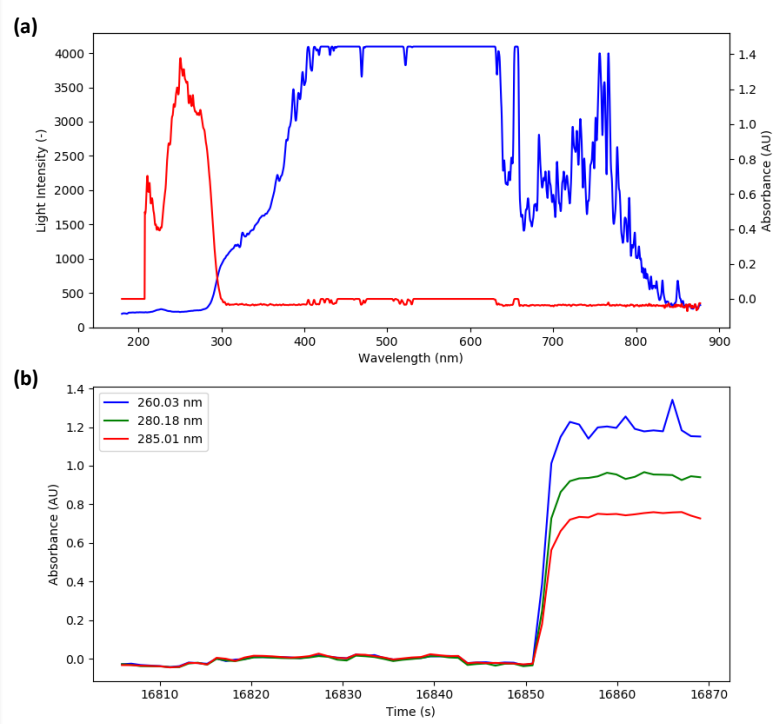

(i=2) Guanosine.

Figure B.2: UV detection for uridine ($i = 1$) and guanosine ($i = 2$) solutions ($c_i = 0.05$ g/L). **(a)** Absorbance Spectrum (–) and Intensity Spectrum (–); **(b)** Chromatogram for three wavelengths (260.0, 280.0, 285.0 nm). The $\lambda = 260$ nm is within the detection range of the Absorbance Spectrum and showed a stable absorbance signal, therefore, this wavelength was chosen for the experiments to be performed with the nucleosides.

B.5 Isotherm.jl

Script run at *Julia* software for Adsorption Isotherms determination, the "Isotherm.jl":

Listing B.3: Isotherm.jl

```
println("\n***Beginning Test now***\n")

println("\n***F = 1.0 E = 4.0***\n")
@step E + F => COL => P
@pump F = 1.0
@pump G = 4.0
sleep(1080)

println("\n***F = 2.0 E = 3.0***\n")
@pump F = 2.0
@pump G = 3.0
sleep(1080)

println("\n***F = 3.0 E = 2.0***\n")
@pump F = 3.0
@pump G = 2.0
sleep(1080)

println("\n***F = 4.0 E = 1.0***\n")
@pump F = 4.0
@pump G = 1.0
sleep(1080)

println("\n***F = 5.0 E = 0.0***\n")
@pump F = 5.0
@pump G = 0.0
sleep(1080)

println("\n***Done***\n")
```

B.6 ColExps.jl

The experimental script submitted to *Julia* software for the uridine-guanosine separation test, the "ColExps.jl", is presented below:

Listing B.4: ColExps.jl

```
% Cycle 1 (Just for cycle 1):

@step F => COL => P
sleep(236.6322)
@step E => COL => P
sleep(240.5298)

```

```
% Cycle 2 to N:

@step E => COL => R
sleep(609.282)
@step R => COL => P
sleep(368.7534)
@step F => COL => P
sleep(236.6322)
@step R => COL => P
sleep(+-240.5298)

% At the end of the N cycle, there is a cleaning command:

@step E => COL => P
sleep(609.282)
@pump F = 0.0
@pump E = 0.0
sleep(1.0)
@valve -all
```

B.7 Simulation Building Blocks

B.7.1 Dispersed plug flow

Model representing the two frits of the recycling device:

$$x = 0: \qquad Qc_i - D_{i\mathrm{L}} \frac{\partial c_i}{\partial x} = (Qc_i)_{\mathrm{in}}, \tag{B.1}$$

$$0 < x < 1 \qquad \frac{\partial c_i}{\partial \theta} = \frac{\tau}{V_f} \left(D_{i\mathrm{L}} \frac{\partial^2 c_i}{\partial x^2} - Q \frac{\partial c_i}{\partial x} \right), \tag{B.2}$$

$$x = 1: \qquad \frac{\partial c_i}{\partial x} = 0, \tag{B.3}$$

where $Q_{i,in}$ and $c_{i,in}$ are the inlet volumetric flowrate, and inlet solute concentration. The material balances to nodes between chromatographic units (admixing or splitting of streams) are easier to write in terms of solute molar (or mass) flowrates. Thus, we shall (i) drop the subscript 'in' in Q_{in} and let Q stand for the working volumetric flowrate through the cell, and (ii) lump Q_{in} and $c_{i,\mathrm{in}}$ into the solute molar (or mass) flowrate, $(Qc_i)_{\mathrm{in}}$.

V_f is the dead volume present in each frit.

Hereafter the time scale is scaled by τ: the dimensional time coordinate t is replaced by a dimensionless time coordinate $\theta = t/\tau$.

And

$$D_{i\mathrm{L}} = D_{i\mathrm{L}}^{(1)} + D_{i\mathrm{L}}^{(2)} Q \tag{B.4}$$

is the dispersion coefficient.

B.7.2 Adsorption column (linear isotherms)

Model representing the chromatographic column:

$$x = 0: \qquad Qc_i - D_{i\mathrm{L}} \frac{\partial c_i}{\partial x} = (Qc_i)_{\mathrm{in}}, \tag{B.5}$$

$$0 < x < 1 \qquad \frac{\partial c_i}{\partial \theta} = \frac{\tau}{[\epsilon + (1-\epsilon)H_i]V_{\mathrm{c}}} \left(D_{i\mathrm{L}} \frac{\partial^2 c_i}{\partial x^2} - Q \frac{\partial c_i}{\partial x} \right), \tag{B.6}$$

$$x = 1: \qquad \frac{\partial c_i}{\partial x} = 0, \tag{B.7}$$

where H_i is the Henry constant of solute i, ϵ is the interparticle porosity, V_{c} is the column volume.

B.7.3 Recycle piston

Piston volume is variable, so:

$$\frac{\partial V}{\partial \theta} = \tau(Q_{in} - Q_{out}) \tag{B.8}$$

1. Model representing the recycle device as dispersed plug flow:

$$x = 0: \qquad VQ_{in}c_i - D_{i\mathrm{L}} \frac{\partial c_i}{\partial x} = V(Qc_i)_{\mathrm{in}}, \tag{B.9}$$

$$0 < x < 1 \qquad \frac{\partial c_i}{\partial \theta} = \frac{\tau}{V^2} \left(D_{i\mathrm{L}} \frac{\partial^2 c_i}{\partial x^2} - V[Q_{in} - (Q_{in} - Q_{out})x] \frac{\partial c_i}{\partial x} \right), \tag{B.10}$$

$$x = 1: \qquad \frac{\partial c_i}{\partial x} = 0, \tag{B.11}$$

   where $c_{i,in} = c_{i,out}^{Frit}$.

2. Model representing the recycle device as perfectly mixed tank:

$$V \frac{dc_{i,out}}{d\theta} = \tau Q_{\mathrm{in}}(c_{i,\mathrm{in}} - c_{i,out}). \tag{B.12}$$

   Brief model explanation:

   As the volume of liquid inside the recycle device, V, changes with time, the global material balance is

$$\frac{dV}{dt} = Q_{\mathrm{in}} - Q_{\mathrm{out}}, \tag{B.13}$$

   where Q_{in} and Q_{out} are the inlet and outlet volumetric flowrates.

   The solute material balance is

$$\frac{d(c_{i,\mathrm{out}}V)}{dt} = c_{i,\mathrm{in}}Q_{\mathrm{in}} - c_{i,\mathrm{out}}Q_{\mathrm{out}}, \tag{B.14}$$

$$V\frac{d(c_{i,\text{out}})}{dt} + c_{i,\text{out}}\frac{d(V)}{dt} = c_{i,\text{in}}Q_{\text{in}} - c_{i,\text{out}}Q_{\text{out}}, \tag{B.15}$$

where $c_{i,\text{in}}$ and $c_{i,\text{out}}$ are the inlet and outlet solute concentrations. Taking into account eq. (B.13), and substituting $\frac{dV}{dt}$ at previous equation:

$$V\frac{d(c_{i,\text{out}})}{dt} + c_{i,\text{out}}(Q_{\text{in}} - Q_{\text{out}}) = c_{i,\text{in}}Q_{\text{in}} - c_{i,\text{out}}Q_{\text{out}}, \tag{B.16}$$

$$V\frac{dc_{i,\text{out}}}{dt} = Q_{\text{in}}c_{i,\text{in}} - Q_{\text{in}}c_{i,\text{out}}). \tag{B.17}$$

Hence, the solute material balance can be rewritten as

$$V\frac{dc_{i,\text{out}}}{dt} = Q_{\text{in}}(c_{i,\text{in}} - c_{i,\text{out}}). \tag{B.18}$$

As the dimensionless time coordinate $\theta = t/\tau$, the final equation is

$$V\frac{dc_{i,\text{out}}}{d\theta} = \tau Q_{\text{in}}(c_{i,\text{in}} - c_{i,\text{out}}), \tag{B.19}$$

which is valid even if V changes with time. This equation gives $c_{i,\text{out}}(\theta)$ as a function of $V(\theta)$, $Q_{\text{in}}(\theta)$, and $c_{i,\text{in}}(\theta)$. The molar flowrate of solute exiting the cell is $c_{i,\text{out}}Q_{\text{out}}$.

Appendix C

Appendix C

C.1 3D Printed Distributor Designs

Examples of designs explored in the SLA method for producing 3D fluid dispensers. Due to the wide variety of conformations, only a few are shown in the image for illustrative purposes.

Figure C.1: Examples of designs explored in the SLA method for producing 3D fluid dispensers.

APPENDIX D

APPENDIX D

D.1 gPROMS Implementation

Brief explanations of implementation in gPROMS are given below. Each section is intended to perform a different task.

D.1.1 Connections between Chromatographic Columns

The below equations (already discussed in Chapter 6):

$$\{s^{\text{in}}, w^{\text{in}}, y^{\text{in}}\}_2 = v_{\text{IC}} \times \{s^{\text{out}}, w^{\text{out}}, y^{\text{out}}\}_1 + (1 - v_{\text{IC}}) \times \{s^{\text{F}}, w^{\text{F}}, y^{\text{F}}\}, \tag{D.1}$$

$$v_{\text{IC}} = \begin{cases} 1 & \text{for the IC steps} \\ 0 & \text{for the B steps,} \end{cases}. \tag{D.2}$$

can be implemented in gPROMS via one easy mechanism. It is necessary to simply introduce a new `SELECTOR`, the `vIC`, which is a special type of variable that can only hold a discrete number of values. For example, in the model we add the following section:

```
SELECTOR
vIC AS (OFF, ON)
```

Then, in the `EQUATION` section we introduce the following block:

```
EQUATION
...
CASE vIC OF
WHEN OFF:
Column(2).sIN = sF ;
Column(2).wIN = wF ;
```

```
Column(2).yIN = yF ;
WHEN ON:
Column(2).sIN = Column(1).sOUT ;
Column(2).wIN = Column(1).wOUT ;
Column(2).yIN = Column(1).yOUT ;
END # CASE
```

D.1.2 Amount of Component i Collected in the Product Fraction

Note that equation, explained in Chapter 6, that describes the amount of component i (mAb or impurity) collected in the product fraction

$$a_i^{\mathrm{P}} = Q_{\mathrm{B}} \int_{\tau_3} c_i^{\mathrm{out}}(t)\, dt, \tag{D.3}$$

is difficult to calculate in gPROMS as is. However, this equation can be recast as follows:

$$\frac{da_i^{\mathrm{P}}}{dt} = Q_{\mathrm{B}} c_i^{\mathrm{out}}(t) \quad \text{for} \quad t \in \text{step 3} \quad \text{s.t.} \quad a_i^{\mathrm{P}} = 0 \ \text{ at the start of step 3.} \tag{D.4}$$

In practice, the actual equation implemented in gPROMS is

$$\frac{da_i^{\mathrm{P}}}{dt} = v^{\mathrm{P}} Q_{\mathrm{B}} c_i^{\mathrm{out}}(t), \qquad v^{\mathrm{P}} = \begin{cases} 1 & t \in \text{step 4} \\ 0 & t \notin \text{step 4} \end{cases}, \tag{D.5}$$

where a_i^{P} is reset to zero at the start of every half cycle.

ANNEX I

ANNEX A1

ChromatographyStudio.jl is the custom-made central program that calls all of the developed drivers, created by J. Antunes & J.P.B. Mota [16], for Single-column Analog process automation and data acquisition.

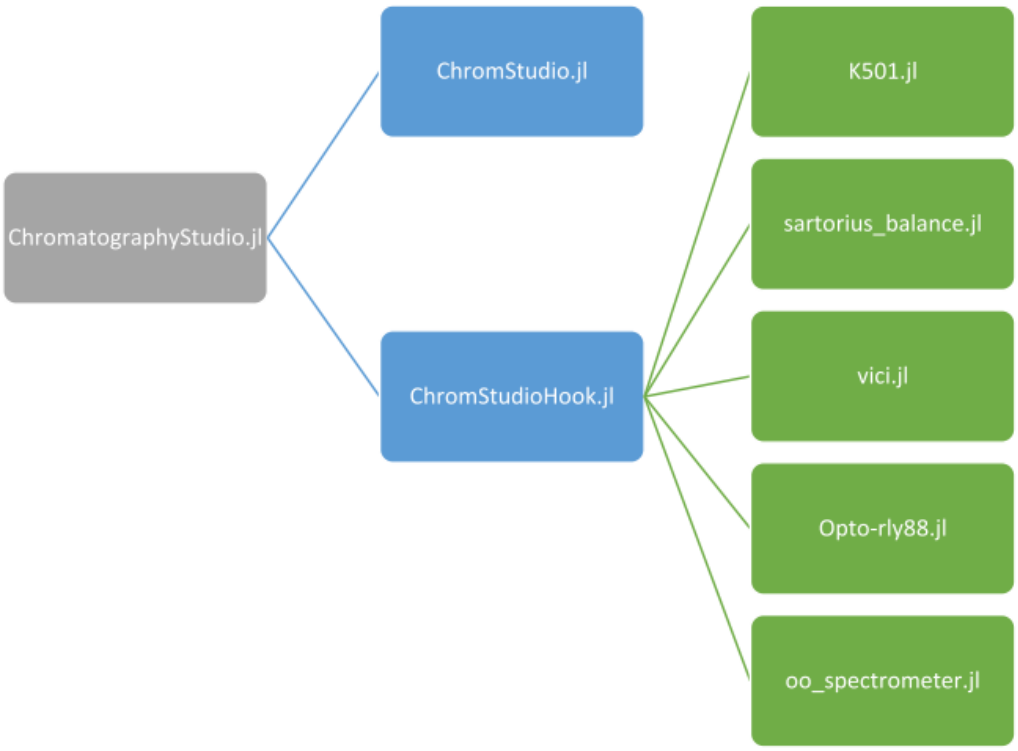

Figure I.1: Hierarchical diagram of programs created for Single-column Analog to SMB process automation and data acquisition. Programs are condensed in an unique easy-to-use interface, the *ChromatographyStudio.jl* module. Source: [16].